

Evaluation of a Detailed Reaction Mechanism for Partial and Total Oxidation of C₁ - C₄ Alkanes

DISSERTATION

Submitted to the
Faculty of Chemistry of the Rupertus-Carola University of Heidelberg, Germany
For the degree of
Doctor of Natural Sciences

Presented by
Raúl Quiceno González
Born in Medellín, Colombia

Examiners: Prof. Dr. Dr. h. c. Jürgen Warnatz
Prof. Dr. Olaf Deutschmann

Heidelberg, November 16, 2007

**Interdisziplinäres Zentrum für Wissenschaftliches Rechnen
Ruprecht – Karls – Universität Heidelberg
2007**

DISSERTATION

Submitted to the

Faculty of Chemistry of the Rupertus-Carola University of Heidelberg, Germany

For the degree of

Doctor of Natural Sciences

Presented by

Raúl Quiceno González, Ms, Sciences

Born in Medellín, Colombia

Heidelberg, November 16, 2007

Title

**Evaluation of a Detailed Reaction Mechanism for Partial
and Total Oxidation of C₁ - C₄ Alkanes**

Examiners: Prof. Dr. Dr. h. c. Jürgen Warnatz
Prof. Dr. Olaf Deutschmann

ACKNOWLEDGMENTS

I would like to acknowledge to all the people who helped me directly or indirectly to accomplish this dissertation: First and foremost, I would like to express all my gratitude towards Prof. Dr. Dr. h. c. Jürgen Warnatz for giving the opportunity to share an unforgettable time in his group in Heidelberg.

To Prof. Dr. Olaf Deutschmann and his family, for his support during my time in Heidelberg, for the useful comments and great support in the development of my work and for his friendship during difficult moments.

To Farid Chejne, my former tutor in Colombia, for his tireless compromise with all of us, for being more than a tutor, a friend.

I am also thankful to my colleagues at IWR: Ingrid for her collaboration with all the administrative details, to Barbara for her unvaluable help, to Jürgen Moldenhauer, Till Katzenmeier, Volker Karbach, Shaik and all my coworkers for their help and understanding.

Este pequeño parrafo me gustaria dedicarlo a mi familia, solo tengo palabras de agradecimiento para ellos por acompañarme desde la distancia, por brindarme amor y comprension, por sufrir el dolor de la separacion, por aceptarlo y ayudarme a sobre llevarlo de la mejor manera posible; solo tengo palabras de agradecimiento para ustedes, y dificilmente podria describir cuanto los quiero, respecto y admiro: mil gracias.

Finally, I would like to thank Sophia, for her boundless love, faith in me, and encouragement and for bring to my life the most beautiful thing that ever happen to me: Madeleine, without both of you this work would still not be completed.

ABSTRACT

In the present work a chemical kinetic mechanism was developed, suitable for modeling combustion and partial oxidation processes of $C_1 - C_4$ alkanes. The gas-phase kinetic mechanism describes intermediate and high temperature chemistry. Accordingly, the formation and evolution of important intermediate gas-phase species: Olefins and oxygenates were described in terms of different pathways typical at those temperature regimes.

A previously developed mechanism suitable for high temperature conditions was extended by including reactions which described the chemistry of total and partial oxidation of methane, ethane, propane, butane, lower alkenes and formation and consumption of their characteristic organic hydro-peroxide radicals and cyclical compounds. The kinetic mechanism was validated by comparing calculated results of ignition delay times, against experimental data obtained in shock tubes, for various hydrocarbons and their mixtures, over a wide range of reaction conditions (temperature, pressure and mixture composition). Further, the kinetic mechanism was evaluated by comparing numerical simulations against experimentally obtained concentration profiles of the main gas-phase species, measured in jet stirred reactors for different hydrocarbons and their mixtures during partial oxidation.

Next, the mechanism was applied to get a better understanding of the interactions between flow, mass transfer and homogeneous-heterogeneous chemistries during the catalytic partial oxidation of methane in a short contact time reactor, which has recently attracted strong scientific and technological interest.

The detailed study of the catalytic partial oxidation of methane to syngas in a single gauze reactor was based on three-dimensional numerical simulations of the flow field coupled with heat transport and multi-step gas-phase and surface reaction mechanisms, including the computation of the surface coverage. Results from the model were compared with experimental data reported in the literature. The gas-phase mechanism was modeled using a reduced mechanism, and for the surface a previously developed mechanism was adapted. The results from the simulation of the partial oxidation of methane in a short contact time reactor were carried out using the commercial computational fluid dynamics code Fluent, which was coupled with external subroutines to model the detailed gas-phase and surface chemistry.

Today, the production of synthesis gas (carbon monoxide + hydrogen) is currently carried out via steam reforming. In that process steam passes over a carbon source, often methane or coal, and is heated to produce the synthesis gas. Synthesis gas is extremely valuable commercially

for the production of methanol, hydrocarbons, higher alcohols for use in detergents, and ammonia to use in fertilizers. There is also a significant interest in the production of hydrogen for fuel cells. However, steam reforming has the major disadvantage of being endothermic and hence requires a large amount of wasted energy to drive the reaction. An alternative to steam reforming is the partial oxidation of the hydrocarbons, especially methane in short contact time reactors. This promising route for natural gas conversion into more useful chemicals has the advantage of being auto thermal.

KURZFASSUNG

In der vorliegenden Arbeit wurde ein chemischer Reaktionsmechanismus entwickelt, mit dem Verbrennungsprozesse und Partialoxidationsprozesse von $C_1 - C_4$ Alkanen modelliert werden können. Der Reaktionsmechanismus der Gasphase beschreibt Prozesse für mittlere und hohe Temperaturen. Die Ausbildung und Entwicklung wichtiger Zwischenprodukte der Gasphase wie Olefine und sauerstoffhaltige Produkte werden hinsichtlich verschiedener Temperaturbereiche geschildert.

Ein bereits entwickelter Mechanismus für Hochtemperaturbedingungen wurde erweitert, indem Reaktionen eingefügt wurden, die die chemischen Reaktionen der vollständigen und partiellen Oxidation von Methan, Ethan, Propan, Butan und kurzkettigen Alkene sowie die Ausbildung und den Verbrauch ihrer charakteristischen organischen hydro-Peroxid Radikalen und zyklische Komponenten beschreibt. Die Überprüfung des Reaktionsmechanismus erfolgte durch Vergleich mit errechneten Ergebnissen von Zündverzugszeiten gegenüber experimentell ermittelte Daten aus Versuchen mit Stossrohren für verschiedene Kohlenwasserstoffe und ihre Mischungen unter verschiedensten Reaktionsbedingungen (Temperatur, Druck und Aufbau der Zusammensetzung). Weiterhin wurde der Reaktionsmechanismus durch Vergleich mit numerischen Simulationen gegenüber experimentell erhaltende Konzentrationsprofile der wichtigsten Spezies in der Gasphase evaluiert. Die Messungen fanden in Reaktionsbehältern für verschiedene Kohlenwasserstoffe und deren Mischungen während der Partialoxidation statt.

Als nächster Schritt wurde der Mechanismus angewandt, um ein besseres Verständnis von den ablaufenden Prozessen und deren Wechselwirkungen (Strömungsfeld, Massentransport, homogener und heterogener Reaktionen) während der katalytischen Partialoxidation von Methan in einem *Short Contact Time Reactor* (SCTR), der derzeit von großem wissenschaftlichen sowie technologischen Interesse ist, zu erlangen.

Die detaillierte Studie der katalytischen Partialoxidation von Methan zu Synthesgas auf einer Platinoberfläche, *Gauze Reactor*, basierte auf dreidimensionale numerische Simulationen reaktiver Strömungen verbunden mit Wärmetransport und mehrstufigen Gasphasenmechanismen sowie Oberflächenreaktionen einschließlich der Berechnung der Oberflächenabdeckung. Die Ergebnisse des Modells wurden mit experimentell ermittelten Daten aus der Literatur verglichen. Der Mechanismus der Gasphase wurde mit einem reduzierten Mechanismus modelliert. Für die Reaktionen auf der Oberfläche wurde ein vorher entwickelter Mechanismus adaptiert. Die Ergebnisse der Partialoxidation von Methan in

einem SCTR wurden mit dem kommerziell erhältlichen CFD-Programm FLUENT simuliert, in dem detaillierte Gasphasen- und Oberflächen-Reaktionsmechanismen berücksichtigt werden.

Derzeit wird die Produktion von Synthesegas (Kohlenstoffmonoxid + Wasserstoff) mit dem Verfahren der Dampfreformierung realisiert. In diesem Prozess passiert Dampf eine Kohlenstoffquelle, oft Methan oder Kohle, und wird erhitzt, um Synthesegas zu produzieren. Synthesegas ist kommerziell sehr nützlich für die Produktion von Methanol, Kohlenwasserstoffe, längerkettige Alkohole für Detergentien sowie Ammoniak für Düngemittel. Außerdem besteht ein erhebliches Interesse an der Produktion von Wasserstoffe für Brennstoffzellen. Allerdings hat die Dampfreformierung den großen Nachteil, daß es ein endothermer Prozess ist und folglich viel Energie benötigt, um die Reaktion zu betreiben. Eine Alternative zur Dampfreformierung stellt die Partialoxidation von Kohlenwasserstoffen dar, insbesondere die Umwandlung von Methan in SCTR. Diese vielversprechende Möglichkeit, Erdgas in wertvollere chemische Grundstoffe zu konvertieren, hat den Vorteil autotherm betrieben werden zu können.

Contents

| | |
|--|-----|
| ACKNOWLEDGEMENTS | i |
| ABSTRACT | iii |
| KURZFASSUNG | v |
| 1. INTRODUCTION | 1 |
| 1.1 Structure of the Thesis | 4 |
| 2. OXIDATION OF HYDROCARBONS | 7 |
| 2.1 Oxidation of Hydrocarbons | 7 |
| 2.2 Ignition Process | 8 |
| 2.3 Continuous Flow Devices | 9 |
| 2.4 Shock Tubes | 9 |
| 2.5 Rapid Compression Machine | 10 |
| 2.6 Stirred Reactors | 13 |
| 3. REACTIVE FLOWS | 15 |
| 3.1 Mathematical and Numerical Model | 15 |
| 3.1.1 Governing Equations for Mass, Momentum and Species | 15 |
| 3.1.2 Heat Transfer | 17 |
| 3.1.3 Equation of State | 18 |
| 3.1.4 Transport Properties | 18 |
| 3.1.5 Thermodynamic Properties | 19 |
| 3.2 Modeling Chemical Reactions | 20 |
| 3.2.1 Rates of Reaction | 20 |
| 3.2.2 Temperature and Pressure Dependence of Rate Coefficients | 23 |
| 3.2.3 Surface Chemistry | 26 |

| | | |
|-------|---|----|
| 3.3 | Coupling of Heterogeneous Chemical Reactions with the Surrounding Flow Field | 29 |
| 3.4 | Methods for Reaction Mechanism Analysis | 30 |
| 4. | DEVELOPMENT AND VALIDATION OF A DETAILED KINETIC MECHANISM FOR COMBUSTION OF C ₄ ALKANES | 33 |
| 4.1 | Bibliographic Review | 33 |
| 4.1.1 | Methane Oxidation and Partial Oxidation | 33 |
| 4.1.2 | Ethane Oxidation and Partial Oxidation | 35 |
| 4.1.3 | Propane Oxidation and Partial Oxidation | 36 |
| 4.1.4 | Butane Oxidation and Partial Oxidation | 38 |
| 4.2 | Reaction Mechanism Development | 39 |
| 4.3 | Low and Intermediate Temperature Oxidation | 39 |
| 4.3.1 | Reaction of Alkyl Radicals | 43 |
| 4.3.2 | Reaction of the Alkylperoxy Radicals RO ₂ | 43 |
| 4.3.3 | Scission of the Alkylhydroperoxide RO ₂ H | 46 |
| 4.3.4 | Scission of the Alkylhydroperoxy Radical QOOH* | 47 |
| 4.3.5 | Oxidation of Hydroperoxyalkyl Radical QOOH* | 47 |
| 4.3.6 | Cycle Ether Formation from HO ₂ Addition to Alkenes | 48 |
| 4.3.7 | Cycle Ether Decomposition | 49 |
| 4.4 | High Temperature Oxidation | 52 |
| 4.4.1 | Reaction of Alkanes | 52 |
| 4.4.2 | Reaction of the Alkyl Radical | 53 |
| 4.4.3 | Reaction of Alkenes | 54 |
| 4.4.4 | Reaction of Aldehydes | 55 |
| 4.5 | Mechanism Base | 56 |
| 4.5.1 | Mechanism for Hydrogen Oxygen Carbon Monoxide | 56 |
| 4.6 | Thermodynamic Data | 63 |
| 5. | EVALUATION OF THE MECHANISM: SIMULATION OF AUTOIGNITION | 65 |
| 5.1 | Ignition Delay Times for the H ₂ -O ₂ System | 66 |
| 5.2 | Ignition Delay Times at Combustion Conditions for Methane and Methane Mixtures | 67 |
| 5.3 | Ignition Delay Times for C ₂ -C ₄ Alkanes | 73 |
| 6. | PARTIAL AND TOTAL OXIDATION OF C1-C4 ALKANES AND ALKENES IN THE GAS PHASE | 81 |
| 6.1 | Partial Oxidation of Methane | 81 |

| | | |
|-------|--|-----|
| 6.2 | Propane Oxidation | 84 |
| 6.3 | Butane Oxidation | 88 |
| 6.4 | Ethene Oxidation at Low and Intermediate Temperature | 91 |
| 7. | CATALYTIC PARTIAL OXIDATION OF METHANE IN A SINGLE GAUZE REACTOR | 95 |
| 7.1 | Introduction | 95 |
| 7.2 | Experiment | 96 |
| 7.2.1 | Experimental Set-Up | 96 |
| 7.2.2 | Results of the Experiments | 99 |
| 7.3 | Kinetic Mechanisms | 100 |
| 7.3.1 | Gas-Phase Mechanism | 101 |
| 7.3.2 | Surface Mechanism | 102 |
| 7.4 | Modeling Approach | 103 |
| 7.4.1 | Channel Simulation of the Catalytic Gauze | 104 |
| 7.4.2 | Fluent Simulation of the Catalytic Gauze | 107 |
| 7.4.3 | Increasing Residence Time | 112 |
| 8. | CONCLUSIONS | 117 |
| | LIST OF FIGURES | 121 |
| | LIST OF TABLES | 127 |
| | ANNEX I | 129 |
| | ANNEX II | 131 |
| | REFERENCES | 133 |

Chapter 1

INTRODUCTION

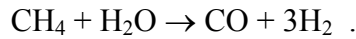
The combustion phenomenon is today still an important research issue for scientists and engineers around the world due to the increasing demand of fossil fuels like crude oil, natural gas and coal to satisfy the energy requirements of our society.

Man has been using combustion since ancient times: People from Greece, Persia, and India discovered natural gas many centuries ago. They were mystified by the burning springs created when natural gas seeps from cracks in the ground and was ignited. They sometimes built temples around these eternal flames so they could worship the fire. Chinese people 2500 years ago recognized that natural gas could be put to work: They piped the gas from shallow wells and burned it under large pans to evaporate sea water for salt. It is known that Romans used coal for fueling their heating system. But it was not until the beginning of the 1800's that the demand of natural gas was increased widely after the city of Baltimore decided to illuminate its streets with natural gas lights. Since then and especially in the past 40 years the use of natural gas has grown dramatically. Today, natural gas accounts for about a quarter of the energy we use.

Beside the use of the fossil fuels as an energy source, they are also the main feedstock for the modern industrial production of chemical compounds. Out of the hydrocarbons, crude oil and natural gas are the main suppliers. The already large prove natural gas reserves and their smaller impact on the greenhouse effect together with the limited crude-oil stocks make natural gas more attractive than its competitors.

However, natural gas utilization faces several limitations due to the existing large distances between the production fields and the consumption centers. Because of this problem, there is an increasing demand for new technologies which might supply a better, faster and more economical conversion of natural gas into liquid, facilitating transport providing an economic advantage.

At the present, methane conversion is carried out through the so called *Steam Reforming* process. In this process a mixture of carbon monoxide and hydrogen (CO and H₂) is obtained; this mixture is called synthesis gas or *syngas*. Raw materials for syngas formation are usually a carbon source (methane or coal in most cases) and water. The global reaction using methane as a carbon source is written as follows



Usually syngas has been used to supply the internal energy demand at energy recovery facilities located at production centers, or in the past syngas was obtained through the coal gasification process to be used for lighting.

After the pioneer work done by Franz Fischer and Hans Tropsch¹ in the 1920's, syngas has been used in the chemistry industry as a raw material during the aliphatic production. The utility of this process is primarily in its role of producing fluid hydrocarbons or hydrogen from a carbon source feedstock, such as coal, methane or solid carbon-containing wastes of various types. Non-oxidative pyrolysis of the carbon source material produces syngas which can be used directly as a fuel without being taken through Fischer-Tropsch transformations. If liquid petroleum-like fuel, lubricant, or wax is required, then the Fischer-Tropsch process can be applied. Finally, if the hydrogen production is to be maximized, the water gas shift reaction can be performed, generating only carbon dioxide and hydrogen and leaving no hydrocarbons in the product stream.

The main disadvantage during the Fischer-Tropsch process is the huge demand of energy that is required in order to keep the process running. Therefore, a more efficient way to achieve natural gas conversion is considered to be one of the most challenging technical topics in modern research.

The direct routes to convert natural gas into syngas would avoid the energy-intensive steam reforming process, but methane is a rather inert substance and apart from its reaction with oxygen, only exhibits a few reactions paths. Due to this challenge, studies on methane activation and further conversion continue to be an open field for research.

One of the direct routes is known as Catalytic Partial Oxidation which offers an alternative means for methane and other hydrocarbons conversion. This alternative method has been widely studied in the last years. Hickman and Schmidt [175, 183] reported syngas production from methane for this kind of reactor, where fuel conversion occurs at extremely short contact times (only a few milliseconds), this feature being one of its most attractive advantages.

Deutschman [28] discussed most of the main features of this process, which are atypical for conventional catalytic reactors. During the catalytic fuel conversion there are some characteristics that can be distinguished:

A highly reactive mixture flows for a few milliseconds through a catalytic monolith operated at temperature around 1200 K.

This reactor is characterized by strong interactions of mass and heat transport.

Chemical reactions can occur either in the homogeneous gas phase or on the surface.

The monolith used during the catalytic conversion is formed for a series of channels which are separated from each other by a thin wall coated with the catalytic material: Inside of each channel the reacting mixture flows and stable or intermediate species are adsorbed or desorbed at and from the catalytic surface. The chemical reactions can occur at the walls of the channels, and further reactions can also take place at the gas phase. Inside each channel different products are obtained, depending on the pressure, temperature and time that are given to the reactive mixture.

¹ Chem. Berg. 1923, 56, 2428

For a better understanding of such a complex process, it is necessary to have an adequate description of the fluid dynamics and the chemistry taking place in both phases, and the interaction between them.

With the development of high performance computers and progress in numerical techniques and algorithms *Computational Fluid Dynamics* (CFD), a research area which solves the mathematical models used to describe the fluid dynamics, chemical engineers have begun to learn more about the interactions between flows and chemistry. CFD has proved to be a potent tool for the analysis of very a complex fluid field; its possibilities cover a vast spectrum of applications including aerospace, energy production, and reactor design. CFD applied to the catalytic process helps us to understand and optimize the required conditions during the partial oxidation process.

In the case of chemistry, both phases are characterized by complex processes that proceed through a large number of elementary steps where the initial hydrocarbon reacts to yield a large number of intermediate species, which finally produce the desired products. A detailed kinetic mechanism should be able to describe these elementary steps in a wide range of operating conditions, accounting for the various molecular and radical species that participate in the reaction network.

The study of surface mechanisms is a new field under continuous development. Surface mechanisms have the particularity that each catalytic surface has its own characteristic reaction scheme and, in contrast to gas phase reactions, there are no unique reaction mechanisms which describe the fuel consumption for all the possible surfaces. This difficulty makes it necessary to include a particular mechanism for each fuel at each material, and special attention must be paid to applying only the kinetic mechanisms which have been obtained at the same conditions of the application of interest.

Most of the reliable gas-phase mechanisms that have been published until now, in particular for hydrocarbon oxidation reactions, are suitable for high temperature combustion only. Stoichiometric flames and low pressures are often characteristic for these high temperature combustion. These mechanisms have for instance been frequently used for the prediction of pollutant formation in combustion processes.

In addition to the known interest in total oxidation of methane and ethane, being principal constituents of natural gas, attention has also been focused on homogeneous partial-oxidation reactions to convert methane into higher valued materials, such as oxygenates (methanol and formaldehyde). Many studies have been devoted to their pyrolysis and partial-oxidation kinetics [6, 18, 28, 33-40]. A large number of experimental and numerical studies have also been conducted on ethane, propane and butane oxidation [52, 55-65].

One of the main characteristics during partial-oxidation methods is that they use fuel-rich mixtures to prevent combustion [178]. However, for very rich conditions, and in the medium temperature range of around 1000°C where partial oxidation occurs, further research is required to develop a more accurate kinetic scheme which considers total and partial-oxidation [69]. At these conditions the detailed reaction mechanisms should be at least as complex as those developed for fuel-rich flames considering that the partial-oxidation reactions pathways can be quite different from the ones during combustion and ignition. The major difference between propagation of low-temperature oxidation and the high-temperature process lies in the importance in the lower temperature regime of organic peroxy radicals, RO₂ [80, 81, 105].

The aim of this work is to extend the applicability of a previous developed mechanism for high temperature combustion [29] for a wider range of conditions by including characteristic steps for the intermediate and low temperature regime. The resultant mechanism is applied to describe experimental results at conditions similar to those that occur during partial oxidation. The mechanism extension was achieved by including reactions which describe the chemistry of total and partial oxidation of methane, ethane, propane, butane, lower alkenes, formation and consumption of their characteristic organic hydro-peroxide radicals and cyclical compounds. The mechanism has been tested for typical combustion conditions by comparing experimental data sets of ignition delay times in shock tubes and concentration profiles in jet-stirred reactors for partial oxidation.

A numerical investigation in two different reactor models (2D and 3D models) was carried out to achieve a better understanding of the interactions between mass and heat transport and homogeneous and heterogeneous chemical reactions in a catalytic gauze reactor during methane partial oxidation. The gas-phase mechanism was modeled using the developed mechanism, and for the surface a previously developed mechanism [25] was adapted. Both mechanisms were coupled with the surrounding flow field.

1.1 Structure of the Thesis

The first three chapters of this thesis describe basic concepts used in combustion:

Chapter 1 includes an overview of combustion phenomena, the ignition process is described, and details about some experimental techniques for its study are presented.

In Chapter 2 the governing equations for modeling reactive flows are presented: The fluid is treated as a continuum and the most accurate description of the flow field of multi-component mixtures is given by the transient three-dimensional Navier-Stokes equations coupled with the species-governing equations.

In Chapter 3 the development of the chemical kinetic mechanism is presented: The mechanism was extended using a set of automatically generated reactions in the C_3 and C_4 sub-mechanisms. The mechanism then was completed including additional reactions which take into account formation or consumption for specified species during experimental conditions. Most of the kinetic data for the newly added reactions were obtained from the National Institute of Standards and Technology (NIST) data base.

In the second part (Chapters 4-6), the evaluation of the mechanism is carried out by comparing experimental data sets of ignition delay times in shock tubes for each alkane inside the C_4 subsystem (Chapter 4). Simulation of the delay times was performed for stoichiometric and rich mixture conditions; an additional evaluation was performed for methane mixtures (hydrogen, ethane and propane were added).

Chapter 6 includes the simulation of the oxidation and partial oxidation for a methane blend, propane and butane at rich conditions and ethene at low temperature in jet-stirred reactors. The experiments were carried out at temperatures close to 1050 K for methane, propane and butane. In the ethene case the experimental conditions were close to 718 K, where a cyclical compound was the main product observed.

Chapter 7 presents the results of the investigation of catalytic partial oxidation of methane to synthesis gas on platinum using a 3D approach. Each chapter includes an introduction into these topics including previous work and at the end a discussion of the results obtained.

Chapter 2

OXIDATION OF HYDROCARBONS

2.1 Oxidation of Hydrocarbons

The chemical reaction of a hydrocarbon with air or oxygen in the gas-phase shows dependence on the external conditions applied which conditioned the response of the mixture. The way in which the chemical reaction proceeds and its dependence on the temperature and pressure are represented in the so-called explosion diagram. Figure 2.1 shows a typical explosion diagram for a hydrocarbon.

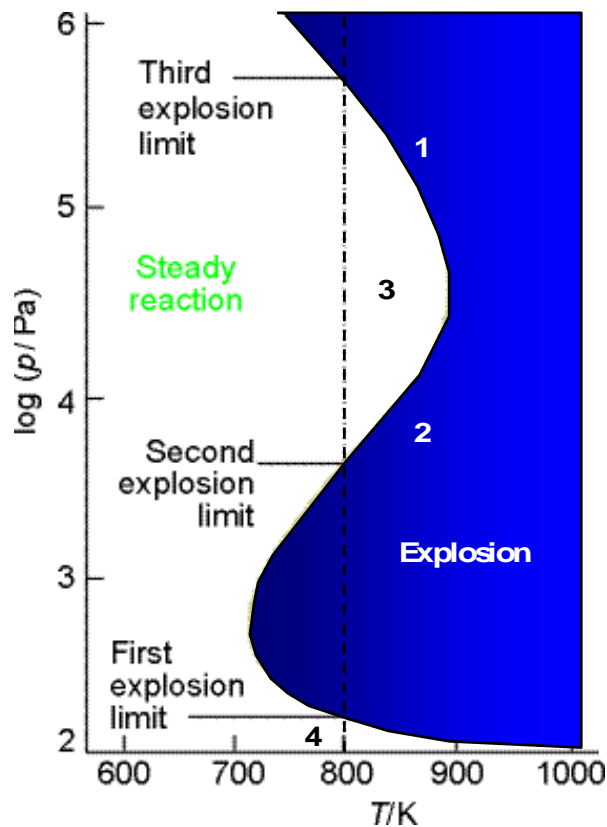


Figure 2.1: Schematic explosion diagram for hydrocarbons: The blue zone at the right represents the different conditions (of temperature and pressure) where the mixture can explode

Depending on the intended purpose, temperature and pressure at which the reaction takes place vary during the hydrocarbon oxidation: For practical applications which seek to convert the chemical energy into mechanical work, like in the case of internal combustion engines, turbojets or turbines used in power plants, the range of pressure and temperature are located near to the points 1 and 2 shown in Figure 2.1. When a transformation of the fuel into potentially more useful chemicals like O-heterocycles, alcohols, ketones and others is the objective, then operating conditions close to the points 3 and 4 are applied.

In the explosion diagram there are two main regions: The area to the left represents the non-explosive reaction region, while the area to the right (in shadow) is the explosive region.

At very low pressures the system is outside the explosion region, and the mixture reacts slowly. The reaction rate is very low, and only a very small fraction of the fuel is consumed.

Increasing the pressure (along a vertical line in the illustration) takes the system through the first explosion limit. The reaction rate is higher and the mixture then explodes.

The reaction is slow when the pressure is above the second explosion limit. The concentration of molecules in the gas is then so high that the radicals produced for the branching reactions combine in the body of the gas. Recombination reactions are facilitated by three-body collisions because a third body (M) removes the excess energy. At low pressures three-particle collisions are unimportant, and recombination is much slower. At higher pressures, where three-particle collisions are important, the explosive propagation of the chain by the radicals is partially quenched, because the branching steps are diverted into simple propagation steps.

After further increases in the pressure, at temperatures between 500 K and 800 K and before the third explosion limit the so-called *cold flame region* appears. Some of the characteristics in this region are: Light blue flames, smooth changes in the reactant concentration, formation of oxygenate species (alcohol, aldehyde, ketone, peroxide and heterocyclic), and a small formation of final combustion products: Carbon dioxide and water.

Explosion is reached when temperature and pressure are over the *explosion limit* in the diagram. Explosion is preceded by an induction phase where the reaction is slow, which ends with a steep (exponential) increase in the reaction rate. During the induction time (ignition delay), highly reactive radicals are formed through branching reactions. The radicals formed react with the fuel quickly, completing its consumption.

2.2 Ignition Process

Ignition processes are usually very complex and involve many intricate physical and chemical steps. Ignition is inherently transient, usually triggered by some transient heating processes. In order to predict or interpret certain ignition phenomena, detailed chemical kinetics must be known; however, the measurement of species concentration in a short time interval is very difficult. As a result, the kinetic mechanism is unknown in most cases. These mechanisms usually significantly vary with ambient conditions and external stimuli like turbulence, time, temperature and pressure. In general there are many parameters which affect the ignition: Mixture composition, pressure, pressurization rate, duration of the heating, velocity of the convective stream, turbulence, thermal and transport properties and catalyst inhibitors are the most common.

Some criterions should be satisfied in order to reach ignition: The temperature must be high enough to allow significant chemical reactions, the time must be long enough to allow the heat input to be absorbed by the reactants so that the thermo-chemical process can occur, and there must be sufficient turbulence to allow a higher mixing between the fuel and the oxidizer.

Besides the ignition process induced by external devices, like sparks, flames or others, there is a process called spontaneous ignition (also known as auto-ignition, self-ignition, or homogeneous ignition) which occurs with no other source than the hot vessel walls. Spalding [1] defined ignition as follows: "When a reactive mixture is formed, raised to a definite temperature and pressure, and then left alone, it may burst into flame after certain time". At the onset of spontaneous ignition, there is usually a rise in temperature, emission of visible radiation, and rapid chemical reaction.

There are different types of ignition devices in research and industrial applications. These include: Spark plugs, hot wires, constant volume bombs, continuous flow test apparatus and shock tubes. Ideal ignition experiments should be independent of the test configuration and free of surface effects. In addition, mixing of the fuel and the oxidizer should be nearly instantaneous; otherwise the effects of mixing must be determined. Shock tube devices and continuous-flow devices have been used extensively due to their ability to fulfill most of the requirements for ignition studies and because of their direct application to practical problems like those posed by gas turbine or ramjet processes.

2.3 Continuous Flow Devices

In a continuous flow device, fuel is injected into a flowing air stream at high temperature, and the combustible mixture ignites at some distance downstream of the fuel injection point, depending on the velocity of the flow. The procedure to acquire the ignition-delay data consists of first establishing the prescribed temperature, pressure, composition and flow rate for the reactant's mixture. Then the inlet air or fuel (if necessary) temperature is gradually increased until auto-ignition occurs within or at the exit of the duct. The occurrence of auto-ignition is determined by observing a visible flame and a rapid increase in temperature at the flame front location. Ignition delay times are calculated from the known length of the test duct, defined as the distance between the injector and the flame location, and the mean free stream flow velocity. Continuous flow devices are widely used. However, due to the fact that they use electrical air heating, they are limited to temperatures up to 1000 K, which is below the range of interest for many combustion problems.

2.4 Shock Tubes

A shock tube is used in ignition studies to produce a high temperature gas under closely controlled test conditions. A limitation of this technique is that the test is of short duration (< 1 ms). A shock tube is a tube of cylindrical or rectangular cross section in which a transverse diaphragm separates two compartments of gas initially at rest. One of the compartments is a high pressure and is considered the driver section of the tube. The other compartment is a low pressure and is considered the driven section; this part forms the ignitable mixture of interest. The diaphragm is burst by either mechanically piercing or by exceeding its structural strength through over-pressurization of the driver section. This action sends a strong shock wave into the low-pressure section increasing the static pressure and temperature of the mix-

ture. The front face or leading edge of this gas flow acts as the head of a 'piston' of gas which drives a pressure pulse ahead of it which rapidly develops into a shock wave. The shock wave is reflected at the end boundary wall of the tube resulting in an additional increase in temperature and pressure (Figure 2.2).

Both the incident and the reflected waves can be used to create test conditions suitable for auto-ignition studies. The reflected wave stagnates the gas and, by reinforcement of the shock strength, produces higher temperature conditions than incident waves. Reflected waves can produce temperatures in the range of 1500 K - 2500 K.

The ignition delay time is defined as the time between shock heating of the gas mixture and the onset of the rapid reaction phase. The properties of the gas mixture prior to ignition are calculated from the ideal shock equations, assuming no chemical reaction occurs ahead of the shock wave and the gases behave ideally with established equilibrium of internal modes. The onset of the rapid reaction phase is detected by one or more of the following types of measurements: Pressure change, piezoelectric types transducers, rate of chemi-ionization probes and by emission from electronically excited species (OH, CH, C₂) or vibrationally excited species (CO, CO₂, H₂O, C_x) or absorption by species (OH, CH₃) by means of a photomultiplier instrumentation.

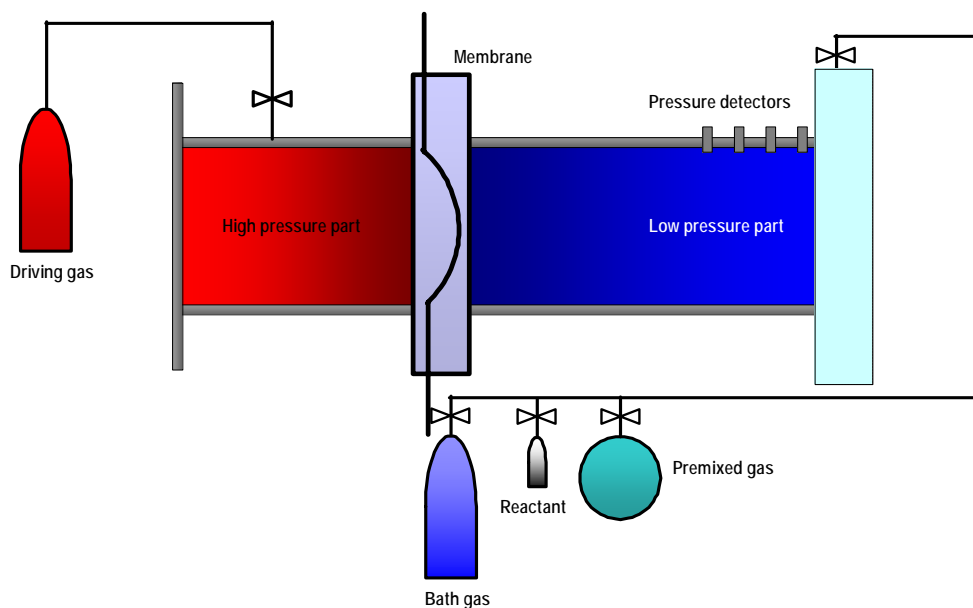


Figure 2.2: Shock tube diagram: In the shock tube, reactions are initiated by a temperature jump behind a shock wave. The shock wave is generated by the pressure jump after a foil which separates the high and the low pressure section is bursting or collapses due to the high pressure induced

2.5 Rapid Compression Machine

A compression machine is suitable for the study of short ignition delays under adiabatic compression. The device should guarantee the compression occurs as quickly as possible, and there must be some means to record the gas pressure and temperature. Species concentrations can also be recorded as function of the time and the piston position.

A rapid compression engine is necessary to reduce heat losses which allow the experimental conditions to closely approximate adiabatic ones. Another attribute of rapid compression engines is that they allow investigation of ignition times for fuels having short delay times.

Piston rebound at the end of the compression must be avoided in order to prevent the attendant adiabatic cooling of the cylinder contents. Cooling of the mixture causes errors in the measurements of the delay periods and of the ignition temperatures. The contamination of the explosive sample by lubricant vapors should also be avoided, because this is another source of inaccuracy.

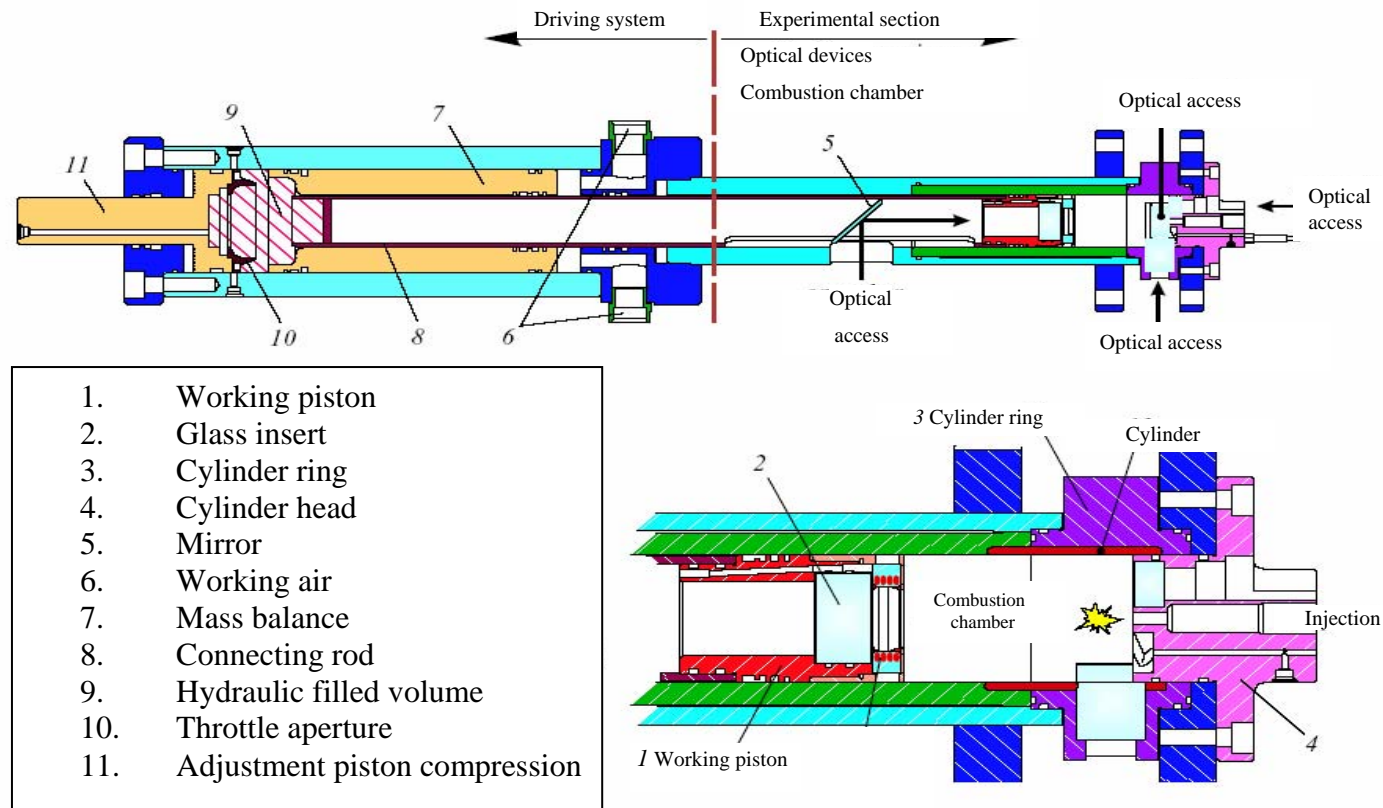


Figure 2.3 Rapid compression machine [2, 3]: A rapid compression machine is designed to simulate a single engine cycle of an internal combustion engine. The conditions inside the combustion chamber are easily controlled and cleaner than in the traditional internal combustion engines. Above: Rapid compression machine. Down: Details of the combustion chamber

In a rapid compression machine the piston adiabatically compresses the testing gas. This compression can be driven pneumatically, hydraulically or by other means. The piston compresses the mixture which is located at the end of the compression camera. Some optical, electrical or other devices are used to investigate the species concentration and ignition times for the test gas. A typical rapid compression machine is shown in Figure 2.3.

2.6 Stirred Reactors

This kind of reactor consists of a closed tank where temperature, pressure and species concentration are given and where the reactions can take place. The main aim is to guarantee homogenous conditions during the operation, reducing the temperature and species concentration gradients along the recipient. During the operation at low temperature there is the possibility that not only homogeneous reactions occur and instead some reactions could take place at the walls of the reactor, although at high temperature this contribution can be neglected in most of the cases. In combustion studies, reactors can be used for the study of non-stationary processes like explosion limits in fuel/oxygen mixtures, cool flame phenomena and others. Some examples of stirred reactors are presented in Figure 2.4.

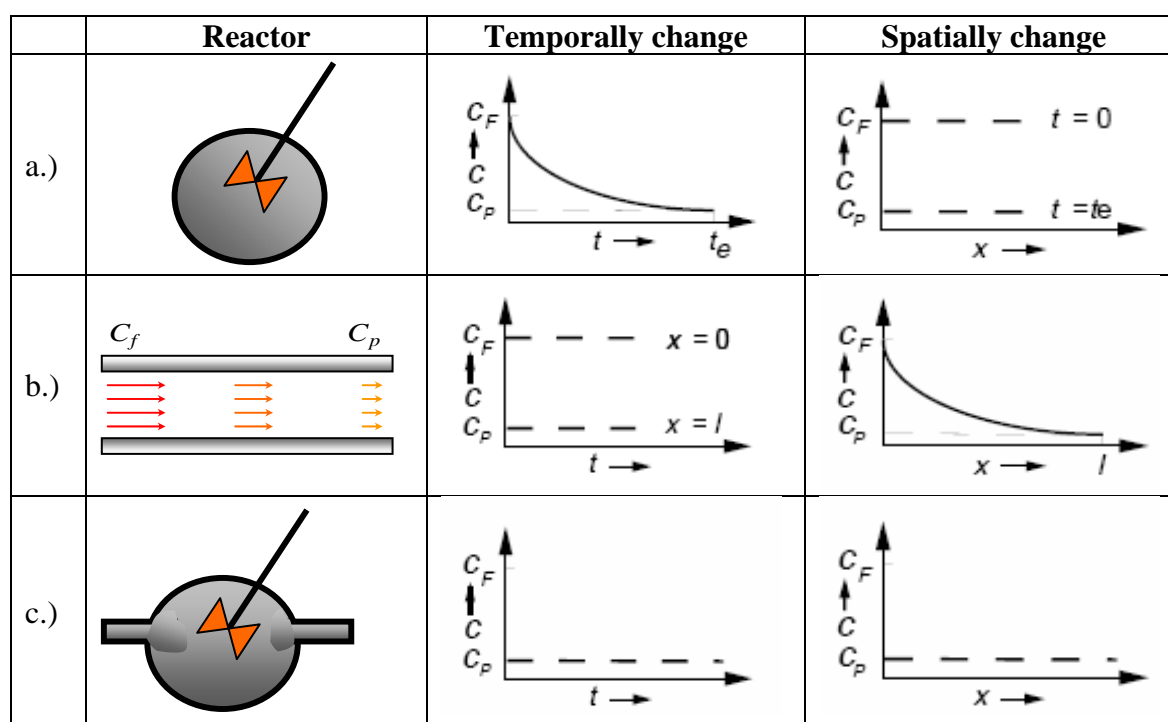


Figure 2.4: Stirred reactors and concentration changes with the time and space: a) Batch reactor; b) Plug-flow tubular reactor (PFTR); c) Continuously stirring tank reactor (CSTR)

While reaction is carried out in the *Batch Reactor* (Figure 2.4a), no reactants or products are added or removed until the reaction is completed. The physical variables such as temperature and pressure are easily controlled by external media. The mixing conditions inside the reactor are guaranteed by mechanical or pneumatic devices, which make sure that a uniform concentration of species is reached inside the vessel. An ideal batch reactor should satisfy with the conditions

$$\frac{\partial c_i}{\partial \bar{r}} = 0; \quad \frac{\partial T}{\partial \bar{r}} = 0 \quad (2-1)$$

with c_i being the concentration ($c_i = n_i/V$) of the species i and n_i = mole number.

For continuous operation, the so called *Continuously Stirred Reactors* are used. Their main advantage is that they can be operating at steady-state conditions with a continuous flow of reactants and products. Figure 2.4 presents two configurations for continuous reactors: The first one is the so called *Plug-Flow Tubular Reactor* (PFTR Figure 2.4b), also known as the *Ideal Flow Reactor*, which is arranged as one long reactor or many short reactors in a tube bank without radial variation in reaction rate (concentration), and with the concentration varying with length along the reactor.

This model is a rough simplification of the real behavior of the flow inside the tube. In the model, no parabolic profile for the flow is considered inside the channel, and there are no turbulence effects being considered. In spite of these simplifications, the PFTR model is widely used.

The thermal condition imposed during the reactor operation establishes that there can be a heat flow to or from the reactor in order to keep a constant temperature. In this case an *isothermal* condition is defined for the boundaries, or the heat flow is restrained inside the reactor and for this case an *adiabatic* condition is defined.

Beside the thermal constrictions, other important variables required to describe the PFTR function are the species concentration $c_i(z)$, the flow velocity $u(z)$, and the temperature $T(z)$.

The PSTR is symmetrical when a cylindrical coordinate system is chosen. Considering r as the radial direction and z as the axial direction, the flow should satisfy the following conditions

$$\frac{\partial c_i}{\partial \bar{r}} = 0; \quad \frac{\partial u}{\partial \bar{r}} = 0; \quad \frac{\partial T}{\partial \bar{r}} = 0 . \quad (2-2)$$

The latter expression means that no variations of the flow properties are considered in the radial direction.

The second kind of continuous reactor is the so called *Continuously Stirred Tank Reactor* (CSTR Figure 2.4c). It is operated at steady-state conditions with a continuous input of reactants and output of products. The feed assumes a uniform composition throughout the reactor, and the exit stream has the same composition as in the tank. The main advantages of these reactors are that they allow a continuous operation (which is required in industrial applications): They easily adapt to two-phase runs and are simple in construction.

There are two main conditions for the model of the reactor: There is an input flow of species, whose composition and temperature are known at each time t (c_i^{in} and T_i^{in}), and the properties of the mixture are uniform, and an ideal mixing is assumed

$$\frac{\partial c_i}{\partial \bar{r}} = 0; \quad \frac{\partial T}{\partial \bar{r}} = 0 . \quad (2-3)$$

Chapter 3

REACTIVE FLOWS

In this section, the governing equations for modeling reactive flows and heterogeneous reactions are summarized. More detailed treatments can be found in a number of textbooks on fluid mechanics, heterogeneous catalysis, and associated phenomena [4, 5, 6, 7]. This chapter is focused on fluid flow, while the chemical processes appear only in simple terms in the equations. Finally, a discussion of modeling chemical reactions will be given.

3.1 Mathematical and Numerical Model

Governing equations can be derived by considering either a given quantity of matter or *control mass* and its extensive properties, such as mass, momentum, and energy or the flow within a certain spatial region called the *control volume*. The *control volume approach* will be applied here. The governing equations are based on conservation principles for an extensive property. By transformation of these laws into a control-volume form, the fundamental variables will be intensive properties, which are independent of the amount of matter considered; examples are density ρ (mass per unit volume) and velocity \vec{v} (momentum per unit mass).

3.1.1 Governing Equations for Mass, Momentum and Species

The principle of *mass conservation* leads to the *mass continuity equation* that is in its differential form

$$\frac{\partial \rho}{\partial t} + \frac{\partial(\rho v_j)}{\partial x_j} = S_m \quad (3-1)$$

Here t is the time, x_j ($j=1, 2, 3$) are the Cartesian coordinates, and v_j denote the Cartesian components of the velocity vector \vec{v} . Even though mass conservation says that mass can be neither created nor destroyed, a source term S_m is introduced on the right-hand side of (3-1). If the continuity equation is applied for modeling the continuous fluid phase of a reactor, mass can be added to that phase for instance due to vaporization of liquid droplets or ablation of solid surfaces. Mass of the fluid can also vanish if, for instance, mass is deposited on a surface

such as in chemical vapor deposition. In (3-1) and throughout this work, the Einstein convention is frequently used, i.e., whenever the same index appears twice in any term, summation over that index is implied, except if the index refers to a chemical species. The principle of *momentum conservation* for Newtonian fluids leads to three scalar equations for the momentum components ρv_i

$$\frac{\partial(\rho v_i)}{\partial t} + \frac{\partial}{\partial x_j}(\rho v_j v_i) = -\frac{\partial p}{\partial x_j} + \frac{\partial \tau_{ij}}{\partial x_j} + \rho g_i \quad (3-2)$$

where p is the static pressure, $\tau_{i,j}$ is the stress tensor, and ρg_i denotes the components of the gravitational acceleration \vec{g} in the direction of the Cartesian coordinates x_j . Gravity, the only body force taken into account in (3-2), can often be neglected when modeling chemical reactors.

The stress tensor is given as

$$\tau_{ij} = \mu \left(\frac{\partial v_i}{\partial x_j} + \frac{\partial v_j}{\partial x_i} \right) - \frac{2}{3} \mu \frac{v_k}{x_k} \delta_{ij}. \quad (3-3)$$

Here, μ is the mixture viscosity and $\delta_{i,j}$ is the *Kronecker* symbol, which is zero for $i \neq j$ and unity for $i = j$. The coupled mass continuity and momentum governing equations have to be solved for the description of the flow field. In multi-component mixtures, not only the flow field is of interest, but also the mixing of chemical species and reactions, which can be described by an additional set of partial differential equations. Here, the mass m_i of each species i in the reactor obeys a conservation law that leads to the following set of governing equations

$$\frac{\partial(\rho Y_i)}{\partial t} + \frac{\partial(\rho v_j Y_i)}{\partial x_j} = -\frac{\partial(j_{i,j})}{\partial x_j} + R_i^{\text{hom}} \quad (i=1, \dots, N_g). \quad (3-4)$$

Here, Y_i is the mass fraction of species i in the mixture ($Y_i = m_i/m$) with m the total mass of the fluid, N_g is the number of gas-phase species, $j_{i,j}$ is the component j of the diffusion mass flux of species i and R_i^{hom} is the net rate of production of species i due to homogeneous chemical reactions. These additional N_g equations are coupled with (3-1) and (3-2). The diffusion of mass is based on gradients of physical properties such as concentration, temperature, pressure, and electromagnetic fields. Only gradients in concentration (*Fick's law*) and in temperature (*thermal diffusion*) are relevant for the problems considered in this work. They are modeled by

$$j_{i,j} = -\rho \frac{Y_i}{X_i} D_i^{\text{M}} \frac{\partial X_i}{\partial x_j} - \frac{D_i^{\text{T}}}{T} \frac{\partial T}{\partial x_j}. \quad (3-5)$$

D_i^{M} in the first term, representing Fick's law, is the effective diffusion coefficient of species i into the mixture. D_i^{T} in the second term is the thermal diffusion coefficient of species i . X_i are mole fractions defined by $X_i = c_i/c$ with c_i and c as concentration of species i and total concentration of the mixture, respectively. The mole fractions can be derived from the mass fractions Y_i using the species molar masses M_j by

$$X_i = \frac{1}{\sum_j^{N_g} \frac{Y_j}{M_j}} \frac{Y_i}{M_i}. \quad (3-6)$$

If the mole fractions are known, the mass fractions can be derived by

$$Y_i = \frac{M_i}{\bar{M}} X_i = \frac{M_i}{\sum_j^{N_g} X_j M_j} X_i \quad (3-7)$$

where \bar{M} is the mean molar mass of the mixture.

3.1.2 Heat Transfer

Heat transport and heat release due to chemical reactions lead to spatial and temporal temperature distributions in chemical reactors. Their prediction is based on the first law of thermodynamics, which says that the total energy of a given system obeys a conservation law. It is generally more convenient to express the corresponding governing equation in terms of the specific enthalpy h by using the thermodynamic expression $\rho h = \rho u + p$, where u is the specific internal energy. For a multi-component fluid flow, this governing equation is stated as

$$\frac{\partial(\rho h)}{\partial t} + \frac{\partial(\rho v_j h)}{\partial x_j} + \frac{\partial j_{q,j}}{\partial x_j} = \frac{\partial p}{\partial t} + v_j \frac{\partial p}{\partial x_j} + \tau_{jk} \frac{\partial v_j}{\partial x_k} + S_h \quad (3-8)$$

with S_h being a heat source, e.g., due to thermal radiation. In multi-component mixtures, the diffusive heat transport \vec{j}_q occurs due to heat conduction (Fourier law) \vec{j}_q^c , mass diffusion \vec{j}_q^d , and concentration gradients (Dufour effect). The Dufour effect is the reverse process to thermal diffusion and it is usually very small and therefore neglected, hence

$$j_{q,j} = j_{q,j}^c + j_{q,j}^d = -\lambda \frac{\partial T}{\partial x_j} + \sum_i^{N_g} h_i j_{i,j} \quad (3-9)$$

where λ is the thermal conductivity of the mixture. The temperature is related to the enthalpy by the definition of the mixture specific enthalpy

$$h = \sum_i^{N_g} Y_i h_i(T). \quad (3-10)$$

The specific enthalpy h_i of species i is a monotonic increasing function of temperature. Therefore, the temperature can also be calculated using 2.10, if the total enthalpy h and the mass fractions Y_i are known [6].

Heat transport in solids such as reactor walls and catalyst materials can also be modeled by an enthalpy equation

$$\frac{\partial(\rho h)}{\partial t} + \frac{\partial(\rho v_j h)}{\partial x_j} = \frac{\partial}{\partial x_j} \left(\lambda \frac{\partial T}{\partial x_j} \right) + S_h \quad (3-11)$$

where h is the specific enthalpy and λ is the thermal conductivity of the solid material. S_h accounts for heat sources, for instance due to electric or radiative heating of the solid and due to heat release by chemical reactions on the solid surface or inside the solid bulk.

3.1.3 Equation of State

The governing equation system discussed above has to be closed by an equation that describes the relation between the thermodynamic variables density ρ , pressure p , and temperature T , which is called the equation of state. For gaseous flows this relation can often be modeled by the *ideal gas equation*

$$p = \rho \frac{R}{M} T \quad (3-12)$$

with R as universal gas constant, $R = 8.314 \text{ J}/(\text{mol}\cdot\text{K})$. In the systems discussed in this work the ideal gas equation is always applied.

3.1.4 Transport Properties

The transport coefficients μ , D_i^M , D_i^T and λ occurring in the governing equations (3-3), (3-5), (3-9) depend on temperature and mixture composition. For multi-component mixtures, they are usually derived from the transport coefficients of the individual species and the mixture composition applying empirical approximations [4, 5, 6] such as

$$\mu = \frac{1}{2} \left[\sum_i^{N_g} X_i \mu_i + \left(\sum_i^{N_g} \frac{X_i}{\mu_i} \right)^{-1} \right]. \quad (3-13)$$

For the mixture viscosity (μ), with μ_i as viscosity of species i , and

$$\lambda = \frac{1}{2} \left[\sum_i^{N_g} X_i \lambda_i + \left(\sum_i^{N_g} \frac{X_i}{\lambda_i} \right)^{-1} \right] \quad (3-14)$$

for the mixture thermal conductivity λ , with λ_i as thermal conductivity of species i . The effective mass diffusion coefficients D_i^M are estimated through [8]

$$D_i^M = \frac{1 - Y_i}{\sum_{j \neq i}^{N_g} \frac{X_j}{D_{i,j}}} \quad (3-15)$$

with $D_{i,j}$ as binary diffusion coefficients. The approximation 3.15 violates mass conservation, therefore the diffusion fluxes have to be corrected by

$$\vec{j}_{\text{corr}} = -\sum_i^{N_g} \vec{j}_i . \quad (3-16)$$

The term \vec{j}_{corr} is either added to the equation of the species that occurs in large excess, or the mass/mole weighted fraction of \vec{j}_{corr} is considered in each species equation. The alternate, multi-component formulation of the transport properties [9, 10] is more accurate than the mixture-averaged form discussed above. This multi-component formulation also guarantees overall mass conservation. The deficiency of this formulation, however, is its computational complexity. Evaluating the ordinary multi-component diffusion coefficients involves inverting an $N_g \times N_g$ matrix, and evaluating the thermal conductivity and thermal diffusion coefficients requires solving a $3N_g \times 3N_g$ system of algebraic equations [10]. Therefore, the mixture-averaged approach is used in this work.

The species transport coefficients need to be modeled considering their temperature-dependence. Experimentally determined data are either given, usually as temperature polynomials, or derived from the *Chapman-Enskog theory* [4,11] of rarefied gases. In the later case the transport coefficients depend on their intermolecular potential, for instance, a *Lennard-Jones (6-12) potential*, which requires the specification of two physical parameters for each species: a characteristic diameter (or *collision diameter*) σ and a characteristic energy of interaction between the molecules ε , that is the maximum energy of attraction between a pair of molecules. In the systems discussed in the present work, the species viscosities, thermal conductivities, and binary diffusion coefficients are derived from this theory. The species parameter σ and ε are taken from data bases developed at the SANDIA National Laboratories [10] and by Warnatz and co-workers at Heidelberg University [6, 8].

3.1.5 Thermodynamic Properties

The specific enthalpy h_i of species i is a function of temperature. According to the first law of thermodynamics, the enthalpy can be expressed in terms of the heat capacity leading to the following expression for the specific species enthalpy

$$h_i(T) = h_i(T_{\text{ref}}) + \int_{T_{\text{ref}}}^T c_{p,i}(T') dT' \quad (3-17)$$

with $c_{p,i}$ the specific heat capacity of species i at constant pressure. The specific standard enthalpy of formation $\Delta h_{f,298,i}^\circ$ can be used as an integration constant $h_i(T_{\text{ref}}=298.15 \text{ K}, p_0=1 \text{ bar})$. The temperature dependence of the specific entropy s_i of species i can analogously be expressed in terms of the species heat capacity using the standard entropy $s_i^\circ(T_{\text{ref}}=298.15 \text{ K}, p_0=1 \text{ bar})$ as an integration constant $s_i(T_{\text{ref}}=298.15 \text{ K}, p_0=1 \text{ bar})$

$$s_i(T) = s_i(T_{\text{ref}}) + \int_{T_{\text{ref}}}^T \frac{c_{p,i}(T')}{T'} dT' . \quad (3-18)$$

The entropies are not directly used in the governing equations, but they are needed for the calculation of the equilibrium constants. Experimentally determined and estimated standard enthalpies of formation, standard entropies, and temperature dependent heat capacities can be looked up in data bases such as the JANAF Table [12] and others [13, 14]. They may also be estimated applying Benson's additivity rules [15].

The temperature dependence of the species heat capacities is often described by polynomials when used in computations [13, 14], e.g., by a polynomial of fourth order according to NASA computer programs [16]. Among others, the CHEMKIN software package developed by Kee and co-workers [13] applies two different polynomials for a low and high temperature interval in order to improve accuracy. For each species i and temperature interval, seven coefficients $a_{i,n}$ are tabulated. The first five are used for the calculation of the temperature dependence of the heat capacity of species i according to

$$c_{p,i}(T) = \frac{R}{M_i} (a_{i,1} + a_{i,2}T + a_{i,3}T^2 + a_{i,4}T^3 + a_{i,5}T^4). \quad (3-19)$$

The other two coefficients are used to define the standard enthalpy of formation and standard entropy of species i : $\Delta h_{f,298,i}^\circ$ and $s_{298,i}^\circ$. Thus, the specific enthalpy and entropy of species i are expressed by

$$h_i(T) = \frac{R}{M_i} \left(a_{i,1}T + \frac{a_{i,2}}{2}T^2 + \frac{a_{i,3}}{3}T^3 + \frac{a_{i,4}}{4}T^4 + \frac{a_{i,5}}{5}T^5 + a_{i,6} \right) \quad (3-20)$$

$$s_i(T) = \frac{R}{M_i} \left(a_{i,1} \ln T + a_{i,2}T + \frac{a_{i,3}}{2}T^2 + \frac{a_{i,4}}{3}T^3 + \frac{a_{i,5}}{4}T^4 + a_{i,7} \right). \quad (3-21)$$

The specific heat capacity of the mixture c_p at constant pressure is calculated by

$$c_p = \sum_i^{N_g} Y_i c_{p,i}. \quad (3-22)$$

3.2 Modeling Chemical Reactions

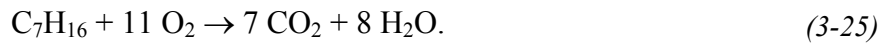
In the equation set for the description of gaseous flow fields in chemical reactors, the source term (R_i^{hom}) appeared, which accounts for the variations of variables due to chemical reactions. Chemical reactions occur either homogeneously in the gas phase or heterogeneously on solid surfaces. While the application of elementary reaction mechanisms has found broad acceptance for homogeneous gas-phase reactions, the extension of this approach to heterogeneous catalytic gas-phase reactions is relatively new and still attracts many discussions about its potential and benefits. In this chapter, models will be discussed for the calculation of R_i^{hom} and R_i^{het} , which are based on the molecular steps.

3.2.1 Rates of Reaction

A one-step chemical reaction can be represented by the following equation



where ν_i' and ν_i'' are the stoichiometric coefficients of the chemical species i , and A_i represents all chemical species. The stoichiometric coefficients have the property that the chemical reaction can be interpreted as a special kind of algebraic equation, in which the sum of the number of atoms must be the same on each side. Examples of chemical reactions are



In nature, the collision of an oxygen molecule and a hydrogen atom can actually lead to the formation of an oxygen atom and a hydroxyl radical as described by Reaction 2.24. In contrast to that, the formation of seven carbon dioxide molecules and eight water molecules by a collision of a heptane molecule with eleven oxygen molecules (3-25) never occurs so directly. A reaction which occurs on a molecular level exactly in the way which is described by the reaction equation is called an *elementary reaction* [17]. Otherwise the reaction is called *global reaction*, *overall reaction*, *complex reaction*, or *net reaction*.

The rate of formation or consumption of a species in a chemical reaction is called *reaction rate* and is described by the rate law. Looking at the reaction rate of species i , the reaction rate is usually expressed according to

$$\frac{dc_i}{dt} = \nu_i k_f \prod_{i=1}^{N_g} c_i^{a_i'} \quad (3-26)$$

with

$$\nu_i = \nu_i'' - \nu_i'.$$

Here, c_i denotes the concentration of species i , k_f is the rate coefficient, and a_i' is the reaction order with respect to species i . Global reactions have complex rate laws where the reaction orders in general are not integers and depend on time and reaction conditions. On the contrary, the reaction orders of elementary reactions always are integers and valid for all experimental conditions. Those reaction orders can easily be derived because they equal the molecularity of the elementary reaction, i.e.,

$$\frac{dc_i}{dt} = \nu_i k_f \prod_{i=1}^{N_g} c_i^{\nu_i'}, \quad (3-27)$$

and for the reverse reactions of 3.23



The rate law analogous to 3.27

$$\frac{dc_i}{dt} = -\nu_i k_r \prod_{i=1}^{N_g} c_i^{a_i''} \quad (3-29)$$

Hence, in the case of an elementary reactions, it is $a_i'' = \nu_i''$.

At chemical equilibrium, forward and backward reactions have the same rate on a microscopic level

$$\nu_i k_f \prod_{i=1}^{N_g} c_i^{a_i'} = \nu_i k_r \prod_{i=1}^{N_g} c_i^{a_i''} \quad (3-30)$$

which means, no net reaction rate can be observed on a macroscopic level. The ratio

$$\frac{k_f}{k_r} = \prod_{i=1}^{N_g} c_i^{\nu_i} \quad (3-31)$$

is called the equilibrium constant K_c of the reaction. For an ideal gas, K_c can be calculated from thermodynamic data according to

$$K_c = \frac{k_f}{k_r} = \left(\frac{p^0}{RT} \right)^{\sum_{i=1}^{N_g} \nu_i} \exp \left[\frac{\Delta_R \bar{S}^0}{R} - \frac{\Delta_R \bar{H}^0}{RT} \right] \quad (3-32)$$

with the molar entropy of reaction

$$\Delta_R \bar{S}^0 = \sum_{i=1}^{N_g} \nu_i \bar{S}_i^0 \quad (3-33)$$

and the molar enthalpy of reaction

$$\Delta_R \bar{H}^0 = \sum_{i=1}^{N_g} \nu_i \bar{H}_i^0 \quad (3-34)$$

Here, $p^0 = 1$ bar is the standard pressure; \bar{S}_i^0 and \bar{H}_i^0 are the standard molar entropies and standard molar enthalpies, respectively, of the species involved in the reaction. For a system of K_g (irreversible) elementary reactions among N_g chemical species, where both forward and reverse reactions are considered individual elementary reactions, the molar reaction rate of species i , denoted by $\dot{\omega}_i$, is given by summation over the rate equations of all elementary reactions

$$\frac{dc_i}{dt} = \dot{\omega}_i = \sum_{k=1}^{K_g} \nu_{ik} k_{fk} \prod_{i=1}^{N_g} c_i^{\nu_{i,k}} \quad (3-35)$$

If a set of elementary reactions (*reaction mechanism*) consists of all reactions occurring among the N_g species in nature, and if all rate coefficients are accurately known, then this mechanism is valid for all external conditions. Hence, elementary reaction mechanisms can be applied for reactor optimization. Furthermore, the reactor behavior can be explored at conditions which are difficult to investigate experimentally. The problem with elementary reactions, however, consists in the completeness of the mechanisms and the accurate

determination of all rate coefficients. Therefore, global reaction rates are still applied in most cases of reactor modeling.

For global reactions, however, the rate law is only valid at conditions which were included in the derivation of the form of the rate law. The determination of the rate law is based on a fitting process using experimentally measured reaction rates as function of temperature, species concentrations, pressure, and other external conditions. An extrapolation to conditions for which no experiments exist or which were not considered in the fitting process is risky and can lead to incorrect conclusions. The use of global reactions for modeling chemically reacting flows can only describe experiments which were already performed. The behavior of the chemical reactor beyond these conditions can therefore not be estimated accurately; hence, reactor optimization and design are limited.

3.2.2 Temperature and Pressure Dependence of Rate Coefficients

In general, the rate coefficients of chemical reactions depend strongly on temperature. According to Arrhenius [18], the nonlinear character of the temperature can be described by an exponential function (*Arrhenius law*). Based on more accurate measurements, an additional small temperature dependence is introduced into the model which leads to the following modified Arrhenius expression for the forward rate coefficient of reaction k

$$k_{fk} = A_k T^{\beta_k} \exp\left[-\frac{E_{ak}}{RT}\right] \quad (3-36)$$

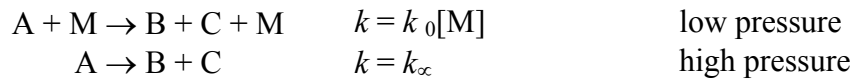
with A_k as pre-exponential factor, β_k as temperature coefficient, E_{ak} as the activation energy and R the gas constant. While these parameters, which are called *rate coefficients*, are fitting parameters when the concept of global reactions is used, they have physical meanings when the concept of elementary reactions is applied. In the case of elementary reactions, the activation energy corresponds to an energy barrier which has to be overcome during the reaction. The pre-exponential A_k or $A_k T^{\beta_k}$ can be connected to a mean lifetime ($1/A_k$) of an activated molecule and a collision rate, for unimolecular and bimolecular reactions, respectively.

The rate coefficients of dissociation (unimolecular) and recombination (trimolecular) reactions have additional pressure dependence. This fact indicates that these reactions are rather a sequence of reactions than a single elementary collision event. To describe it simply, in these reactions another collision partner has to be present during the reaction to provide or absorb energy. Therefore, the rate coefficients of those reactions depend on the number of collisions, and therefore also on the pressure. Since the different chemical species, here also called third bodies, differ in their efficiency for providing and absorbing energy in a collision, the rate coefficient also depends on the kind of that partner, i.e., a single dissociation or recombination reaction has to be expressed by a large number of elementary reactions. For brevity's sake those reactions are commonly summarized by writing, e.g.,



For low pressure, the rate of reaction is proportional to the third body concentration ($k \sim [A][M]$, bimolecular), for high pressure, the rate is independent of the pressure ($k \sim [A]$, unimolecular). A typical graph for pressure dependence of the rate coefficient is shown in

Figure 3.1. The position and the shape of the fall-off area depend on the reactive bonds. For small particles, the fall-off area moves to higher pressures. For particles with a high number of atoms, the fall-off region becomes wider.



with

$$k_0 = A_0 T^{\beta_0} \exp\left[-\frac{E_{a0}}{RT}\right] \quad (3-38)$$

$$k_\infty = A_\infty T^{\beta_\infty} \exp\left[-\frac{E_{a\infty}}{RT}\right]. \quad (3-39)$$

The reaction rate for recombination and dissociation reactions for the H₂-O₂ system, considered here is dependent on the third body concentration for the interval between 0.01 bar and 40 bars, i.e.,

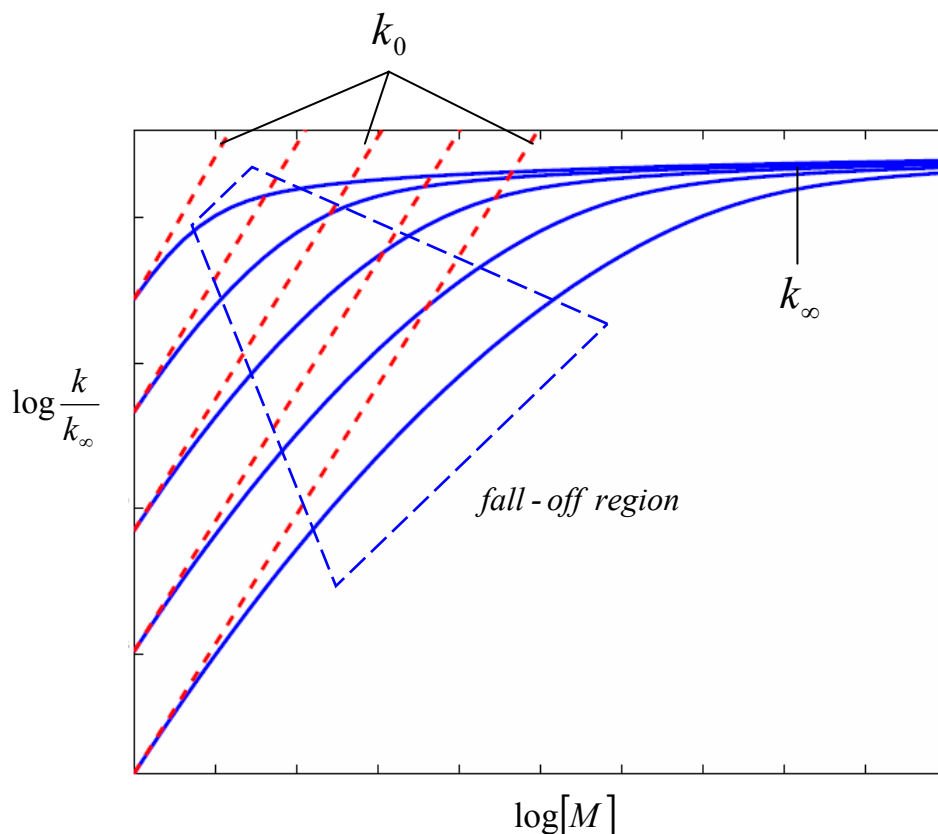
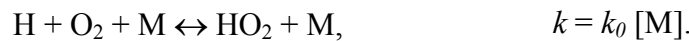


Figure 3.1: Characteristic dependence on the pressure for the rate coefficient (k). At low pressure $k \sim k_0[M]$, in the fall-off region $k = f(T, [M])$. At high pressure $k = k_\infty \neq f([M])$

The different effectiveness for the third body molecules is expressed by the collision efficiency η_M , for instance [19]

| Species | H ₂ | N ₂ | H ₂ O | CO | CO ₂ | CH ₄ | CH ₃ OH | Ar | He |
|----------|----------------|----------------|------------------|------|-----------------|-----------------|--------------------|------|------|
| η_M | 1.0 | 0.4 | 0.4 | 0.75 | 1.5 | 3.0 | 3.0 | 0.35 | 0.35 |

The different collision efficiencies of the third bodies where i corresponds to the species and N_g to the reaction are then taken into account by efficiency coefficients η_i in the following way

$$c_M = \sum_{i=1}^{N_g} \eta_i c_i. \quad (3-40)$$

For the thermal decomposition of alkanes containing more than three carbon atoms, the pressure dependence reaction rate is low, therefore only the high pressure rate is considered



If the rate coefficient is in the pressure-dependent zone within the fall-off region, as is the case for methyl recombination, it is possible to calculate the dependence on the rate coefficient with a quantum mechanical model (Kassel model [20])

$$\frac{k_{uni}}{k_\infty} = (1-\alpha)^s \sum_{p=0}^{\infty} \frac{\alpha^p (p+s-1)!}{\frac{A_\infty}{k_{coll}[M]} \frac{(p+m)!(p+s-1)!}{[(p+m+s-1)!p!]}} \quad (3-42)$$

with $p = n-m$, $m = E_\infty/h\nu$, $\alpha = \exp(-h\nu/kT)$; A_∞ and E_∞ being the Arrhenius parameters for the rate coefficient k_∞ at high pressure; ν is the geometrical center of the vibration frequency (s) of the dissociating molecule. The term $k_{coll}[M]$ depends on the product of the number of collisions Z and the efficiency of the collision λ

$$k_{coll}[M] = \lambda Z. \quad (3-43)$$

The collision efficiency is used to adapt the calculated rate coefficient. The bimolecular collision number Z is calculated under the assumption of a Lennard-Jones potential according to

$$Z = 2.078 N_A \pi \sigma^2 \left(\frac{8kT}{\pi\mu} \right)^{0.5} \left(\frac{\varepsilon}{kT} \right)^{0.5} \quad (3-44)$$

where σ and ε are the specific Lennard-Jones parameters. Here, σ represents the molecular diameter and ε the depth of the intra-molecular potential. μ is the reduced mass (for two compounds it is defined as: $m_1 \cdot m_2 / (m_1 + m_2)$), and N_A is the Avogadro number ($6.023 \cdot 10^{+23}$).

Another method to calculate the rate coefficient of this kind of reactions is known as *Troe formalism* [21,22], which is an improvement of the Lindemann-Hinshelwood original work [23]:

$$k = \frac{k_0 k_\infty [M]}{k_0 [M] + k_\infty} F$$

$$k_0 = A_0 T^{\beta_0} \exp\left(-\frac{E_{a0}}{RT}\right) \quad (3-45)$$

$$k_\infty = A_\infty T^{\beta_\infty} \exp\left(-\frac{E_{a\infty}}{RT}\right).$$

The additional broadening factor F is equal to the unit in the Lindemann expression. In the Troe formulation, F is calculated as

$$\log F = F_{\text{cent}} \left(1 + \left\{ \frac{\log P_r + c}{n - d(\log P_r + c)} \right\}^2 \right)^{-1} \quad (3-46)$$

where

$$P_r = \frac{k_0 [M]}{k_\infty} \quad (3-47)$$

$$c = -0.4 - 0.67 \log F_{\text{cent}}$$

$$n = 0.75 - 1.27 \log F_{\text{cent}} \quad (3-48)$$

$$d = 0.14$$

and,

$$F_{\text{cent}} = (1-a) \exp\left(-\frac{T}{T^{***}}\right) + a \exp\left(-\frac{T}{T^*}\right) + a \exp\left(-\frac{T^{**}}{T}\right). \quad (3-49)$$

Under atmospheric conditions, the first two terms in the F_{cent} expression are important; the last term becomes significant only for high temperature. The four parameters a , T^{***} , T^* and T^{**} are along with A_0 , β_0 , E_{a0} , A_∞ , β_∞ and $E_{a\infty}$ parameters needed for the rate coefficient calculation at high and low pressure, and their values can be found in the literature [24, 25, 26].

3.2.3 Surface Chemistry

Gas-phase species may not only react in the gas-phase but also on solid surfaces. These reactions sometimes are undesirable, for instance when radicals formed in homogeneous combustion recombine on the reactor wall. More importantly, however, the inclusion of a surface in the reaction pathway often offers the only possibility to obtain the desired product. This section focuses on modeling heterogeneous reactions among gas-phase species on solid surfaces that serve as catalyst as it was exhausted discussed in [27].

The catalyst provides an alternate reaction pathway between reactants and products by lowering the activation energy of the reaction as shown in Fig. 3.2. After diffusion from the gas-phase to the catalyst, the reactants adsorb on the surface, which can involve dissociation and decomposition reactions. The rates of surface reactions and desorption depend on surface coverage and temperature.

Heterogeneous reactions on solid surfaces can principally be treated by formalism very similar to that applied for gas-phase reactions if the mean-field approximation is applied [28]. This means that the adsorbates are assumed to be randomly distributed on the surface, which is viewed as being uniform. The state of the catalytic surface is described by the temperature T and a set of surface coverages μ_i which is the fraction of the surface that is covered with surface species i . The surface temperature and the coverage depend on the macroscopic position in the reactor, but are averaged over microscopic local fluctuations.

Under those assumptions a chemical reaction can be defined analogously to Equation 3.23 by

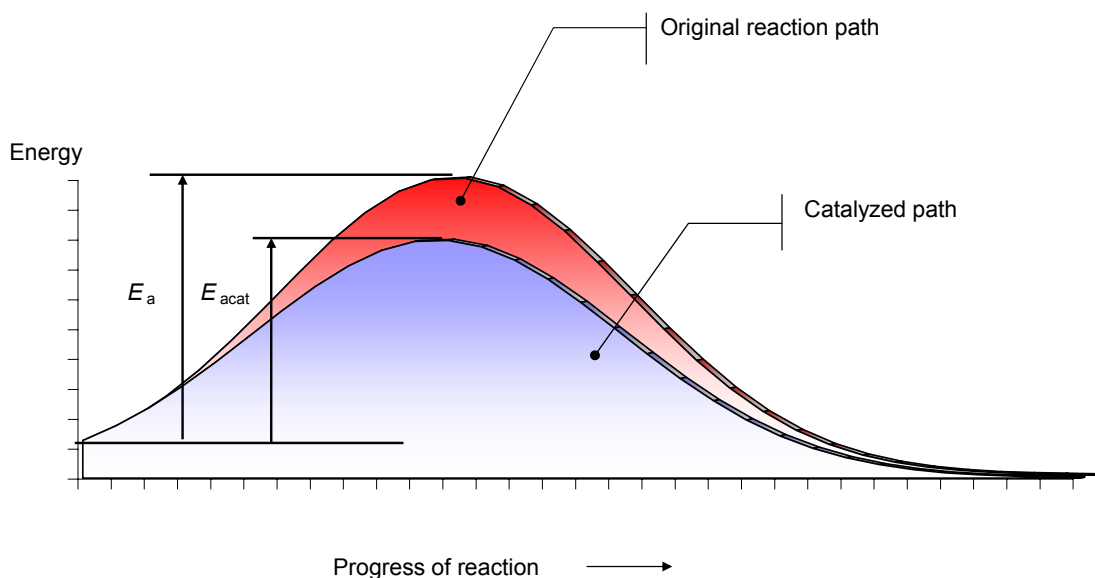


Figure 3.2: Activation energy for the catalytic and non-catalytic pathway for a chemical reaction

The only difference is that now the A_i denotes not only gas-phase species (e.g., H_2) but also *surface species* (e.g., $H(s)$) and *bulk species* (e.g., $H(b)$). The N_s surface species are species that are adsorbed on the top atom layer of the solid while the N_b bulk species are species that are diffused in the inner solid material. An uncovered site of the top layer of the solid surface, which is generally available for species adsorption is also counted as surface species and is denoted for instance by $Pt(s)$.

Steric effects of adsorbed species and various configurations, e.g., the type of the chemical bonds between adsorbate and solid, can be taken into account using the following concept: The surface structure is associated with a surface site density Γ that describes the maximum

number of species that can adsorb on a unit surface area, given, e.g., in mol/m². Then each surface species is associated with a coordination number σ_i , the number of surface sites which are covered by the species. For a surface reaction, possibly an adsorption process, a reaction between adsorbed reactants, desorption process, or species diffusion into and from the bulk phase, the total number of surface sites is constant

$$\sum_{i=N_g+1}^{N_g+N_s} \nu_i' \sigma_i = 0. \quad (3-51)$$

Under the assumptions done, multi-step (quasi-elementary) reaction mechanisms can be set up. The molar net production rate s_i of a gas-phase species or an adsorbed species due to heterogeneous reactions on the solid surface is then given as

$$\dot{s}_i = \sum_{k=1}^{K_s} \nu_{ik} k_{f_k} \prod_{i=1}^{N_g+N_s+N_b} c_i^{\nu_{i,k}}. \quad (3-52)$$

Here, K_s is the number of surface reactions, c_i are the species concentrations, which are given, e.g., in mol/m² for the N_s adsorbed species and in, e.g., mol/m³ for the N_g and N_b gaseous and bulk species. According to (3-52), the definition of the surface site density Γ , and surface coverages θ_i , the variations of surface coverages, follow

$$\frac{\partial \theta_i}{\partial t} = \frac{\dot{s}_i}{\Gamma} = 0 \quad (i = N_g + 1, \dots, N_g + N_s). \quad (3-53)$$

The surface coverages always refer to a single monolayer, hence the condition

$$\sum_{i=1}^{N_s} \theta_i = 1, \quad (3-54)$$

must be obeyed. The temperature dependence of the rate coefficients is described by a modified Arrhenius expression

$$k_{fk} = A_k T^{\beta_k} \exp\left[-\frac{E_{ak}}{RT}\right] \prod_{i=1}^{N_s} \theta_i^{\mu_{ik}} \exp\left[\frac{\varepsilon_{ik} \theta_i}{RT}\right]. \quad (3-55)$$

The parameters μ_{ik} and ε_{ik} describe the dependence of the rate coefficients for several surface reactions on the surface coverage of species i . For adsorption reactions, sticking coefficients are commonly used. They are converted to conventional rate coefficients by

$$k_{fk}^{\text{ads}} = \frac{S_i^0}{\Gamma_i^\tau} \sqrt{\frac{RT}{2\pi M_i}}, \quad (3-56)$$

with S_i^0 the initial (uncovered surface) sticking coefficient and τ the number of sites occupied by the adsorbing species.

The rate coefficient of the reverse reaction k_r can again be calculated using thermodynamic data (3-57). However, here, the change in number of occupied surface sites has to be taken into account

$$K_c = \frac{k_f}{k_r} = \left(\frac{p^0}{RT} \right)^{\sum_{i=1}^{N_g} \nu_i} \exp \left[\frac{\Delta_R \bar{S}^0}{R} - \frac{\Delta_R \bar{H}^0}{RT} \right] \Gamma^{\sum_{i=N_g+1}^{N_g+N_s} \nu_i} \prod_{i=N_g+1}^{N_g+N_s} \frac{\sigma_i^{\nu_i'}}{\sigma_i^{\nu_i}}. \quad (3-57)$$

3.3 Coupling of Heterogeneous Chemical Reactions with the Surrounding Flow Field

The chemical processes at the surface are coupled with the surrounding flow field by balance equations at the gas-surface interface. The species mass fractions Y_i are determined by N_g species mass balances considering diffusive \vec{j}_i and convective \vec{v}_{Stef} mass transport from and to the gaseous flow as well as the net production rate of the species by homogeneous gas-phase reactions (R_i^{hom}) and heterogeneous surface reactions (R_i^{het}) [29]

$$\int \rho \frac{\partial Y_i}{\partial t} dV_{\text{gas}} = - \int (J_i + \rho \vec{v}_{\text{Stef}} Y_i) \vec{n} dA + \int R_i^{\text{het}} dA + \int R_i^{\text{hom}} dV_{\text{gas}} \quad (i=1, \dots, N_g). \quad (3-58)$$

V_{gas} is the gas-phase control volume adjacent to the surface and \vec{n} is the outward pointing unit vector normal to the surface. R_i^{het} is given per unit geometric surface area, corresponding to the reactor geometry. It is linked with the molar reaction rate by

$$R_i^{\text{het}} = \dot{s}_i M_i F_{\text{cat/geo}}, \quad (3-59)$$

with $F_{\text{cat/geo}}$ the ratio of catalytic active surface area to geometric surface area. This procedure accounts for the fact that the total catalytic surface area exposed to the gas-phase commonly differs from the area of the reactor or support, which is coated with the catalyst. The heterogeneous reaction mechanisms are developed for a given number of adsorption sites (mole/m²) depending on the catalyst material and its intrinsic structure. Referring to the fluid flow equations with boundary conditions based on the geometric reactor coordinates, the total catalytic surface area can be much smaller ($F_{\text{cat/geo}} < 1$) if only few catalyst clusters exist, or it can be much larger ($F_{\text{cat/geo}} > 1$) if the catalyst is dispersed on a washcoat. $F_{\text{cat/geo}}$ is determined by experimental characterization of the catalyst, namely the catalyst weight and dispersion measured. The dispersion can be estimated, e.g., by hydrogen chemisorption measurements.

The so-called *Stefan-velocity* occurs at the surface if there is a net mass flux between the surface and the gas phase

$$\vec{n} \vec{v}_{\text{Stef}} = \frac{1}{\rho} \sum_{i=1}^{N_g} R_i^{\text{het}}. \quad (3-60)$$

At steady-state conditions, this mass flux vanishes unless mass is deposited on the surface, e.g., chemical vapor deposition, or mass ablation occurs, e.g., materials etching. The growth rate \vec{v}_{growth} is then defined as

$$\vec{v}_{\text{growth}} = \frac{\rho}{\rho_s} \vec{v}_{\text{Stef}}, \quad (3-61)$$

with ρ_s the density of the material deposited or ablated. At steady-state conditions, (3-58) results in the following boundary conditions for the species-continuity equations (3-4) at the gas-surface interface [29]

$$\vec{n}(\vec{j}_i + \rho \vec{v}_{\text{Stef}} Y_i) = R_i^{\text{het}} \quad (i = 1, \dots, N_g). \quad (3-62)$$

If the Stefan velocity does not vanish, a mass source term has to be included in the continuity equation at the gas-surface boundary (3-1). Here, no-slip boundary conditions are chosen, i.e., all velocity components vanish at the gas-surface interface unless a net mass flux occurs. These velocity components represent the boundary condition for the momentum equations (3-2). There are several ways to specify a boundary condition for the enthalpy (Equation (3-8)). Generally, either a *Dirichlet boundary condition* is chosen by giving a fixed value for the variable under consideration or a *Neumann boundary condition* is chosen by specifying a flux at the boundary. In the first case, a surface temperature is usually given, in the latter case a heat flux q_h is specified for the enthalpy equation. The heat flux accounts for (temperature-dependent) heat transfer at the boundary and external radiative heat loss

$$q_h = q_h^T (T - T_0) + \varepsilon \sigma (T^4 - T_0^4) + q_h^{\text{const}}, \quad (3-63)$$

with q_h^T a heat transfer coefficient given, e.g., in $\text{W}/(\text{m}^2\text{K})$, ε the thermal emissivity, σ the *Stefan-Boltzmann* constant, T_0 a reference temperature, and q_h^{const} the constant heat flux. If a heat balance equation is solved not only in the gas-phase but also in the solid-phase (3-11), local thermal equilibrium is assumed in this work, i.e., the gas-phase temperature equals the solid temperature at the gas-surface boundary. The heat released by heterogeneous chemical reactions

$$S_h^{\text{het}} = \sum_{i=1}^{N_g+N_s} h_i R_i^{\text{het}} + \sum_{i=N_g+N_s+1}^{N_g+N_s+N_b} h_i s_i M_i \quad (3-64)$$

is either added as source term to the heat transport equation in the solid (3-11) or in the gas-phase (3-8) at the gas-surface boundary. The latter choice is followed unless a heat transport equation in the solid is solved. The heat release due to heterogeneous surface reactions can also be split by depositing the heat of desorption reactions in the gas-phase, and the heat of adsorption reactions and reactions between adsorbed and/or surface bulk species into the solid.

3.4 Methods for Reaction Mechanism Analysis

In combustion modeling, the parameters describing the thermo-chemical and transport properties of the chemical species and the rates of the elementary reactions may include many values. The relative importance of these parameters spans a very wide range, meaning that model predictions usually are affected by the values of only a small fraction of the model parameters: Only a few parameters really matter. The study of relationships between parameter values and model predictions is called *sensitivity analysis* [30]. Parameters which

prove to strongly influence model predictions are *sensitive parameters*, those with little influence are insensitive ones. The set of sensitive values for the whole parameters set is the sensitivity spectrum.

For a chemical system the results for the concentration variables can be inferred from the governing Navier-Stokes equations, where the following assumptions are made: (1) the ideal gas is valid, and (2) the heat flux caused by radiation of gases is negligible [31].

At pressure p and constant temperature T

$$\dot{c}_i = \omega_i + c_i \left\{ \frac{\dot{p}}{p} - \frac{RT \sum_{i=1}^{N_g} \dot{\omega}_i}{i} - \frac{\dot{T}}{T} \right\}; i = 1, \dots, N_g. \quad (3-65)$$

At pressure p and constant V

$$\dot{c}_i = \omega_i - c_i \left\{ \frac{\dot{V}}{V} \right\}; i = 1, \dots, N_g. \quad (3-66)$$

The temperature can be specified or calculated from the enthalpy conservation assuming adiabaticity. The rate laws for a reaction mechanism consisting of R reactions among N_g species can be written as a system of first order ordinary differential equations

$$\begin{aligned} \frac{dc_i}{dt} &= F_i(c_1, \dots, c_n; k_1, \dots, k_n); i = 1, \dots, N_g. \\ c_i(t = t_0) &= c_i^0 \end{aligned} \quad (3-67)$$

The time t is the independent variable, the concentrations c_i of species i are the dependent variables, and k_r the parameters of the system; c_{i0} denotes the initial conditions at t_0 . Only the rate coefficients of the chemical reactions taken into account shall be considered here as parameters of the system. Nevertheless, initial concentrations, pressure, etc. can be treated as system parameters too, if desired. The solution of the differential equation system depends on the initial conditions as well as on the parameters.

For a few elementary reactions, changes in their rate coefficients have a very significant effect on the outcome modeling result of the system. These important reaction steps are rate-determining steps or rate-limiting steps. The dependence of the solution c_i on the parameters k_r is called absolute and relative sensitivity. Sensitivities and can be defined as

$$\begin{aligned} E_{i,r} &= \frac{\partial c_i}{\partial k_r} \\ E_{i,r}^{\text{rel}} &= \frac{k_r}{c_i} \frac{\partial c_i}{\partial k_r} = \frac{\partial \ln c_i}{\partial \ln k_r}. \end{aligned} \quad (3-68)$$

A second tool for interpretation of computed profiles is called *flux analysis*. The aim is to seek the channels in which chemical reactions “flow”. The procedure consists of scanning of

all the net rates (Equation 3-67) at interesting times during the reaction to determinate the fastest, and the noncontributing reactions and to determinate reactions which are so fast in both directions that they are essentially equilibrated.

Chapter 4

DEVELOPMENT AND VALIDATION OF A DETAILED KINETIC MECHANISM FOR COMBUSTION OF C₄ ALKANES

4.1 Bibliographic Review

4.1.1 Methane Oxidation and Partial Oxidation

Several high range temperature oxidation mechanisms for C₁ to C₄ hydrocarbons already exist in the literature [32, 33]. Other mechanisms (Warth [34], Chevalier [35] and Ranzi [36]) have been generated automatically and evaluated by comparing ignition delay times and species concentrations.

Different authors have reported methane autoignition investigations. Asaba [37] et al. conducted autoignition experiments for methane oxygen mixtures with equivalence ratios between 0.2 and 6.0 at temperatures between 800 K and 2200 K. The pressure range was between 7 bar and 10 bar.

Asaba suggested that, depending on the methane content, two different mechanisms exist. For lean mixtures a branching chain mechanism at low temperatures governs the reaction during the induction period. For rich mixtures, the thermal chain mechanism governs the reactions at high temperatures.

Bowman [38] reports ignition delay times for methane oxygen mixtures diluted in Argon in the range of temperatures between 1700 K and 2200 K, equivalence ratios of 0.25 to 4.0 and pressures between 0.55 bar and 2.6 bar.

Lifshitz et al. [39] confirmed that dilution has no effect on the induction time. In their investigation, Lifshitz and coworkers deduced a correlation for determining the induction time for methane mixtures which showed a good agreement in the range of temperature between 1300 K and 2500 K which was used with good results by other authors [40].

Tsuboi and Wagner [41] studied the homogeneous thermal oxidation of methane oxygen mixtures highly diluted in Argon with equivalence ratios between 0.2 and 2.0, and pressures from 3 bar to 300 bar at temperatures around 1800 K. A correlation for the induction time was obtained similar to the earlier proposed by Lifshitz.

Roth and Just [42] studied the kinetics of the oxidation of methane at high temperatures. The temperatures used in their studies ranged between 1850 K and 2500 K, pressures were about 1.8 bar and the fuel-oxygen ratio was between 0.01 and 0.5. In their experiments, oxygen (O) and hydrogen (H) atom concentrations were directly measured. A kinetic mechanism consisting of 25 elementary reactions was used to model the concentration profiles of the main species.

Spadaccini and Colket [43] reported a comprehensive literature search related to ignition delay of methane and methane mixtures. Spadaccini also reports results from measurements of ignition delays of methane and methane mixtures where, ethane, propane and butane were used as additives for their experiments. Experiments were carried out between 1300 K and 1900 K and pressures of 3.5 atm to 15 atm. Equations based on the empirical results were developed for predicting the ignition delay of various binary methane hydrocarbon mixtures. A detailed kinetic model that included methane, ethane and propane chemistry was reported, and suggested the importance of hydrogen peroxide in the autoignition process.

Partial oxidation of methane has also been studied by several authors. Zanthoff and Baerns [44] studied the oxidative coupling of methane in the gas phase in the absence of a catalyst. The main products found in their experiments were ethane and ethylene and minor amounts of C₃ hydrocarbons as coupling products and carbon oxides as total oxidation products. Experiments were done in the range of pressures between $1.84 \text{ bar} < p(\text{CH}_4) < 8 \text{ bar}$, $0.18 \text{ bar} < p(\text{O}_2) < 0.8 \text{ bar}$ and temperatures of $878 \text{ K} < T < 1071 \text{ K}$. It was found that selectivity to C₂₊ hydrocarbons species increases with temperature and with CH₄/O₂ ratio, while selectivity to carbon oxides decreases. For the dependence on the C₂₊ selectivity on pressure, Zanthoff found that the C₂H₄/C₂H₆ ratio decreases with increasing pressure. Maximum C₂₊ selectivities were on the order of 50%. Zanthoff proposed a kinetic mechanism, which included 163 reactions and 28 species. The kinetic data used for the simulation were the ones proposed by Warnatz [18], CODATA [25-26] and Cohen and Westberg [45].

Goralski and Schmidt [46] modeled a short contact time catalytic methane combustor as a plug flow tubular reactor using homogeneous and heterogeneous chemistry. For different species composition, the pressure was ranged from 1 atm to 25 atm, and temperatures were between 1000°C and 1800°C. Homogeneous chemistry alone was found to produce NO and CO, but in the presence of a catalyst this was inhibited as result of the adsorption of radicals into the surface of the catalyst. The gas-phase mechanism used was the GRI mechanism 2.11 [47], initially proposed by methane oxidation. The mechanism consisted of 277 reversible reactions and 49 gas-phase species.

Catalytically stabilized combustion of hydrogen-air mixtures has been studied under lean conditions and turbulent flow [48]. The authors developed a two-dimensional elliptic model including heterogeneous and homogeneous chemical reactions assuming that the temperature at the walls was constant. After a comparison between laminar and turbulent flows using the same initial conditions, the authors concluded that in the turbulent case, combustion was inhibited due to an increased heat transport away from the near wall layer where gaseous combustion was confined.

Chen et al. [49] studied the oxidative coupling of methane in the presence and absence of a catalyst with ethane co-feeding. Ethane was found to increase the conversions of methane and be beneficial for the production of ethane and C₂ species due to the lower C-H bond energy in ethane, which led to higher propagation rates and then to higher branching rates in a branched chain mechanism. Chen and Marin proposed a mechanism which consists of 39 reversible reactions, optimized for temperatures around 1073 K and pressures up to 400 kPa. The model was based on a previous one developed by the same authors [50].

Baerns [51] studied the oxidative coupling of methane between 700°C and 900°C. Ethane, ethylene, and small quantities of higher hydrocarbons were found in the presence and absence of a catalyst. A kinetic model was used to model the concentration profiles. This model considered 193 reactions among 33 species and included propane, propylene, ethane, ethylene and methane chemistry. Reactions between methyl radicals and oxygen to form CH₃O₂ and the characteristic secondary radical CH₃O₂H were also included. These last steps are present in the low temperature regime.

Wiele et al. [52] studied the roles of the gas phase and the heterogeneous chemistry in the oxidative coupling of methane. The authors modeled the oxidative coupling of methane, assuming that the catalyst kinetically controlled the reaction steps for the formation of ethane, ethylene and carbon monoxides through an initial hydrogen abstraction, which in each case produces the respective radical. In the case of ethane, methyl radicals were produced in the catalyst, and the coupling process took place in the gas phase. Conversion of ethane to ethylene was also controlled by the catalyst, which initialized the reactions by a hydrogen abstraction, and was followed by radical reactions which occurred in the gas phase. For the modeling of the gas-phase reactions, Wiele developed a kinetic scheme consisting of more than 400 reactions which were later reduced to 164. The references used for the kinetic data of the reactions are from the previous works developed by Warnatz [18], Tsang and Hampson [53], Westley and Herron [54], Vardanyan and Nalbandyan [55], Dagout et al. [56], and Albright et al. [57].

4.1.2 Ethane Oxidation and Partial Oxidation

Cooke and Williams [58] performed studies of autoignition of ethane oxygen mixtures in the temperature range from 1400 K to 1800 K, in their experiments the equivalence ratios were ranged between 0.5 to 2. A mechanism consisting of 34 reversible reactions among 34 chemical species was proposed. According to the authors, a rapid degradation of the fuel due to cracking occurred before the ignition and suggested the conversion of ethane to ethylene via ethyl radical formation before ignition and the formation of ethylene during ignition. Ethylene is then converted to acetylene, whose concentration decays once the hydroxyl radicals reach a maximum, leading to the formation of combustion products.

Marinov et al. [59] performed a chemical kinetic modeling to investigate aromatic and polyaromatic hydrocarbon formation pathways in rich, sooting methane and ethane premixed flames. Experiments were carried out at equivalence ratio of 2.5 for both fuels (CH₄/O₂/AR 30.4/24.3/45.3 and C₂H₆/O₂/AR 22.8/31.9/45.3) at atmospheric pressure. The proposed mechanism consists of 661 reversible reactions among 161 species. To develop the mechanism, Marinov used previous work on propane and propylene from Tsang [60, 61], n-butane from Pitz et al. [62] and the mechanism from Miller-Melius [63] for benzene formation. The mechanism was able to predict stable species concentration in rich premixed laminar flames.

Rota et al. [64] experimentally investigated the oxidation of several fuel mixtures, involving methane, ethane, ethylene and acetylene, in a jet-stirred reactor. Conditions used in their experiments cover a range of temperature between 864 K and 1248 K at atmospheric pressure. Binary mixtures of methane and ethane were used and the effects of adding ethylene and acetylene to the binary mixture were investigated. The authors reported no changes in the reactivity of the methane and ethane when ethylene was added with similar conversions obtained in both cases. Ethylene reactivity is strongly influenced by the C_2H_6/C_2H_4 ratio: Conversions were negative for high ethane-ethylene ratios and increased for lower C_2H_6/C_2H_4 ratios, which indicates that for higher ratios thermal decomposition of ethane to ethylene occurred before ethylene decomposition started; similar results were reported by Cooke and Williams [58].

Westbrook et al. [65] studied the oxidation of ethylene in a well-stirred reactor at temperatures ranging from 1003 K to 1253 K and atmospheric pressure. Fuel oxygen ratios were 0.36 to 0.48. Westbrook reported a kinetic mechanism that described formation of the main products and consumption of reactants. From this study, the main consumption of ethylene for this range of temperature was via hydrogen atom abstraction by hydroxyl radicals and oxygen atoms.

Wilk et al. [66] investigated the oxidation of ethylene in the low temperature range in a static reactor. Experiments were done at 696 K and 718 K at 0 atm to 0.79 atm (2 torr to 600 torr.) At these low temperatures, products such as aldehydes and oxiranes are expected. The main reactions involving ethylene consumption involved OH and HO_2 radicals. A detailed chemistry mechanism, which describes oxiranes formation, was developed and evaluated by comparison of the concentration profiles of the species. The chemical mechanism developed included addition reactions of the O_2 , HO_2 and OH radicals to the fuel, and decomposition of the oxygenated species to aldehydes following the scheme proposed by Waddington [67].

Zerkle et al. [68] studied the role of the homogeneous and heterogeneous chemistry in the catalyzed partial oxidation of ethane. A two-dimensional model for a short contact time reactor including mass and heat transport was employed to model the partial oxidation of ethane to ethylene; the model used a detailed heterogeneous and homogeneous chemical kinetics mechanism to describe the chemistry. Production of ethylene and hydrogen was found to be due to combined homogeneous and heterogeneous processes of ethane dehydrogenation. Gas-phase reactions were modeled using a subset of the mechanism proposed by Marinov et al. [59], and the evaluation of the reduced mechanism was done by comparison against experimental data for flame velocities from Egolfopoulos et al. [69] and species concentration profiles from Dagaut et al. [70]. The authors proposed an exothermal heterogeneous process, which releases the necessary energy to drive the reactor, and an endothermic gas-phase process which produces ethylene. Behavior of the reactor was strongly dependent on the conditions, e.g., it was found that in mixtures of ethane and oxygen with ratio 1.5 ($C_2H_6/O_2 = 1.5$) gas-phase reactions are predominant for ethane consumption and ethylene formation, but when this ratio was increased to 1.7 and 1.9 both the heterogeneous and the gas-phase were competitive.

4.1.3 Propane Oxidation and Partial Oxidation

Propane combustion has been studied extensively. Burcat and Lifshitz [71] reported ignition delay times for propane/oxygen/argon mixtures measured in shock-tubes experiments. Temperature was varied between 1250 K and 1600 K and pressure between 2 atm and 10 atm.

Equivalence ratios used during the experiments ranged from 0.125 to 2. No dependence on the ignition delay times with the third body was found and self-decomposition was the main path that was responsible for the ignition process ($C_3H_8 \leftrightarrow CH_3 + C_2H_5$). Ethylene and propylene were the main species formed before ignition under the conditions examined. Equivalence ratio was an important variable in the delay times measured: For stoichiometric mixtures, the radical recombination process slowed down the ignition of the mixture while for lean mixtures oxygen shortened the ignition and recombination reactions which were exceeded by the branching reactions which involved oxygen ($H + O_2 \leftrightarrow OH + O$).

Burcat and Radhakrishnan [72] studied the high temperature oxidation of propene in a shock-tube. Measurements of ignition delay times are reported over a range of temperature from 1274 K to 1840 K and pressures from $6.5 \cdot 10^{-2}$ atm to 0.175 atm (50 torr to 133 torr) The fuel-oxygen ratio of the mixtures was kept between 0.55 and 2.22. The main products found before ignition occurred were acetylene and ethylene, and minor traces of methane. The authors suggested two different mechanisms: In the high temperature range (1700 K), the main reaction was the hydrogen abstraction from the fuel to produce allyl radicals (C_3H_5) and hydrogen (H_2), followed in importance by ($H + O_2 \leftrightarrow O + OH$). In the low temperature region (1366 K) ($H + O_2 \leftrightarrow O + OH$) was the most important reaction, followed by ($HCO + HO_2 \leftrightarrow CH_2O + O_2$) and the scission to produce methyl radicals and vinyl ($C_3H_6 \leftrightarrow CH_3 + C_2H_3$). The authors proposed a kinetic mechanism which consists of 59 reversible reactions, but only partial agreement between experimental data and simulation was achieved.

Experiments in a laminar flow quartz reactor have also been made to study propane oxidation. Cathonnet et al. [73], studied reacting mixtures in a range of equivalences ratios from 0.05 to 25 and a temperature near to 1000 K. The main products found were olefins (C_2H_4 and C_3H_6), methane, carbon monoxide and ethane. The authors proposed a kinetic scheme which consists of 110 non-reversible reactions which included propane and butane chemistries and predicted with good agreement the experimental data. According to the mechanism proposed, initially the fuel is attacked by hydroxyl radicals (OH) in the case of lean mixtures, and hydrogen (H) for the case of rich mixtures, or it proceeds to self-decomposition, which produces methyl (CH_3) and ethyl (C_2H_5) radicals. Further, the methyl radical produced in the initial step reacts with the fuel, increasing its consumption.

Catalytic dehydrogenation of propane was investigated by several authors [74, 75, 76]. Beretta et al. [76] studied the oxidative dehydrogenation of propane in the presence and absence of a catalyst, and suggested that two different processes occur. The first one is the full oxidation of the propane on the surface of the catalyst, which can occur at low temperatures and the second is the olefin production in the gas phase at high temperatures. In their experiments, Beretta et al. reported no olefin production at temperatures below 773 K. At this temperature only combustion species were found in the products, but over 823 K (550°C) large amounts of olefins were formed with propylene-ethylene selectivities higher than 55%, at conversions of 90% and 100% of fuel and oxygen, respectively. Experiments in absence of a catalyst at conditions similar to those used in the catalytic study showed that the homogeneous phase can produce the same amount of olefins as observed in the heterogeneous case, and the process can be operated adiabatically, if the proper conditions of preheating and mixture composition were chosen. According to the authors, under these conditions the role of the heterogeneous phase was to reduce the contact times necessary to run the process. Details from the homogeneous chemistry in the process are reported later [77]. Two main channels are considered for the chain radical initiation steps: In the presence of oxygen, oxygen and the fuel react to produce hydroperoxy (HO_2) radicals and propyl (C_3H_7) radicals, or in the absence of oxygen, decomposition of the fuel into methyl and ethyl radicals is the predominant

channel. These two paths (in absence or presence of oxygen) are the most important for the fuel consumption. The kinetic scheme for pyrolysis and oxidation of propane proceeded through the well-known path of successive reactions of *n*-C₃H₇ and *i*-C₃H₇ radicals and further decomposition to olefin or smaller radicals.

4.1.4 Butane Oxidation and Partial Oxidation

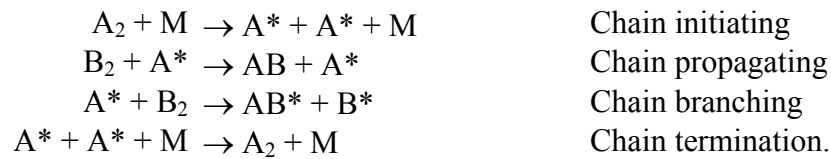
Rapid compression experiments were performed by Kojima [78, 79, 80] to study the combustion of butane in the low temperature range (720 K - 830 K). Kojima reported a detailed chemical kinetic model, which consists of 461 reactions among 141 species. For the evaluation of the mechanism, a comparison between calculated ignition delay times and the ones found during the experiments was done. Additionally, a further evaluation was performed in the high temperature range (1200 K - 1400 K) by comparison of a simulation with experimental data from Burcat et al. [81]. For the experiments performed in shock tubes, a good agreement was achieved between simulations and experiments. In accordance with the results of the simulations, Kojima suggested two main channels for the high temperature range which control the ignition process: External hydrogen abstraction from the fuel for a radical which can be hydrogen or hydroxyl (H, OH), via the reactions ($C_4H_{10} + H(OH) \leftrightarrow 2 C_4H_9 + H_2(H_2O)$), or thermal decomposition of the fuel to ethyl radicals ($C_4H_{10} \leftrightarrow 2C_2H_5$). In both cases the alkyl radicals will decompose to an olefin (C₃H₆ or C₂H₄). For 2 C₄H₉, its decomposition leads to a chain termination step ($2 C_4H_9 \leftrightarrow CH_3 + C_3H_6$; $CH_3 + CH_3 \leftrightarrow C_2H_6$) and two branching steps ($CH_3 + HO_2 \leftrightarrow CH_3O + OH$, and $O_2 + H \leftrightarrow OH + OH$), while the ethyl radicals lead to a chain propagation step ($C_2H_5 + O_2 \leftrightarrow C_2H_4 + HO_2$). In the middle temperature range hydrogen peroxide decomposition is the most important branching step ($H_2O_2 \leftrightarrow OH + OH$), and in the low temperature range two termination steps govern the ignition delay time: ($Alkyl + O_2 \leftrightarrow Olefin + HO_2$), and ($C_4H_9O_2 \leftrightarrow C_4H_9 + O_2$).

Cathonnet et al. [73] studied experimentally and theoretically the oxidation of butane at high temperature and atmospheric pressure for different equivalence ratios. Simulations of their experiments were done using the kinetic scheme already proposed for propane oxidation, and including a set of additional reactions for butane; some of them were not elementary ones. The mechanism was able to reproduce the experimental data well.

Karbach [33] and Nehse [82] developed a complex kinetic mechanism for the combustion of small alkanes. The proposed mechanism consists of 765 irreversible reactions among 60 chemical species. The mechanism was evaluated by comparison of simulation and experimental data for flame velocities of the following species: Hydrogen (H₂), carbon monoxide-hydrogen (H₂) mixtures, methane (CH₄), ethanal, methanol (CH₃OH), ethyne (C₂H₂), ethene (C₂H₄), ethane (C₂H₆), propene (C₃H₆), propane (C₃H₈), 1-butene (C₄H₈), n-butane (C₄H₁₀), and ignition delay times for hydrogen (H₂), methane (CH₄), ethane (C₂H₆), propane (C₃H₈) and butane (C₄H₁₀). The values for the rate coefficients required for the different reactions were taken from Baulch [26], or in the case that some specified rate was not included in this report, other sources were consulted, such as the NIST Database [83]. Below, more explanation will be given for some of the most important reactions of this mechanism, which was initially used in the present thesis.

4.2 Reaction Mechanism Development

Combustion of hydrocarbons can involve a great number of chemical reactions. They consist of a series of consecutive, competitive, and opposing reaction steps with differences in reaction rate constants. In a reaction process, the most active species are called free radicals. Combustion is a radical chain process, where elementary reactions are called chain initiating or chain terminating reactions according to whether they produce or destroy radicals. With regard to the ratio of the number of free radicals in the products to the reactants, elementary reactions are called chain propagating (or chain carrying) reactions if the ratio is equal to 1 and chain branching reactions if the ratio is larger than 1. Some examples of elementary reactions are



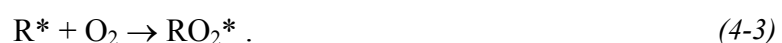
The construction of an elementary reaction mechanism has the advantage that the order of the reaction for a single reaction is independent from the time and test conditions. Other advantage from the elementary mechanism is that they allow extrapolation of results at conditions, where there are no experimental measurements available, which is not possible when a global mechanism is used.

4.3 Low and Intermediate Temperature Oxidation

The initial reaction that describes the fuel consumption in the low temperature range is accepted to be an H atom abstraction to yield an alkyl radical



This reaction is slow, selective and endothermic, having a high activation energy for each of the four alkanes included in the butane mechanism (around 200 kJ mol^{-1} [26]), and despite producing two radicals does not accelerate the reaction [84]. This initiation step was suggested initially by Cullis and Hinshelwood [85], and later substantiated by Semenov [86]. The oxygen attack on the fuel is thought to favor the secondary C-H bond instead of the primary due to the difference in their strength ($\sim 12 \text{ kJ mol}^{-1}$), which, although small, becomes more important in the lower temperature range [87]. The tertiary C-H bond is preferred broken over the secondary on the same basis. In the low temperature regime (temperature around 700 K), reactions of hydrocarbons show that the alkyl radicals mainly react with oxygen. Other types of reactions such as decomposition, disproportionation, isomerization recombination and reaction with the fuel will only be competitive when the partial pressure of oxygen is low or the temperature is high [88]. The two main reactions for the alkyl radicals (olefin production and oxygen addition) are described as follows



There are two theories related to the consumption of the alkyl radicals: The first of them, proposed by Knox [89], suggests that the primary route for alkyl oxidation leads to the formation of the conjugate alkene. Knox found during his experiments with several small alkanes (with less than four carbon atoms) that nearly 80% of the alkanes that are consumed appeared in the products as alkenes. These experiments were carried out at low and high temperature, and in each condition the products were the same at lower fuel conversion (< 1%).

The second theory which has been developed from observations during the oxidation of larger hydrocarbons (> C₄) and at later stages of reaction (80% < Fuel Conversion) proposed an addition of oxygen to the alkyl radical to yield alkylperoxy radicals which further rearrange to a hydroperoxide alkyl radical through an internal H atom abstraction. The hydroperoxide formed (R'OOH) is then decomposed into stable products (R'O) and hydroxyl by fragmenting the O-O bond. In this theory, the fuel consumption is then completed by the unselective attack by the OH that is formed



The degenerated branching species RO₂* should accumulate to significant concentrations before chain-branching reactions become important. Only after this accumulation has taken place self-acceleration occurs.

For the low temperature region, the oxygen addition to the alkyl radical is the predominant path for the alkyl consumption. Although at higher temperature the hydrogen atom abstraction is the main route. The transition region from the low temperature to the high temperature regime is characterized by an increase in the induction time and a decrease in the rate of species production. This behavior is attributed to the negative temperature coefficient phenomenon which is associated with hydrocarbons oxidation.

From the chemical point of view R'OOH, which is the main branching agent in the low temperature regime, decomposes into R'O and OH during the transition. This chain-branching reaction accelerates the reaction, producing a rapid increase in temperature and pressure. However, as the temperature increases, acceleration is stopped as the R'OOH radicals are rapidly consumed. The further rise in temperature makes alkene formation from the alkyl radical more competitive with the oxygen addition, and as a consequence there is a decrease in RO₂* production that leads to OH formation.

When temperature increases, alkene and hydroperoxy radical (HO₂) production becomes more important, and the hydroperoxy radical (HO₂) replaces the characteristic low temperature R'OOH radical as the most abundant. In spite of this, the reaction does not accelerate, even if HO₂ is more reactive than the R'OOH. HO₂ does not increase the rate of reaction as it does not have as many possible routes for its consumption as R'OOH, which accounts for the observed decrease in the reaction rate as the temperature continues to rise. HO₂ will tend to abstract hydrogen from a hydrogen donor species (fuel or an aldehyde) to form peroxide



With a further rise in temperature, the hydrogen-peroxide dissociation rate increases leading to hydroxyl radical formation, which is the main branching reaction at temperatures above the

negative coefficient region. This reaction is extremely accelerating and again a decrease in the induction time is observed as the temperature continues to increase



H_2O_2 production is more significant at higher temperature reactions, and HO_2 and OH become the dominant radicals. Functionally, HO_2 replaces the RO_2 radicals while H_2O_2 replaces $\text{R}'\text{OOH}$. These changes characterize the transition between the low and the intermediate temperature mechanisms of hydrocarbon oxidation. Figure 4.1 presents the main paths for the hydrocarbons oxidation at low temperature.

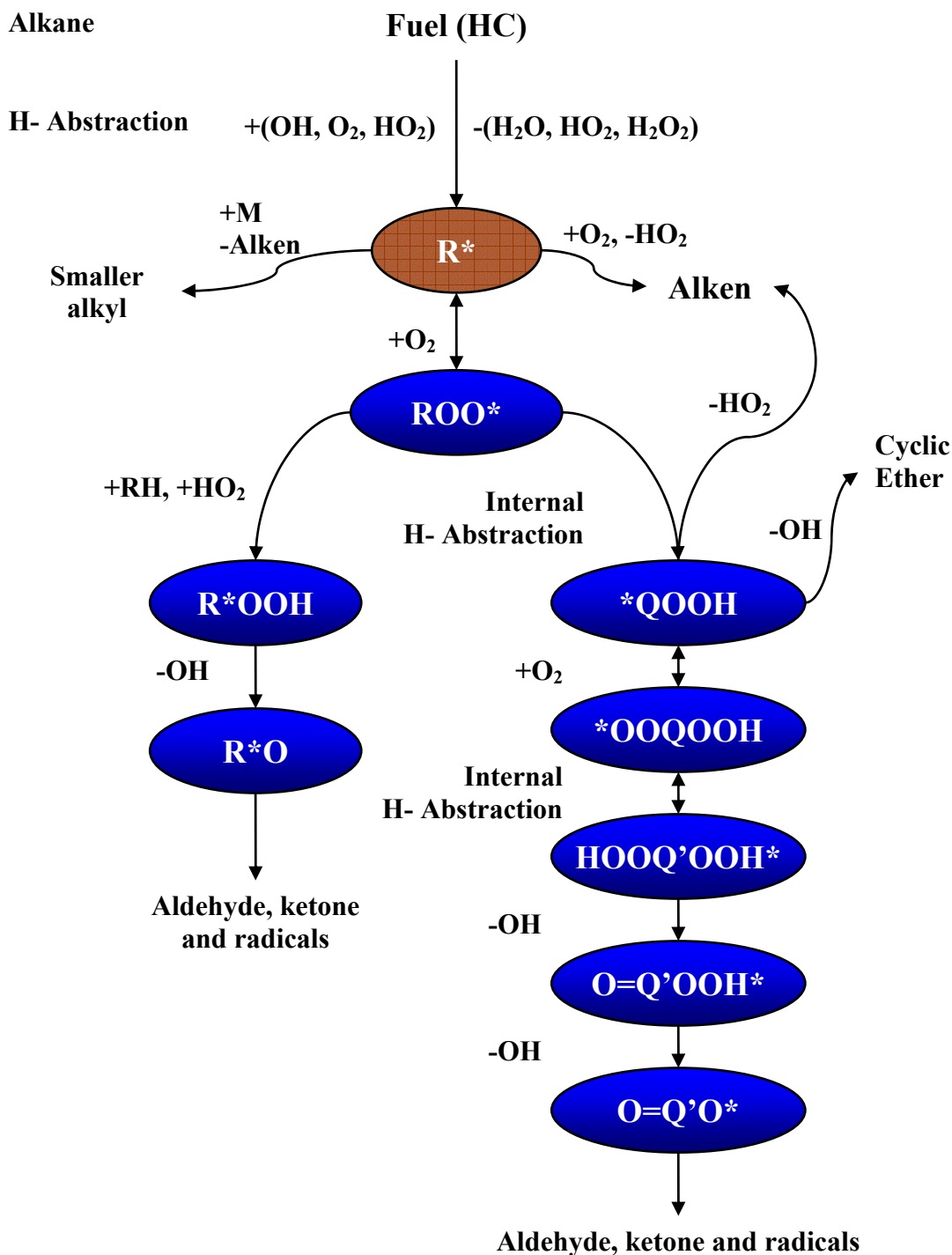


Figure 4.1: Schematic mechanism for the combustion of hydrocarbons at 500K - 800K. $R = C_nH_{2n+1}$; $Q = C_nH_{2n}$; $Q' = C_nH_{2n-1}$. First step involves a hydrogen abstraction from the fuel to yield the alkyl radical. At low temperature, the alkyl formed is oxidized and peroxy radicals appears: Further they are decomposed into aldehydes (main species found during experiments in cold flames [88]) ketones and others small radicals

4.3.1 Reaction of Alkyl Radicals

The predominant mode of oxidation of alkyl radicals is by oxygen addition and an alkylperoxy radical is formed and then undergoes homogeneous intramolecular rearrangement. Decomposition of the rearranged radical usually leads to hydroxyl radicals and stable products which include O heterocycles, carbonyl compounds and alcohols. In the middle and low temperature regime, there are two different reactions between the alkyl radicals and oxygen



For the first channel (oxygen addition), and for both radicals (propyl and butyl) an activation energy of 0 kJ mol⁻¹ is accepted in the literature. The pre-exponential factors are different for each particular radical. Kinetic parameters that have been used are listed in Table 4.1.

Table 4.1 Arrhenius parameters for the reaction: $R^* + O_2 \leftrightarrow RO_2^*$
(A in $cm^3 mol^{-1} s^{-1}$, E_a in $kJ mol^{-1}$)

| Alkyl Radical | $A/n/E_a$ |
|---|----------------------------|
| <i>n</i> -C ₃ H ₇ | $3.50 \cdot 10^{12}/0/0.0$ |
| <i>i</i> -C ₃ H ₇ | $8.50 \cdot 10^{12}/0/0.0$ |
| 1 C ₄ H ₉ | $4.50 \cdot 10^{12}/0/0.0$ |
| 2 C ₄ H ₉ | $1.00 \cdot 10^{13}/0/0.0$ |

Different kinetic data have been used for the reaction between the propyl and oxygen: Tsang [61] and Warth [34] proposed kinetic data after a bibliographic review, including a temperature dependence of the pre-exponential factor. Atkinson et al. [90] proposed for the same reactions kinetic data for modeling atmospheric chemistry (temperatures in the range of 200 K- 300 K). Slage et al. [91] presented experimental work in the range of 297 K – 635 K and Ruiz and Bayes [92] proposed kinetic data at 298 K and low pressure based on their experimental work. The proposed values from Slage, which are consistent with the ones from Ruiz, were used here.

For the butyl radical, the selected kinetic parameters are taken from the experimental work performed by Lenhardt et al. [93]. The hydrogen atom abstraction to produce hydroperoxy radicals and olefin was already included in the high-temperature mechanism. The kinetic parameters used were proposed by Baker et al. [94] and were calculated at a temperature of 753 K and 0.67 bar.

4.3.2 Reaction of the Alkylperoxy Radicals RO₂

There are several reactions reported that could occur with the alkylperoxy radicals





The dissociation of the alkylperoxy radical in alkyl and oxygen is the back-reaction of the reversible Reaction (4-8), and it becomes more important in the temperature range of 700 K - 800 K. For higher hydrocarbons, the internal hydrogen abstraction Reaction (4-11) prevails. The internal abstraction drives the formation of stable products as cycle compounds and aldehydes. The radical isomerization chain can be described as follows:



Once the alkylhydroperoxide is decomposed, OH radicals that are being formed proceed to the unselective attack of the fuel. Table 4.2 presents the kinetic parameters used for the internal hydrogen abstraction.

Table 4.2 Arrhenius parameters for the internal H abstraction $\text{RO}_2^* \rightarrow \text{QOOH}^*$. Kojima[78]
(A in $\text{cm}^3 \text{mol}^{-1} \text{s}^{-1}$, E_a in kJ mol^{-1})

| $\text{C}_3\text{H}_7\text{O}_2^*$ | $A/n/E_a$ | $\text{C}_4\text{H}_9\text{O}_2^*$ | $A/n/E_a$ |
|------------------------------------|--------------------------------|------------------------------------|--------------------------------|
| 2→1 | $1.39 \cdot 10^{12}/0.0/118.0$ | 2→1 | $1.39 \cdot 10^{12}/0.0/118.0$ |
| 3→1 | $2.60 \cdot 10^{11}/0.0/110.0$ | 3→1 | $1.73 \cdot 10^{11}/0.0/92.0$ |
| 1,3→2 | $4.16 \cdot 10^{12}/0.0/138.0$ | 4→1 | $3.26 \cdot 10^{10}/0.0/91.0$ |
| | | 1→2 | $2.00 \cdot 10^{12}/0.0/138.0$ |
| | | 3→2 | $1.39 \cdot 10^{12}/0.0/118.0$ |
| | | 4→2 | $2.60 \cdot 10^{11}/0.0/110.0$ |

The internal hydrogen abstraction (Reaction (4-11)) is a reversible reaction and hence the reverse isomerization of hydroperoxyalkyl radical can compete with its decomposition and further oxidation. The estimated values for the kinetic data for the isomerization had been reported by Pollard [88], Fish [95] and Baldwin et al. [96]. Nehse [82] proposed a pre-exponential factor for the back reaction similar to the one for the forward reaction and an activation energy of 33 kJ mol^{-1} lower, considering that an OH bond in the hydroperoxy group is 33 kJ mol^{-1} weaker than in a CH bond considering the kinetic parameters from Fish and Pollard. After a review of the early proposed values from Baldwin, Kojima [80] proposed the kinetic values used here; they are presented in Table 4.3.

The external H abstraction is the other reaction channel that is considered (Reactions (4-12) and (4-13)). In the low temperature regime, it is common to consider only HO_2 radicals and the fuel as H atom donors because of the lower alkane concentration at these conditions, although for the case of rich mixtures, high concentration of radical species are expected to be present in the intermediate stage of the reaction. Wilk et al. [84] include in their work on ethene and propene oxidation at low temperature the H atom abstraction by smaller alkanes and radical species. Their proposed kinetic data for reactions that include those radicals were applied here. Table 4.4 presents a summary of them.

Table 4.3 Arrhenius parameters for the reverse internal H abstraction $QOOH^* \rightarrow RO_2^*$. Kojima [78-80]. (A in $cm^3 mol^{-1} s^{-1}$, E_a in $kJ mol^{-1}$)

| $C_3^*OOH^*$ | $A/n/E_a$ | $C_4^*OOH^*$ | $A/n/E_a$ |
|--------------|----------------------------------|--------------|----------------------------------|
| 1→2 | $2.98 \cdot 10^{09}/-0.044/63.8$ | 1→2 | $2.99 \cdot 10^{04}/63.9$ |
| 1→3 | $1.04 \cdot 10^{09}/-0.095/41.5$ | 1→3 | $3.74 \cdot 10^{08}/0.044/37.9$ |
| 2→1,3 | $2.22 \cdot 10^{10}/-0.138/69.6$ | 1→4 | $1.30 \cdot 10^{08}/-0.095/22.5$ |
| | | 2→3 | $3.81 \cdot 10^{09}/0.01/63.9$ |
| | | 2→1 | $1.06 \cdot 10^{10}/-0.131/69.6$ |
| | | 2→4 | $1.33 \cdot 10^{09}/-0.131/41.6$ |

Table 4.4 Arrhenius parameters for the external H abstraction: $RO_2^* + RH \rightarrow ROOH + R^*$. Wilk [84] (A in $cm^3 mol^{-1} s^{-1}$, E_a in $kJ mol^{-1}$)

| $C_3H_7O_2$ | Primary Position | | | Secondary Position | | |
|---------------|----------------------|-----|-------|----------------------|-----|--------|
| | A | n | E_a | A | n | E_a |
| +radical | $1.00 \cdot 10^{12}$ | 0.0 | 42.0 | $1.00 \cdot 10^{12}$ | 0.0 | 42.0 |
| + C_2H_4 | $7.10 \cdot 10^{11}$ | 0.0 | 104.5 | $7.10 \cdot 10^{11}$ | 0.0 | 104.50 |
| + C_3H_6 | $3.20 \cdot 10^{11}$ | 0.0 | 62.28 | $3.20 \cdot 10^{11}$ | 0.0 | 62.28 |
| + C_3H_8 | $6.00 \cdot 10^{12}$ | 0.0 | 81.0 | $6.00 \cdot 10^{12}$ | 0.0 | 71.20 |
| + C_4H_{10} | $1.68 \cdot 10^{13}$ | 0.0 | 85.50 | $1.12 \cdot 10^{13}$ | 0.0 | 74.00 |
| $C_4H_9O_2$ | | 0.0 | | | 0.0 | |
| +radical | $1.00 \cdot 10^{12}$ | 0.0 | 42.0 | $1.00 \cdot 10^{12}$ | 0.0 | 42.0 |
| + C_2H_4 | $7.10 \cdot 10^{11}$ | 0.0 | 104.5 | $7.10 \cdot 10^{11}$ | 0.0 | 104.50 |
| + C_3H_6 | $3.20 \cdot 10^{11}$ | 0.0 | 62.28 | $3.20 \cdot 10^{11}$ | 0.0 | 62.28 |
| + C_4H_{10} | $1.68 \cdot 10^{13}$ | 0.0 | 85.50 | $1.12 \cdot 10^{13}$ | 0.0 | 74.00 |

Disproportion reactions (like Reaction (4-14)) are important in the low temperature regime because under the right experimental conditions (e.g., higher oxygen concentration, high pressure) they represent an important path that precedes the termination step, which leads to the formation of acetaldehyde and alcohol. The kinetic mechanism is as follows:



Pollard [88] reported the kinetic data at 600 K for the disproportion reaction of methylperoxy radicals calculated by Heicklen [97]. Propylperoxy radicals disproportionations were experimentally studied by Adachi et al. [98] at 298 K and low pressure (0.49 bar). Others authors (Wallington et al. [99], Atkinson et al. [90], Lightfoot et al. [100]) proposed kinetic parameters for the reaction of propyl peroxides at 298 K which produces oxygen and other unspecified products. Sochet et al. [101] reported the kinetic parameters for the termination step of some alkylperoxy radicals in the C_4 submechanism. Table 4.5 presents the kinetic values that are used in the mechanism where the partner radical RO_2^* is represented by CH_3O_2 , $C_2H_5O_2$ and $C_3H_7O_2$ radicals.

Table 4.5 Arrhenius parameters for the disproportionation reaction: $RO_2^* + RO_2^* \rightarrow 2RO^* + O_2$ Adachi [98]. (A in $\text{cm}^3 \text{mol}^{-1} \text{s}^{-1}$, E_a in kJ mol^{-1})

| | Primary Position | Secondary Position |
|----------------------|------------------------------|---------------------------------|
| $C_3H_7O_2 + RO_2^*$ | $A/n/E_a$ | $A/n/E_a$ |
| CH_3O_2 | $1.30 \cdot 10^{11}/0.0/0.0$ | $1.30 \cdot 10^{12}/0.0/42.00$ |
| $C_2H_5O_2$ | $1.30 \cdot 10^{11}/0.0/0.0$ | $1.00 \cdot 10^{11}/0.0/104.50$ |
| $C_3H_7O_2$ | $1.30 \cdot 10^{11}/0.0/0.0$ | $1.00 \cdot 10^{11}/0.0/62.28$ |

4.3.3 Scission of the Alkylhydroperoxide RO_2H

The alkylhydroperoxy that is formed by external H atom abstraction is decomposed by the splitting of the O-O bond from the hydroperoxy group into OH radical and an alkoxy radical (RO^*),



This is a chain-branching reaction which produces the highly reactive OH radical, although several studies (Pollard [88], Fish [95] and Antonik and Lucquin [102]) showed that at very low temperatures (near to room temperature) and pressures ($p < 265$ mbar) this branch reaction is somewhat slower than the internal H atom abstraction. Therefore, the rate of production of the branching agent is slower in comparison to the rate of formation for other products.

Some kinetic data have been proposed for alkylhydroperoxides decomposition in the C_4 sub-system [103, 104]. In these studies the activation energy varies between 158 kJ mol^{-1} and $170.12 \text{ kJ mol}^{-1}$, with a pre-exponential factor of 10^{13} s^{-1} . Pollard [88] proposed a range for a C_nH_{2n+1} type alkylhydroperoxide between $179.74 \text{ kJ mol}^{-1}$ and $183.92 \text{ kJ mol}^{-1}$, with a pre-exponential factor of 10^{15} s^{-1} .

In the specific case of the C_3 and C_4 radicals, for the scission into OH radicals there are experimental and theoretical kinetic data for their decomposition: In the range of temperatures around $553 \text{ K} < T < 653 \text{ K}$ Kirk and Knox [104] proposed a value for the rate coefficient of $1.58 \cdot 10^{+15} \exp(167 \text{ kJ/mol}^{-1}/RT) \text{ cm}^3 \text{ mol}^{-1} \text{ s}^{-1}$ which must be considered with an uncertainty factor of 2; Sahetchian et al. [105] gave a value of $0.83 \cdot 10^{+15} \exp(179 \text{ kJ/mol}^{-1}/RT) \text{ cm}^3 \text{ mol}^{-1} \text{ s}^{-1}$ for this reaction and Konnov proposed a value of $4.00 \cdot 10^{+15} \exp(179.7 \text{ kJ/mol}^{-1}/RT) \text{ cm}^3 \text{ mol}^{-1} \text{ s}^{-1}$. Here, the values used are the ones proposed by Sahetchian. Table 4.6 presents the values used for the decomposition reaction of alkylhydroperoxide radical.

Table 4.6 Arrhenius parameters for the decomposition of hydroperoxides: $RO_2H \rightarrow RO^* + O$. Sahetchian [105]. (A in $\text{cm}^3 \text{mol}^{-1} \text{s}^{-1}$, E_a in kJ mol^{-1})

| $RO_2H \rightarrow RO^* + OH$ | | $RO_2H \rightarrow RO^* + OH$ | |
|-------------------------------|--------------------------------|-------------------------------|--------------------------------|
| $C_3 \text{ O}_2H$ | $A/n/E_a$ | $C_4 \text{ O}_2H$ | $A/n/E_a$ |
| p-C3H7OOH | $1.10 \cdot 10^{16}/0.0/182.0$ | p-C4H9OOH | $7.00 \cdot 10^{15}/0.0/174.0$ |
| s-C3H7OOH | $8.30 \cdot 10^{14}/0.0/179.0$ | s-C4H9OOH | $1.10 \cdot 10^{16}/0.0/182.0$ |

4.3.4 Scission of the Alkylhydroperoxy Radical QOOH*

The decomposition of the alkylhydroperoxy radical usually leads to a hydroxyl radical formation and stable products which include O-heterocycles, carbonyl compounds and alcohols. The alkylhydroperoxy radical can be consumed by three channels: Self-decomposition into a heterocyclic and OH radical (4-19), loss of the hydroperoxy group and production of an olefin and hydroperoxy (4-20) or reaction with oxygen in a second oxygen addition (4-21),



The simple decomposition of a hydroperoxyalkyl radical to an O-heterocycle with elimination of OH is an irreversible unimolecular process [88] with an activation energy of approximately $62.70 \text{ kJ mol}^{-1}$ to $75.24 \text{ kJ mol}^{-1}$ according to the reported data from Benson [106], and a pre-exponential factor of 10^{11} s^{-1} . Kojima [78] modeled the autoignition of butane at low temperature using the original literature by Hindmarsh [107], who proposed for the same channel a pre-exponential factor of $1.3 \cdot 10^{10} \text{ s}^{-1}$ and an activation energy of 65.5 kJ mol^{-1} . The scission of the hydroperoxy radical is a characteristic path that has been observed in cool flames and especially in the range of temperature of 568 K - 678 K where oxirane and alkenes are the primary products. Table 4.7 presents the kinetic data for the decomposition and the scission of the hydroperoxyalkyl radical.

Table 4.7: Arrhenius parameters for the decomposition of hydroperoxyalkyl QO_2H^* radical: $\text{QO}_2\text{H}^* \rightarrow \text{QO} + \text{OH}$. Kojima [78]

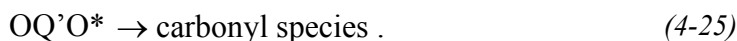
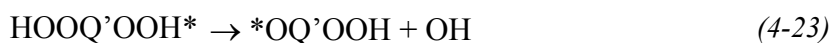
| $\text{C}_3\text{-O}_2\text{H}^* \rightarrow \text{QO} + \text{OH}$ | $A/n/E_a$ | $\text{C}_4\text{-O}_2\text{H}^* \rightarrow \text{QO} + \text{OH}$ | $A/n/E_a$ |
|--|-------------------------------|--|-------------------------------|
| $2\text{C}_3\text{OOH}_1$ | $1.30 \cdot 10^{10}/0.0/65.5$ | $(2,3,4)\text{C}_3\text{OOH}_1$ | $1.30 \cdot 10^{10}/0.0/65.5$ |
| $3\text{C}_3\text{OOH}_1$ | $1.30 \cdot 10^{10}/0.0/65.5$ | $(1,3,4)\text{C}_3\text{OOH}_2$ | $1.30 \cdot 10^{10}/0.0/65.5$ |
| $1\text{C}_3\text{OOH}_2$ | $1.30 \cdot 10^{10}/0.0/65.5$ | | |
| $\text{C}_3\text{-O}_2\text{H}^* \rightarrow \text{C}_3^- + \text{HO}_2$ | $A/n/E_a$ | $\text{C}_4\text{-O}_2\text{H}^* \rightarrow \text{C}_4^- + \text{HO}_2$ | $A/n/E_a$ |
| $2\text{C}_3\text{OOH}_1$ | $2.00 \cdot 10^{13}/0.0/83.8$ | $2\text{C}_4\text{OOH}_1$ | $2.00 \cdot 10^{13}/0.0/83.8$ |
| $1\text{C}_3\text{OOH}_2$ | $2.00 \cdot 10^{13}/0.0/83.8$ | $1\text{C}_3\text{OOH}_2$ | $2.00 \cdot 10^{13}/0.0/83.8$ |
| | | $3\text{C}_3\text{OOH}_2$ | $2.00 \cdot 10^{13}/0.0/83.8$ |

Formation of alkenes from the decomposition of the hydroperoxyalkyl (Reaction (4-20)) has been experimentally shown to be an important channel to be considered especially during the oxidation of larger alkanes [108,109] over the temperature range of 568 K - 678 K. Some kinetic parameters have been estimated for the decomposition: The activation energy has been calculated in the range 83.6 kJ mol^{-1} - $104.5 \text{ kJ mol}^{-1}$ and the pre-exponential factor between 10^{13} s^{-1} and $10^{13.7} \text{ s}^{-1}$ [89, 106]. The kinetic expression that was selected is $2.0 \cdot 10^{13} \exp(-83.8 \text{ kJ mol}^{-1}/RT) \text{ cm}^3 \text{ mol}^{-1} \text{ s}^{-1}$.

4.3.5 Oxidation of Hydroperoxyalkyl Radical QOOH*

Further oxidation of hydroperoxyalkyl radicals completes the hydroperoxyalkyl consumption. The oxygen addition reaction (Reaction (4-21)) is important especially at a high oxygen pres-

sure and normally is followed by an internal H abstraction (Reaction 4.22) to yield dihydroperoxide, which decomposes into carbonyl or dicarbonyl compounds,



The sequence of Reactions (4-21) to (4-25) plays an important role in the combustion of hydrocarbons due to the chain branching reactions which produce OH radicals. The oxygen addition reaction is analogous to Reaction (4-8) and is expected to proceed with zero activation energy, and a similar pre-exponential factor ($A = 10^{13} \text{ cm}^3 \text{ mol}^{-1} \text{ s}^{-1}$). Internal H abstraction (Reaction (4-22)) is similar to Reaction (4-11), and similar kinetic data have been used. The first scission of the OH radical in Reaction (4-23) has been modeled with a rate coefficient of $10^9 \exp(-31.4 \text{ kJ mol}^{-1} / RT) \text{ s}^{-1}$ similar to that used for the $QOOH^*$ scission in Reaction (4-19). For the second OH scission, values similar to the ones in Table 4.6 have been used in literature (Nehse [82]). Devush et al. [110] reported experimentally an activation energy of 138 kJ mol^{-1} for the decomposition into products for the propane peroxy acid ($C_3H_6O_3$) with a pre-exponential factor of $1.35 \cdot 10^{13} \text{ s}^{-1}$. The kinetic data reported by Devush were considered for modeling C_3 radicals and the ones used by Nehse for the $OQ'OOH^*$ radicals in the respective C_4 sub-mechanism. The final decomposition of the peroxidized $OQ'O$ radical follows a similar path as the alkoxy radical (RO^*) decomposition in Reaction (4-18). They proceed via β scission of the C-C bond into carbonyl products. The kinetic value used was $2.0 \cdot 10^{13} \exp(-62.8 \text{ kJ mol}^{-1} / RT) \text{ cm}^3 \text{ mol}^{-1} \text{ s}^{-1}$.

4.3.6 Cycle Ether Formation from HO_2 Addition to Alkenes

Cycle ether formation from alkenes has been found to be an important intermediate product during the oxidation of several alkenes in the low temperature regime [66, 84]. In addition to the path described in Figure 4.1, the authors proposed that formation of the cyclic species is due to the direct reaction between the alkene and the hydroperoxy radical to yield hydroxyl and the respective cycle ether species. Table 4.8 presents the kinetic parameters for the alkenes inside the C_4 mechanism that have been used.

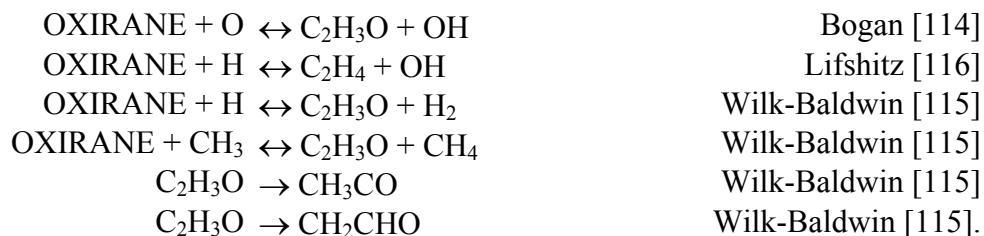
Table 4.8: Arrhenius parameters for the reaction: $C_nH_{2n} + HO_2 \leftrightarrow QO + OH$. (A in $\text{cm}^3 \text{ mol}^{-1} \text{ s}^{-1}$, E_a in kJ mol^{-1})

| Alkene \rightarrow Cycle Ether | $A/n/E_a$ | |
|----------------------------------|------------------------------|---------------------------|
| $C_2H_4 \rightarrow$ Oxirane | $3.79 \cdot 10^{12}/0/74.74$ | Codata2005 [111] |
| $C_3H_6 \rightarrow$ 2Moxi | $1.09 \cdot 10^{12}/0/59.31$ | Baldwin et al. [112] |
| $1-C_4H_8 \rightarrow$ 2-3 Moxi | $4.71 \cdot 10^{11}/0/49.90$ | Stothard and Walker [113] |
| $2-C_4H_8 \rightarrow$ 2-3 Moxi | $4.71 \cdot 10^{11}/0/49.90$ | Stothard and Walter [113] |

4.3.7 Cycle Ether Decomposition

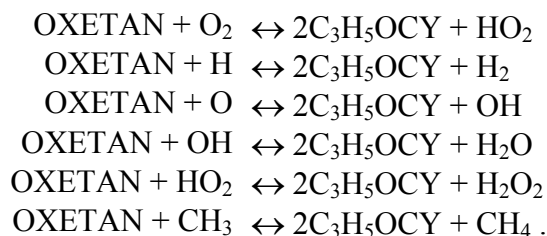
From the original scheme shown in Figure 4.1, there are some missing paths that describe the further O heterocyclic reactions which lead to their decomposition or to the formation of other products. Since cyclical ethers are expected as major intermediate species during the low temperature oxidation of alkanes and alkenes, it is necessary to incorporate those reactions that take into account their consumption. From the literature there are three main routes reported which describe the cyclical ether consumption: Self-decomposition, isomerization and external H atom abstraction. The main O heterocycles that are included in the mechanism are presented in Table 4.10.

The consumption of the cyclical ether formed in the ethane sub-mechanism (oxirane, C₂H₄O) was modeled with the kinetic data from the studies of Bogan and Hand [114], Baldwin et al. [115] and Lifshitz and Ben [116]. The oxiranyl (C₂H₃O) that is formed decomposes to carbon monoxide and aldehyde, the reactions are as follows:



The kinetic values for the isomerization or decomposition of C₂H₃O are however still unclear. Chen et al. [117] proposed for the isomerization to CH₂CHO a value for $k = 2 \cdot 10^4 \text{ s}^{-1}$, Wilk et al. [66] proposed an activation energy of 58 kJ mol⁻¹ for both isomerization channels and Baldwin [115] proposed a ratio between the rate coefficients of 8.55. The kinetic parameters used in this study consider the values for the activation energy for both reactions according to Wilk, and a pre-exponential factor of $1 \cdot 10^{14} \text{ s}^{-1}$ with the ratio between the channels of 8.55 proposed by Baldwin.

A similar approach was made for the cyclical ether in the C₃ system (Oxetan, C₃H₆O). An external abstraction of hydrogen was implemented with kinetics parameters taken from Duke and Holbrook [118]:



The radicals that are formed proceed to decompose into olefins (C₂H₄, C₃H₆) or into oxygenated species (CHO, CH₂O, CH₃CHO) according to the kinetic parameters given by Warth [34].

For the C₄ sub-mechanism, different possible heterocyclic species are expected: 2,3-Dimethyloxirane (2-3MOXI), Tetrahydrofuran (THF) or Ethyloxirane (2EOXI).


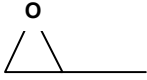

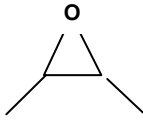
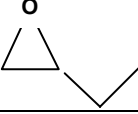
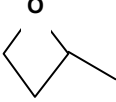
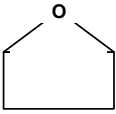
Each one of these species can be formed by the reaction of $2 \text{ C}_4\text{H}_9 + \text{O}_2 \leftrightarrow \text{OH} + 2\text{-3MOXI}$,

(THF or 2EOXI), or through the previously described mechanism illustrated in Figure 4.1. For the first reaction channel (butyl radical and oxygen reactions), the kinetic parameters used are taken from Baker et al. [119] and are presented in Table 4.9.

Table 4.9: Arrhenius parameters for the reaction: $2 C_4H_9 + O_2 \leftrightarrow OH + QO$. Baker [119]
(A in $cm^3 mol^{-1} s^{-1}$, E_a in $kJ mol^{-1}$)

| $2 C_4H_9 + O_2$ | $A/n/E_a$ |
|----------------------------|-----------------------------|
| \rightarrow 2-3 MOXI | $1.042 \cdot 10^{10}/0/0.0$ |
| \rightarrow THF | $2.601 \cdot 10^{10}/0/0.0$ |
| \rightarrow Ethyloxirane | $1.198 \cdot 10^{09}/0/0.0$ |

Table 4.10: O-Heterocyclic in the C_4 mechanism

| | Cycle species | |
|-------|-----------------------------|---|
| C_2 | Oxirane |  |
| C_3 | 2 Moxi Methyloxirane |  |
| | Oxetan |  |
| C_4 | 2-3 Moxi Dimethyloxirane |  |
| | 2 Eoxi Ethyloxirane |  |
| | 2 Moxe |  |
| | THF Tetrahydrofuran |  |

The self-decomposition that has been included for each of the cyclical ethers is as follows: Dimethyloxirane will decompose to propylene and formaldehyde. The kinetic data are the

ones from Zalatoi et al. [120]. Tetrahydrofuran decomposes to propylene and ethylene or to ethylene and oxirane, the kinetic data are from Lifshitz et al. [121]. Ethyloxirane will lead to propylene and formaldehyde and was modeled with Zalatoi's [120] data. Figure 4.2 shows the additional steps that have been included for the C₄ mechanism, including the direct formation of cyclical ether from olefins, decomposition of cyclical compounds and direct formation of O-cyclical ether from alkyl radicals.

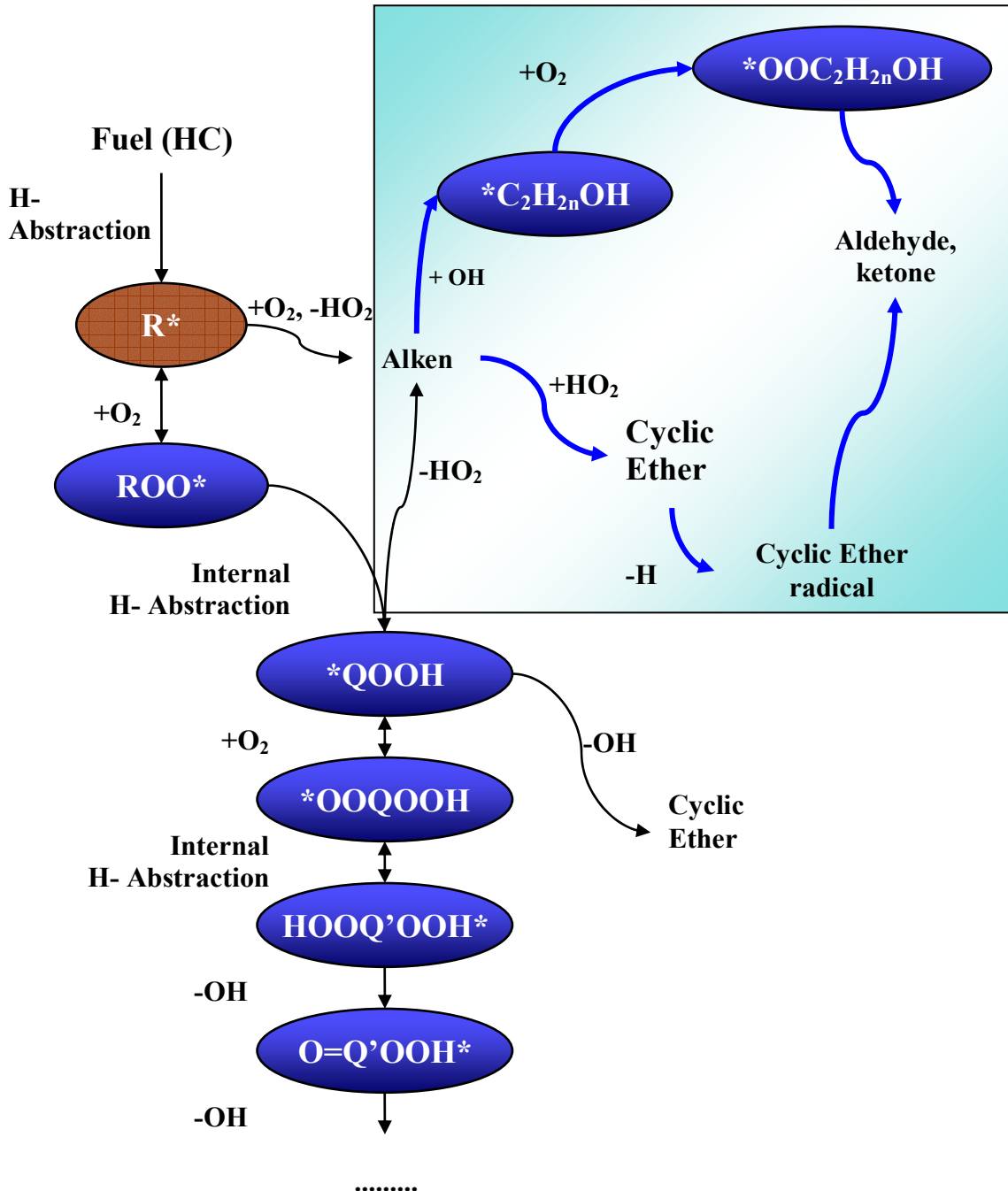


Figure 4.2: Schematic mechanism for the combustion of hydrocarbons at 500 K – 800 K, including additional steps proposed in [66]. Blue zone represents the new paths considered: Hydroxyl addition to the olefin, decomposition of the hydroperoxy radical into olefin, and ether formation via HO₂ addition to the olefin $R = C_nH_{2n+1}$; $Q = C_nH_{2n}$; $Q' = C_nH_{2n-1}$

4.4 High Temperature Oxidation

To understand the chemistry that occurs in flames it is most important to focus on processes that take place at temperatures above 1000 K. At this temperature, the products are alkyl radicals, alkene and C_1 and C_2 species. The high temperature oxidation of alkanes is characterized by an initial thermal decomposition of the fuel and abstraction of H atoms from the fuel molecules, forming radicals that fragment and react in various ways to give smaller olefins and partially oxidized carbon containing species [122]. Figure 4.3 shows the scheme for the combustion of alkanes in the high temperature regime.

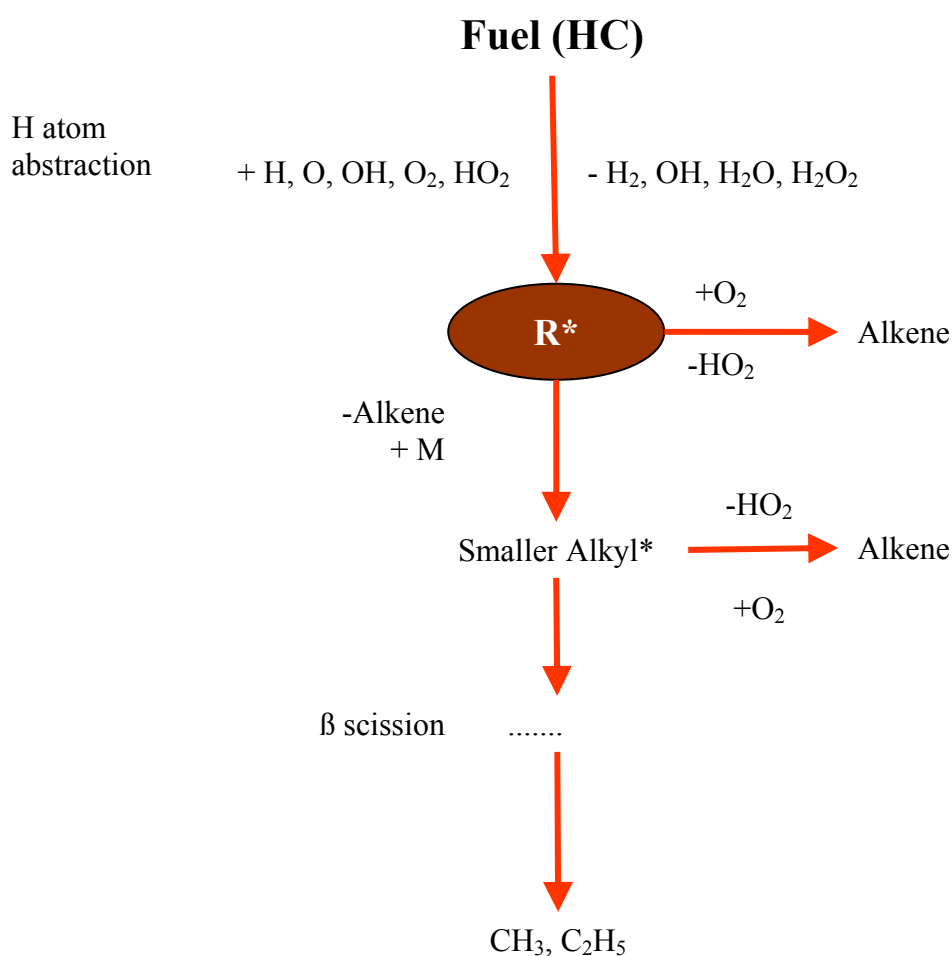


Figure 4.3: Schematic mechanism for the combustion of hydrocarbons at high temperature

4.4.1 Reaction of Alkanes

The initial reaction during the combustion of alkanes at high temperature involves the abstraction of an H atom from the fuel through a reactive radical species or molecule. Main radical species are H, O, OH, and HO₂ and methyl radical CH₃. The reaction of the alkane and the reactive species is as follows:



The initial radical attack is not selective and all the possible isomeres appear in the products. The radical position is different and depends from the C-H bond which is broken: For a C-H primary bond the activation energy is higher than for a secondary C-H bond, for a C-H secondary bond its activation energy will be higher than for a tertiary C-H bond. The reactivity from the radicals and their concentration play another important role: OH radicals are more reactive than others like CH₃, and the rate coefficient should include this effect. In Annex 1 the reactions that have been included in the mechanism and their respective reference are listed. The mechanism includes initial radical abstraction for the species: H, O, OH, HO₂, CH₃, CH₃O, CHO, CH₃CO, CH₃O₂ and C₃H₅.

Besides the H atom abstraction, self-decomposition of alkanes is another important path in the initial stages of the oxidation, when the radical species concentration is low. There are two possible decomposition reactions for the alkanes,



For propane, its decomposition into smaller alkyl radicals leads to methyl and ethyl radical formation. The kinetic data for these reactions have been taken from Baulch et al. [26]. In the butane case decomposition leads to two different reactions: In the first one, two ethyl radicals are produced [26], for the second reaction, methyl and propyl radicals are the products [123]. The H atom abstraction, which produces propyl radicals for the propane case and butyl from butane, is modeled using the kinetic values calculated by Dean [124]. Table 4.11 lists the values used for each reaction in the C₃ and C₄ sub-mechanism.

Table 4.11: Arrhenius parameters for the decomposition $RH \rightarrow R^* + R'^*$; and $RH \rightarrow R^* + H$. (A in $cm^3 mol^{-1} s^{-1}$, E_a in $kJ mol^{-1}$)

| $C_3H_8 \rightarrow R^* + R'^*$ | $A/n/E_a$ | $C_4H_{10} \rightarrow R^* + R'^*$ | $A/n/E_a$ |
|---------------------------------|-------------------------------------|------------------------------------|------------------------------------|
| $CH_3 + C_2H_5$ | $1.10 \cdot 10^{17} / 0.0 / 352.10$ | $CH_3 + C_3H_7$ | $1.00 \cdot 10^{17} / 0.0 / 357.9$ |
| | | $C_2H_5 + C_2H_5$ | $3.62 \cdot 10^{16} / 0.0 / 344.8$ |
| | | | |
| $C_3H_8 \rightarrow R^* + H$ | $A/n/E_a$ | $C_4H_{10} \rightarrow R^* + H$ | $A/n/E_a$ |
| $n C_3H_7$ | $1.58 \cdot 10^{16} / 0.0 / 408.24$ | $1 C_4H_9$ | $9.51 \cdot 10^7 / 0.0 / 409.0$ |
| $s C_3H_7$ | $6.31 \cdot 10^{15} / 0.0 / 396.60$ | $2 C_4H_9$ | $6.023 \cdot 10^7 / 0.0 / 397.4$ |

4.4.2 Reaction of the Alkyl Radical

At high temperature alkyl radicals have a thermal decomposition which produces small radicals and alkenes due to the breaking of the C-C bond at the radical position. Alternatively they can decompose due to the breaking of the C-H bond, producing an alkene and an H atom,



The kinetic parameters used for this group of reactions are presented in Table 4.12.

Due to the rich conditions that prevail during the partial oxidation process, there are a significant number of radical species which could be present in the reacting mixture. These species can react additionally, and it is necessary to take their reaction into account. Reactions between the parent alkyl from the fuel with methyl, ethyl, propyl and butyl radicals are incorporated. The kinetic data used for these reactions are from Tsang [60, 61]. Annex I presents all the additional reactions that were included in the final mechanism.

Table 4.12 Arrhenius parameters for the decomposition of alkyl radical $R^* \rightarrow R^* + \text{Alkene}$, and $R^* \rightarrow H + \text{Alkene}$. Annex I includes references used for those reactions. (A in $\text{cm}^3 \text{mol}^{-1} \text{s}^{-1}$, E_a in kJ mol^{-1})

| C₃ | | C₄ | |
|---|-------------------------------------|--|------------------------------------|
| Propyl \rightarrow R*+C₂H₄ | A / n / E_a | Butyl \rightarrow R*+Alken | A / n / E_a |
| $n\text{-C}_3\text{H}_7 \rightarrow \text{CH}_3 + \text{C}_2\text{H}_4$ | $1.05 \cdot 10^{13} / 0.0 / 127.08$ | 1 $\text{C}_4\text{H}_9 \rightarrow \text{C}_2\text{H}_5 + \text{C}_2\text{H}_4$ | $3.00 \cdot 10^{13} / 0.0 / 120.6$ |
| $s\text{-C}_3\text{H}_7 \rightarrow \text{CH}_3 + \text{C}_2\text{H}_4$ | $2.00 \cdot 10^{10} / 0.0 / 123.50$ | 1 $\text{C}_4\text{H}_9 \rightarrow \text{CH}_3 + \text{C}_3\text{H}_6$ | $1.26 \cdot 10^{12} / 0.0 / 113.1$ |
| | | 2 $\text{C}_4\text{H}_9 \rightarrow \text{CH}_3 + \text{C}_3\text{H}_6$ | $3.60 \cdot 10^{14} / 0.0 / 139.0$ |
| Propyl \rightarrow H+C₃H₆ | A / n / E_a | Butyl \rightarrow H+Alken | A / n / E_a |
| $n\text{-C}_3\text{H}_7 \rightarrow \text{H} + \text{C}_3\text{H}_6$ | $1.26 \cdot 10^{13} / 0.0 / 161.30$ | 1 C_4H_9 | $1.26 \cdot 10^{13} / 0.0 / 161.6$ |
| $s\text{-C}_3\text{H}_7 \rightarrow \text{H} + \text{C}_3\text{H}_6$ | $1.07 \cdot 10^{11} / 1.16 / 161.2$ | 2 $\text{C}_4\text{H}_9 \rightarrow 1 \text{C}_4\text{H}_8$ | $2.00 \cdot 10^{13} / 0.0 / 169.2$ |
| | | 2 $\text{C}_4\text{H}_9 \rightarrow 2 \text{C}_4\text{H}_8$ | $5.00 \cdot 10^{13} / 0.0 / 158.7$ |

At temperatures around 1000 K, reactions between alkyl radicals and oxygen, which produce alkenes and HO_2 , are faster than the oxygen addition to the radical (which prevails at low temperature). The hydrogen abstraction reaction, which produces hydroperoxy radicals, is the main reaction which leads to the build-up of HO_2 concentration, and which will produce OH after recombination and further decomposition. For this reaction Tsang [61], Slagle et al. [91] and others proposed an activation energy of zero (0) and a pre-exponential factor of around $5 \cdot 10^{10} \text{ cm}^3 \text{ mol}^{-1} \text{ s}$. Cathonnet et al. [56] proposed for the same path an activation energy between 8.4 and 24 kJ mol^{-1} and a pre-exponential factor of $10^{12} \text{ cm}^3 \text{ mol}^{-1} \text{ s}$. The kinetic data used for reactions between alkyl radicals and oxygen are presented in Table 4.13.

Table 4.13: Arrhenius parameters for the alkyl radical and oxygen reaction $R^* + \text{O}_2 \rightarrow \text{HO}_2 + \text{Alken}$. Annex I includes the references. (A in $\text{cm}^3 \text{mol}^{-1} \text{s}^{-1}$, E_a in kJ mol^{-1})

| C₃H₇+O₂ | | C₄H₉+O₂ | |
|---|------------------------------------|---|-----------------------------------|
| \rightarrowHO₂+Alken | A / n / E_a | \rightarrowHO₂+Alken | A / n / E_a |
| $n\text{-C}_3\text{H}_7$ | $1.00 \cdot 10^{12} / 0.0 / 20.00$ | 1 C_4H_9 | $1.00 \cdot 10^{12} / 0.0 / 8.4$ |
| $s\text{-C}_3\text{H}_7$ | $1.00 \cdot 10^{12} / 0.0 / 20.00$ | 2 C_4H_9 | $2.00 \cdot 10^{13} / 0.0 / 18.4$ |

4.4.3 Reaction of Alkenes

At high temperature alkenes can be decomposed thermally by the scission of the double bond. They can be attacked by radical species, mainly OH, O, H, and HO_2 or react with oxygen and other small radicals like methyl, ethyl or propyl. There are several studies which report the kinetic parameters for the decomposition of alkenes. Karbach's [33] mechanism already described the kinetic values used for high temperature combustion for C_2H_4 , C_3H_6 , and C_4H_8 species. Here, there are two additional decomposition paths which were included for propylene based on the studies from Hidaka et al. [125] and Barbe et al. [126]. In both cases stable products (CH_4 , C_2H_2 , and H_2 , C_3H_4) are obtained.

There are three additional reactions between ethylene and radicals that have been implemented: Initially oxygen, hydromethyl and methoxy attack the fuel, producing hydroperoxy and vinyl radicals ($C_2H_4 + O_2 \rightarrow HO_2 + C_2H_3$), methanol and vinyl radicals ($C_2H_4 + CH_2OH \rightarrow CH_3OH + C_2H_3$), and formaldehyde and ethyl radicals ($C_2H_4 + CH_3O \rightarrow CH_2O + C_2H_5$). The first of these reactions is an important initiation reaction at low and intermediate temperatures. The second abstraction reaction is the main methanol formation step at low temperature oxidation. The last abstraction is an alternative path for formaldehyde formation. The bibliographic references for these reactions were taken from Tsang [53] and their importance increases for ethene combustion in the intermediate temperature regime ($T \sim 700$ K).

For the other alkenes (C_3H_6 , C_4H_8) no further changes were made with respect to the original mechanism proposed by Karbach, who was following the kinetic scheme proposed by Cathonnet [56].

4.4.4 Reaction of Aldehydes

Aldehydes are decomposed after a hydrogen atom abstraction. The abstraction occurs at the aldehyde hydrogen atom position, and is due to radical species like O, OH, O_2 , HO_2 , and CH_3 . For each of the aldehydes included in the mechanism there are additional reactions which were added: For ethyl aldehyde (CH_3CHO), the proposed value for the H atom abstraction by methyl radicals which yield CH_2CHO and CH_4 from Berces [127] was included. Propyl aldehyde (C_2H_5CHO) reactions from Singleton et al. [128], Atkinson et al. [90] and Baldwin and Walker [96] were considered. For butyl aldehyde (C_3H_7CHO) the proposed reactions from Singleton et al., Baldwin et al. [129] and Birrell and Trotman [130] were implemented. Table 4.14 presents the reactions and the kinetic values used in the mechanism.

Table 4.14: Arrhenius parameters for the aldehydes reactions. (A in $cm^3 mol^{-1} s^{-1}$, E_a in $kJ mol^{-1}$)

| $CH_3CHO + R^* \rightarrow$ | $A/n/E_a$ | Reference |
|---|-------------------------------|----------------------|
| $CH_3 \rightarrow CH_2CHO + CH_4$ | $1.58 \cdot 10^{00}/4.0/32.0$ | Berces [127] |
| $C_2H_5CHO + R^* \rightarrow$ | | |
| $O \rightarrow C_2H_5CO + OH$ | $5.68 \cdot 10^{12}/0.0/6.43$ | Singleton [128] |
| $H \rightarrow C_2H_5CO + H_2$ | $9.38 \cdot 10^{06}/0.0/32.2$ | Singleton [128] |
| $OH \rightarrow C_2H_5CO + H_2O$ | $1.21 \cdot 10^{13}/0.0/0.0$ | Atkinson [90] |
| $HO_2 \rightarrow C_2H_5CO + H_2O_2$ | $1.52 \cdot 10^{09}/0.0/0.0$ | Baldwin [96] |
| $CH_3 \rightarrow C_2H_5CO + CH_4$ | $2.20 \cdot 10^{11}/0.0/48.6$ | Atkinson [90] |
| $CH_3O_2 \rightarrow C_2H_5CO + CH_3O_2H$ | $2.20 \cdot 10^{12}/0.0/42.0$ | Atkinson [90] |
| $C_3H_7CHO + R^* \rightarrow$ | | |
| $O \rightarrow i C_3H_7CO + OH$ | $7.16 \cdot 10^{12}/0.0/5.81$ | Singleton [128] |
| $O \rightarrow n C_3H_7CO + OH$ | $6.20 \cdot 10^{12}/0.0/5.97$ | Singleton [128] |
| $O_2 \rightarrow i C_3H_7CO + HO_2$ | $1.20 \cdot 10^{02}/0.0/0.0$ | Baldwin et al. [131] |
| $HO_2 \rightarrow i C_3H_7CO + H_2O_2$ | $1.80 \cdot 10^{09}/0.0/0.0$ | Baldwin et al. [129] |
| $HO_2 \rightarrow n C_3H_7CO + H_2O_2$ | $2.40 \cdot 10^{09}/0.0/0.0$ | Baldwin et al. [129] |
| $CH_3 \rightarrow i C_3H_7CO + CH_4$ | $3.98 \cdot 10^{12}/0.0/40.9$ | Birrl-Trotman [130] |
| $CH_3 \rightarrow n C_3H_7CO + CH_4$ | $6.32 \cdot 10^{11}/0.0/30.5$ | Birrl-Trotman [130] |

4.5 Mechanism Base

The high temperature mechanism of Karbach [33] was complemented by adding reactions paths characteristic for the low and intermediate temperature regime. The additional set of reactions used includes the paths already described in Section 4.3 for propane and butane. Additional reactions, which were not automatically generated, have been added for ethene, propene and normal butene mechanisms following the studies from Wilk et al. [66, 84] on combustion of small olefins (Section 4.3.6). Here, the original mechanism for C₁ and C₂ will be described and some further changes that were made will be presented.

Originally, the mechanism was developed by Chevalier [32]. An update from this mechanism was made by Karbach using newly known kinetic and thermodynamic data which had been proposed in the literature. The thermodynamic data for HO₂, CH₃, CH₂OH, CH₃O₂H, C₂H₅O, CH₃CHOH, CH₂CHO, C₃H₄ and C₃H₅ were modified with respect to the original ones from Chevalier. Additionally, the mechanism was extended, and new reaction steps that include reactions of consumption-formation for iso-butane were considered.

4.5.1 Mechanism for Hydrogen Oxygen Carbon Monoxide

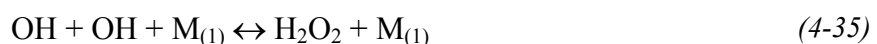
The original mechanism proposed was kept and no further changes were included. The original mechanism includes reactions between H₂ and O₂ species, radical species recombination and reactions to describe formation and consumption for HO₂ and H₂O₂ radicals. During the studies of flame velocities, Karbach reported the following reactions as the most sensitive ones:

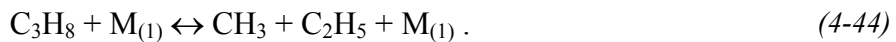
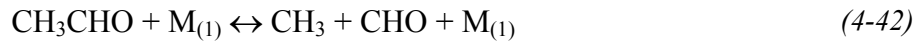
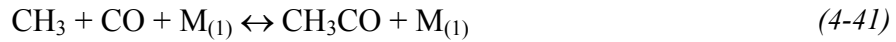
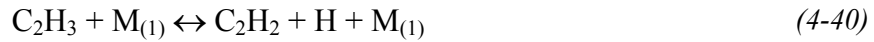
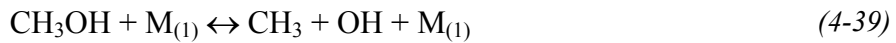
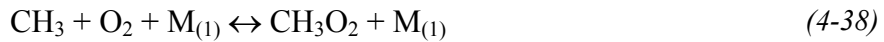
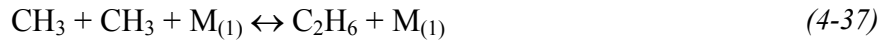


The kinetic data used for these reactions were taken from Baulch et al. [26]. For modeling the pressure-dependent reactions, the Troe formalism was used. Four different sets of coefficients for the collision partners are defined [18]:

| | H ₂ | H ₂ O | O ₂ | AR | N ₂ | CO | CO ₂ | CH ₄ |
|-------------------|----------------|------------------|----------------|------|----------------|------|-----------------|-----------------|
| η _{M(1)} | 1.0 | 6.5 | 0.4 | 0.35 | 0.4 | 0.75 | 1.5 | 3.0 |
| η _{M(2)} | 1.0 | 2.55 | 0.4 | 0.15 | 0.4 | 0.75 | 1.5 | 3.0 |
| η _{M(3)} | 1.0 | 6.5 | 0.4 | 0.29 | 0.67 | 0.75 | 1.5 | 3.0 |
| η _{M(4)} | 1.0 | 6.5 | 0.4 | 0.35 | 0.4 | 0.75 | 1.5 | 0.66 |

Further, pressure-dependent elementary reactions, which are included in the original mechanism, are



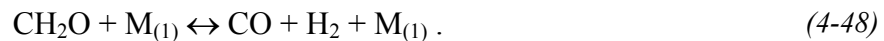
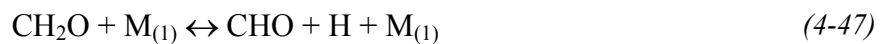


³CH₂ Reactions. Reactions of triple methylene radicals with atom oxygen have two channels:



The kinetic data for these reactions are chosen from recommendations giving by Baulch et al. [24-26], [111]. That report does not include a back reaction for Reaction (4-45).

CH₂O Reactions. Thermal decomposition of formaldehyde occurs via two channels:



According to the kinetic data in Baulch et al. [25-26, 111], for the thermal decomposition the first reaction channel is predominant, $k_{\text{cin}}/k_{\text{tot}} = 0.7$, although both channels have been implemented. Other reactions that occur at high temperature like hydrogen atom abstraction form hydroxyl radicals, methyl or other radical species are predominant in this temperature regime. The kinetic data used for these radical abstractions are taken from Baulch et al. [25-26, 111].

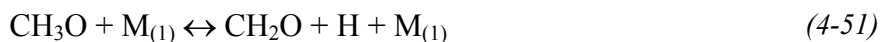
CH₃ Reactions. Oxidation of methyl radical with hydroxyl radicals can occur through two paths:



The rate coefficient used for the first reaction was the one proposed by Sloane [132]. For the second reaction, the kinetic values were changed to the new values proposed by Deters et al. [133]. In rich mixture conditions (such as those in methane partial oxidation), methyl recombination is an important step which describes ethane production. The kinetic values used for these reactions are recommended by Baulch et al. [25-26, 111]. An additional reaction for the recombination of methyl to ethene and hydrogen ($\text{CH}_3 + \text{CH}_3 \leftrightarrow \text{C}_2\text{H}_4 + \text{H}_2$) was included,

even if this reaction is expected to occur only in the high temperature interval. The reference used for the kinetic data of this reaction was taken from the shock-tube experiments carried out by Hidaka et al. [134].

CH₃O Reactions. The high temperature mechanism for methoxy radicals includes the thermal decomposition to formaldehyde and hydrogen atom abstraction through the radical species: Hydroxyl, oxygen atom, hydrogen atom and molecular oxygen. The mechanism is as follows:



In the original mechanism the kinetic data for the reaction with molecular oxygen were given as two separate reactions according to the kinetic data from Baulch et al. [25-26, 111]. The kinetic data for this reaction have been changed, and the experimental kinetic data from Yu et al. [135] have been used. Yu's values are slightly smaller than those recommended in [25-26, 111], but they lie in the tolerance range specified by that report.

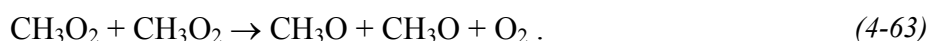
CH₃O₂ Reactions. Two new paths were added to the kinetic mechanism for the reactions of methyl-peroxy radicals:



Both paths are taken from Tsang [53]. The first reaction accounts for methanol formation and the second considers the direct oxidation. The other reactions included are as follows:



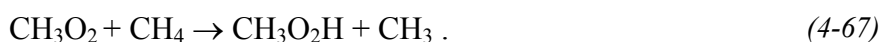
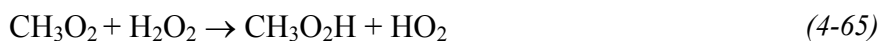
For the first two reactions, the kinetic data from Konnov were chosen. The recommendation from [25-26, 111] was used for the last reaction. The original mechanism includes the disproportion reactions



Recommendations from Baulch et al. [25-26, 111] were implemented for the kinetic values.

CH₃OH Reactions. The original mechanism follows the proposed reaction scheme from Konnov. Only a few changes were made: The reaction between methoxy radicals that produces methanol ($\text{CH}_3\text{O} + \text{CH}_3\text{O} \leftrightarrow \text{CH}_3\text{OH} + \text{CH}_2\text{O}$) has been included (Hassinen and Koskikallio [136]), and the kinetic values for the reaction between methanol and hydroperoxy radicals have been set to the original values as proposed by Tsang [137].

CH₃O₂H Reactions. The mechanism includes the CH₃O₂H self-decomposition to produce methoxy and OH radicals ($\text{CH}_3\text{O}_2\text{H} \leftrightarrow \text{OH} + \text{CH}_3\text{O}$) and hydrogen atom abstraction from hydroxyl radicals ($\text{CH}_3\text{O}_2\text{H} + \text{OH} \leftrightarrow \text{H}_2\text{O} + \text{CH}_3\text{O}_2$). The kinetic data used for these reactions are from the Baulch et al. report [25-26, 111]. Some additional hydrogen atom abstraction reactions were considered. The kinetic values used for this group of reactions were taken from the Tsang [137] mechanism. The reactions included in the mechanism are as follows:

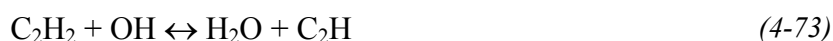


C₂H Reactions. The original mechanism includes three channels for the ethynyl radical consumption: Reaction with oxygen atoms ($\text{C}_2\text{H} + \text{O} \leftrightarrow \text{CO} + \text{CH}$), reaction with methane ($\text{C}_2\text{H} + \text{CH}_4 \leftrightarrow \text{C}_2\text{H}_2 + \text{CH}_3$) and oxidation with molecular oxygen. For this last step there are five different channels which are included in the Baulch et al. report [25-26, 111], although Karbach's mechanism [33] includes only two of them:



The sum of both kinetic values gives the preferred value recommended in that report. The kinetic values for both channels were changed, and the new experimental data available from Thiesemann and Taatjes [138] have been used. There are also new kinetic data available, which have been used for the reaction between the ethynyl and the atomic oxygen. The experimental values from Devriendt and Peeters [139] were chosen.

C₂H₂ Reactions. The kinetic values for the reaction $\text{C}_2\text{H} + \text{H}_2 \leftrightarrow \text{C}_2\text{H}_2 + \text{H}$ have been changed; the experimental values reported by Peeters et al. [140] have been included. The mechanism was completed with the kinetic data from the Baulch et al. reports; the reactions included are as follows:





C₂H₃ Reactions. Reaction between the vinyl radical and oxygen leads to three different channels



Information about the branching ratios is not clear, although the first channel is predominant at low temperature and pressure. But at temperatures above 1400 K the second channel is predominant. The rate expression from Slage and Knyazed [141] was chosen for the first path, and for the branching paths the proposed values from Bozelli and Dean [142] and Mebel et al. [143] were used.

CH₃CO Reactions. A new step (Reaction 4-78) which leads to methyl and formyl radical formation has been included in the mechanism, with kinetic values from Bartels et al. [144]:

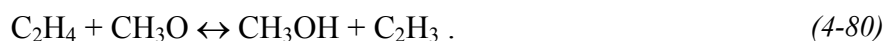


C₂H₄ Reactions. Beside the already described mechanism for ethylene oxide (see Chapters 4.3.6 and 4.3.7), there are some additional steps that have been considered.

The reaction between ethylene and oxygen has four reaction paths. In the original combustion mechanism from Karbach only three of the four reaction paths were included due to the low contribution of the fourth to the product formation. Nevertheless, here the fourth path was also implemented:



During ethene oxidation at low temperature the main initiation reaction involves the reaction of the fuel with oxygen ($\text{C}_2\text{H}_4 + \text{O}_2 \leftrightarrow \text{C}_2\text{H}_3 + \text{HO}_2$). This path has been included in the mechanism. The kinetic data from Tsang and Hampson [53] has been used. Some experimental results [65,145] showed that methanol is one of the more relevant products during ethylene oxidation. Tsang proposed the following path to describe its formation:

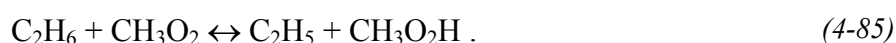
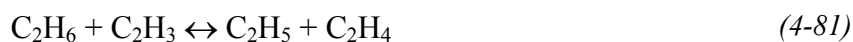


The methyl radical and ethylene reaction rates have been changed, and the kinetic values from Zhang and Back [146] have been used; this value is lower than the one recommended in the Baulch et al. report. Although new experiments (Ahonkhai and Back [147] and Ahankhai et al. [148]) suggest that the values recommended in [25-26, 111] had been overestimated.

C₂H₅ Reactions. In the mechanism for the ethyl radical the kinetic values for the pressure-dependent reaction $\text{C}_2\text{H}_4 + \text{H} + \text{M} \leftrightarrow \text{C}_2\text{H}_5 + \text{M}$ have been modified in order to get a better agreement with the experimental results for species concentration. The pre-exponential value was divided by two, still inside the tolerance range from the kinetic report by Baulch et

al.[111] For the reaction $C_2H_5 + H \leftrightarrow CH_3 + CH_3$, Karbach doubled the kinetic factor. The original value in [25-26, 111] was used.

C₂H₆ Reactions. The ethane mechanism was complemented by including external hydrogen abstraction reactions from the radical species: C₂H₃, CH₃O, C₂H, CHO, and CH₃O₂. The reactions considered are as follows:



The kinetic data for the first reaction was taken from Zhang and Back [146], the others from Tsang [53].

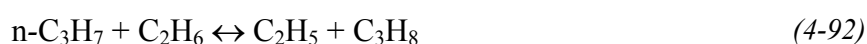
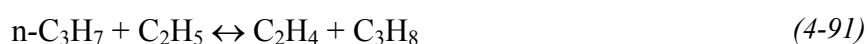
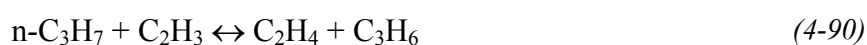
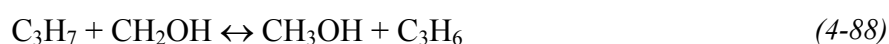
C₃H₅ Reactions. The reaction between the allyl radical and the ethyl radical has been included. There are two different paths expected:



The kinetic values used for the reactions are from Tsang [60].

C₃H₆ Reactions. The original propylene mechanism was completed by including the automatically generated reactions and adding the proposed mechanism from Wilk [66] as described in Sections 4.3.6 and 4.3.7. The high temperature mechanism was completed with some additional reactions. Hidaka [125] proposed two more possible decomposition paths for propylene for modeling shock tube experiments with propene. The first of them leads to methane and acetylene ($C_3H_6 \leftrightarrow CH_4 + C_2H_2$), and the second one to hydrogen and allene ($C_3H_6 \leftrightarrow H_2 + C_3H_4$).

n(i)-C₃H₇ Reactions. The original mechanism from Karbach included only a few reactions for the propyl radical. Therefore, the mechanism was extended by including more reactions. The reactions considered are as follows:

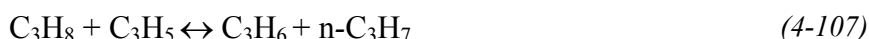
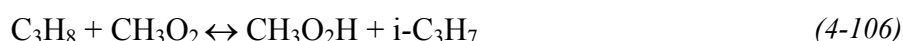
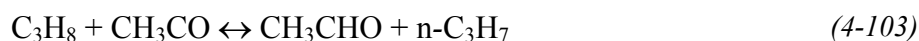
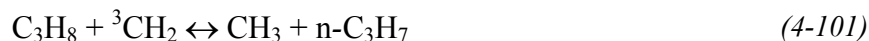
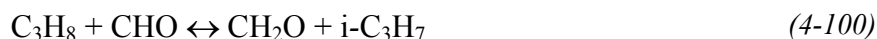
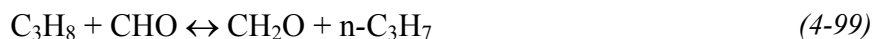




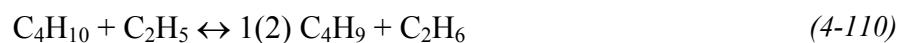
These reactions take into account other additional paths for the formation of olefins and light alkanes during oxidation of C₃ and C₄ alkanes. The described reaction scheme was proposed by Tsang [61]. In a similar way the *i*-C₃H₇ radical mechanism was complemented including its reaction with the same radical species as in the *n*-C₃H₇ case:



C₃H₈ Reactions. The propane mechanism was completed adding further hydrogen atom abstraction reactions that include formaldehyde, methyl and propene formation. Tsang [61] proposed the kinetic data used. Reactions (4-99) to (4-108) present the new channels included:



C₄ Mechanism. The C₄ mechanism for high temperature was complemented by including additional channels reported in the literature: Butyl radical decomposition to olefin and methyl radical was reported by Marshall [149] ($1(2) \text{C}_4\text{H}_9 \leftrightarrow \text{C}_3\text{H}_6 + \text{CH}_3$). Methane formation through hydrogen atom abstraction from butyl radical ($1(2) \text{C}_4\text{H}_9 + \text{CH}_3 \leftrightarrow 1(2) \text{C}_4\text{H}_8 + \text{CH}_4$) was considered by Thynne [150]. Butane decomposition into butyl and hydrogen atom ($\text{C}_4\text{H}_{10} \leftrightarrow 1(2) \text{C}_4\text{H}_9 + \text{H}$) from Dean's work was used [124] (see Section 4.4.1). Hydrogen atom abstraction from vinyl, ethyl and allyl radicals (Reactions (4-109) to (4-111)) from Yampol'skii [151] and Cathonnet [73] were used:



4.6 Thermodynamic Data

Thermodynamic data used are from Chemkin Thermodynamic Database [12], Burcat [152], Konnov [153] and Thergas [154].

Chapter 5

EVALUATION OF THE MECHANISM: SIMULATION OF AUTOIGNITION

Ignition delay time, a characteristic of combustion, is interesting due to its wide range of different practical applications such as in determining the knocking in Otto IC engines, or in the study of combustion in Diesel engines. Autoignition is a spontaneous process, whereby a combustible mixture undergoes chemical reactions leading to the rapid release of energy. The rate of this energy release is sufficient to sustain combustion even in the absence of an external energy source such as a flame or spark [43].

Reasons for studying ignition processes derive from specific objectives: Preventing fire hazards, developing igniters and reproducible energy sources for ignition and combustion, gaining knowledge of the ignitability of a material under given initial conditions, determining minimal energy required for ignition, and gaining knowledge of physical and chemical parameters for ignition delay times.

In the ignition of a fuel-air mixture, a series of physical and chemical processes, which have characteristic times, is combined to form an overall induction or ignition delay time. In early stages, the induction period is probably dominated by physical processes like diffusion, heating, mixing and reactant transport, and at later stages by chemical ones like kinetics.

During ignition, there is a rapid depletion of the primary fuel, very high radical concentrations, and an exponential rise in temperature and pressure. The ignition delay time can be defined as the period between the creation of a combustible mixture and the onset of the rapid reaction phase leading to a rise in temperature and pressure.

Chain-branching reactions result in oxidative decomposition of fuel hydrocarbon species and an increase in the concentration of intermediate free radical species. These radical species are called ignition precursors. They rise to a level where ignition will occur.

The ignition delay time is a readily measurable quantity, that is a function of initial temperature, pressure, composition of the reactant mixture and level of mixing of the reactants. In the low ($T < 750$ K) and high temperature ($T > 1100$ K) ranges, the induction time is reduced with a rise of temperature. In the intermediate temperature range ($750 \text{ K} < T < 1100 \text{ K}$), the induction time shows a strong non-linear temperature dependence.

In this chapter simulations of ignition delay times for homogeneous gas-phase mixtures for different hydrocarbons will be calculated. A comparison with experimental results will be made. The simulations were performed in the high and intermediate temperature ranges, and adiabatic conditions were assumed. The experiments were performed in shock-tube devices.

For comparison it is necessary to carefully consider the criteria used in the experiments. Experimental data were given for a defined initial mixture at different initial temperatures or pressures. In other experiments the temperature was fixed and different initial conditions of the mixtures were used.

5.1 Ignition Delay Times for the H₂-O₂ System

The ignition delay times for the H₂-O₂ sub-mechanism were calculated and compared with the experimental data available at 1 bar and 5 bar for different initial mixtures: H₂/O₂/Ar: 8.0/2.0/90.0 mole fraction ($\phi = 2$) and $p = 5$ bar; H₂/O₂/Ar : 4.0/2.0/94.0 mole fraction ($\phi = 1$) at $p = 1$ bar and H₂/O₂/Ar: 1.0/2.0/97.0 mole fractions ($\phi = 0.25$) at $p = 1$ bar. Results from the simulation are presented in Figure 5.1 and, as can be seen, the simulated values are in all the instances slightly higher than the ones that are reported in the experiments. Though there exists an acceptable agreement between the calculated ignition delay times and the experimental data for the cases studied here.

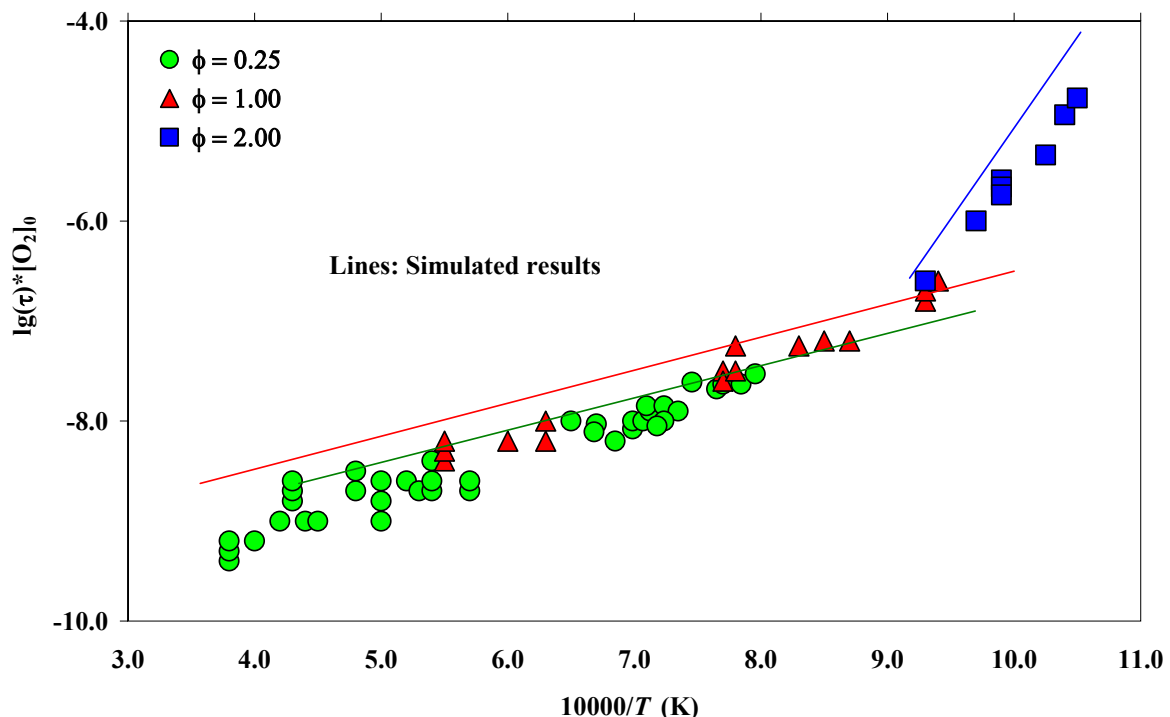


Figure 5.1: Ignition delay times (τ) for H₂/O₂/Ar mixtures as function of the initial temperature and inlet mixture composition. Points: Experimental data, Lines: Simulated results. Experimental data taken from [31]. H₂/O₂/Ar (vol.%): □: 8.0/2.0/90.0 ($\phi = 2$), $p = 5$ bar. Δ : 4.0/2.0/90.0 ($\phi = 1$), $p = 1$ bar. O: 1.0/2.0/90.0 ($\phi = 0.25$), $p = 1$ bar

Sensitivity analyses were performed for each of the mixtures at different temperatures. In all cases, the reaction between H and O₂ to produce hydroxyl radicals and atomic oxygen ($\text{H} + \text{O}_2 \leftrightarrow \text{O} + \text{OH}$) was the most sensitive, and to a lesser degree the reaction between hydrogen and oxygen atomic to produce hydroxyl radicals and atomic radicals ($\text{H}_2 + \text{O} \leftrightarrow \text{OH} + \text{H}$). A typical sensitivity analysis is presented in Figure 5.2 for a mixture at $p = 1$ bar and $\phi = 1$ and 90% Ar dilution.

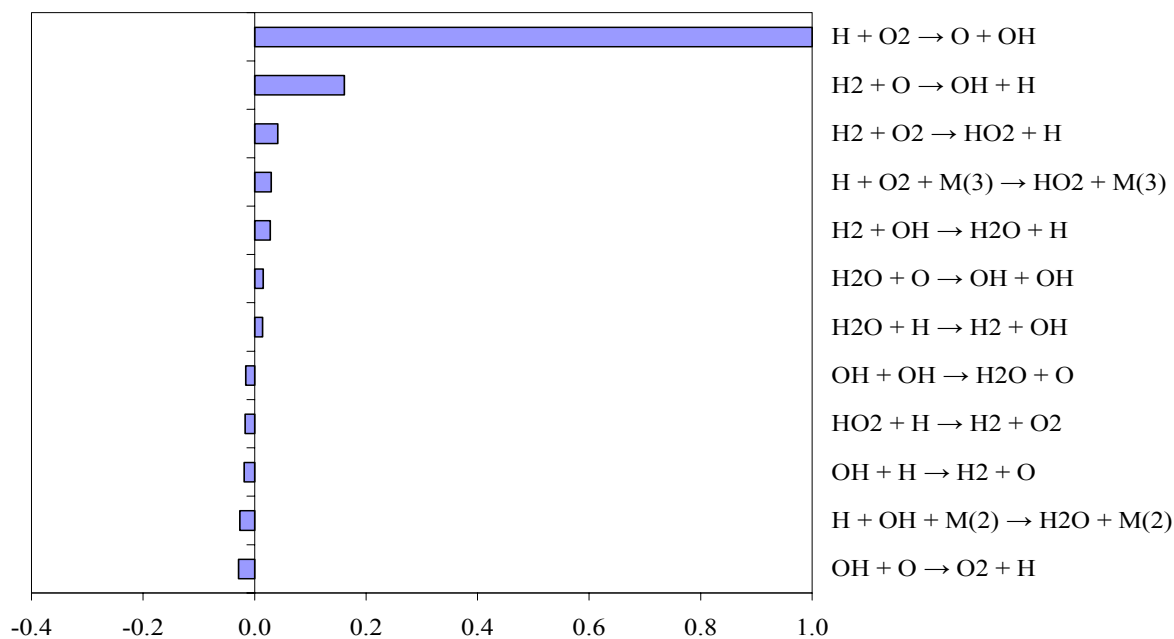


Figure 5.2: Sensitivity analysis for a $\text{H}_2/\text{O}_2/\text{Ar}$ mixture calculated at $p = 1$ bar and $\phi = 1.4.0\%$. H_2 : 2.0%, O_2 : 90% Ar

5.2 Ignition Delay Times at Combustion Conditions for Methane and Methane Mixtures

The ignition delay times in methane and methane mixtures were simulated under different experimental conditions reported in the literature: Methane-oxygen-diluent and methane-oxygen-additives-diluent, with hydrogen (H_2), ethane (C_2H_6) and propane (C_3H_8) used to study the influence of the additives in the mixture.

Figure 5.3 presents the results for calculated ignition delay times and the corresponding experimental data reported by Cooke and Williams [58] and Frenklach and Bornside [155] for two different initial compositions in methane-oxygen-argon mixtures.

In both cases results from the simulations are in agreement with the experimental data. Sensitivity analysis for the mixture revealed that the computed ignition delay times were more sensitive to reaction of a methyl radical with an oxygen molecule to produce methoxy and molecular oxygen ($\text{CH}_3 + \text{O}_2 \leftrightarrow \text{CH}_3\text{O} + \text{O}$) and ($\text{CH}_3 + \text{O}_2 \leftrightarrow \text{CH}_2\text{O} + \text{OH}$), to the reaction of methane with a hydrogen atom to produce molecular hydrogen and a methyl radical ($\text{CH}_4 + \text{H} \leftrightarrow \text{H}_2 + \text{CH}_3$), and to the reaction of a hydrogen atom with molecular oxygen to form hydroxy radicals and molecular oxygen ($\text{H} + \text{O}_2 \leftrightarrow \text{OH} + \text{O}$). All the references used for these reactions are from Baulch et al. [25-26,111].

In oxidative coupling of methane the fuel does not contain any single alkane species. Therefore, knowledge of ignition delay times for mixtures of methane and other fuels is important. Lifshitz et al. [39] reported experiments for ignition delay times of methane seeded with hydrogen. Figure 5.4 presents the data from the experiments carried out by Lifshitz and a comparison with simulated results in a mixture with an initial density of $\rho_0 = 7.5 \cdot 10^{-5}$ mol/cm³ at stoichiometric conditions and 90% of dilution. Hydrogen was added and reported measurements were taken at 0.073 mole fraction and 0.52 mole fraction.

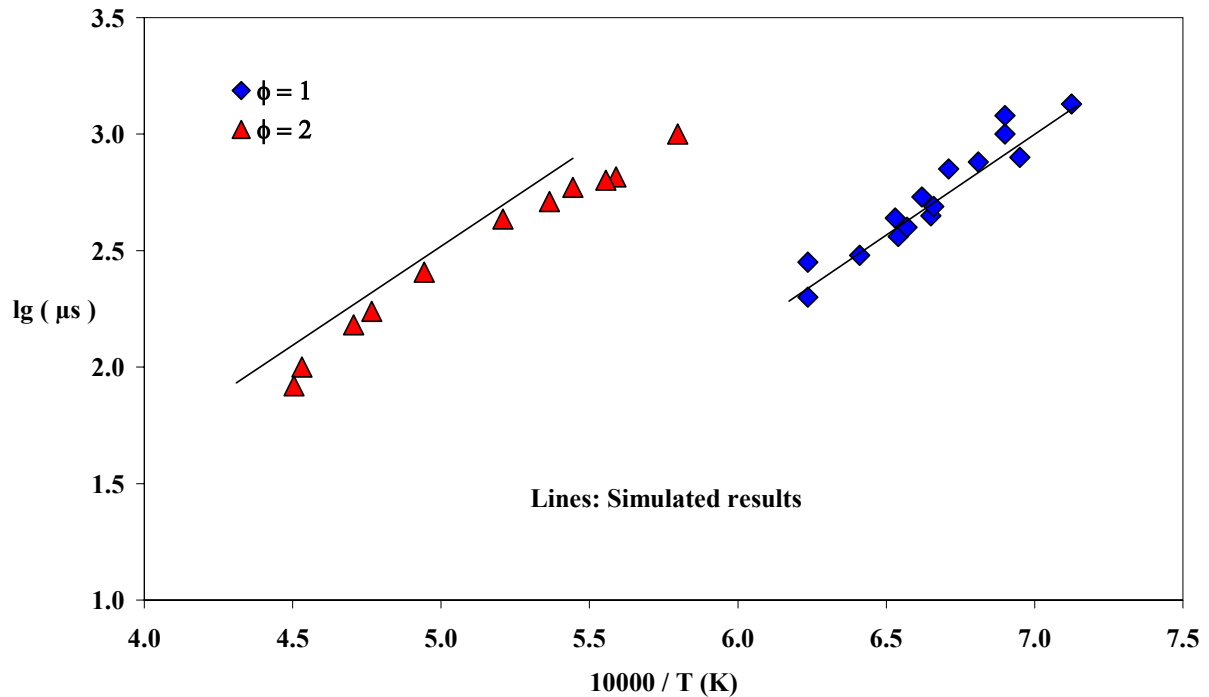


Figure 5.3: Ignition delay times (τ) for methane-oxygen-argon mixture as function of the initial temperature: CH₄/O₂/Ar (vol.%). \diamond : 9.5/19.0/71.5 ($\phi = 1$), $\rho \sim 2 \cdot 10^{-5}$ mol/cm³. Experimental data from Frenklach [155]. Δ : 5.0/5.0/90.0 ($\phi = 2$), $p = 0.2$ bar. Experiments from Cooke and Williams [58]

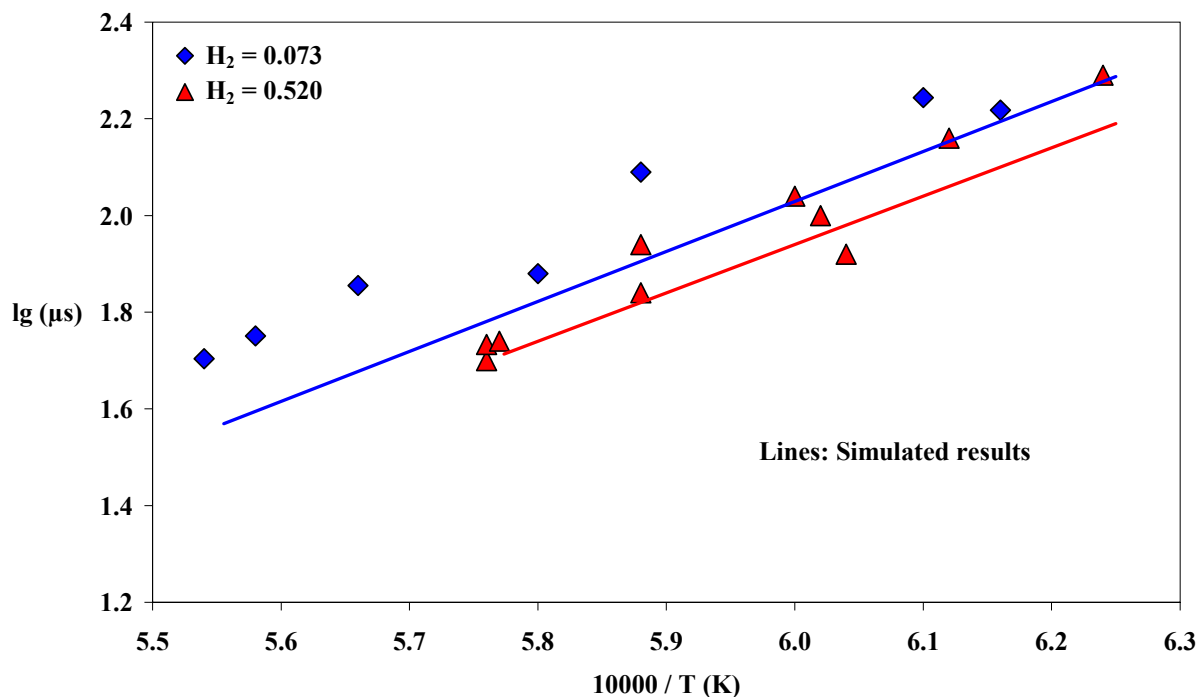
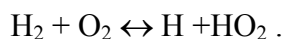
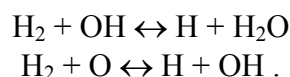


Figure 5.4: Ignition delay times $\text{CH}_4:\text{H}_2$ mixtures as function of the initial temperature and mixture composition. $\text{CH}_4/\text{O}_2/\text{H}_2/\text{Ar}$, (vol.%). Δ : 3.5/7.0/0.52/88.98; \diamond : 3.5/7.0/0.073/89.42. $\rho_o = 7.5 \cdot 10^{-05} \text{ mol/cm}^3$. Experimental data from Lifshitz et al. [39]

For the ignition delay times in the methane-hydrogen mixtures presented in Figure 5.4, sensitivity analysis showed that the OH concentration was in all instances sensitive to the changes in the reactions of atomic hydrogen with oxygen to produce hydroxyl radicals and atomic oxygen ($\text{H} + \text{O}_2 \leftrightarrow \text{O} + \text{OH}$) and to the reaction between molecular hydrogen and the fuel to produce molecular hydrogen and methyl radicals ($\text{CH}_4 + \text{H} \leftrightarrow \text{H}_2 + \text{CH}_3$). The ignition process involves the decomposition of the fuel (methane), its reaction with O_2 and the consumption of the hydrogen with which the mixture had been seeded. A description of the main reaction that occurs is as follows: The hydrogen which is being used as an additive is decomposed by the reaction with oxygen, and it produces hydrogen atoms and hydroperoxy. The initial step is



The hydrogen atom that is formed during this first stage of the reaction is then consumed by the reaction with oxygen ($\text{H} + \text{O}_2 \leftrightarrow \text{OH} + \text{O}$). This is the initial path which increases the OH radical concentration. OH and O that are produced react with the hydrogen, and they are responsible for the hydrogen consumption:



The methane is then attacked by the radicals that have been formed (OH, H, O), causing the ignition. Figure 5.5 presents the sensitivity analysis, which was carried out for a mixture with 0.52 H_2 added at 1 bar initial pressure and at 1600 K initial temperature.

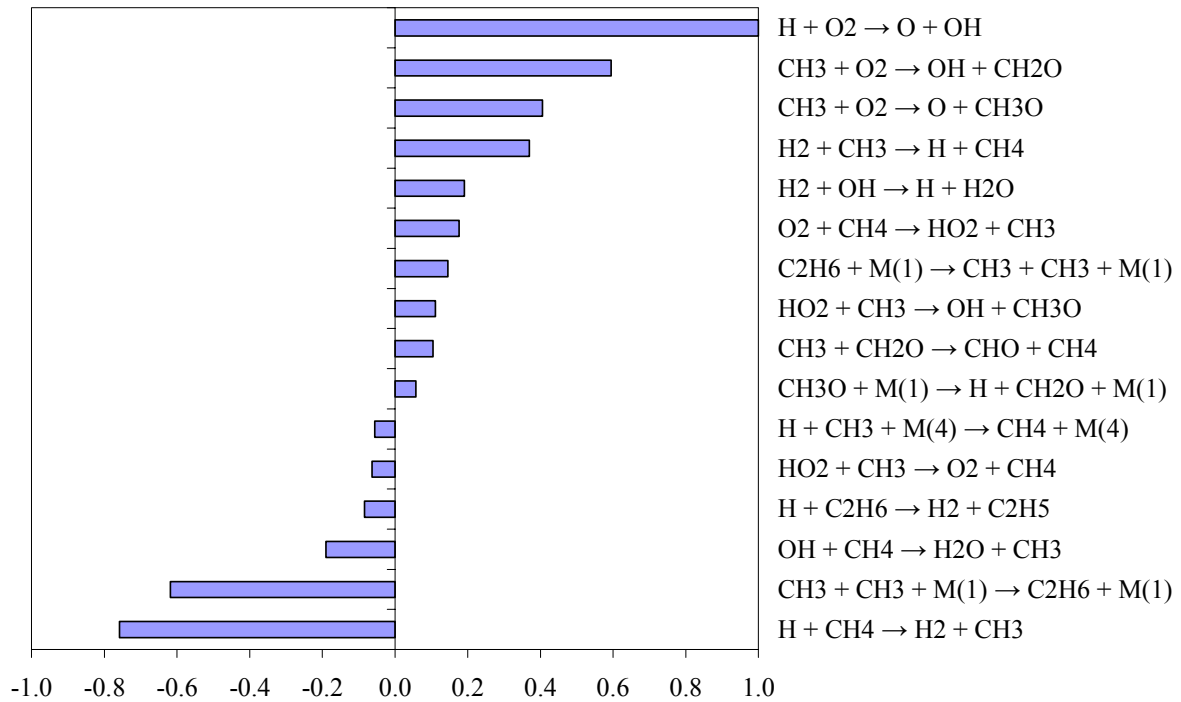


Figure 5.5: Sensitivity analysis for a $\text{CH}_4/\text{O}_2/\text{H}_2/\text{Ar}$ mixture. $\text{CH}_4/\text{O}_2/\text{H}_2/\text{Argon}$ (vol.%): 3.5/7.0/0.052/89.0. $p = 1 \text{ bar}$, $T = 1600 \text{ K}$

Experiments in methane-ethane mixtures were reported by Crossley et al. [156] for stoichiometric conditions, 0.05 C_2H_6 and 0.164 C_2H_6 added. Figure 5.6 presents the comparison of the simulation with the experimental data.

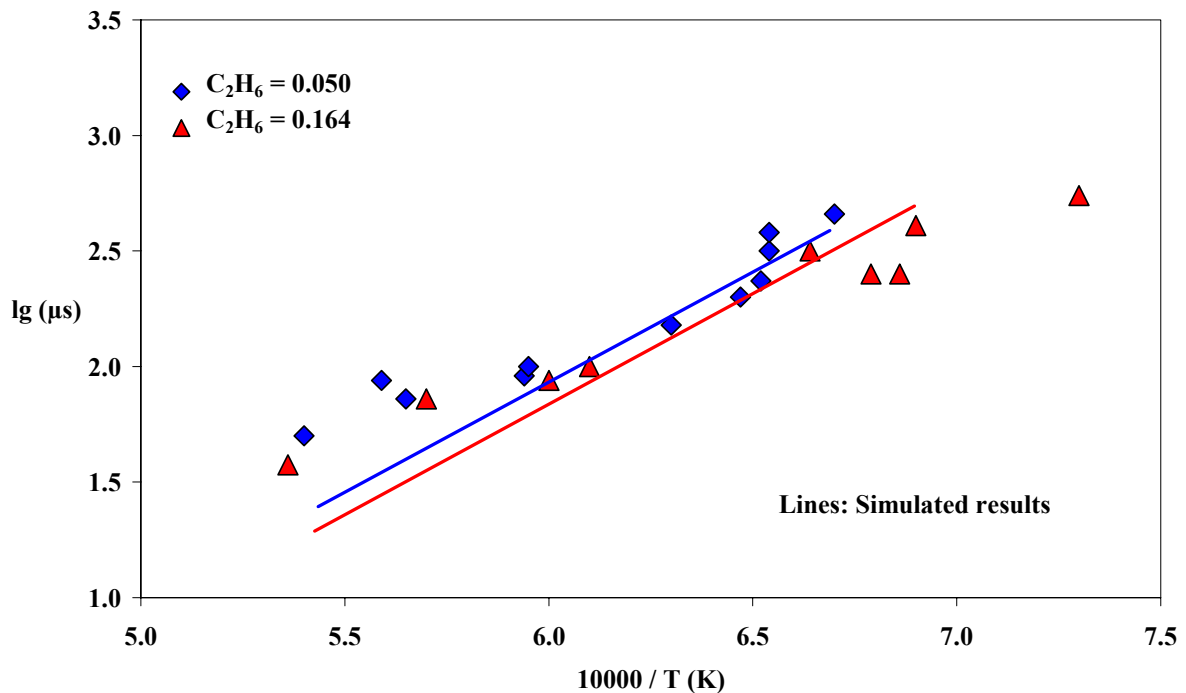


Figure 5.6: Ignition delay times (τ) for $\text{CH}_4/\text{O}_2/\text{C}_2\text{H}_6/\text{Ar}$ mixture as function of the initial temperature and inlet composition. $\text{CH}_4/\text{O}_2/\text{C}_2\text{H}_6/\text{Ar}$ (vol.%) \diamond : 3.5/7.0/0.050/89.450. Δ : 3.5/7.0/0.164/89.336. $\rho_0 = 6.3 \cdot 10^{-05} \text{ mol/cm}^3$. Experimental data from Crossley [156]

For the methane-ethane mixtures presented in Figure 5.6, ignition is led by the decomposition of C_2H_6 into CH_3 radicals and by the reaction of methyl radicals with O_2 , which produces hydroxyl radicals (OH) and CH_2O ($CH_3 + O_2 \leftrightarrow CH_2O + OH$), and by the reaction of methyl with O_2 , which produces methoxy radicals (CH_3O) and oxygen ($CH_3 + O_2 \leftrightarrow CH_3O + O$). According to the sensitivity analysis and the flow path analysis, hydroxyl radicals (OH) and oxygen atoms (O) are the most reactive species which consume the methane.

Another possible reaction that happens between the radicals that were formed is the one that produces hydrogen atoms (H) through the reaction of hydroxyl and oxygen atoms ($OH + O \leftrightarrow H + O_2$).

These are the main channels that describe formation of the three main methane consuming radicals (O, OH and H) before the ignition takes place. The kinetic data used for this group of reactions during the simulations for modeling the ignition are the ones proposed by Baulch et al. [25-26, 111]. Results from the sensitivity analysis for OH concentration are presented in Figure 5.7.

Some of the reactions that have a negative effect on the OH concentration are connected to the termination steps which deplete radicals and slow down the reaction. These include the methyl recombination which was the reaction with the highest negative value of sensitivity; the reaction of hydrogen atoms and the fuel ($CH_4 + H \leftrightarrow H_2 + CH_3$), which, although it is important for the consumption of the fuel at early stages of the reaction, “transforms” the more active hydrogen atom radicals into methyl radicals.

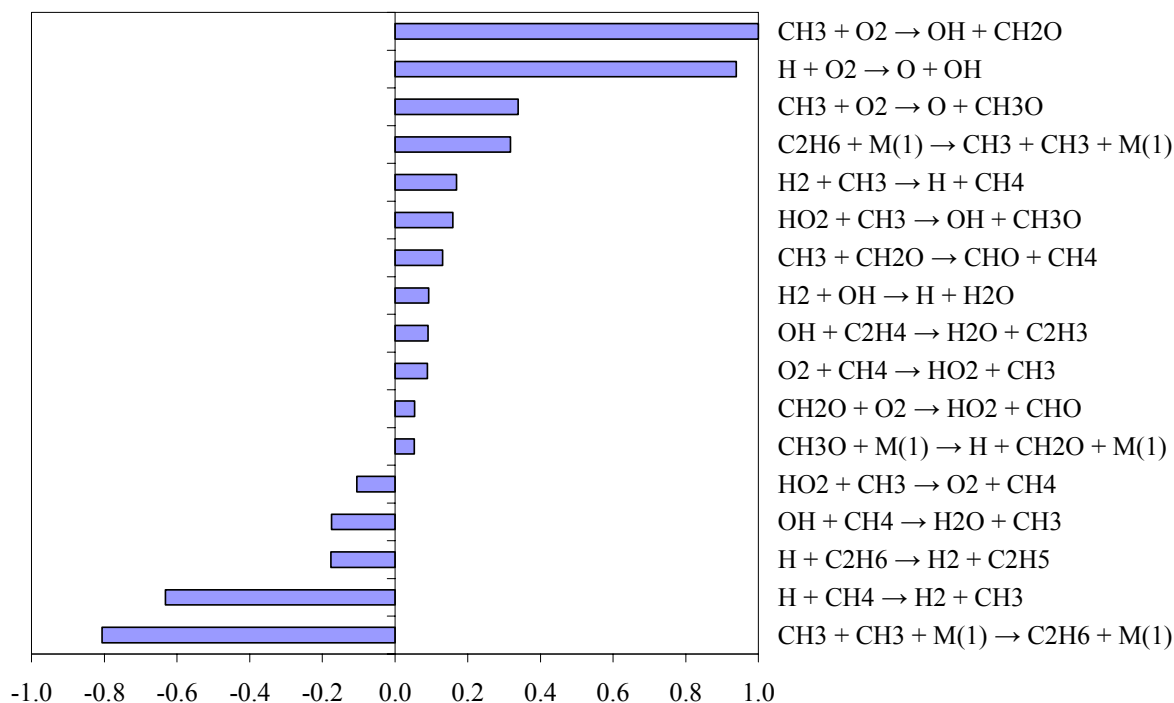


Figure 5.7: Sensitivity analysis for a $CH_4/O_2/C_2H_6/Ar$ mixture (vol.%)
 $CH_4/O_2/C_2H_6/Ar$: 3.5/7.0/0.164/89.336. $p = 8$ bar, $T = 1600$ K

Methane-propane mixtures were studied by Frenklach [155] in a shock tube experiment for a stoichiometric mixture and with 0.19%, 0.475%, 0.95% and 1.9% of propane added. The experiments were carried out at nearly constant density ($\rho_0 \sim 2 \cdot 10^{-05} \text{ mol/cm}^3$), and in the range of temperature of $1300 \text{ K} < T < 1600 \text{ K}$. Figure 5.8 presents the results from the simulation and the comparison with the corresponding experimental data.

Ignition delay times for methane-propane mixtures show a behavior similar to those described for methane-ethane mixtures, but in the case of $\text{CH}_4/\text{C}_3\text{H}_8$ the initial reaction is the decomposition of the added propane. Its self-decomposition reaction into methyl CH_3 and ethyl C_2H_5 radicals ($\text{C}_3\text{H}_8 \leftrightarrow \text{CH}_3 + \text{C}_2\text{H}_5$) is a most important decomposition reaction. The kinetic data used for this reaction are from Baulch et al. [25-26, 111].

The build-up of the radical pool involves several steps: Methyl radicals that were formed from the propane added follow a similar path to the one already described for methane-ethane mixtures (reaction with oxygen, formaldehyde formation, acetyl radical formation and finally combustion products). During these reactions OH, O and H radicals are formed, especially during methyl consumption by oxygen ($\text{CH}_3 + \text{O}_2 \leftrightarrow \text{OH} + \text{CH}_2\text{O}$), which, as shown, has a high sensitivity to OH concentration. On the other hand, the ethyl radicals which are produced during the propane decomposition are mainly decomposed into hydrogen atoms and ethylene ($\text{C}_2\text{H}_5 \leftrightarrow \text{H} + \text{C}_2\text{H}_4$). From there, hydrogen atoms are formed and along with the methyl from the first stage (propane decomposition), the OH produced by the methyl and oxygen reaction, the radical pool grows and ignition occurs. These results are in agreement with those reported by Frenklach and Bornside [155]. Results of the sensitivity analysis are presented in Figure 5.9.

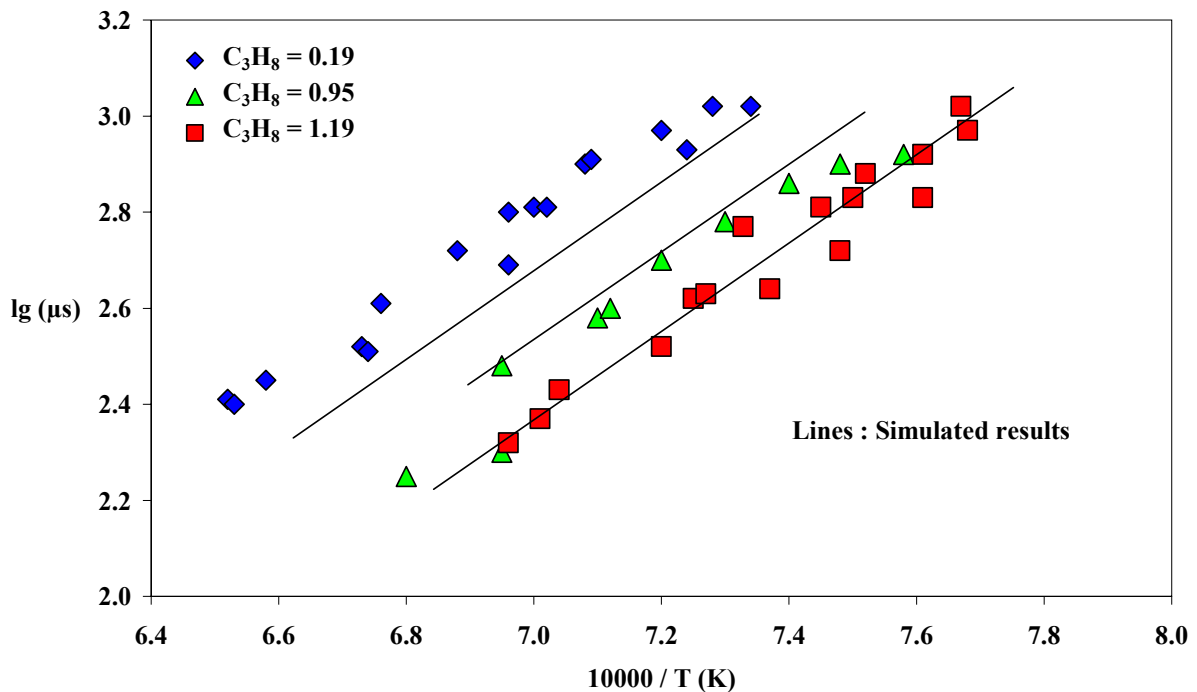


Figure 5.8: Ignition delay times (τ) for $\text{CH}_4/\text{O}_2/\text{C}_3\text{H}_8/\text{Ar}$ mixtures. $\text{CH}_4/\text{O}_2/\text{C}_3\text{H}_8/\text{Ar}$ (vol.%): \diamond : 9.5/19.0/0.19/71.31. \triangle : 9.5/19.0/0.95/70.60. \square : 9.5/19.0/1.19/70.31. $\rho \sim 2 \cdot 10^{-05} \text{ mol/cm}^3$. Experiments: Frenklach and Bornside [155]

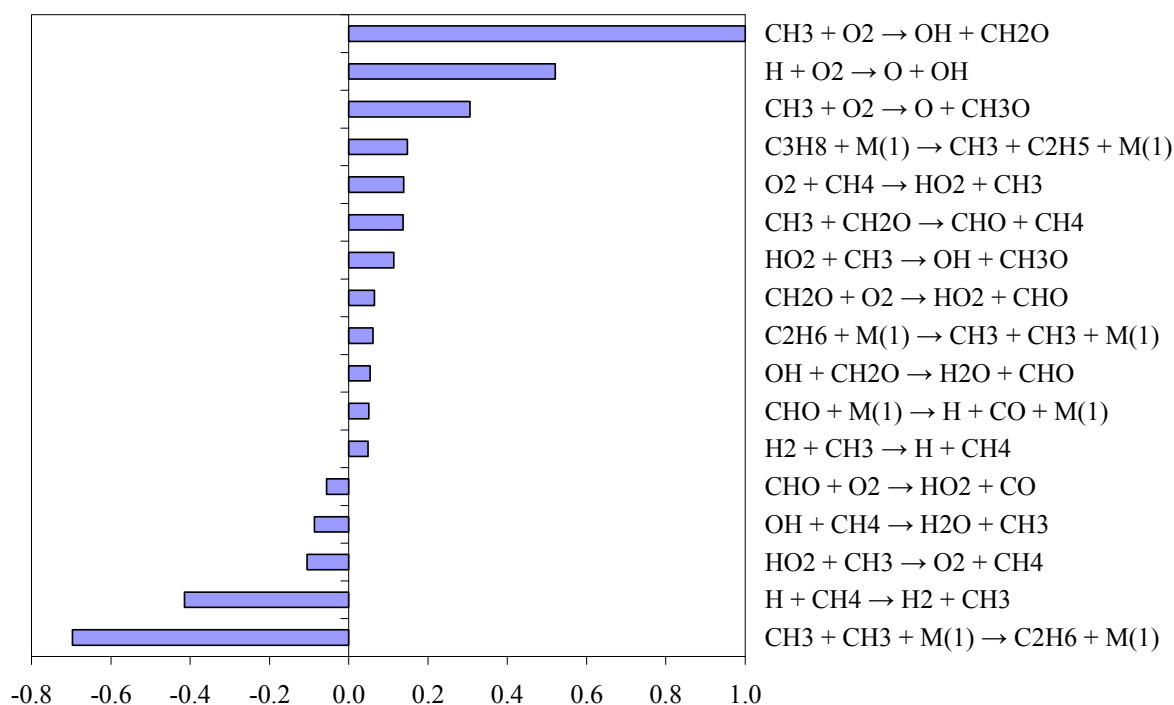


Figure 5.9: Sensitivity analysis for a $\text{CH}_4/\text{O}_2/\text{C}_3\text{H}_8/\text{Ar}$ mixture (vol.%).
 $\text{CH}_4/\text{O}_2/\text{C}_3\text{H}_8/\text{Ar}$: 9.5/19.0/1.9/69.6. $p = 2.5$ bar, $T = 1300$ K

5.3 Ignition Delay Times for C_2 - C_4 Alkanes

The following mechanism was evaluated for ignition delay times of the linear alkanes: Ethane (C_2H_6), propane (C_3H_8) and butane (C_4H_{10}) at stoichiometric and rich mixture conditions. For the experiments high dilution conditions were used. Argon is in most cases the carrier gas acting as diluent. The calculated ignition points were taken from the OH radical profile according to the reported experimental results, which in most cases are based on measurements of OH concentration profiles.

The calculated ignition delay times for ethane mixtures and their comparison with the experimental data reported by Cooke and Williams [58] are presented in Figure 5.10 for mixtures with equivalence ratios of 1 and 2. Mixtures used had 90% argon dilution and the pressure was set to 0.3 bars.

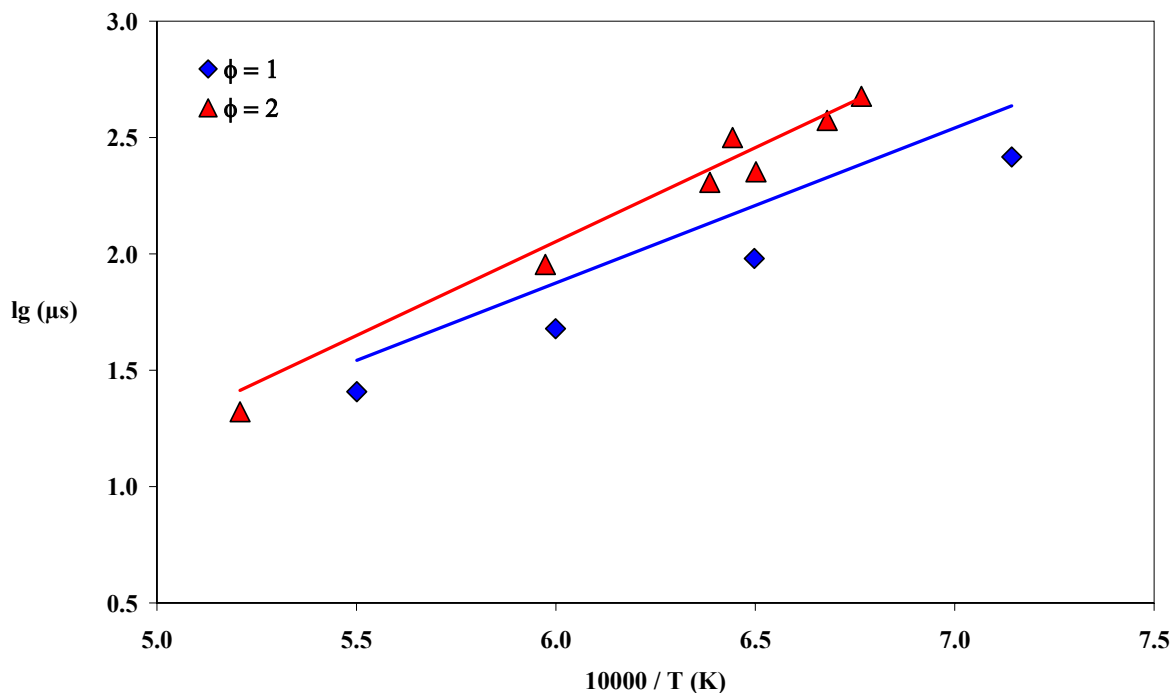


Figure 5.10: C_2H_6 ignition delay times for $C_2H_6/O_2/Ar$ mixtures as function of the initial temperature and composition. Experimental data from Cooke and Williams [58], $C_2H_6/O_2/Ar$ (vol.%). \diamond : 2.22/7.78/90.0 ($\phi = 1$), Δ : 6.36/3.64/90.0 ($\phi = 2$). $p = 0.3$ bar

In the case of C_2H_6 , a sensitivity analysis was performed before the ignition at a temperature of 1500 K and a pressure of 0.3 bar with a mixture 90% diluted in Ar. Under these conditions, the sensitivity of OH concentration displayed a highly negative dependence on the external hydrogen abstraction from the fuel ($C_2H_6 + H \leftrightarrow H_2 + C_2H_5$) and on the decomposition reaction of the ethyl radicals into methyl ($C_2H_5 + H \leftrightarrow CH_3 + CH_3$). On the other hand, sensitivity of OH concentration was positively affected by the decomposition reaction of ethyl radical into ethylene and atomic hydrogen ($C_2H_5 + M_{(1)} \leftrightarrow H + C_2H_4$), by fuel decomposition into methyl radicals ($C_2H_6 \leftrightarrow CH_3 + CH_3$) and by the oxygen and hydrogen atom reaction to produce hydroxyl and molecular oxygen ($H + O_2 \leftrightarrow OH + O$). Results of the sensitivity analysis are presented in Figure 5.11.

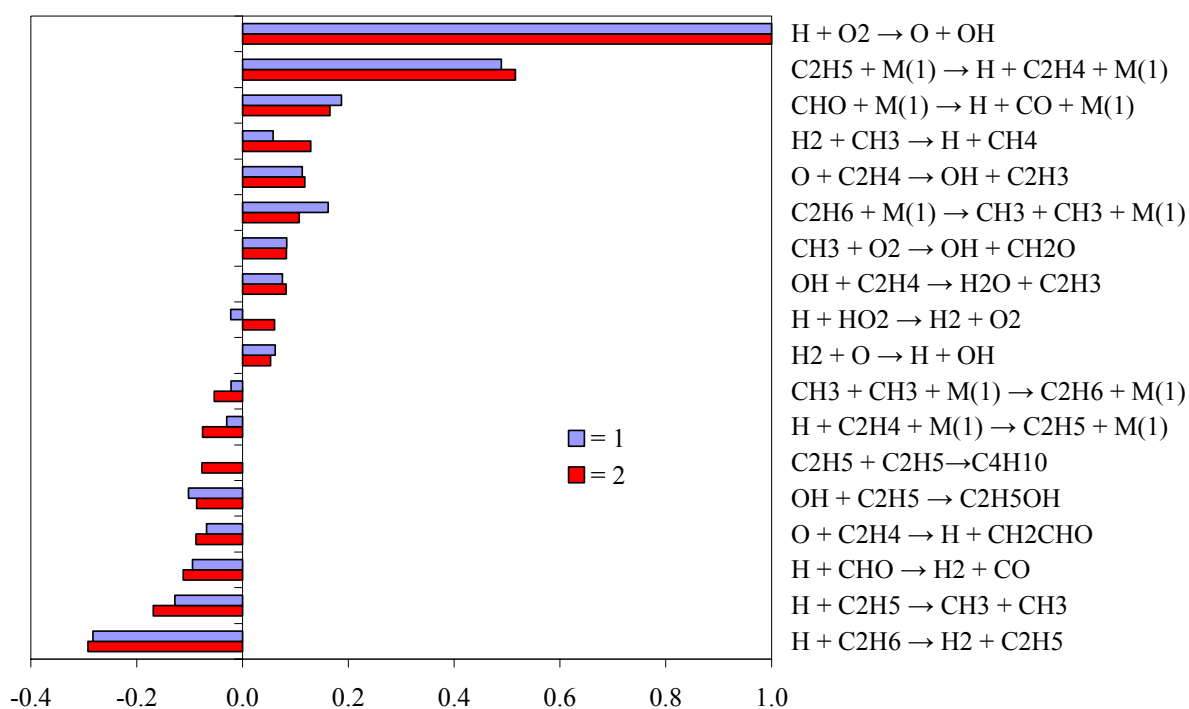


Figure 5.11: Sensitivity analysis for $C_2H_6/O_2/Ar$ mixtures: $C_2H_6/O_2/Ar$: 2.22/7.78/90.0, $\phi = 1$.
 $C_2H_6/O_2/Ar$: 3.64/6.36/90.0, $\phi = 2$. $p = 0.3$ bar, $T = 1500$ K

Under stoichiometric conditions ethane degradation initiates the attack of the radicals on the fuel: H and OH are the main radicals that consume fuel and form ethyl radicals. The kinetic data used for these reactions were taken from [47] in the first of the cases (hydrogen reaction) and the ones proposed by Baulch et al. [25-26, 111] for the reaction with hydroxyl.

The ethyl formed decomposes into ethylene according to the performed flow analysis. Reactions between ethyl radicals and hydrogen and the self-decomposition consume 100% of the ethyl formed. The kinetic data used are in both cases proposed by Baulch et al. [25-26, 111].

Ethylene is consumed through different channels: vinyl radical formation, via the reaction between olefins and H, and atomic oxygen O and hydroxyl radical OH. Vinyl radical formation via radical attack consumes 60% of the ethylene formed; the vinyl radicals are consumed in the reactions with molecular oxygen ($C_2H_3 + O_2 \leftrightarrow CHO + CH_2O$) and ($C_2H_3 + O_2 \leftrightarrow O + CH_2CHO$), and self-decomposition to acetylene ($C_2H_3 + M_{(1)} \leftrightarrow C_2H_2 + H + M_{(1)}$); the values for the kinetic parameters for the first reaction are from the experimental study by Slage et al. [157], for the second case from Bozzelli and Dean [158], and for the last reaction from Baulch et al. [25-26, 111].

The second channel which consumes the last 40% of the olefin includes the oxygen reaction to form formyl radicals ($C_2H_4 + O \leftrightarrow CH_3 + CHO$ and $C_2H_4 + O \leftrightarrow H + CH_2CHO$) and both of these products react to yield CO and CO_2 .

Figure 5.12 presents the comparison between the simulated results and the experimental data reported by Burcat and Radhakrishnan [72] for propane-oxygen mixtures at equivalence ratios of 1 and 2 and for different initial pressures.

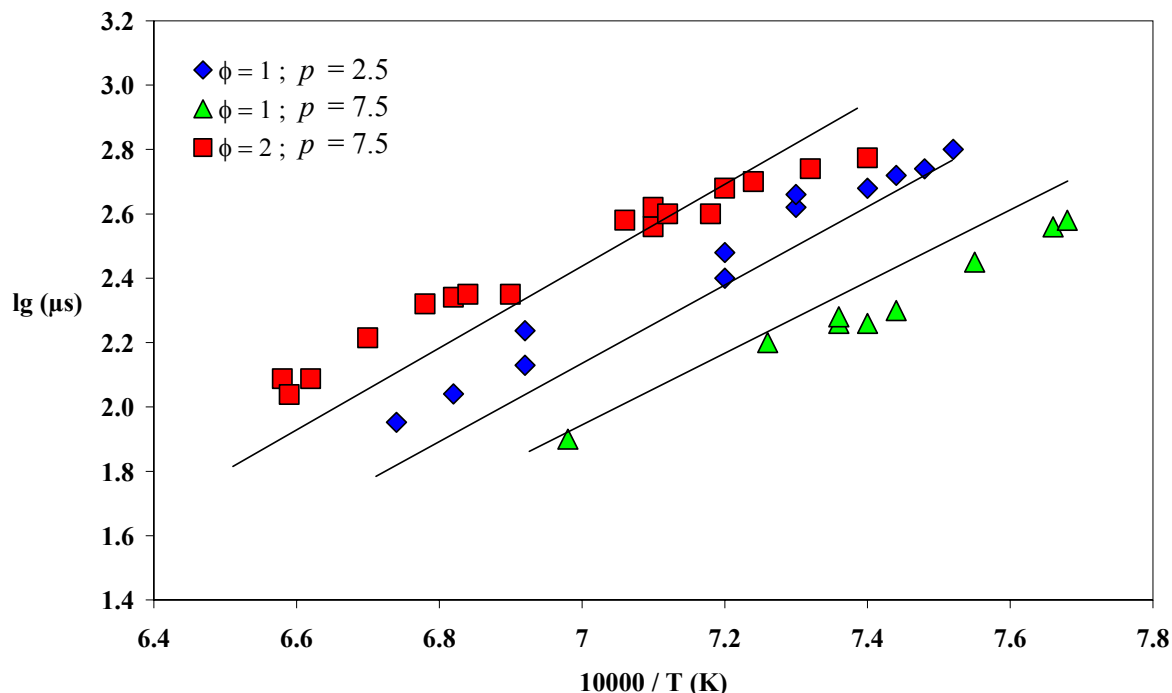


Figure 5.12: C_3H_8 ignition delay times as a function of the initial temperature. $C_3H_8/O_2/Ar$ (vol.%)
 \diamond : 1.6/8.0/90.4, $p = 2.5$ bar. \triangle : 1.6/8.0/90.4, $p = 7.5$ bar. \square : 1.6/4.0/94.4, $p = 7.5$ bar. Experimental data from Burcat and Radhakrishnan [72]

The results presented in Figure 5.12 for the ignition delay times of C_3H_8 were calculated for three mixtures at different pressures and compositions: 7.5 bar ignition delay times were calculated for a stoichiometric ($\phi = 1$) and a rich mixture ($\phi = 2$), and at lower pressure ($p = 2.5$ bars) for a stoichiometric mixture.

Sensitivity analysis at 1300 K was performed at each of these conditions. It showed that at high pressure and stoichiometric conditions the most important reactions are: Hydrogen atom abstraction from the fuel ($C_3H_8 + H \leftrightarrow H_2 + n(i)-C_3H_7$), methyl radical recombination ($CH_3 + CH_3 \leftrightarrow C_2H_6$), and hydroxyl attack on the formed olefin ($OH + C_3H_6 \leftrightarrow H_2O + C_3H_5$). All of these reactions presented a negative value for sensitivity. On the other hand, the fuel decomposition to ethyl and methyl radicals ($C_3H_8 \leftrightarrow CH_3 + C_2H_5$), the reaction between methyl and oxygen ($CH_3 + O_2 \leftrightarrow OH + CH_2O$) and the oxygen hydrogen reaction ($H + O_2 \leftrightarrow OH + O$) had a positive effect on the calculated sensitivity. For rich conditions in the high pressure range only few minor changes were observed for the most important reactions. Figure 5.13 presents the comparison for the high pressure range at stoichiometric and rich conditions.

The major changes that were observed involved reactions among oxygen and other radical species: Oxidation of formyl radicals to produce carbon monoxide was sensitive at stoichiometric conditions, but was not sensitive at rich conditions. There was a similar behavior with the decomposition of methoxy radicals and the hydrogen atom abstraction from formaldehyde by OH which were not sensitive in the rich mixture case.

Propane decomposes before ignition occurs. Stable species (especially olefins: C_3H_6 and C_2H_4) appear in the intermediate products, and reactions that are connected to their consumption play a key role during the ignition, as is shown in the sensitivity analysis for both cases.

The ignition delay is influenced by the olefin consumption due to the fact that, once olefins are formed, they ignite much more easily than the propane itself. Figure 5.14 presents the calculated species concentration profiles before the ignition occurs for C_2H_4 , C_3H_6 , C_3H_8 and OH, in a stoichiometric mixture with 90% Ar dilution and for an initial temperature of 1120 K.

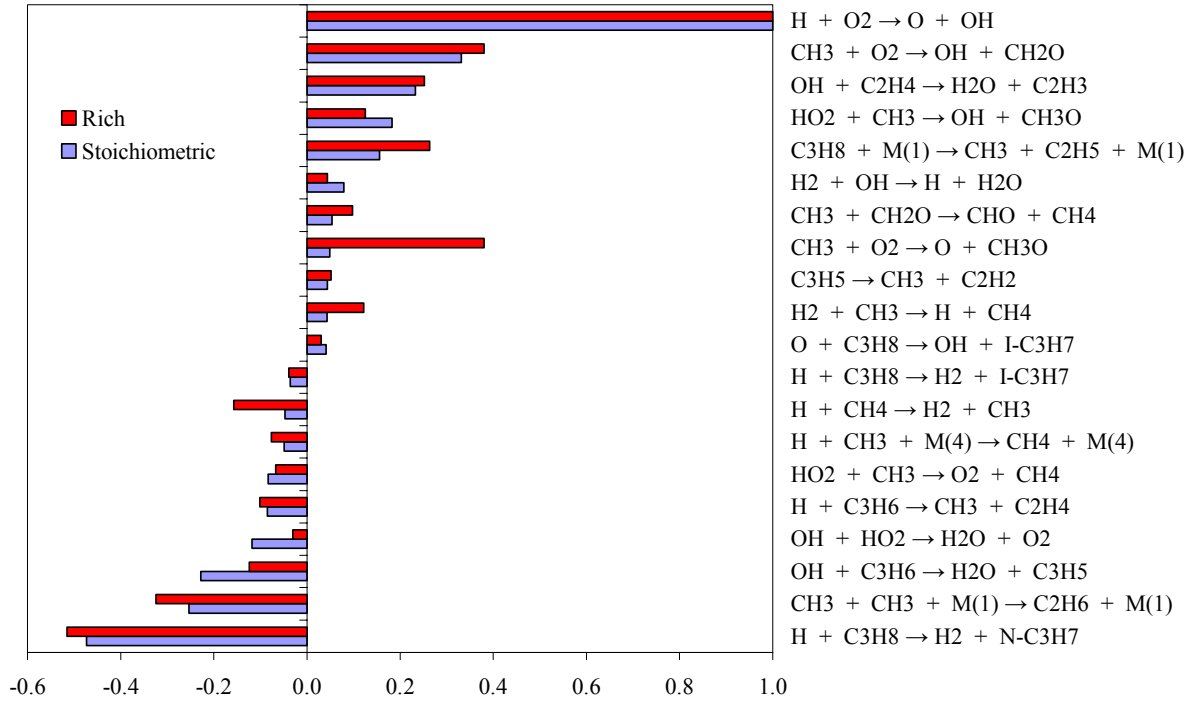


Figure 5.13: Sensitivity analysis for high pressure propane combustion ($C_3H_8/O_2/Ar$): Stoichiometric and rich conditions: $\phi = 1$ and $\phi = 2$, at 90% Ar dilution, $p = 7.5$ bar, $T_0 = 1120$ K

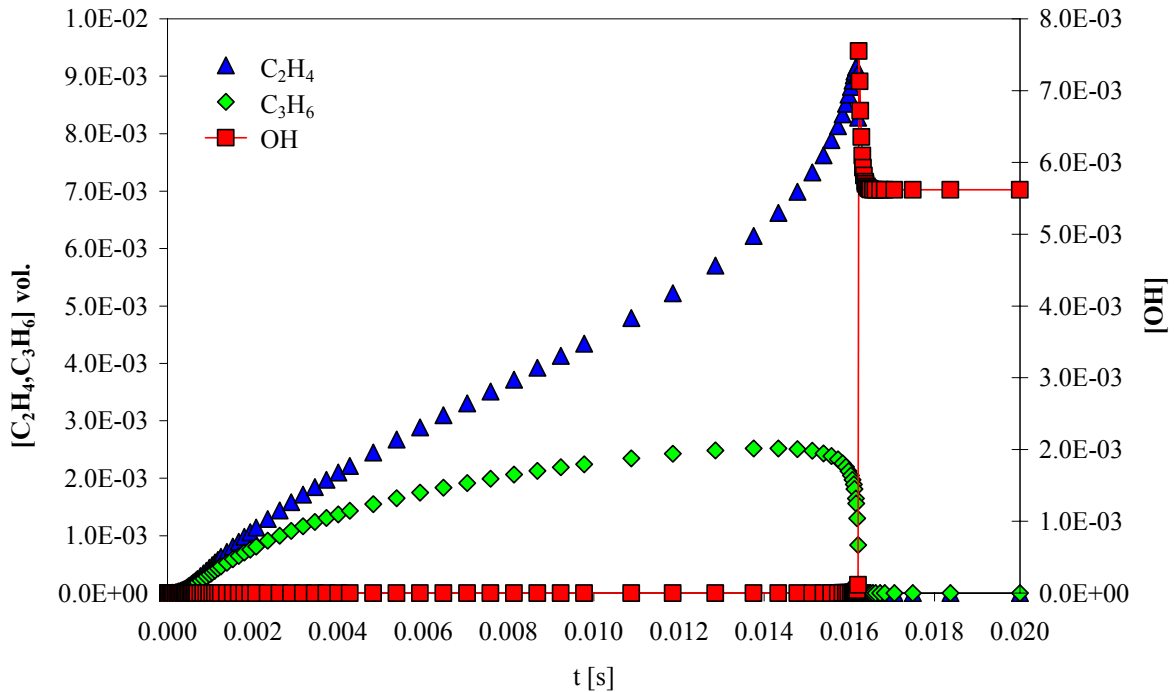


Figure 5.14: Calculated species mole fraction prior to ignition: In early stages propylene is formed, later ethylene appears in the system preceding the ignition. $C_3H_8/O_2/Ar$: 1.6/8.0/90.0 (vol.%), $p = 2.5$ bar, $T_0 = 1120$ K

Figure 5.15 presents the comparison between the experimental data from Burcat et al. [81] and the results of the simulation for the ignition delay times of butane-oxygen mixtures at stoichiometric conditions and 81% of argon dilution. The experiments were performed at a pressure of 10 bar.

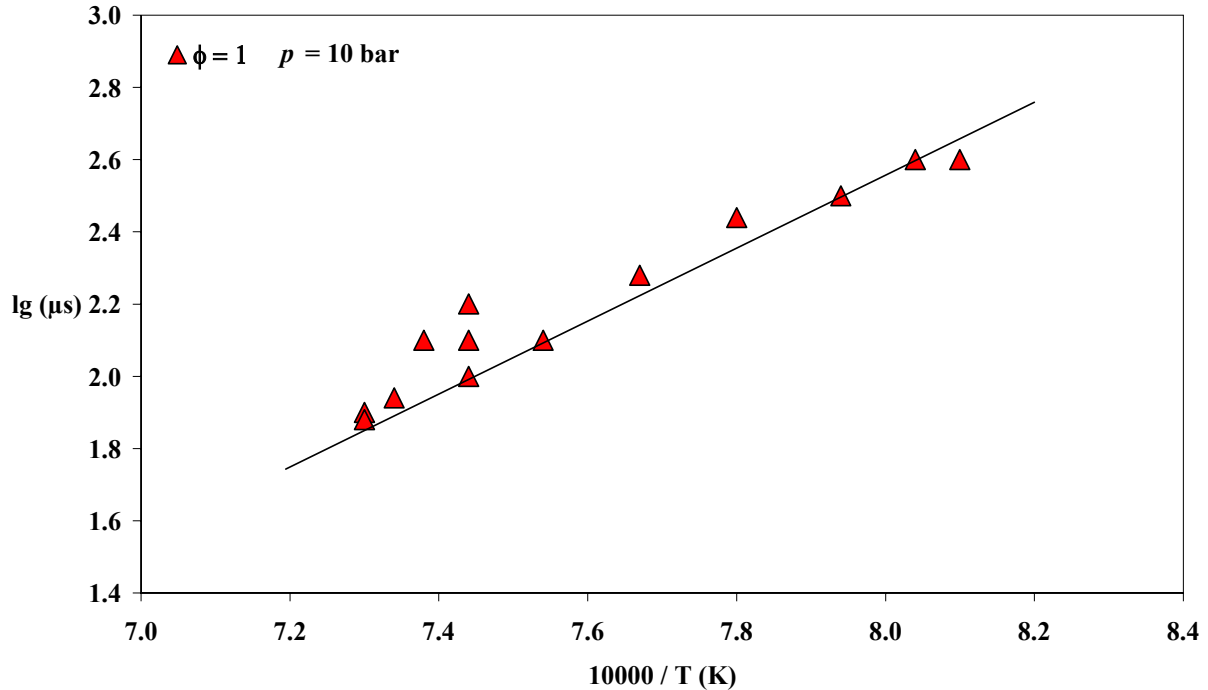


Figure 5.15: Ignition delay times for a $C_4H_{10}/O_2/Ar$ mixture as a function of the initial temperature. $C_4H_{10}/O_2/Ar$: 2.5/16.3/81.0, (vol.%). $p = 10$ bar. Experimental data from Burcat et al. [81]

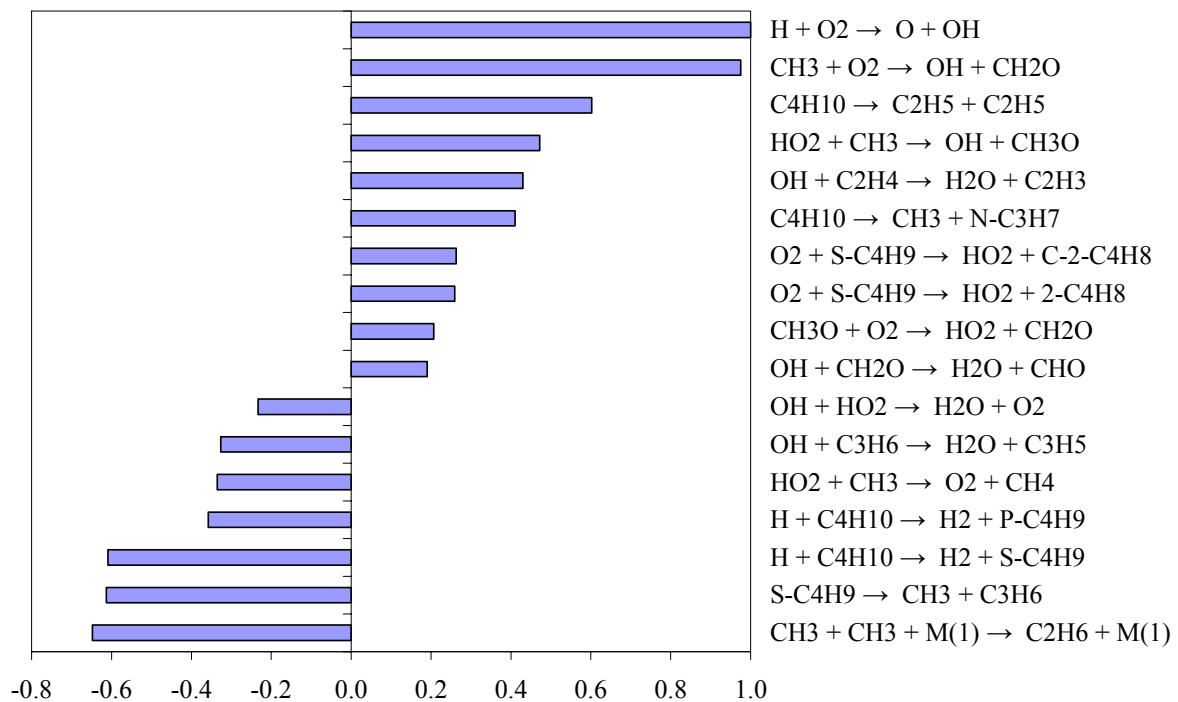


Figure 5.16: Sensitivity analysis for a $C_4H_{10}/O_2/Ar$ mixture. $C_4H_{10}/O_2/Ar$: 2.50/16.30/81.20, (vol.%). $p = 10$ bar, $T_0 = 1250$ K

A sensitivity analysis for the butane oxygen mixture is presented in Figure 5.16 for a mixture with $C_4H_{10}/O_2/Ar$: 2.5/16.3/81.20 and an initial temperature and pressure of 1250 K and 10 bar, respectively.

In the high temperature range the most sensitive reactions to the OH concentration at $t = \tau$ are the reaction among hydrogen radicals and oxygen leading to OH formation ($H + O_2 \leftrightarrow OH + O$) and the reaction of methyl radicals with oxygen to produce aldehydes ($CH_3 + O_2 \leftrightarrow OH + CH_2O$). Aside from these two reactions there are three additional paths, which are important for OH formation: The decomposition of butane into ethyl radicals ($C_4H_{10} \leftrightarrow C_2H_5 + C_2H_5$), the reaction of methyl radicals with oxygen and hydroperoxy radicals to form OH and aldehydes or methoxy radicals ($CH_3 + O_2 \leftrightarrow OH + CH_2O$), $CH_3 + HO_2 \leftrightarrow OH + CH_3O$ and the self-decomposition to methyl and normal propyl radicals ($C_4H_{10} \leftrightarrow CH_3 + n-C_3H_7$).

The hydrogen abstraction from the fuel ($C_4H_{10} + H \leftrightarrow 1(2) C_4H_9 + H_2$), the methyl recombination ($CH_3 + CH_3 \leftrightarrow C_2H_6$), and the radical recombination for hydroperoxy and hydroxyl radicals to form water ($HO_2 + OH \leftrightarrow H_2O + O_2$) are also important reactions for the sensitivity, but they have a negative value of sensitivity.

Butane starts its decomposition before the ignition occurs: Self-decomposition to two ethyl radicals and to methyl and normal propyl radicals is responsible for 20% of its consumption until the moment of ignition, according to the performed flow analysis. Radical attack on the fuel by atomic hydrogen and hydroxyl radicals consumes the last 80% of the butane and leads to butyl radical formation. Both butyl radicals which are formed follow different decomposition channels: The primary butyl (1- C_4H_9) decomposes to ethylene and ethyl radicals ($1 C_4H_9 \leftrightarrow C_2H_4 + C_2H_5$). This is the main formation channel for ethylene, while the secondary butyl (2- C_4H_9) leads to the formation of propylene and methyl radicals ($1 C_4H_9 \leftrightarrow C_3H_6 + CH_3$), or it reacts with oxygen to produce butene. As in the case of propane, the olefins formed play a key role during the ignition, because they are the main intermediate products before ignition at the conditions of the experiments. Figure 5.17 shows the concentration profile for the main species formed prior to ignition as well as the temperature profile and the OH radical concentration.

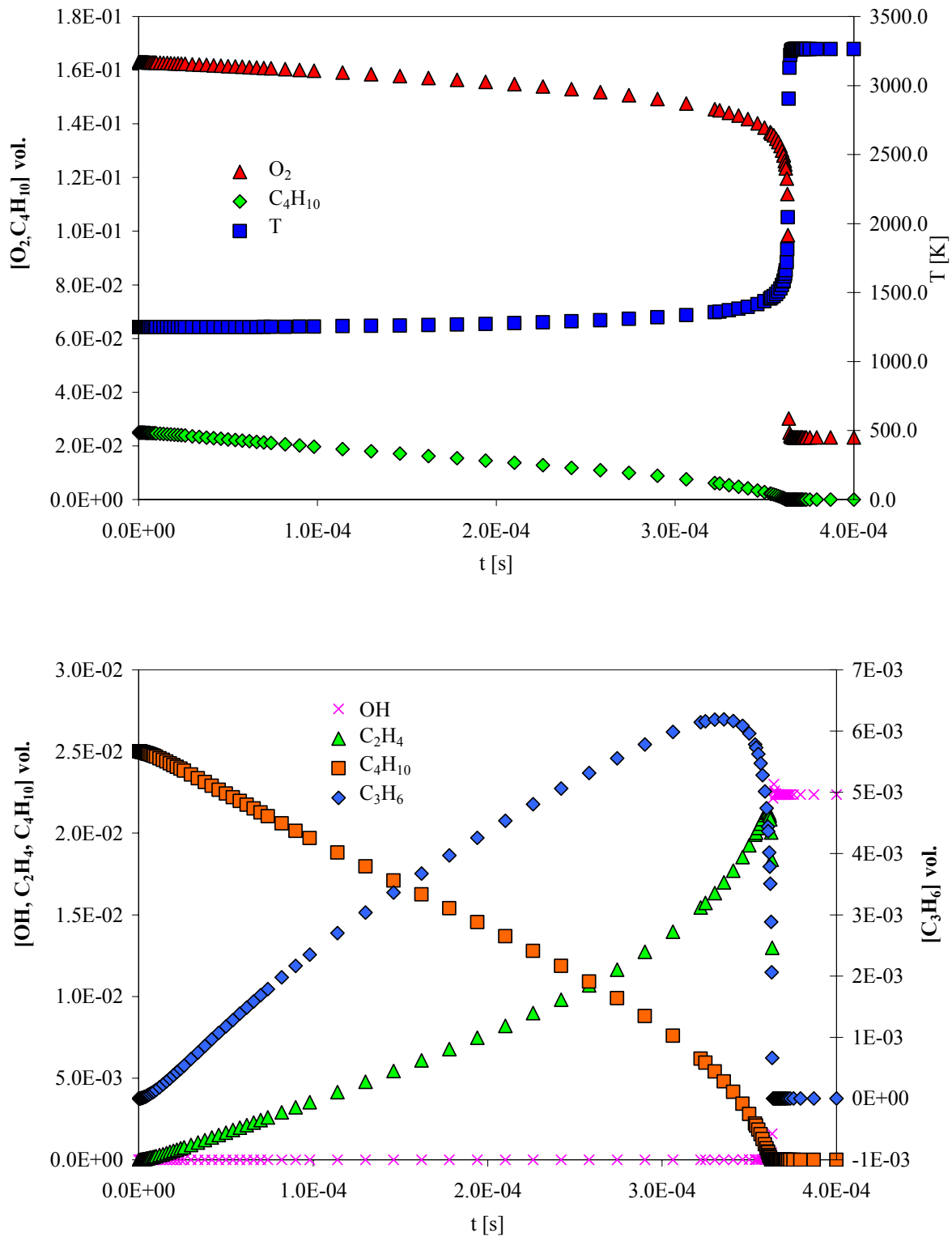


Figure 5.17: Mole fraction profiles for the main species formed prior to ignition during the C_4H_{10} ignition. $C_4H_{10}/O_2/Ar$: 2.5/16.3/81.20 mixture. $p = 10$ bar, $T_0 = 1250$ K

Chapter 6

PARTIAL AND TOTAL OXIDATION OF C₁-C₄ ALKANES AND ALKENES IN THE GAS PHASE

The study of pure gas-phase oxidative coupling is of great interest, because it produces the same products as in the catalytic processes, but at a different rate due to the absence of the catalyst, which strongly accelerates the reaction during the catalytic process.

A vast number of experimental and theoretical studies on methane oxidative coupling to produce ethane and ethylene as main products have been carried out. For the catalytic coupling of methane, temperatures between 650°C and 950°C are used alongside methane-rich mixtures. In the case of methane it was suggested that the catalyst would act as a “methane activator”, which produces methyl radicals and initiates a process occurring in the gas phase (methyl combination). Although this is a considerable simplification, it shows the importance that the homogeneous process has and that its contribution should be included during the study of the methane catalytic coupling.

According to the experimental results from different authors [44, 52], the partial oxidation process is characterized by several facts: When the temperature is increased at constant flow (or at constant residence time), conversion of fuel and the oxygen are sharply increased. Ethane has a maximal selectivity in the lower temperature region; at higher temperatures ethylene is predominant. However, after reaching the maximal ethylene selectivity, a further increase in the temperature leads to a decrease in ethylene selectivity. Miele et al. [44] concluded from their experimental work that the synthesis of ethylene is possible only considering the gas-phase chemistry. The temperature was the key factor which controlled the reaction rates, whereas selectivities are controlled by the conversion grade.

In this section, results for partial oxidation of methane, propane and butane will be presented. Simulations were performed for the conditions used in [66, 73, 159] in a jet-stirred reactor. The temperature profiles reported from the experiments were used in the simulations.

6.1 Partial Oxidation of Methane

Zanthoff and Baers [44] examined the homogeneous gas-phase reaction of methane and oxygen in the absence of a catalyst at the usual concentration compositions applied for the cata-

lytic conversion of methane. In their work the authors developed a kinetic scheme, which allowed the calculation of the time dependence of the concentrations of the various compounds as a function of the conversion degree. The results from his simulations were compared with experimental data obtained in the temperatures range $878 \text{ K} < T < 1071 \text{ K}$ and the partial pressure ranges $1.84 \text{ bar} < p_{\text{CH}_4} < 8 \text{ bar}$ and $0.18 \text{ bar} < p_{\text{O}_2} < 0.8 \text{ bar}$.

Zhu et al. [159] reported the reduction of complex kinetic models using a new algorithm to produce a reduced mechanism based on a normal sensitivity analysis from Warnatz et al. [6], and a new approach defining a global sensitivity coefficient. Validation of the methodology developed by Zhu was made using the experimental data from Zanthoff [44] and running both the complex and the reduced mechanism for a complex initial mixture, which includes methane, ethane, hydrogen, carbon monoxide and oxygen. These data were taken for comparison purposes. The conditions used during the simulation are given in Table 6.1.

Table 6.1: Selected operation conditions for oxidative coupling of methane

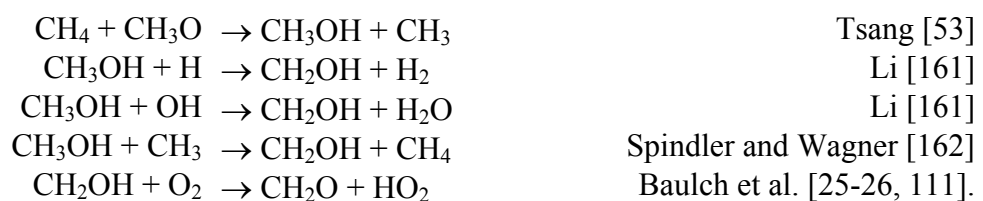
| vol. % | | | | | | | | p | T |
|-----------------|-------------------------------|-------------------------------|-----------------|------|----------------|------------------|----------------|-----|------|
| CH ₄ | C ₂ H ₆ | C ₂ H ₄ | CO ₂ | CO | O ₂ | H ₂ O | H ₂ | bar | K |
| 64.60 | 0.30 | 0.30 | 0.60 | 1.80 | 26.50 | 4.70 | 1.20 | 1.7 | 1052 |

The results of the comparison between the results from Zhu [159] based on the experiments from Zanthoff [44] and the results using our mechanism are presented in Figure 6.1.

Figure 6.2 presents the calculated reaction path for the consumption and formation of the main species according to the mechanism. Different reactions between radicals are presented in the complex mixture, which involves a large number of species and important intermediate compounds. The initial reaction is the decomposition of the C₂H₆ to CH₃. The CH₃ formed reacts with C₂H₆ to produce C₂H₅, and this decomposes into C₂H₄ and hydrogen atoms. This path, according to the flow analysis, is the main channel for ethylene formation and plays an important role in the CH₄ decomposition, because the hydrogen atoms formed in these initial steps attack the CH₄, increasing its consumption.

The CH₃ radicals follow a similar reaction path as in the case of ignition; they react with oxygen to produce CH₂O and OH (CH₃O₂ ↔ OH + CH₂O), and the OH formed is consumed in the reaction with CH₄ to form H₂O and CH₃.

CO formation follows the well known route CH₃ → CH₂O → CHO → CO (Warnatz et al. [6], Smith et al. [47], Konnov [153], Pilling et al. [160]); however, there is another path for CO formation which should be considered according to the results from the mechanism: Reaction of CH₃O with CH₄ to produce methanol (CH₃O + CH₄ ↔ CH₃OH + CH₃). The reference used is from Tsang [53]. Further methanol consumption via OH, H and CH₃ radicals form hydroxymethyl radicals (CH₂OH), which react with oxygen to produce CH₂O (CH₂OH + O₂ → CH₂O + HO₂), and finally reaction of the formed CH₂O into CO. The chain reaction is described as follows:



This reaction scheme, although differing from those proposed by Zhu and Zanthoff, can also predict the concentration of the main species.

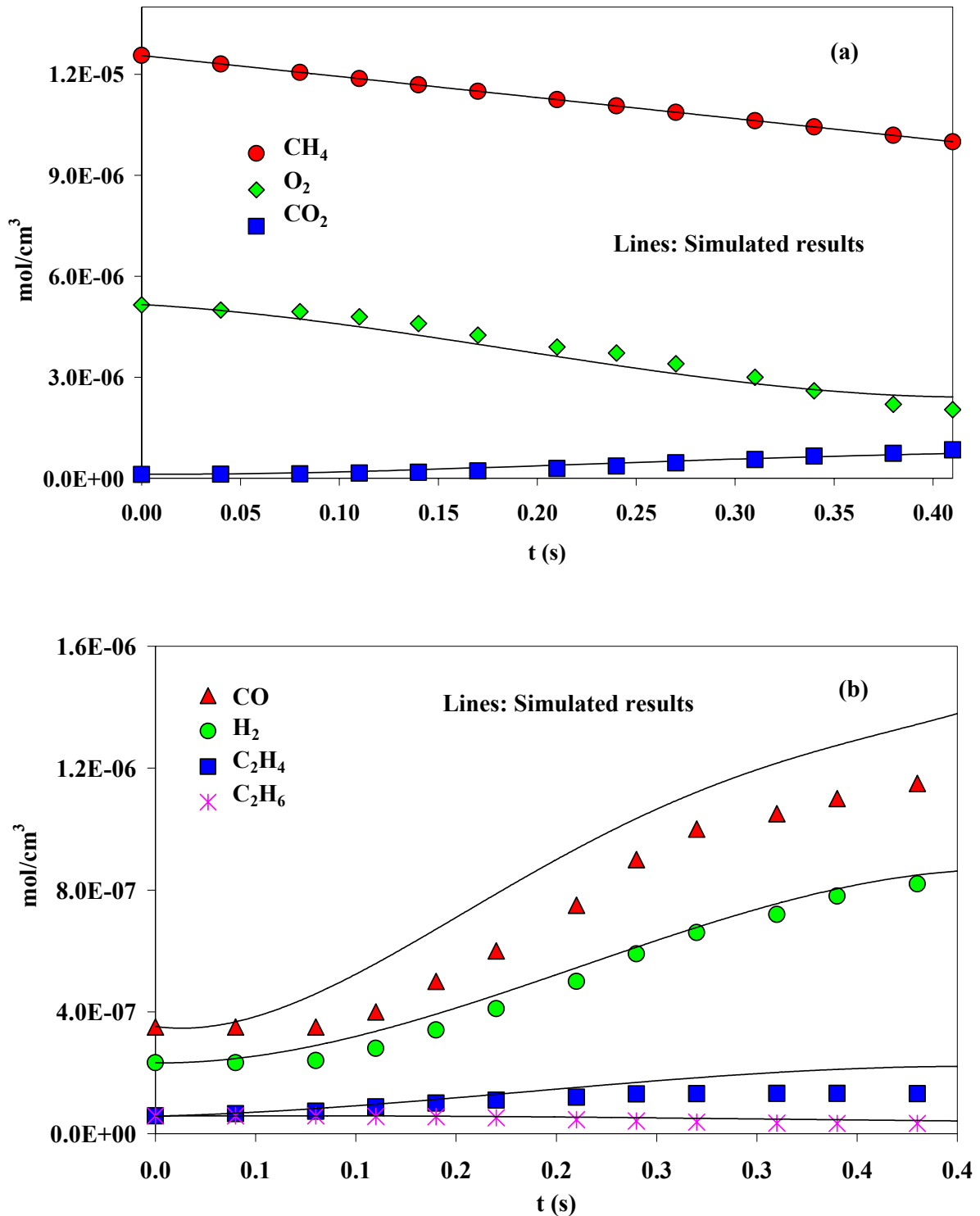


Figure 6.1: Comparison between the simulated results using the gas-phase mechanism and the results reported by Zhu et al. [159] for partial oxidation of a complex methane mixture. (a) Methane and oxygen consumption and carbon dioxide production. (b) Main species reported: Carbon monoxide, hydrogen and coupling products ethylene and ethane. Symbols: results reported by Zhu, lines: Simulation using the kinetic mechanism. Initial conditions used for the simulations are given in Table 6.1

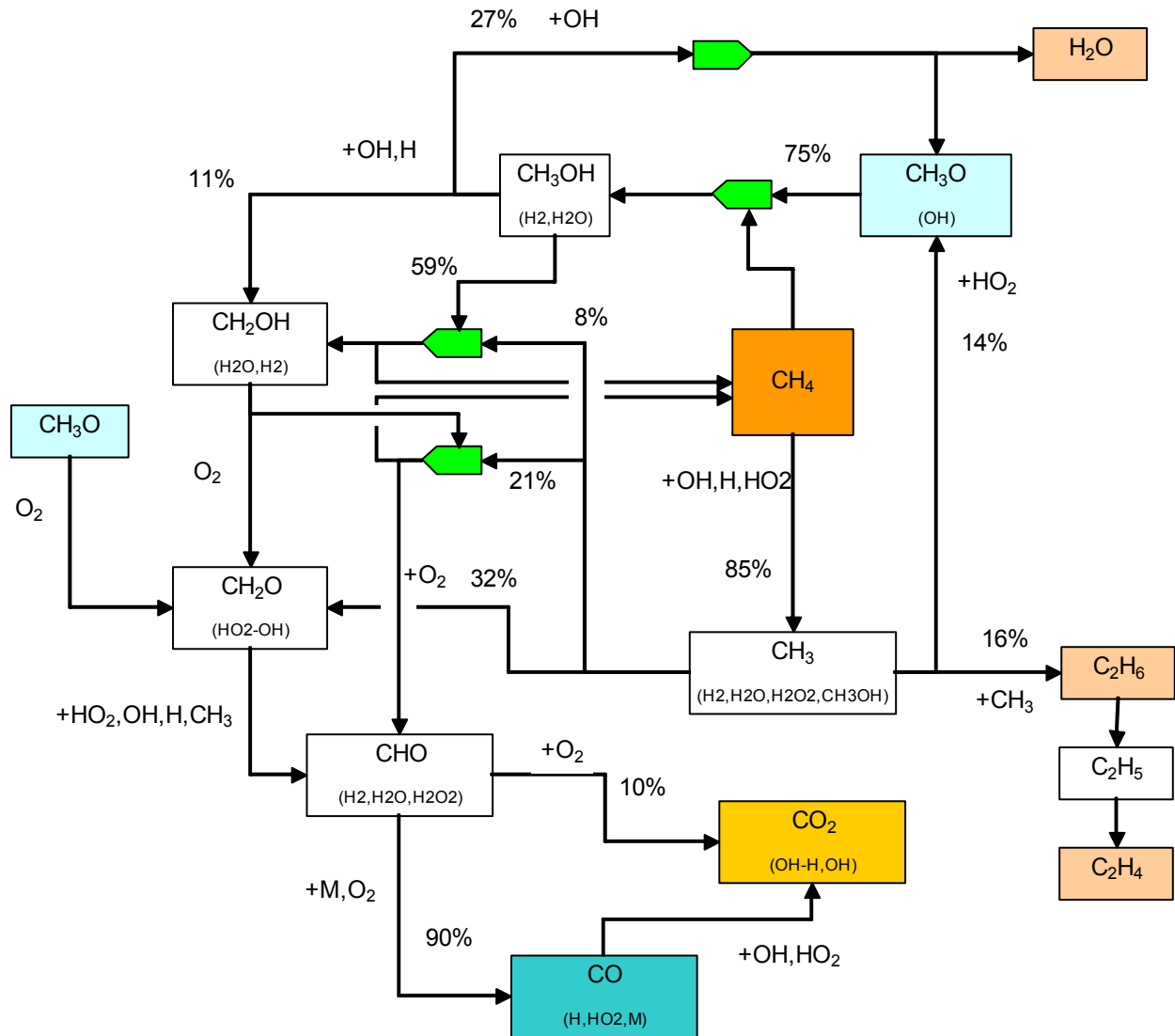


Figure 6.2: Reaction path analysis for the partial oxidation of the complex mixture presented in Table 6.1. Methane main consuming paths are due to radicals attack: OH, H and HO₂ (85% of the decomposed fuel is through this channel). Methoxy radicals (CH₃O) consume the 15% left. Coupling product (C₂H₆) is produced due to recombination of the methyl radicals formed in the first stage of the fuel decomposition, ethylene is secondary specie produced from the ethane decomposition

6.2 Propane Oxidation

Oxidation of propane and butane was studied analytically and experimentally by Cathonnet et al. [73] with the initial temperature in the range of 1023 K < T < 1053 K and pressures in the range 1 bar < p < 6 bar. Experiments were performed with highly diluted samples (nitrogen was used as the oxygen carrier) with equivalence ratios between 0.05 and 25. In both cases it was found that the major products were C₂H₄, C₃H₆, CH₄, CO and C₂H₆.

In the case of propane oxidation, the simulation was made for a mixture with an equivalence ratio of 2.8 and a pressure of 4 bar. A temperature profile was given according to the experimental data ($T_0 = 1033$ K). Results for the calculated species profiles are presented in Figure 6.3.

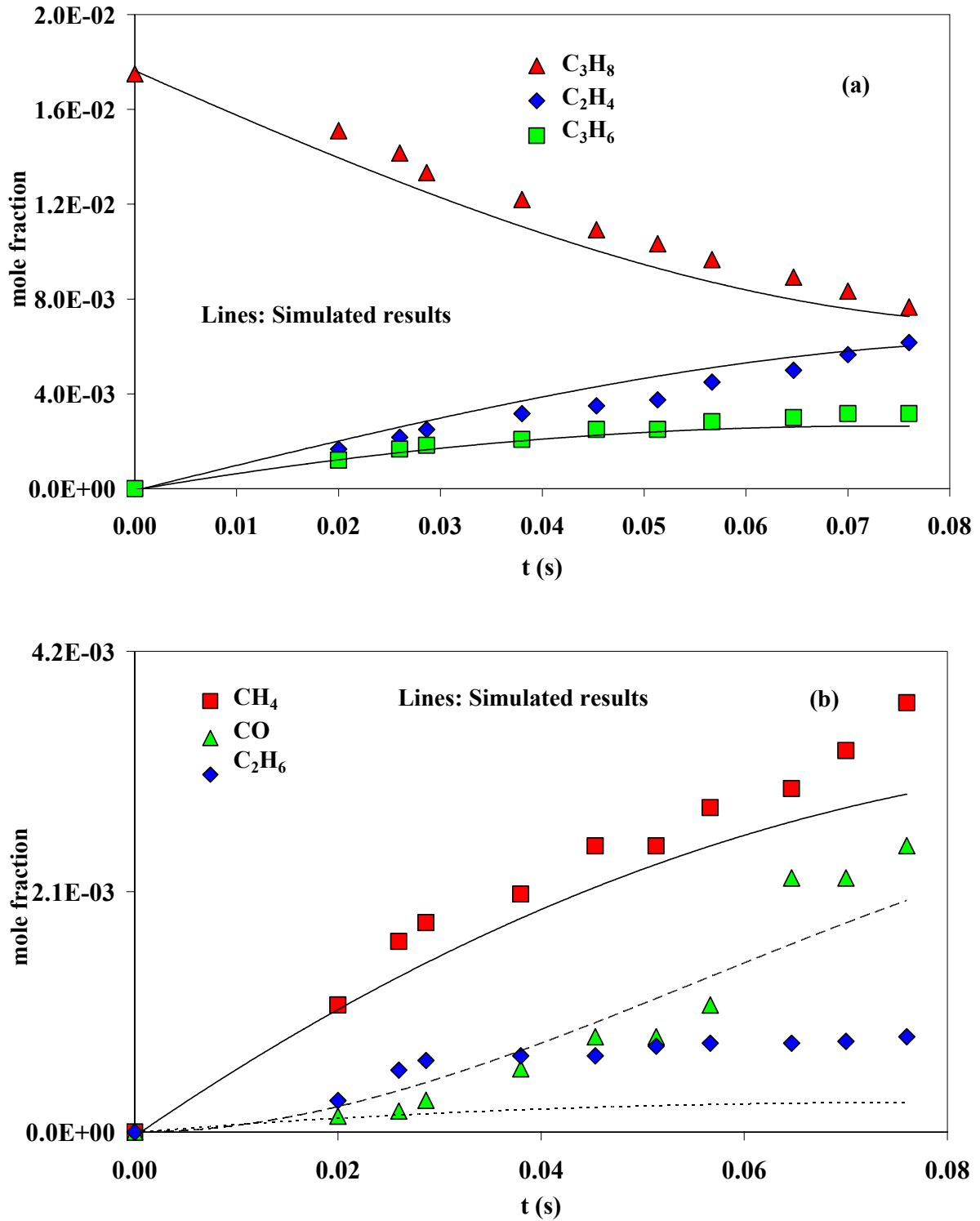


Figure 6.3: Comparison between calculated results and experimental data for the high temperature partial oxidation of propane. Initial conditions: $\phi = 2.8$, $[C_3H_8]_0 = 0.0175\%$ mole, $p = 4$ bar, $T_0 = 1033$ K. Lines: Simulation results; symbols: Experimental data [73]: (a) Propane consumption and olefins production (C_2H_4 and C_3H_6), (b) Methane, carbon monoxide and ethane vol. fraction. At high temperature the decomposition of propyl radicals into CH_3 and C_2H_4 (main product) leads to high yields of methane (methyl further reacts with the fuel) which is similar to those for propylene

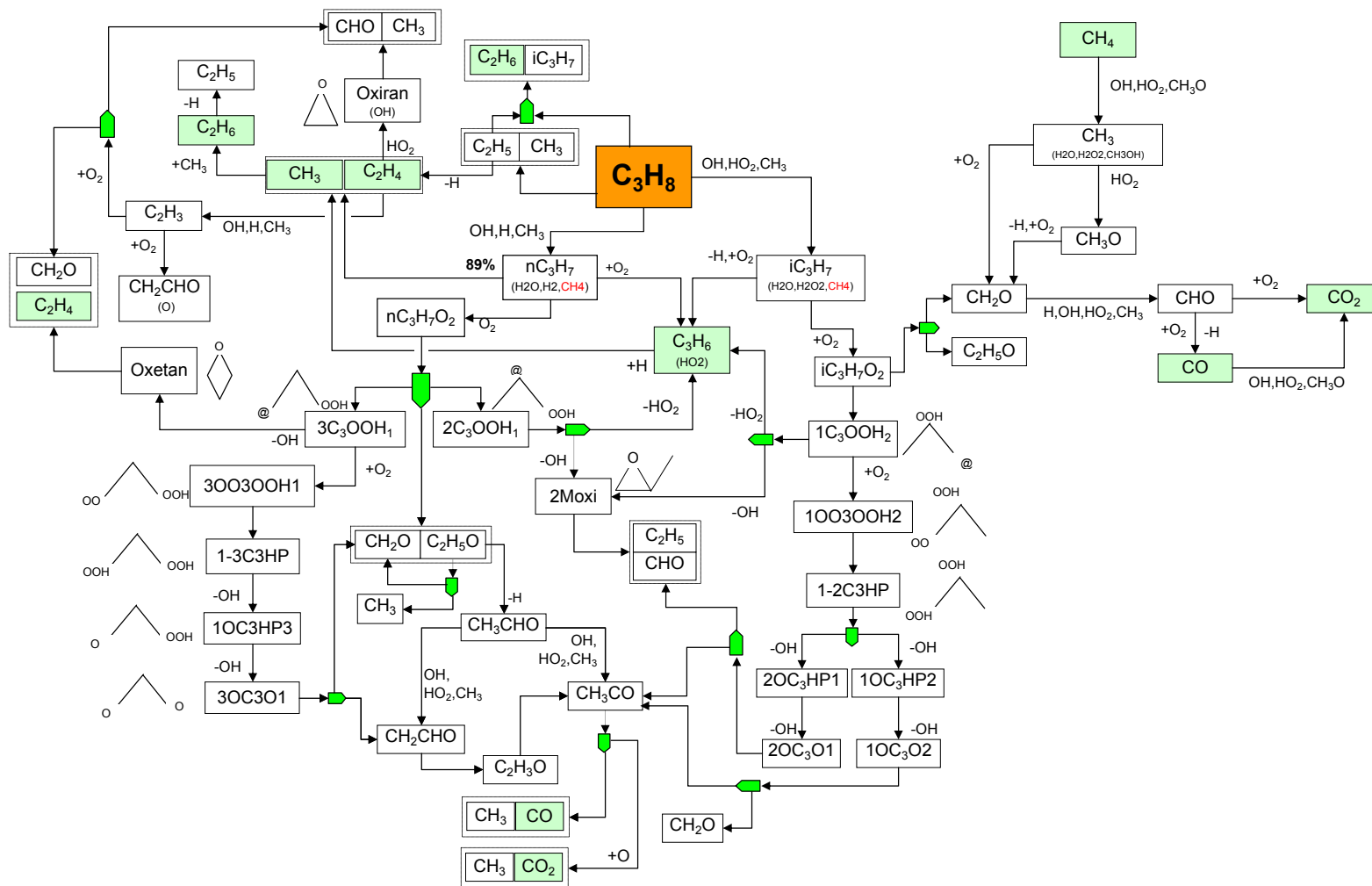


Figure 6.4: Reaction flow analysis for the partial oxidation of propane. Conditions: $\phi = 2.8$, $[C_3H_8]_0 = 0.0175$ mole fraction, $p = 4$ bar, $T_{(t=0)} = 1033$ K. Initially propane is attacked by radical species leading to *n(i)*-propyl formation. Ethylene (largest species formed) is produced mainly from *n*-propyl decomposition in early stages of the reaction. Propylene, other of the largest species experimentally found, is formed during the reaction between *i*-propyl and radical species ($i-C_3H_7 + R \rightarrow C_3H_6 + RH$). Other reaction paths involving oxygen addition, isomerization of the peroxide radical formed and its decomposition are responsible for nearly 14% of the C_3H_6 obtained

The experimentally measured and the calculated data of concentrations presented in Figure 6.3 display similarities. The reaction path calculated at the conditions of the experiments is presented in Figure 6.4.

Propane consumption is mainly due to radical attack. The first step is a hydrogen abstraction reaction. The main abstracting species are OH, hydrogen atoms (H) and methyl radicals (CH₃), which lead to propyl formation. The propyl radicals formed in the first step decompose to ethylene C₂H₄ ($n\text{-C}_3\text{H}_7 \rightarrow \text{C}_2\text{H}_4 + \text{CH}_3$) (Tsang [61]) or to propylene C₃H₆ ($i\text{-C}_3\text{H}_7 \rightarrow \text{C}_3\text{H}_6 + \text{H}$) (Konnov [153]). These two channels consume nearly 85% of the propyl formed, and they are the main channels for olefin production, which were observed in the simulations.

There is, however, a secondary path for propylene formation. This route involves an oxygen addition to the parent propyl ($n(i)\text{-C}_3\text{H}_7$), isomerisation of the peroxyalkyl radicals formed ($n(i)\text{C}_3\text{H}_7\text{O}_2$) and their decomposition to propylene. This second channel represents nearly 14% of the propylene formed and is an indication that this channel should be considered to explain the olefin production during the propane oxidation, especially for low temperatures, where the route via scission is more energy demanding.

Ethylene is formed by the n -propyl scission (85% according to the flow analysis), and by the attack of hydrogen atoms to propylene (7%) ($\text{C}_3\text{H}_6 + \text{H} \leftrightarrow \text{C}_2\text{H}_4 + \text{CH}_3$). Cathonnet [73] proposed that ethylene formation is due solely to propyl scission and did not consider the direct decomposition of propylene to ethylene. The rate coefficient used for the reaction between the propylene and hydrogen atom to ethylene was taken from Hidaka et al. [120].

Methane, which is the other main product found in the experiment, is formed, according to the flow analysis, via two channels: The first includes the reaction between methyl radicals and the fuel; 85% of the methane is formed through this channel. The second channel, which is responsible for 5% of the methane formation, includes a hydrogen atom abstraction from formaldehyde ($\text{CH}_3 + \text{CH}_2\text{O} \leftrightarrow \text{CH}_4 + \text{CHO}$). The kinetic parameters for the reactions between methyl radicals and the fuel are from Tsang [61] and Mintz et al. [163], the formaldehyde reaction from Baulch et al. [25-26, 111].

Methyl recombination plays an important role in the formation of ethane. It is the principle channel which produces ethane, but it is not the only one; 40% of the ethane is formed by the hydrogen atom abstraction from the fuel by ethyl radicals. Ethyl radicals are formed to a lesser extent by the self-decomposition of fuel ($\text{C}_3\text{H}_8 + \text{M}_{(1)} \rightarrow \text{C}_2\text{H}_5 + \text{CH}_3 + \text{M}_{(1)}$), or by the decomposition of ethane that is formed at the first stage of the reaction. This means that, once the ethane has been formed and begins its decomposition, the ethyl that is being formed accelerates the rate of production of ethane from the fuel.

Carbon monoxide and carbon dioxide are formed from methyl radicals, which follow the characteristic path $\text{CH}_3 \rightarrow \text{CH}_2\text{O} \rightarrow \text{CHO} \rightarrow \text{CO} \rightarrow \text{CO}_2$. Other channels involved in the carbon monoxide formation are: direct formation of formaldehyde from the reaction between vinyl radical and oxygen ($\text{C}_2\text{H}_3 + \text{O}_2 \leftrightarrow \text{CH}_2\text{O} + \text{CHO}$) and the low-temperature steps: oxygen addition to propyl radicals \rightarrow internal hydrogen abstraction \rightarrow second oxygen addition \rightarrow second internal abstraction \rightarrow scission OH \rightarrow decomposition into CH₂CHO. This last path is responsible for 15% of the formaldehyde formation.

6.3 Butane Oxidation

Butane oxidation was simulated for an initial mixture with an equivalence ratio of 1.66 at a pressure of 1 bar. The temperature profile was taken from the experimental results given by Cathonnet et al. [73] with an initial temperature of $T_0 = 1033$ K. A comparison between simulation results and experimental data is presented in Figure 6.5.

A similar study for propane and butane oxidation was carried out by Glasmann et al. [164]. In their study three different stages during the reactions were identified. During an initial consumption of the fuel, a non-saturated hydrocarbon species is formed. In the following step there is carbon monoxide formation with some energy being liberated. In the final stage carbon monoxide is converted into carbon dioxide with high energy liberation. Cathonnet [73] limited his study to the first two phases described by Glassman, where a moderate increase in temperature was observed.

The kinetic mechanism reproduces the consumption of the fuel and the production of olefins well, as shown in Figure 6.5 (b). In Figure 6.5 (b), ethane formation is adequately reproduced by the mechanism, however after 0.1 seconds of reaction there is a gap between the calculated values and the experimental data, which indicates a much larger consumption of ethane in the simulation than the one observed during the experiments. Ethane is mainly consumed in the reactions with H and OH (90%). The kinetic data used for these reactions were taken from Baulch et al. [25-26, 111]. The reaction with CH_3 to produce methane and ethyl radicals is responsible for the last 10% of consumption. Kinetic values observed in the experimental work from Moller et al. [165] in the temperature range 1100 K - 1400 K were used.

The prediction of methane production is underestimated by the mechanism and presents the most significant deviation from the experimental data. Experimental values were 25% higher than those of the simulation. In order to improve the correlation between experimental and simulated results, several kinetic values proposed in the literature have been tested (Cathonnet et al. [73], Yampol'skii [166], Sway [167]). The final parameters used are from Sway (abstraction from the secondary position) and Yampol'skii (abstraction from the primary position). The fact that the methane concentration calculated with the mechanism can have a better performance indicates that an adjustment should be done in some of the reactions considered.

Figure 6.6 presents the flow analysis for the butane oxidation under the conditions of the Cathonnet [73] experiments. Butane is consumed by radical attack; H, OH and CH_3 are main reactive species and on a minor scale. Self-decomposition (2%) plays a role in the consumption. Butyl and ethyl radicals, which will conduct the olefin production, are produced in these early stages of the reaction.

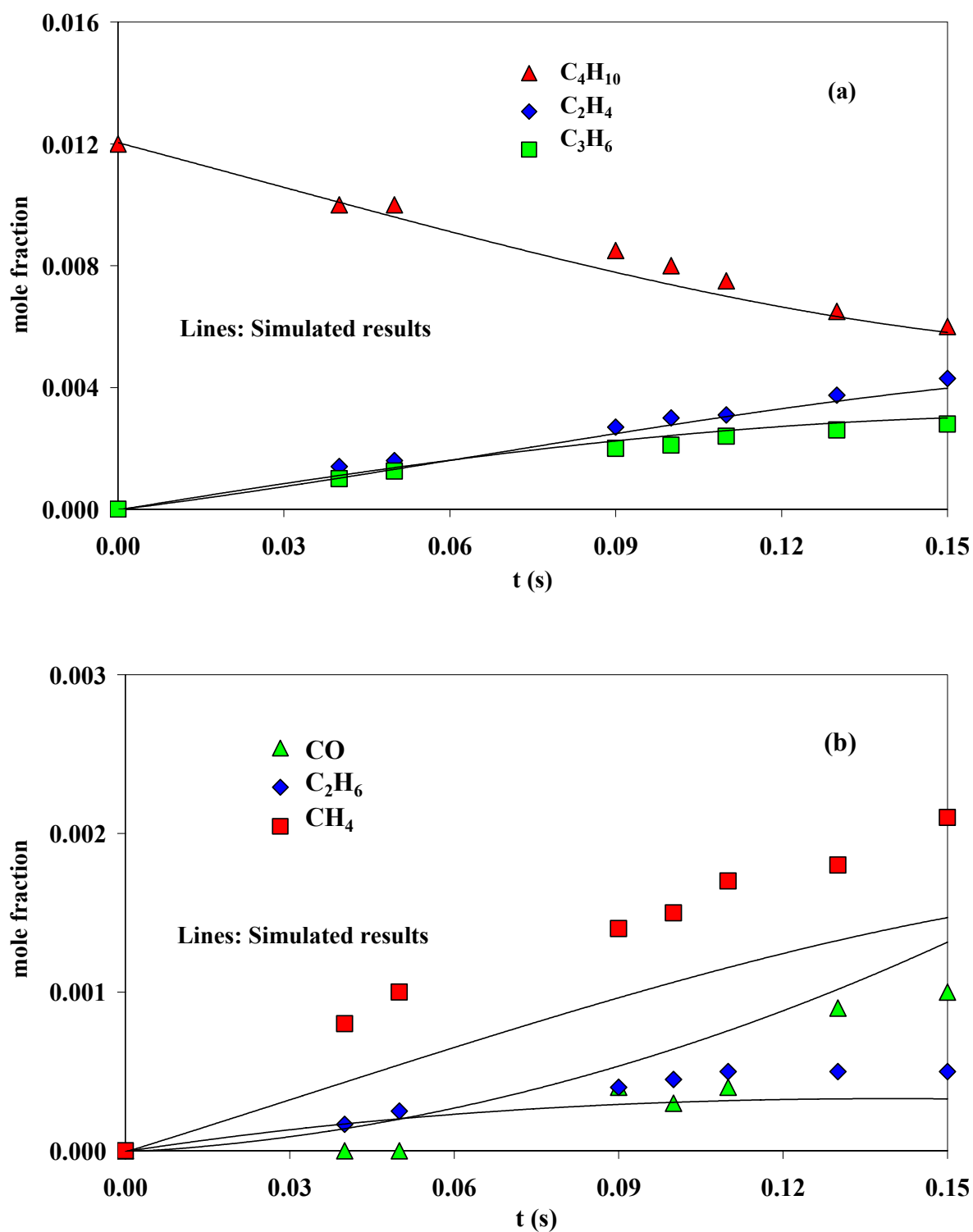


Figure 6.5: Comparison between calculated results and experimental data for the high temperature partial oxidation of butane. Initial conditions: $\phi = 1.66$, $[C_4H_{10}]_0 = 0.012\%$ mole, $p = 1$ bar, $T_0 = 1033$ K. Lines: Simulation results, symbols experimental data [73]. (a) Butane consumption and olefins production, yields of ethylene and propylene are similar at < 0.09 s, after propylene is consumed and higher concentration of ethylene was found. (b) Methane production increases continuously: Initially methane is formed via reactions between methyl radicals and butane; in later stages reactions involving decomposition of ethane, ethylene and aldehydes drive methane formation

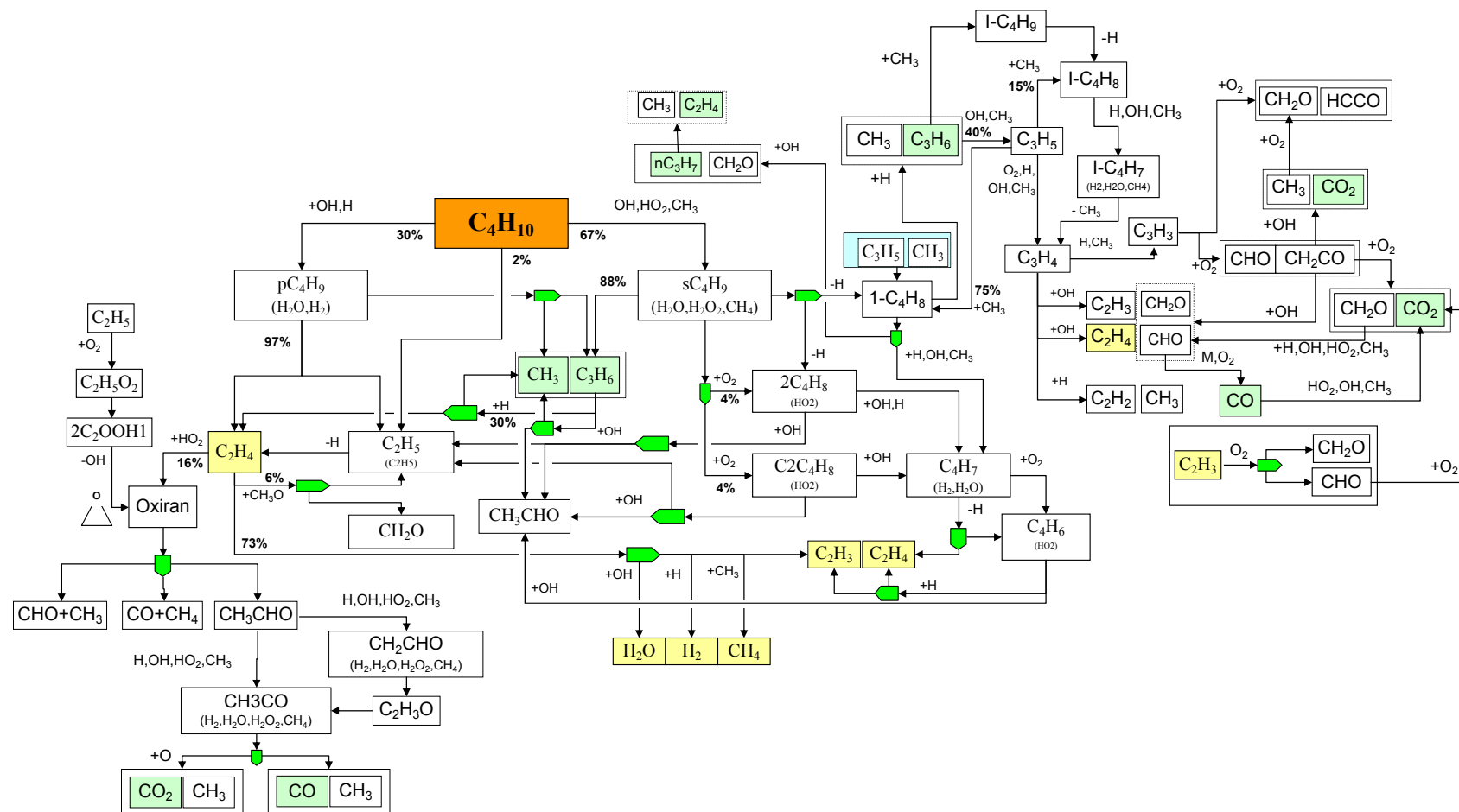


Figure 6.6: Reaction flow analysis for the high temperature partial oxidation of butane. Conditions: $\phi = 1.66$; $[C_4H_{10}]_0 = 0.012$ % mole, $p = 1$ bar, $T_0 = 1033$ K. Propylene is mainly formed (95%) from scission of *s*-butyl radical ($sC_4H_9 \rightarrow C_3H_6 + CH_3$), this step consumes almost all the butyl radicals being formed (88%). Ethylene formation includes two main channels: 1. Direct decomposition of *n*-butyl radicals ($nC_4H_9 \rightarrow C_2H_4 + C_2H_5$) (45% of the C_2H_4 formed). 2. Decomposition of the ethyl radicals formed ($C_2H_5 \rightarrow C_2H_4 + H$) (41% of the C_2H_4 produced). In later stages, propylene to ethylene conversion accounts for the 10% left of the ethylene yield. Formation of C_2H_6 occurs by methyl recombination. Methane formation is explained by the reaction of methyl radical with butane.

For butane, the path for production of olefins is less complex than in the case of propane, and they are formed mainly from butyl radicals. From the flow analysis it was found that nearly 95% of propylene is formed from the scission of $2C_4H_9$ ($2C_4H_9 \rightarrow C_3H_6 + CH_3$) (Cathonnet [73]), whereas ethylene was formed (41%) directly by scission of $1C_4H_9$ ($1C_4H_9 \rightarrow C_2H_5 + C_2H_4$) (Cathonnet [73]), and a second channel (45% of the production) which includes the decomposition of the ethyl radical previously formed to hydrogen atoms and ethylene ($C_2H_5 \rightarrow H + C_2H_4$) (Baulch [25-26, 111]). The last 10% of the ethylene formation results from propylene consumption: 30% of the propylene goes to ethylene. According to the experimental results, in early stages of the reaction selectivities for ethylene and propylene are nearly the same ($t < 0.05$ s), but thereafter the selectivity to propylene decreases in favor of ethylene. In later stages of the reaction, the propylene reaction with hydrogen atoms leads to ethylene formation.

The lighter alkanes CH_4 and C_2H_6 are formed mainly from reactions which involve methyl radicals: Methane is formed from their reaction with the fuel ($C_4H_{10} + CH_3 \rightarrow$ Butyl + CH_4) and ethane by their recombination reaction ($CH_3 + CH_3 + M_{(1)} \rightarrow C_2H_6 + M_{(1)}$). For the conditions given, the reaction between formaldehyde and methyl radicals which produces methane ($CH_3 + CH_2O \leftrightarrow CH_4 + CHO$) also makes an important contribution to the methane formation; 18% is produced due to this channel. During ethane formation, along with the methyl recombination, the hydrogen atom abstraction from the fuel is an important channel; ethyl radicals which are formed from butyl react with the fuel and increase the ethane formation. Nearly 40% of ethane is produced via this channel.

In both cases carbon monoxide is formed from reactions of methyl radicals with oxygen to produce formaldehyde (CH_2O), which then becomes formyl (CHO) and finally produces carbon monoxide. Other paths which lead to CHO formation are concerned with the low temperature reactions; 8% of the formyl radicals is formed from the decomposition of oxirane ($Oxirane \leftrightarrow CHO + CH_3$), which itself is produced by the addition of hydroperoxy radicals to ethylene ($C_2H_4 + HO_2 \leftrightarrow Oxirane + OH$) [111], and (this is the main channel 90%) via oxygen addition, isomerization and follow scission ($C_2H_5 \leftrightarrow C_2H_5O_2 \leftrightarrow 2-C_2OOH-1 \leftrightarrow Oxirane$).

6.4 Ethene Oxidation at Low and Intermediate Temperature

Ethene is a major intermediate product in the oxidation of many hydrocarbon fuels (n-octane, n-pentane, n-butane, propane, propene, and ethane). Its formation is especially important in the oxidation of these fuels in the intermediate and high temperatures.

Alkenes are unsaturated hydrocarbons characterized by the presence of at least one carbon-carbon double bond. Because of that feature, alkene consumption involves free radicals addition at the double bond position: H, O, OH and HO_2 . These reaction channels lead to products such as aldehydes and oxiranes.

Several studies have been performed for the ethane and ethene oxidation: Thornton et al. [168] used a jet-stirred reactor to study the high temperature oxidation of ethene; Wilk et al. [169] used a static reactor to investigate the intermediate temperature oxidation of ethene and Baldwin, Walker and coworkers [170, 171, 172] used a static reactor to determine the mechanism and certain rate coefficients in the ethene reaction.

Wilk et al. [66] theoretically and experimentally studied the ethene oxidation at low and intermediate temperatures; here, their experimental data were used for comparison. Experiments were performed in a static reactor. The experiments were carried out at an initial pressure of 800 mbar with initial temperatures of 696 K and 718 K and an equivalence ratio of 2.

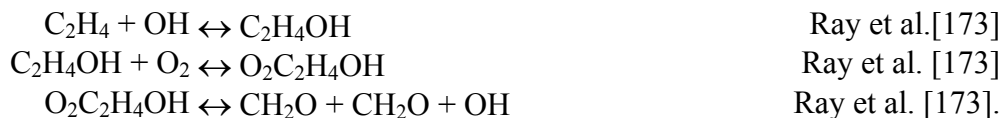
At these conditions the authors reported CO and CO₂ as the main products, alongside oxirane (C₂H₄O) and CH₂O. Methane (CH₄) and methanol (CH₃OH) were the second largest species that were found. Fuel conversion was nearly 66% after 400 s reaction time when the temperature was fixed at 718 K. Figure 6.7 presents the comparison between the experimental data of concentration from Wilk [66] and the results from the simulation.

The calculated and the experimental fuel consumption profiles are in agreement. At 718 K Wilk proposed that most of the ethylene is consumed by the reactions with OH and HO₂. The two main reaction channels are the radical addition to the double bond and a hydrogen atom abstraction. After performing a flow analysis, it was found that ethylene was consumed as follows: During the reaction with OH, 21% is consumed by a hydrogen abstraction reaction and 18% by the addition reaction. The reaction with hydroperoxy radicals to produce ethene oxide consumed 10% of the fuel. The reaction between methoxy radicals and the fuel to produce methanol was another important abstraction path for fuel consumption, and 22% of the fuel was consumed by this channel.

The production of ethene oxide, which is the largest intermediate species, is controlled by the addition of hydroperoxy radicals to ethene, followed by a scission from the radicals formed. The chain reaction is as follows:

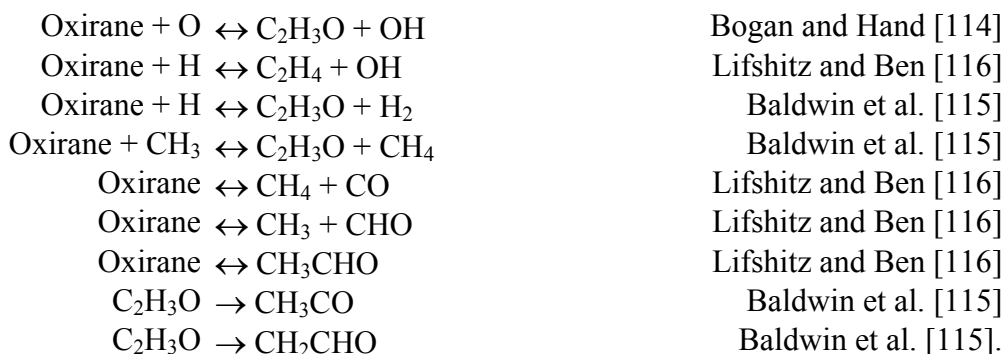


This sequence is responsible for ethene oxide formation and transforms HO₂ radicals into the more reactive OH radical. Formaldehyde (CH₂O) is mainly formed (30%) through the so-called *Waddington mechanism* [173],



30% of the CH₂O formed is due to this mechanism. CH₂O formation also includes C₂H₄OOH decomposition (C₂H₄OOH ↔ CH₂OH + CH₂O) and the further oxidation of CH₂OH to CH₂O and HO₂. Based on the flow analysis, 15% of CH₂O was formed due to this route, and reaction of vinyl radicals with oxygen generated the last 55% of CH₂O.

The mechanism describing ethene oxide formation was already described in the previous section; for its consumption a new set of reactions was included. The channels considering the ethene oxide consumption include a hydrogen atom abstraction by radicals (kinetic parameters used for these reactions are from the studies of Bogan and Hand [114], Baldwin et al. [115] and Lifshitz and Ben [116]), isomerization, and decomposition. From these reactions, OH hydrogen atom abstraction is the most important and consumes 50% of the fuel. After the abstraction, the oxyranyl formed (C₂H₃O) has two isomerization reactions to CH₂CHO or to acetyl radicals (CH₃CO). The reactions included here are as follows:



It is still unclear which are the correct kinetic values for the isomerization or decomposition of C₂H₃O. Chen [117] proposed for the isomerization to CH₂CHO a value for $k = 2 \cdot 10^{+04} \text{ s}^{-1}$, Wilk et al. [169] proposed an activation energy of 58 kJ/mol for both isomerization channels and Baldwin proposed a ratio of 8.55 between their rate coefficients. The kinetic parameters used in this study consider the values for the activation energy for both reactions according to Wilk, and the ratio of formation of 8.55 proposed by Baldwin. From the flow analysis, oxirane formed is mainly consumed in the reaction to acetyl radical, and the path to CH₂CHO was not important. Finally, acetyl radicals formed decompose to methyl and carbon monoxide (90% of it), and a small part goes directly to carbon dioxide and methyl (CH₃CO + O \leftrightarrow CH₃ + CO₂). The kinetic values used for both reactions are the ones given by Baulch et al. [25-26, 111].

The model underestimates the quantity of methanol that is formed. Results from Wilk et al. [66] agree with the experimental values. Wilk proposed that methanol is mainly formed by methoxy radicals by a hydrogen atom abstraction (CH₃O + C₂H₄ \leftrightarrow CH₃OH + C₂H₃; CH₃O + CH₂O \leftrightarrow CH₃OH + HCO). These two reactions had already been implemented in the mechanism. The kinetic data used were proposed by Konnov [153] for the abstraction from the fuel and by Tsang [53] for the second reaction. The underestimation of methanol indicates that the predicted consumption is faster than it occurs experimentally. The reaction with OH is the most important and consumes 90% of the methanol formed.

CO and CO₂ were the largest products found during the experiments. Carbon monoxide was formed during the oxidation of formyl radicals (90%) and by decomposition of acetyl radicals (10%). Carbon dioxide is formed by the reaction of carbon monoxide with OH (25%), the reaction of carbon monoxide with hydroxyl radicals (15%), the reaction with methoxy (5%), and direct oxidation of formyl (CHO + O₂ \leftrightarrow CO₂ + OH).

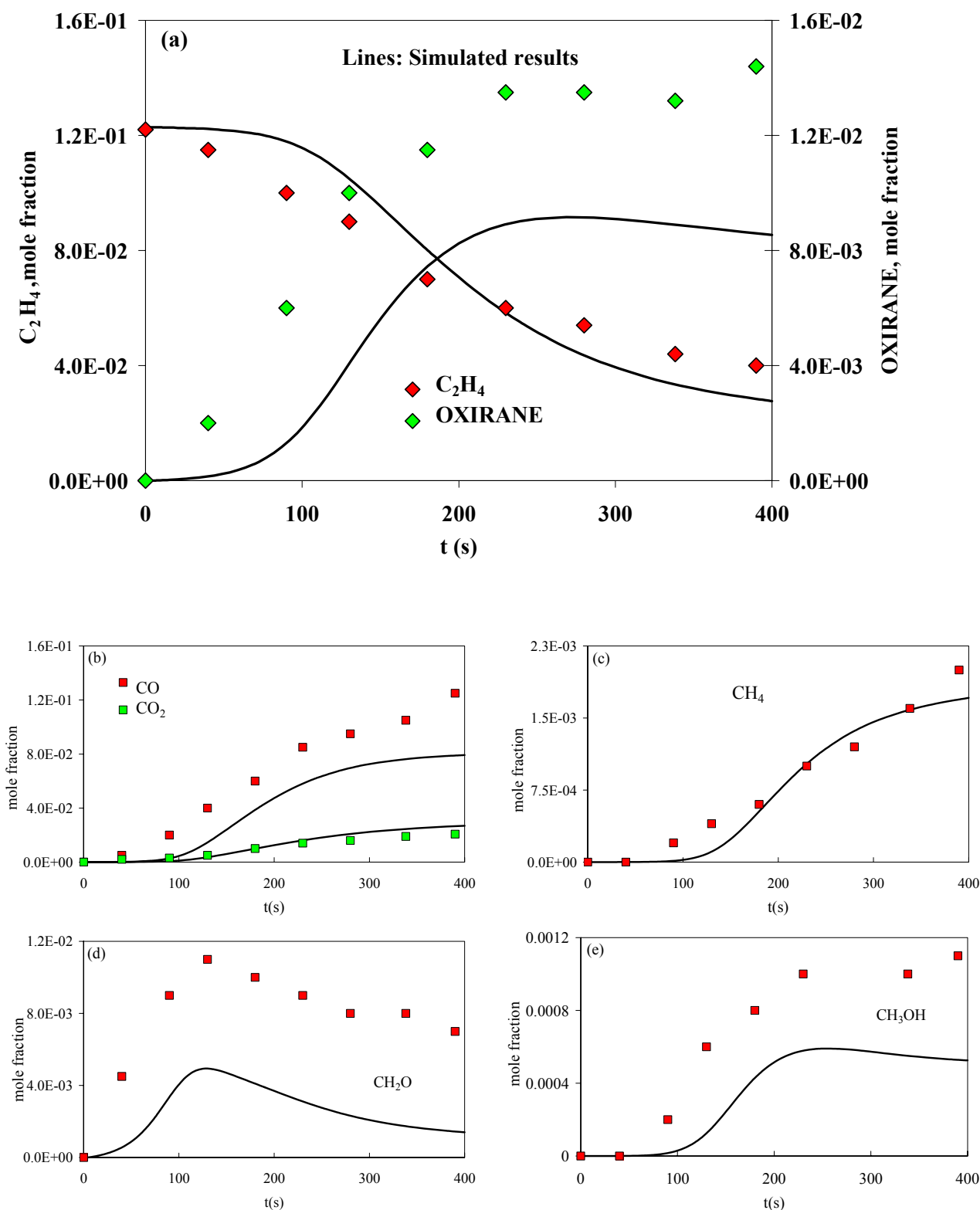


Figure 6.7: Comparison between the calculated species profiles and the experimental data reported in [66] for the C₂H₄ oxidation at low temperature. Experimental conditions: [C₂H₄]₀ = 0.122 mole fraction; [O₂]₀ = 0.1842 mole fraction. T = 718 K, p = 800 mbar

Chapter 7

CATALYTIC PARTIAL OXIDATION OF METHANE IN A SINGLE GAUZE REACTOR

7.1 Introduction

The production of synthesis gas (carbon monoxide + hydrogen) is currently carried out via steam reforming. In that process steam passes over a carbon source, often methane or coal, and is heated to produce the synthesis gas. Synthesis gas is extremely valuable commercially for the production of methanol, hydrocarbons, and higher alcohols for use in detergents and ammonia for use in fertilizers. There is also significant interest in the production of hydrogen for fuel cells.

Steam reforming has the major disadvantage of being endothermic, and hence requires a large amount of wasted energy to drive on the reaction. An alternative to steam reforming is the partial oxidation of the hydrocarbons, especially methane, in short-contact-time reactors, which is commonly referred to as CPOX. The major advantage here is that the process is exothermic, so energy is not consumed in order to drive the reaction. The partial oxidation of methane is described by the global reaction



Several studies have been performed in order to find a more efficient route to convert methane into syngas as well as for the coupling process to obtain higher hydrocarbons: Zanthoff and Baerns [44] studied the oxidative coupling of methane in the gas phase, Chen et al. [49] studied the oxidative coupling of methane, in the presence and absence of a catalyst, with ethane co-feeding. Baerns [51] studied the oxidative coupling of methane from around 700°C to 900°C and found that ethane, ethylene, and small quantities of other higher hydrocarbons were present in the presence and absence of a catalyst. Wiele et al. [52] studied the roles of the gas-phase and the heterogeneous chemistry in the oxidative coupling of methane. Goralski and Schmidt [174] modeled a short-contact-time catalytic methane combustor as a plug-flow tubular reactor using homogeneous and heterogeneous chemistry. Initially, Hickman and Schmidt [175] developed a multi-step surface mechanism for partial oxidation of methane on rhodium and later Deutschmann and Schmidt [176] performed a two-dimensional numerical

simulation for a single monolith channel using the experimental work of Bodke et al. [177]. Deutschmann et al. [29] also studied the catalytic combustion of methane on platinum foil and syngas formation in a short-contact-time reactor combining the catalytic process with the surrounding flow.

Hickman and Schmidt [175] applied adiabatically operated monoliths containing platinum and rhodium catalysts and reported hydrogen and carbon monoxide selectivities as well as methane conversion above 90% for methane partial oxidation on rhodium-coated foam monoliths. The main advantage of their reactor was the fact that the reactor could be operated auto-thermally at residence times of a few milliseconds.

Recent studies (Schwiedernoch [178]) reported, experimentally and theoretically, results for the total and partial oxidation of methane over platinum, palladium, and rhodium catalysts for a wide range of operating conditions. The experiments were carried out in such a way that transient processes such as light-off were investigated. Simulations were performed for methane conversion on catalytic monoliths, taking into account detailed mechanisms of surface and gas-phase reactions as well as mass and heat transport processes in the channels and heat transport in the solid monolithic structure.

Detailed modeling and simulation support a better understanding and the technical realization of those high-temperature catalytic reactors, which are characterized by complex interactions between reactive flow and catalytic surface, heterogeneous and homogeneous chemistry, and the competition between complete and partial oxidation.

Here, a detailed study of the catalytic partial oxidation of methane in a single gauze reactor is presented, which is based on three-dimensional numerical simulations of the flow field coupled with heat transport and multi-step gas-phase and surface reaction mechanisms, including the computation of the surface coverage. Results from the model were compared with experimental data by Smet et al. [179].

The results from the simulation of the partial oxidation of methane in a short contact time reactor were carried out using the commercial computational fluid dynamics code FLUENT [180], which is coupled with external subroutines to model the detailed gas-phase and surface chemistry.

7.2 Experiment

Smet et al. [179] studied the partial oxidation of methane with oxygen to synthesis gas by performing steady state experiments in a continuous flow reactor set-up containing a single Pt metal gauze. The results of their experiments will be used in order to model the effects of the gas-phase and surface reactions.

7.2.1 Experimental Set-Up

The gauze used in the simulations, schematically shown in Figure 7.1c, reproduced that reported by Smet et al. [179, 181]. The gauze catalyst consists of two rows of six parallel platinum wires placed on top of each other (Figure 1a). The average distance between the centers of two individual wires (diameter = 0.20 mm) was $8.2 \cdot 10^{-4}$ m (Figure 1b).

The quartz reactor contained three zones: In the first zone the reactant gases were preheated, the Pt gauze catalyst was located at the end of the preheating zone. The final zone was for cooling the products that were formed after the reacting mixture crossed the gauze.

The gas-phase temperature was measured upstream and downstream of the Pt gauze by Nisil-Nicrosil thermocouples. Surface temperature was determined directly by means of a surface thermocouple.

Due to symmetry considerations, only a quarter of a single mesh of the gauze catalyst had been taken into account in the computational grid, including a single contact point between two wires. The domain extends for half of the distance between centres of two individual wires (amount $4.1 \cdot 10^{-4}$ m) in the “Y” direction (Figure 1c).

Results of temperature measurements are presented in Figure 7.2. The bulk gas-phase temperature was defined as the average gas-phase temperatures measured upstream and downstream of the gauze catalyst; its value was nearly 200 K less than the catalyst temperature.

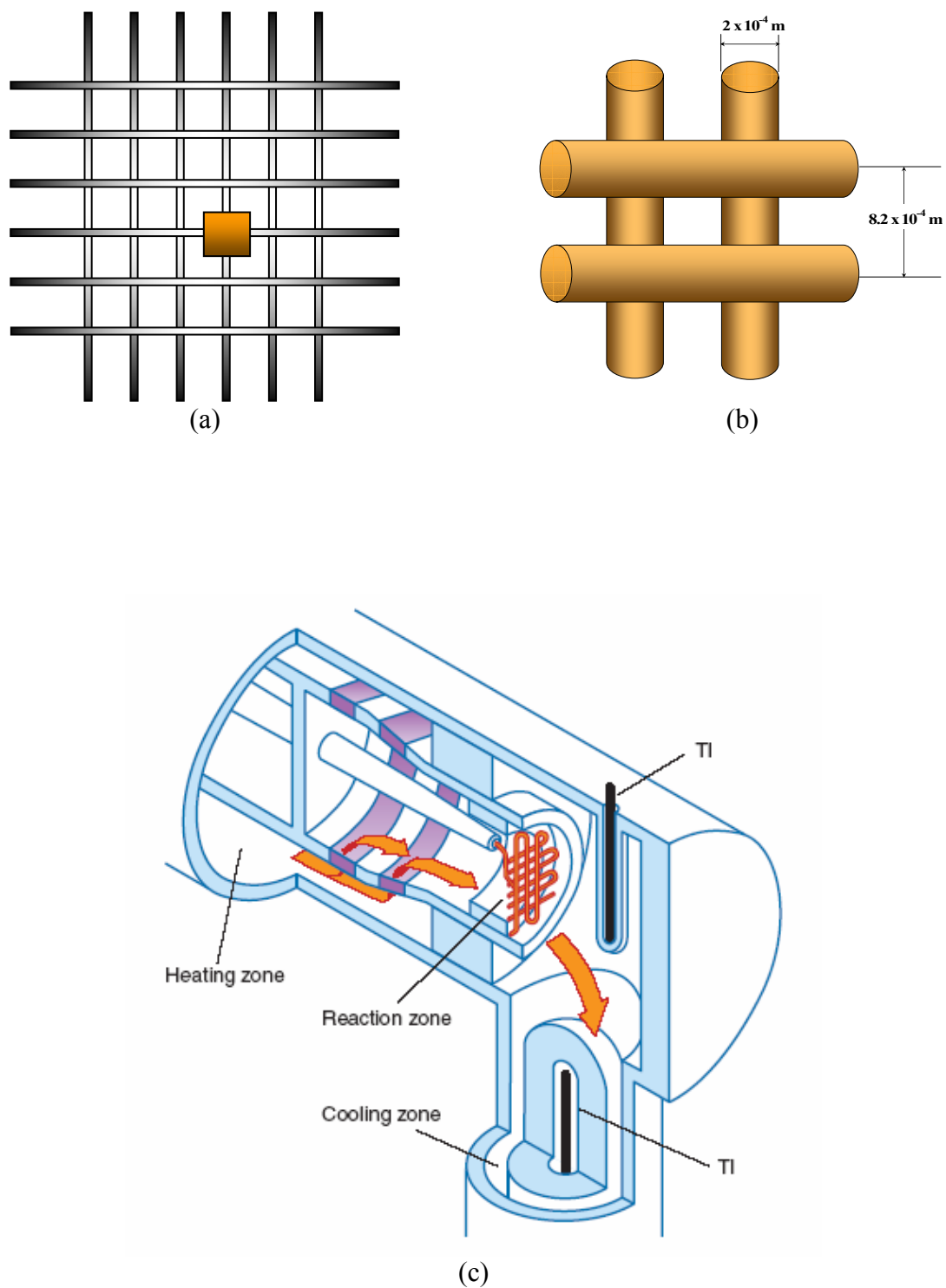


Figure 7.1: Schematic illustration of the reactor used by Smet et al. [179, 181] for the study of methane partial oxidation. (a) The illustration of the Pt gauze builds up using a single Pt wire. (b) Pt gauze geometry. (c) Reactor set-up. Original figure from [181]

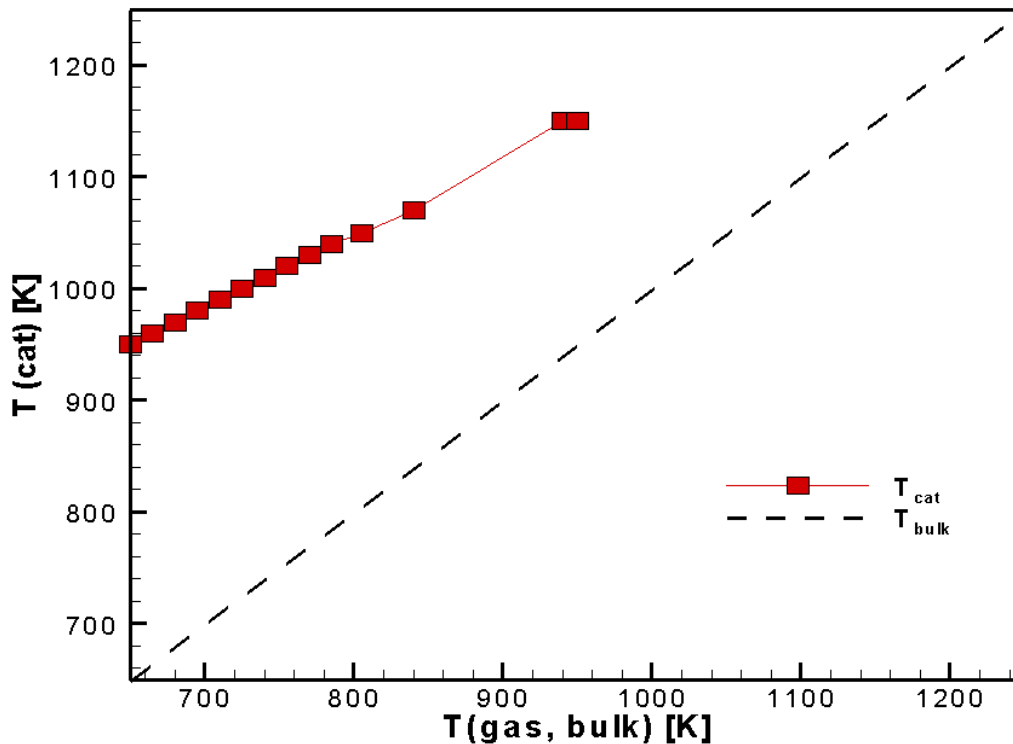


Figure 7.2: Comparison between measured temperature at the catalyst surface and the gas-phase bulk temperature. Conditions: $p_{\text{tot}} = 130 \text{ kPa}$, $F_{\text{tot}} = 1 \cdot 10^{-2} \text{ mol s}^{-1}$, $W/F_{\text{CH}_4, \text{O}} = 39.9$; $\text{CH}_4/\text{O}_2/\text{He} : 14.3/5.7/80.0$. Experiments of Smet et al. [179]

The conversion of reactants and the product selectivities were calculated based on the mole fractions of C, O, and H in the product stream. During the experiments the total molar flow rate was varied in the range $1.5 \text{ mmol} \cdot \text{s}^{-1}$ to $20 \text{ mmol} \cdot \text{s}^{-1}$ at the position of the gauze catalysts, which resulted in linear gas velocities of $1.5 \text{ m} \cdot \text{s}^{-1}$ to $20 \text{ m} \cdot \text{s}^{-1}$ corresponding to Reynolds numbers (with the density, velocity, and viscosity calculated at the gauze) of 1000, which indicates that the flow pattern was laminar.

7.2.2 Results of the Experiments

At all conditions the authors reported CO, CO₂ and H₂O as the main products, H₂ was found only at high temperatures (above 1270 K). Figure 7.3 shows the influence of the temperature on the conversions and selectivities. Methane and oxygen conversions were independent of the catalyst temperature. In the CO case there is a strong temperature dependence: the selectivity increased from 20% at 1025 K to 50% at 1200 K. These results are in agreement with the earlier ones reported by Hofstadt et al. [182] and Hickman and Schmidt [183]; both studies used Pt and Pt-10% Rh gauzes.

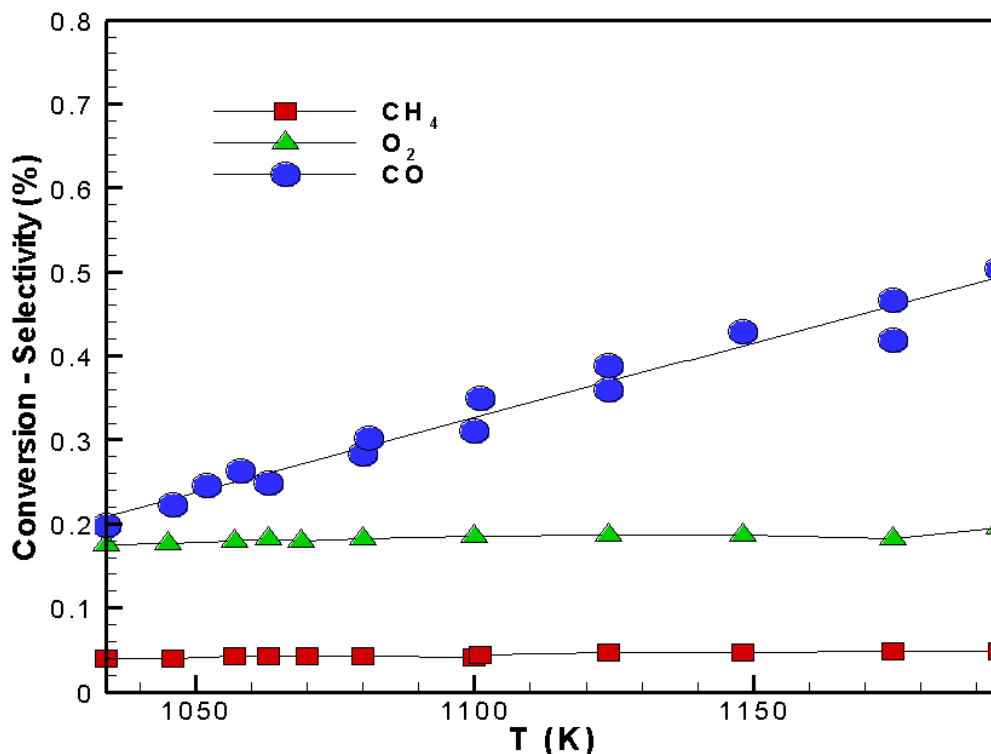


Figure 7.3: Conversion and selectivity as a function of the catalyst temperature. $p_{tot} = 130$ kPa, $F_{tot} = 1 \cdot 10^{-2}$ mol s^{-1} . $CH_4/O_2/He = 14.3/5.7/80.0$. Lines: Results of the simulation. Symbols: Experimental data [179]

7.3 Kinetic Mechanisms

Partial oxidation of methane can take place over a wide range of catalyst types and surfaces, although certain common features of the mechanism can be discerned [184]: In general the formation of C_2 hydrocarbons only takes place at temperatures above $600^\circ C$. The highest selectivity to C_2 species occurs at the lowest methane conversion. Increase in temperature or decrease in CH_4/O_2 ratio increases the methane conversion; the CO_x field (CO and CO_2) increases with temperature and O_2 mole fraction.

The first step in the catalytic partial oxidation of methane involves the breaking of a C-H bond in the catalysis surface (Hickman and Schmidt [175], Deutschmann et al. [176], Mackie [184]); afterwards the free radicals species formed may undergo reaction with the oxidant. Dependent on the catalyst nature, a portion of the subsequent reaction will take place on the surface, or some fraction of the total reaction will comprise a sequence of partial reactions in the gas-phase.

Originally a coupling process was thought to take place only on the catalytic surface [185]. Ito et al. [186] proposed that the recombination of two methyl radicals resulting from the H atom abstraction from the fuel on the surface can occur either in the gas-phase or on the surface, which is the responsible path for ethane formation. Later, Campbell et al. [187] identified methyl radicals in the gas-phase during the partial oxidation of methane and demonstrated that this is an important channel in the C_2H_6 formation. CO_x was thought to arise from surface reactions of methyl with oxygen or secondary gas-phase oxidation of the C_2 species.

The above experimental evidence underlines the importance of coupling gas-phase and surface reaction mechanisms for developing robust kinetic schemes able to simulate the high-temperature catalytic partial oxidation of methane in the millisecond regime.

7.3.1 Gas-Phase Mechanism

Simulations performed in the homogeneous reactor at contact times, temperature and pressure as in the gauze reactor showed that isolated gas-phase reactions did not occur although interactions between surface and the gas processes happen, as it was previously mentioned. Therefore, a gas-phase mechanism suitable to be implemented in the CFD model should be used. To this end, a reduction of the already complex mechanism was performed, taking care to include those reactions which occur at the conditions in the catalytic gauze. This means that several assumptions should be made:

The first consideration was to extend the time for the gas-phase calculations until reaching reactant conversion as it was found experimentally in the gauze: The final time was set at 5% of fuel conversion. The methane/oxygen ratio used for the initial mixture prior to the reduction was 2.5, the pressure 1 bar and the temperature 1100 K.

The final reduced mechanism consists of 150 reactions and 30 species; the reaction path for the consumption of the fuel and the formation of the main products is presented in Figure 7.4.

From sensitivity and flow analysis it was inferred that the most important steps in the gas phase are the following ones: initial abstraction of hydrogen from the methane molecule by a free radical or oxygen; main channels include abstraction by hydroxyl (OH), atomic hydrogen (H), HO₂ and atomic oxygen (O). The methyl that is formed at this stage will react to produce formaldehyde CH₂O. Reaction of formaldehyde with radical species (hydroxyl and hydroperoxy) yields the formyl radical (CHO), which further is oxidized to carbon monoxide (CO) and carbon dioxide (CO₂).

There is an alternative path that consumes the methyl that is formed: Methyl is oxidized, and as a result methoxy radicals are formed (CH₃O). The methoxy attacks the fuel, increasing its consumption and leading to the production of CO by the parallel channel CH₃OH → CH₂OH → CHO → CO. A final channel consuming the methyl is its recombination reaction (ethane (C₂H₆) is produced). Later the ethane proceeds to be dehydrogenated and ethene and other C₂ gas-phase species appear.

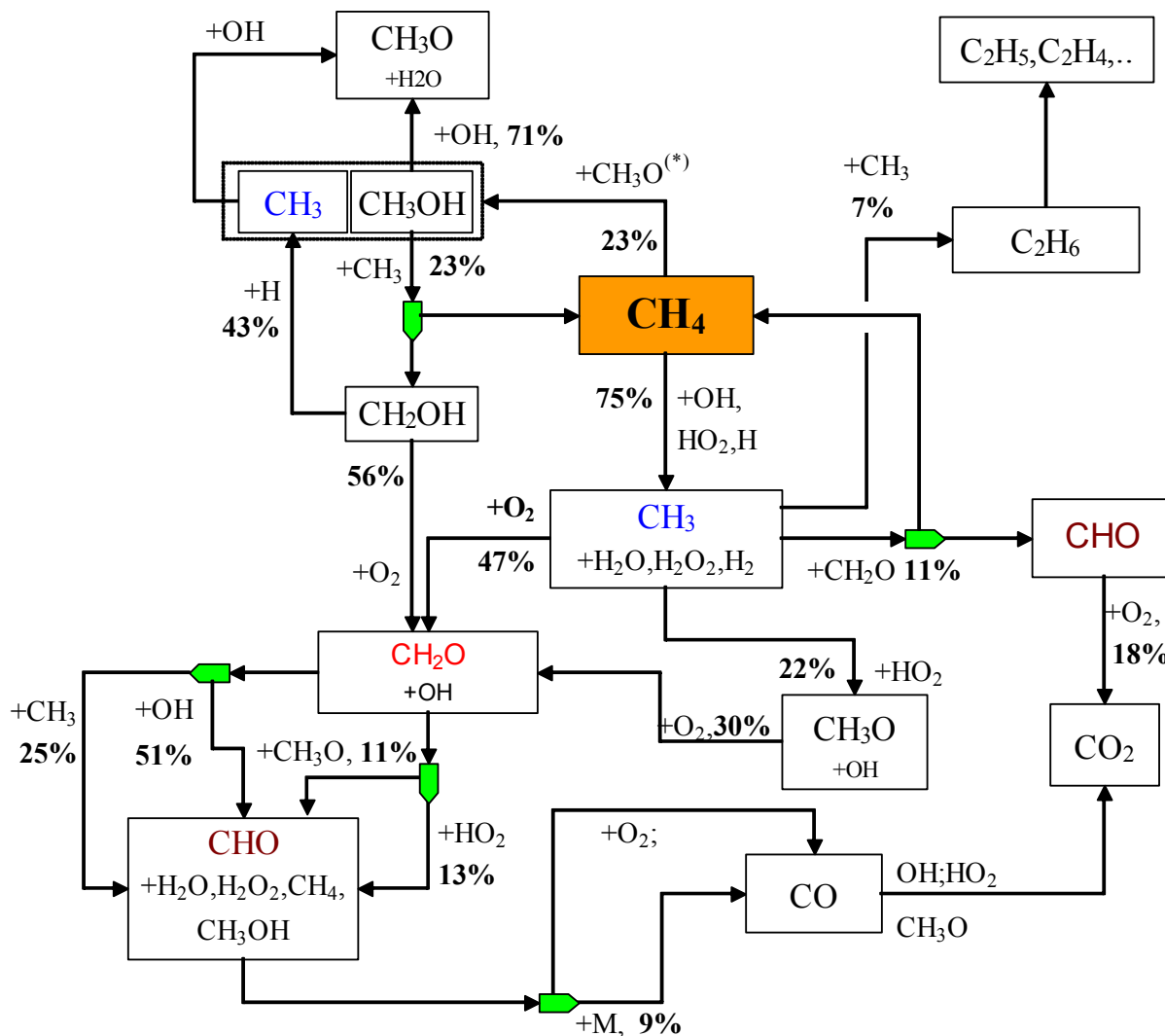


Figure 7.4: Reaction path analysis for methane oxidation in the gas phase. Percentages in the flow analysis quantify the consumption of the species due to that elementary step. Conditions: CH_4/O_2 ratio = 2.5 (vol.), $T = 1050$ K, $p = 1$ bar. The residence time was fixed in order to achieve a methane conversion of 5% (see text)

7.3.2 Surface Mechanism

The mechanism used for these calculations is based on the initial mechanism proposed by Deutschmann et al. [29] to predict ignition and steady state operation for the catalytic combustion of methane on Pt surfaces. The original mechanism includes 10 surface species, 9 reversible reactions, and 8 irreversible reactions. The scheme assumes interaction between the gas-phase mechanism and the surface mechanism via the molecular species of hydrogen, oxygen, methane (via dissociative adsorption), carbon monoxide, carbon dioxide and water, as well as the radical species hydrogen, oxygen and hydroxyl.

Some modifications have been made in order to improve the performance over a wider range of conditions; Zerkle et al. [68] developed a mechanism to model the C_1 and C_2 partial oxidation reactions in a short-contact-time reactor. The mechanism consists of 19 surface species and 41 reversible reaction steps and includes a complete C_1 surface mechanism, with initial adsorption steps for the methane with atomic oxygen and hydroxyl radicals. These two

steps are included in a modified Deutschmann mechanism as well as the desorption steps for the fuel, which were not included in the original one. A summary of the reaction steps with their associated rates can be found in Annex II.

7.4 Modeling Approach

Deutschmann [28] discusses the most relevant works on catalytic modeling. The following is a summary of these:

The earliest simulation by Hickman and Schmidt [175] assumed tubular plug flow behavior for the short-contact-time reactor. In their work, the authors assumed uniform distribution for the temperature, which could be determined by a heat balance consistent with the reactor exit-product distribution. Gas-phase reactions were not considered, and with a purely heterogeneous mechanism, these authors were able to predict CO and H₂ product selectivities that are consistent with those observed experimentally.

Wolf et al. [188] studied mass and heat transfer limitations to the partial oxidation of methane over a Pt/MgO catalyst, comparing experimental results to simulations employing a simple four-step heterogeneous kinetic model and one-dimensional plug flow analysis.

Veser and Frauhammer [189] applied a one-dimensional two-phase reactor model for the oxidation of methane to synthesis gas over platinum in a monolith reactor. The model incorporates a detailed surface reaction mechanism and a simplified gas-phase reaction mechanism.

Deutschmann applies more sophisticated transport and chemistry models for the description of catalytic partial oxidation of methane on rhodium. A reactor was modeled in two dimensions with full mass transport and heterogeneous reaction chemistry using FLUENT coupled with the DETCHEM [190] software to simulate coverage-dependent surface reactions. In the gas-phase, full heat transport was employed, but an isothermal condition was imposed on the wall with the temperature chosen to be consistent with experimental observations [176].

A three-dimensional simulation of the catalytic partial oxidation of methane to synthesis gas in a wire-gauze configuration has previously been performed by Smet et al. [179], also using a simple surface reaction model.

Schwiedernoch [178] performed detailed numerical simulations of the physical and chemical processes using the DETCHEM package and the commercially available CFD code FLUENT. The numerical codes take into account detailed mechanisms of surface and gas-phase reactions as well as mass and heat transport processes in the channels and heat transport in the solid monolithic structure. The channels are simulated under steady-state conditions in three dimensions by an elliptic approach using FLUENT and in two dimensions by a parabolic approach using DETCHEM^{CHANNEL}. Transient phenomena are simulated using the DETCHEM^{MONOLITH} package.

Results from a multidimensional model using complex gas and surface chemistry will be presented. Multidimensional simulations using multi-step chemical mechanisms are highly demanding with respect to computing resources and time. Therefore, a simpler CFD model was used to evaluate effects of the new surfaces steps on the original Deutschmann [29]

surface mechanism. Once the evaluation was performed, the kinetic mechanism was implemented in a three-dimensional gauze reactor model, coupled with the flow field and heat transfer. Results from both cases were compared.

7.4.1 Channel Simulation of the Catalytic Gauze

A two-dimensional simulation including mass and heat transport effects was performed using the CHANNEL code, which is part of the DETCHEM package [190]. The following assumptions were made to approximate the gauze to the conditions used by the code:

The diameter size was chosen considering a hydraulic diameter that was calculated with the free path to the flow in the gauze. The dimension of the channel was chosen so that the contact area was the same as the exposed area of the gauze. With these geometrical parameters fixed, only the residence time of the mixture remains unspecified; to determine residence time, initial velocity was tuned, making the residence of the mixture inside the channel coincide with the contact time for the mixture at the gauze. A summary of the conditions used for this simulation is given in Table 7.1.

Table 7.1 Conditions used for the simulations with the channel reactor model

| | |
|---------------------------------------|----------------------|
| Catalytic wall temperature (K) | 1025 - 1175 |
| Internal diameter (m) | $1.55 \cdot 10^{-4}$ |
| Longitude (m) | $5.30 \cdot 10^{-4}$ |
| Mixture molar composition | |
| vol.% CH ₄ | 14.3 |
| vol.% O ₂ | 5.7 |
| vol.% He | 80.0 |
| Residence time ($1 \cdot 10^{-3}$ s) | 0.02 - 0.2 |

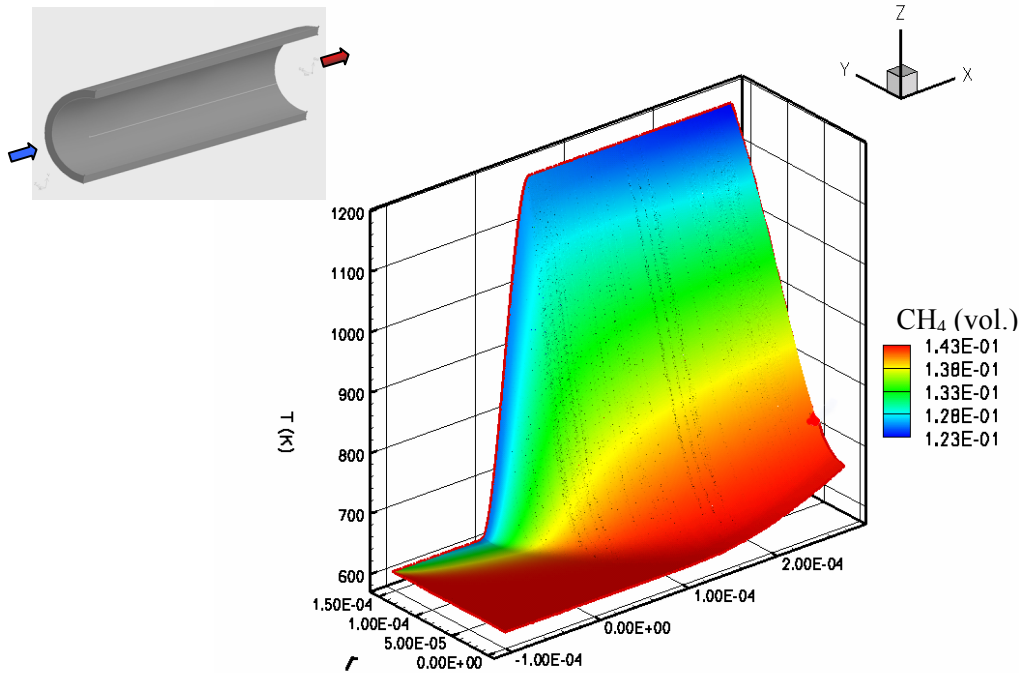
Lines in Figure 7.3 present the results of the simulation for the influence of the catalyst temperature and the conversion (selectivity) using the modified mechanism. The mechanism was able to predict the selectivity and conversions from the experiments in the range of conditions considered. The numerical results are close to those observed in the experiments with the gauze with oxygen conversions overestimated by 2% to 3%.

Figure 7.5 presents the species concentration and temperature profile including gas-phase and surface mechanisms. The mixture flows from left to the right in the picture, the radial position (r) is set to zero at the tube axis so that the catalytic wall is at $r = r_{\max}$. The wall temperature (located at the back side) was kept at 1175 K for the mixture.

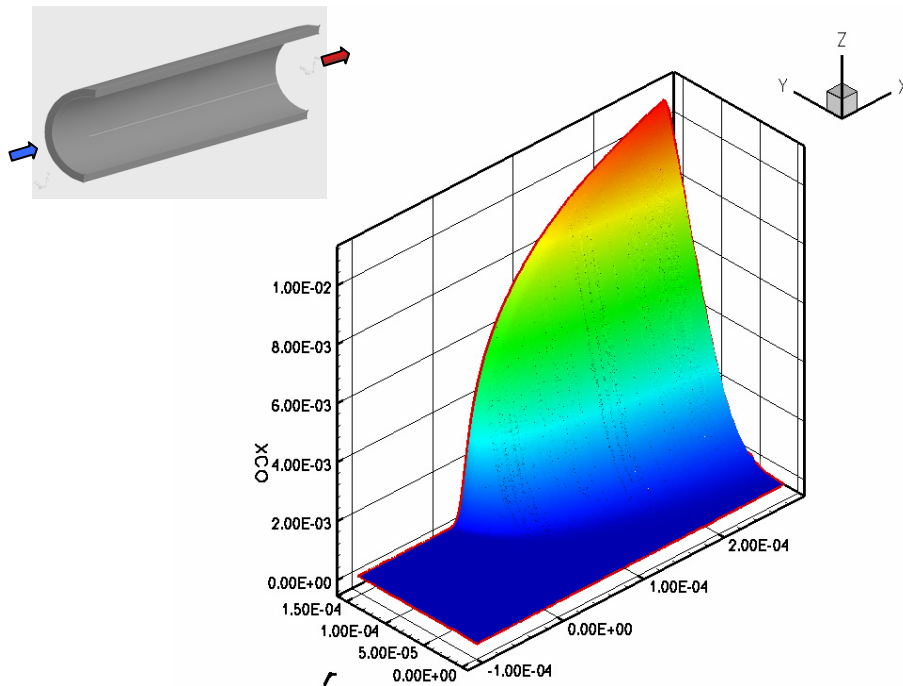
Figure 7.5a includes CH₄ concentration (represented by the colored area) and temperature profile (represented by the boundary of the colored area). Initially the mixture enters at 600 K (experimental conditions), but later is set up by the contact with the catalytic wall. Temperature distribution inside the channel showed that only the part of the mixture, which is in direct contact with the catalytic wall reaches the catalyst temperature; for the remaining part of the mixture values between 700 K (at the center of the channel) and 1175 K at the wall were observed.

Methane concentration varies along the radial direction: At the center line (axis of the channel) no changes were observed, while higher consumption occurred at the catalytic wall,

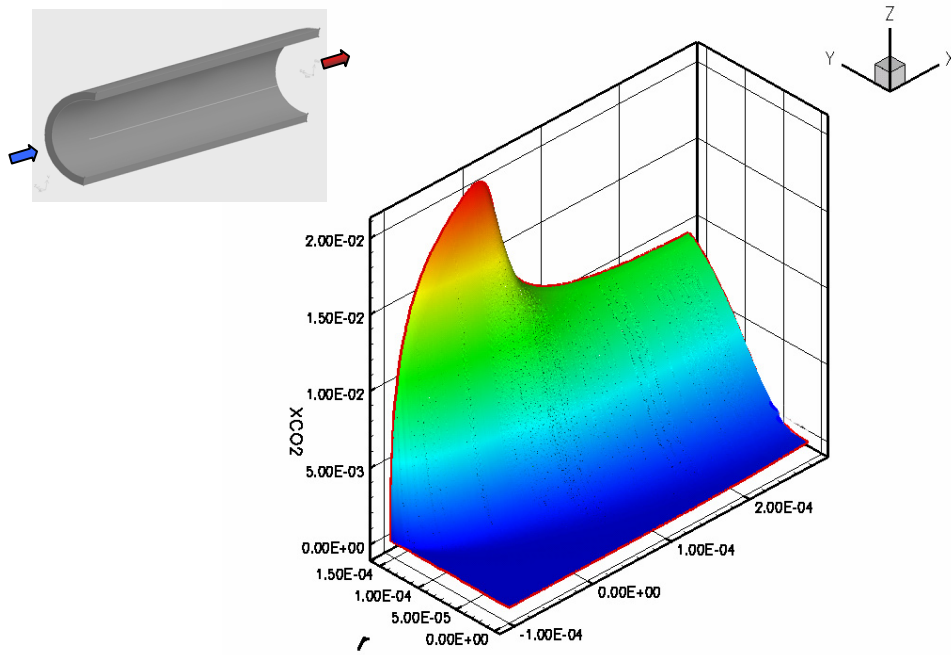
pointing out that gas-phase reactions play a small role for the fuel consumption. The calculated fuel conversion was 4% (Figure 7.3) and agrees with the value found experimentally. The calculated oxygen conversion was 21%; its pattern has a similar behavior as methane and it is omitted here.



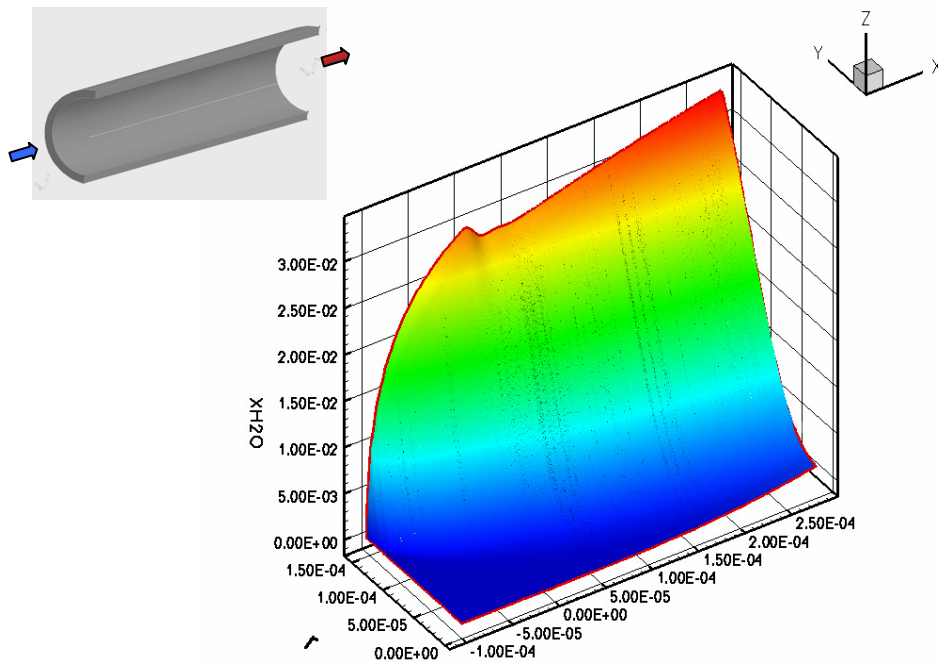
(a) Temperature profile colored by CH_4 mole fraction concentration. Back side corresponds to the reactor wall at $T_{\text{fix}} = 1175 \text{ K}$, methane concentration falls to zero at that point and stays nearly unchanged at the channel centre



(b) CO mole fraction inside the channel, maximal value at $r = r_{\text{max}}$ corresponding to the reactor wall. Carbon monoxide is mainly formed at latest stages near to the reactor exit



(c) CO_2 mole fraction is formed at the reactor inlet, the maximum value coincides with the reactor zone where oxygen still is available for the oxidation reaction, and at the channel centre no reaction was observed



(d) H_2O mole fraction, initially H_2O reaches a maximum which coincides with the maximum CO_2 formation (total oxidation of the methane at the reactor inlet), and continuously increases until the reactor exit

Figure 7.5: Mole fraction calculated inside the channel for the different species. X = distance from the channel inlet (m), Y = radial distance from the channel center (m), Z = corresponding variable

The formation of carbon monoxide, carbon dioxide and water are presented in Figure 7.5b-d. For all of them their formation is due to surface reactions involving methane consumption. Carbon dioxide is the main product that is formed in early stages inside the reactor; later carbon monoxide starts to gain importance, as they have nearly the same concentration. Carbon monoxide (that for the partial oxidation process is the main product) indicates an incomplete combustion and is formed in the later stages of the reaction. For the oxygen, its consumption at early stages by surface reactions leads to CO₂ formation. Later, when no more oxygen is available on the surface, incomplete combustion reactions occur and carbon monoxide (CO) appears in the products. The absence of both CH₄ and O₂ reactants at the catalytic walls (back side of the figures) indicates a strong mass transfer limitation, and even if there are still oxygen and methane available inside the system, their transport from the center line of the channel (in the gas phase) to the surface (where the core of the consumption reactions takes place) is not efficient, inhibiting complete combustion from occurring.

Here a 2D model was used to describe the gauze geometry and the main species formation. The proposed chemical mechanism for the surface satisfactorily describes selectivities and reactants consumption, and these data will be used for a 3D model of the gauze.

7.4.2 FLUENT Simulation of the Catalytic Gauze

The model developed in the previous section gave us important information about the quantitative and qualitative behavior of the mixture in the gauze reactor, although there are several assumptions that have been made which could introduce some distortion in the results obtained. This is the reason why a more sophisticated model was introduced to compare the results already found and to consider in more detail the variables that are included.

The commercial software FLUENT [180] was used to solve the basic conservations equations, which were described in Chapter 3 (Reactive Flows). FLUENT solves these equations using a control volume based finite difference method. A non-staggered system is applied for storage of discrete velocities and pressure. The resulting equation system is solved using a SIMPLE algorithm. The gas and surface chemical mechanisms are the same that have been used in the CHANNEL-code simulations.

Due to symmetry considerations, only a quarter of a single mesh of the gauze catalyst has been taken into account in the computational grid. Initially, the methane/oxygen mixture (volumetric ratio 2.5 and 80% helium dilution) flows at a uniform inlet velocity of 10 m/s and at 600 K from the right to the left. In the model only a single contact point between two Pt wires (each 0.20 mm diameter, Figure 7.1) is considered. The domain extends for half of the distance between centers of two individual wires (amount $4.1 \cdot 10^{-4}$ m) in the “Y” direction as sketched in Figure 7.6. The axial direction “X” was extended in order to get a better visualization of the patterns.

The total number of grid cells was 35.675, the number of computational cells with surface reactions boundaries was 1.412, and the total number of nodes was 7571. The conditions used for the calculations are presented in Table 7.2.

Table 7.2: Boundary conditions used during the simulation

| | |
|-------------------------------------|------|
| Catalyst temperature (K) | 1100 |
| Inlet mixture temperature (K) | 600 |
| Total pressure (MPa) | 0.13 |
| Initial molar composition: | |
| CH ₄ | 14.3 |
| O ₂ | 5.7 |
| He | 80.0 |
| Inlet velocity (m s ⁻¹) | 10.0 |

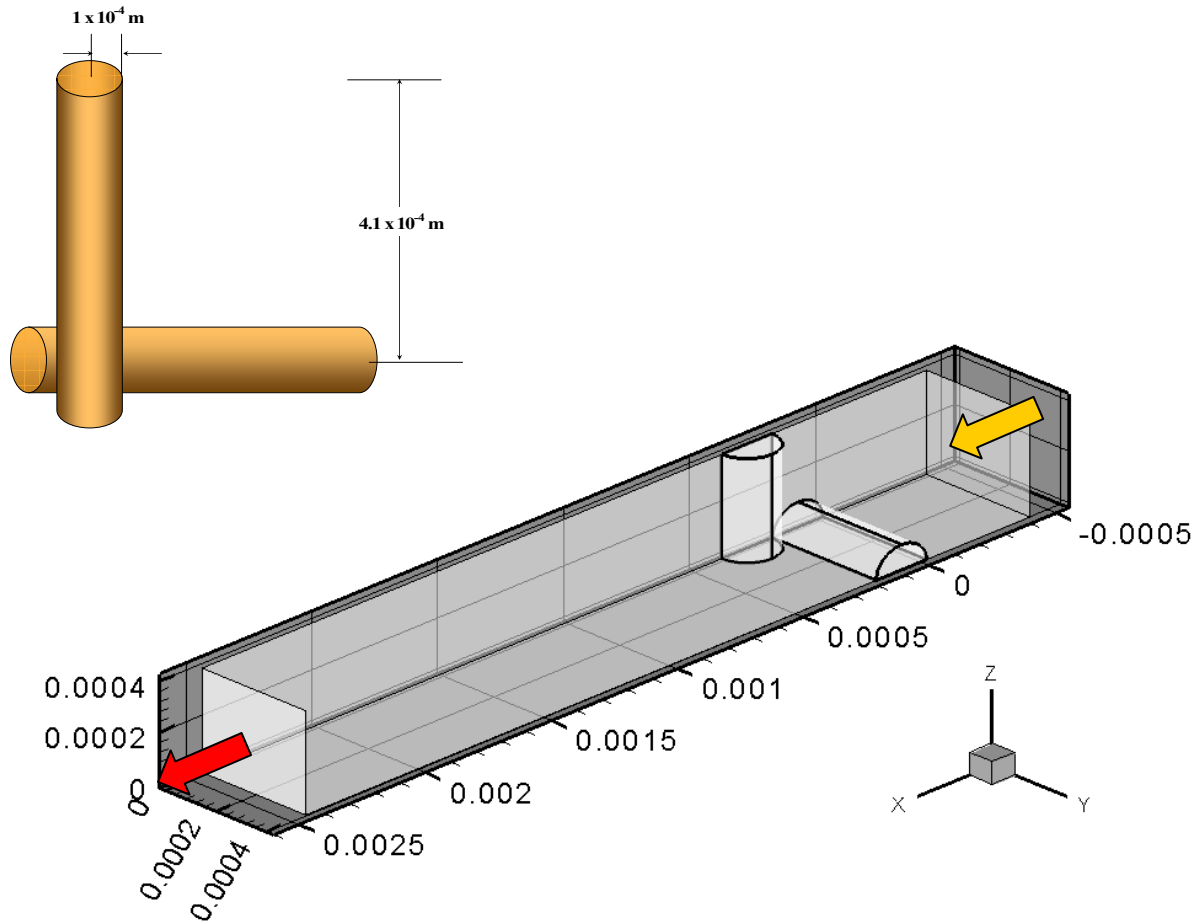


Figure 7.6: Selected domain used for the 3D simulations of the catalytic gauze, the reactive mixture flows from the right side to the left and crosses the first catalytic wire at $X = 0$. Due to geometrical symmetry only half of both (horizontally and vertically placed) wires have been included

Initially, the mixture flows at uniform inlet velocity of 10 m/s and an initial temperature of 600 K (preheating) into the gauze reactor. The surface temperature at the gauze was kept constant at 1100 K (boundary condition $T = \text{constant}$). Once the solution converged, a new boundary condition was imposed at the surface of the gauze: The energy source term was calculated by external subroutines using the thermodynamic data set for each species, and a coupled boundary condition was used. After this change, the maximum temperature falls to 1090 K.

Figure 7.7 presents representative temperature and velocity profiles calculated for the gauze. In the temperature profile (Figure 7.7a), two different zones can be stabilized: The first one is a cold zone located on the top of the mesh and more distant from the wires (center of the gauze in the real reactor) where temperature does not rise more than 200 K in comparison to the initial temperature given; the values for the temperature in this zone are between 600 K and 800 K. The second zone, which is at the bottom of the mesh and near to the wires, is characterized by a thin layer where the gas-phase temperature reaches almost the same value as in the wires and is extended for nearly half of the wire diameter downstream.

The velocity profiles (Figure 7.7b) show a different behavior than temperature profiles: The maximal velocity occurs on the top of the mesh at the free-path zone of the gauze, while on the backside of the mesh and near to the wires the velocity almost vanishes.

Species concentrations presented in all cases display large gradients along the axis of the wires. Figure 7.8 presents profiles of concentration for CO, CO₂ and CH₄ species. For the reactants, the maximal consumption occurs on the surface of the wires. The methane concentration near to the wires is zero, which indicates that all methane in contact with the catalyst is consumed; in a similar way oxygen is exhausted next to the wires surface. These results point out that a more efficient catalyst design, which enhances the contact time between the reactive mixture and the catalytic material without increasing the drop pressure is expected to increase the performance of the catalytic gauze (higher conversions and products yields).

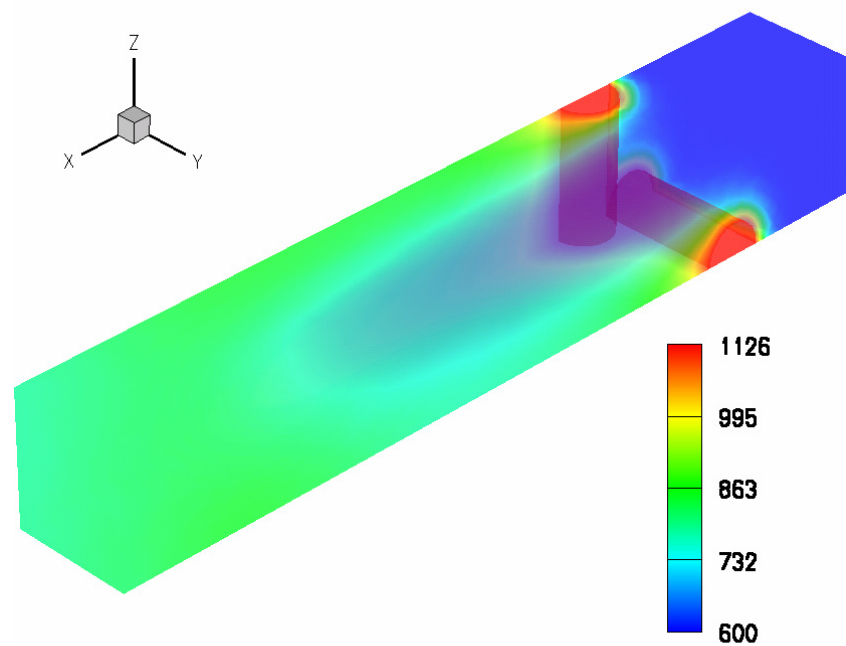
Carbon monoxide and carbon dioxide formation occur on the surface of the catalytic wires (Figure 7.8); the maximal product concentration is located at the contact point between the catalytic wires. This zone is characterized by a low or zero value for velocity which favors higher residence times for the products that are being formed, concentration of monoxide carbon and a decrease in the axial direction, e.g., in direction to the center of the gauze where the flow has a higher velocity. Water is produced only on the surface. Carbon dioxide is mainly formed at the catalyst surface, and its contours of concentration do not differ from the ones in carbon monoxide.

Water is another of the main products in the experiments; water production occurs on the surface of the catalyst.

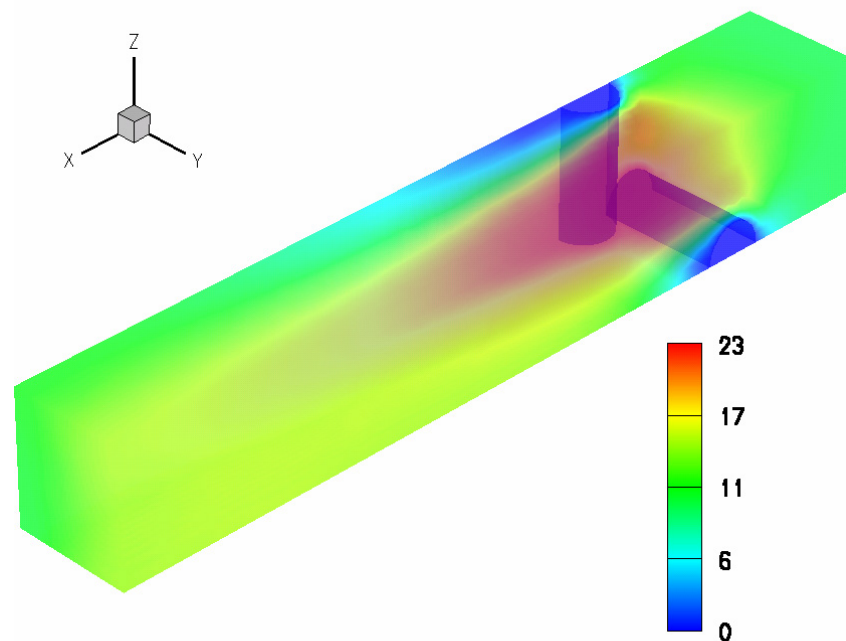
A comparison between the numerical results from the calculated conversion and selectivity of the products obtained with the 3D model and the experimental data is presented in Table 7.3. The numerical results and the experimental data showed an agreement: the conversion of reactants is well predicted and selectivity of CO and CO₂ are close to the experimental ones. No hydrogen was found during the simulation and water was the other main product.

Table 7.3: Results 3D numerical simulation

| Selectivity/Conversion | Simulation | Experiment |
|--------------------------------|------------|------------|
| CH ₄ (% conversion) | 3 | 4 |
| O ₂ (% conversion) | 19 | 18 |
| CO (%) | 50 | 48 |
| CO ₂ (%) | 50 | 52 |
| H ₂ (%) | 0 | 0 |
| H ₂ O (%) | 100 | 100 |

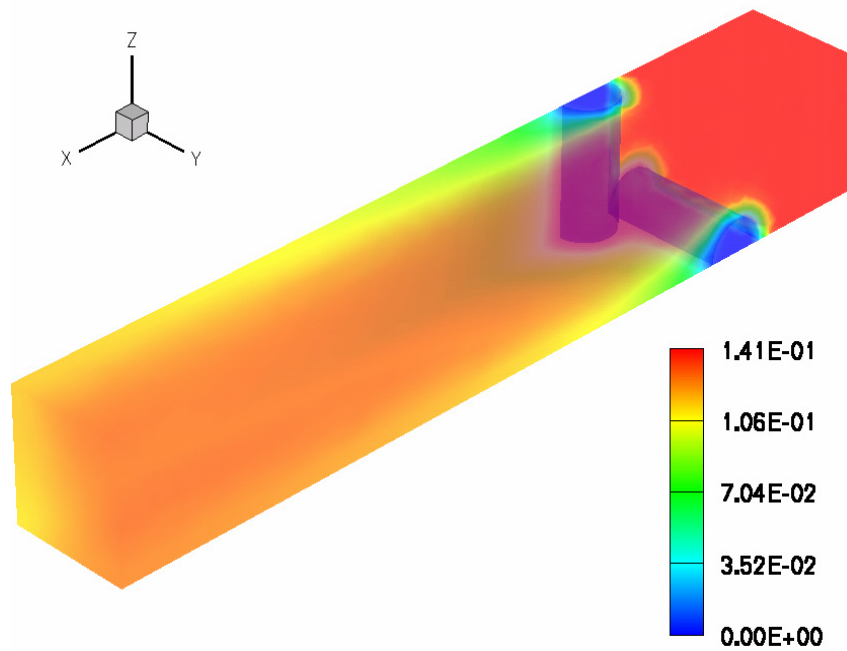


a) Temperature profile (K) obtained with the simulations considering the 3D geometric of the gauze and the gas-phase and surface kinetic mechanisms

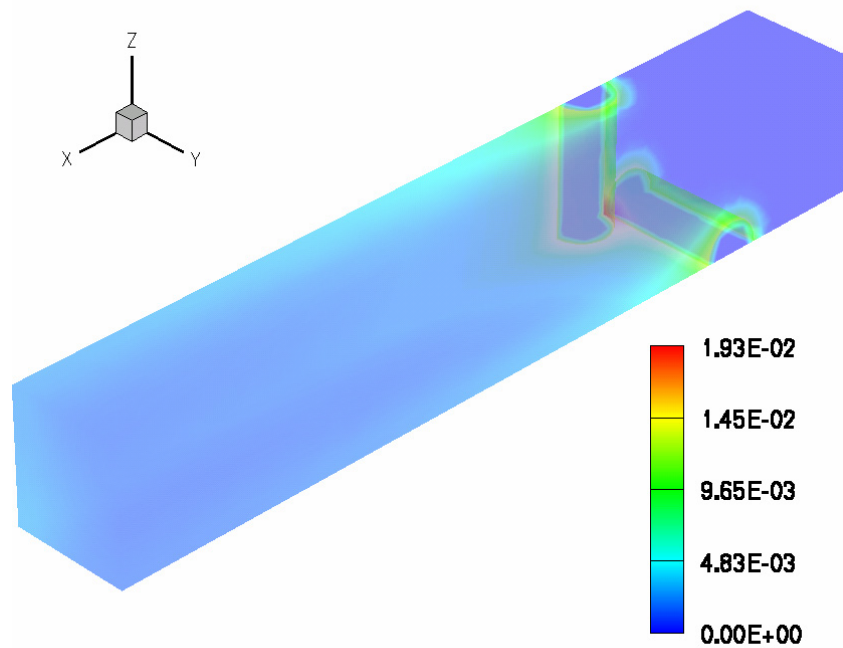


b) Velocity magnitude (m/s)

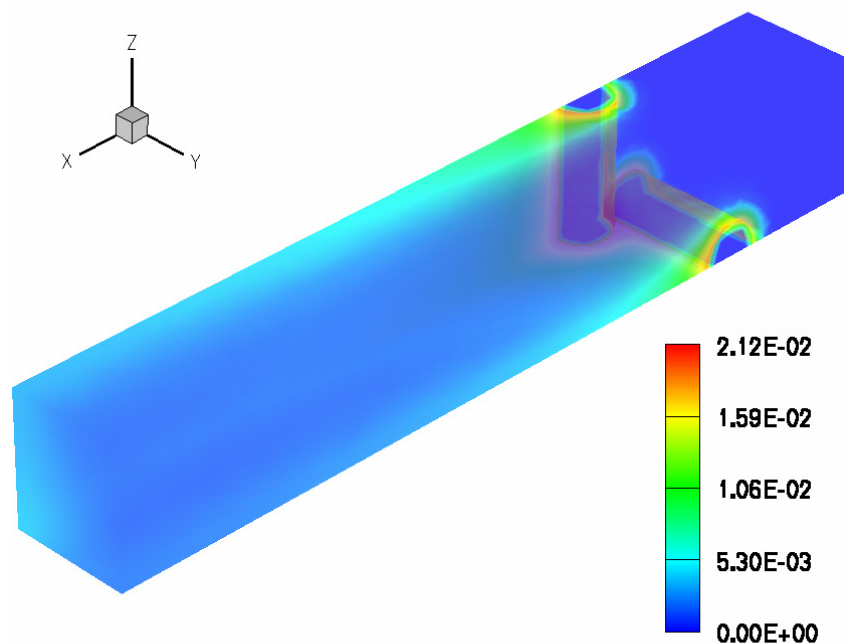
Figure 7.7: Calculated temperature and velocity profiles: $p_{tot} = 130\text{kPa}$, $V_0 = 10\text{ m/s}$, $T_0 = 600\text{K}$
 $\text{CH}_4/\text{O}_2/\text{He}: 14.3/5.7/80.0$



a) Methane profiles (mole fraction): Initial methane concentration (feed at the right side) is 0.14 mole fraction which falls to zero in the region next to the wires, where the catalytic reactions occur. Most of the methane remains without reacting and escapes implying low methane conversions



b) Carbon monoxide profiles (mole fraction): Most of the carbon monoxide is formed at the catalyst surface; the maximal concentration occurs at the join of the catalytic wires where accumulation of the products formed is feasible



c) Carbon dioxide profiles (mole fraction): As it occurs with CO, CO₂ formation occurs via catalytic reactions, maximal concentration is similar to those found for CO

Figure 7.8: Main species concentration: CH₄, CO and CO₂. $p_{tot} = 130\text{kPa}$, $V_0 = 10\text{ m/s}$, $T_0 = 600\text{K}$.
 $\text{CH}_4/\text{O}_2/\text{He} = 14.3/5.7/80.0$

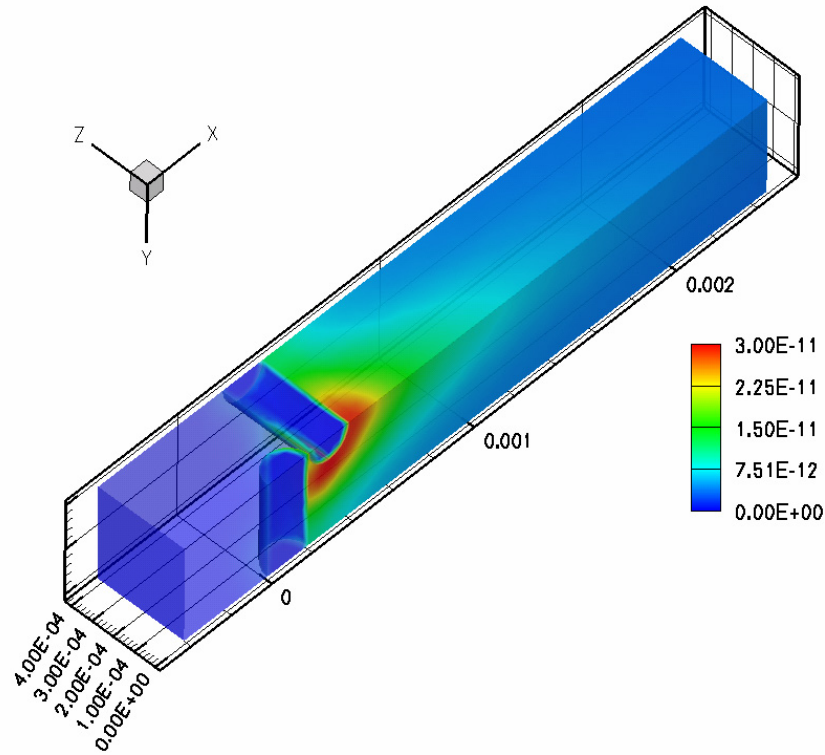
7.4.3 Increasing Residence Time

For the experimental conditions, gas-phase chemistry does not play a major role and molar concentration for the radical species is low. No difference was observed in the main products after including the gas-phase chemistry into the model.

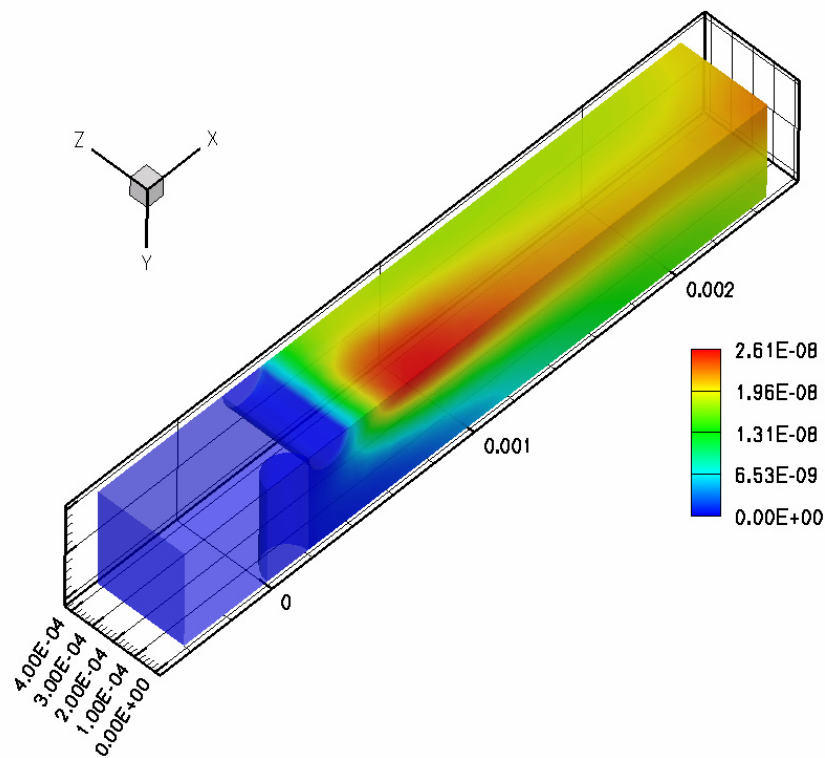
The influence of the gas-phase chemistry in the overall process becomes significant with increasing pressure and residence time [184]. Under these conditions, the formation of oxidative coupling products, e.g., C₂H₆, and total combustion products, i.e., CO₂ and H₂O, are expected to occur in the homogeneous phase as well, which was observed by simulation of the purely homogeneous partial oxidation of methane. The influence of the residence time on the homogeneous reactions was studied by decreasing the inlet gas velocity from 10 m/s to 1 m/s.

Figure 7.9a-d illustrates the concentration profiles of gas-phase radical species (HO₂, OH, and CH₃) and the coupling product (C₂H₆) for an inlet flow velocity of 10 m/s at 1.3 bar and 600 K for a CH₄/O₂ volumetric ratio of 2.5. In all cases, these species are formed homogeneously downstream of the gauze. The domain of maximum production rate of homogeneous reactions coincides with the zone of the reactor with lower velocity and higher temperature. For the conditions considered, HO₂ is the first radical species formed, followed by hydroxyl radicals (OH) appearing at a short distance downstream. Afterwards, methyl radicals are obtained, recombining and forming ethane further downstream. This result draws parallels

with the reaction scheme proposed by Pollard [88] for the gas-phase oxidation of hydrocarbons in the intermediate temperature regime.



a) HO_2 (mole fraction)



b) OH (mole fraction)

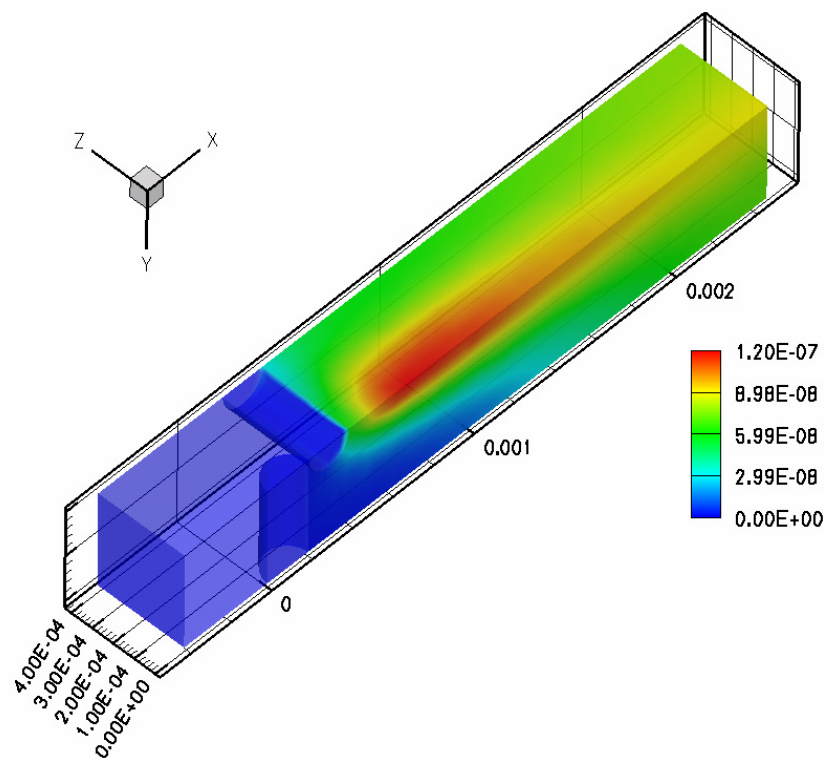
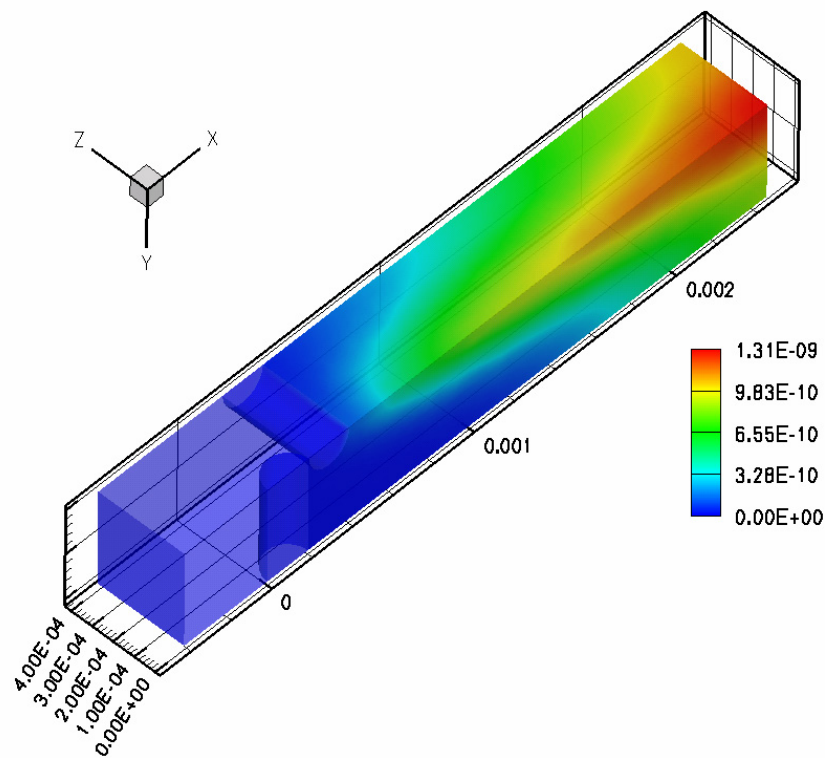
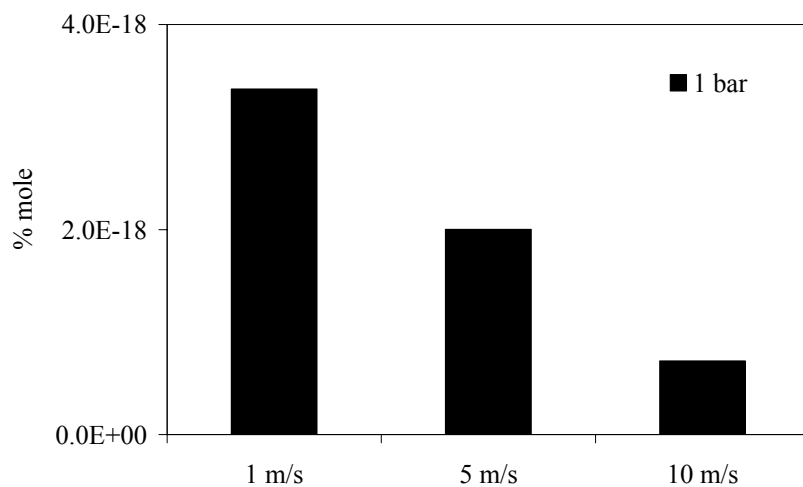
c) CH_3 (mole fraction)d) C_2H_6 (mole fraction)

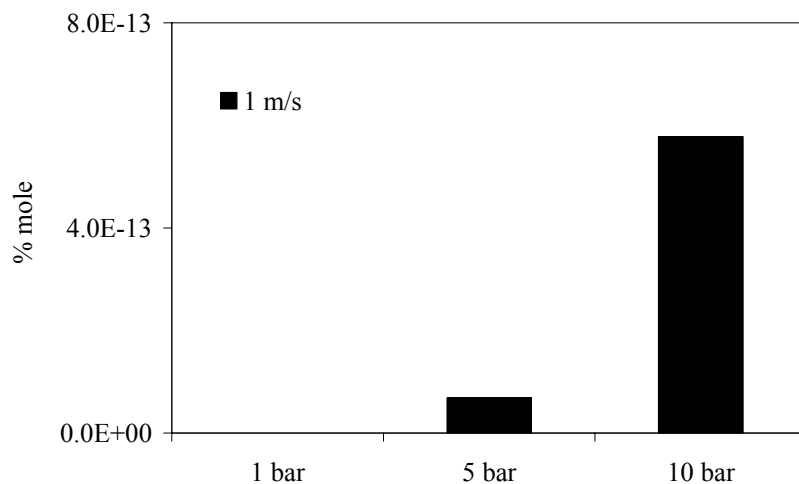
Figure 7.9: Gas-phase effects: Radicals and coupling products. HO_2 , OH , CH_3 and C_2H_6 formed after increasing the contact time between the mixture and the catalyst. $V_0 = 1\text{m/s}$, $p = 1\text{bar}$, $T_0 = 1175\text{K}$

Decreasing the inlet velocity from 10 m/s to 1 m/s at fixed temperature, pressure and composition leads to an increase in conversion (4% to 7% for CH_4 and 20% to 30% for O_2), as well as a higher CO_2/CO ratio at the reactor outlet (1.0 to 2.0). In spite of the relevance of gas-phase processes at an increased residence time, surface chemistry is still the main route for methane conversion. It should be noted that the surface reaction mechanism does not include the adsorption/desorption of all possible radicals formed in the gas-phase due to the missing knowledge of the kinetic data, which surely affects the discussion above.

Figure 7.10 shows the predicted concentration of ethane at different pressures and inlet gas velocities. The C_2H_6 production decreases as the velocity increases (Figure 7.10a), i.e., at shorter residence times. An increase in pressure favors ethane production (Figure 7.10b). 5 orders of magnitude higher C_2H_6 yields were obtained upon increasing the pressure from 1 bar to 10 bar. Altogether, the total amounts of coupling products are still very low.



a) C_2H_6 (mole fraction) after changes in the inlet velocity: An increase from 1 m/s to 10 m/s reduces the C_2H_6 yields by a factor of 3: Transport of mass due to diffusion from the main stream to the catalytic walls is less efficient at high speed values



(b) Effect of the pressure on the C_2H_6 yields: Increases of pressure has an opposite effect in the yields of coupling products, and their amounts rise several orders of magnitude as it has been reported by several authors [176, 179, 184]

Figure 7.10: Impact of (a) inlet gas velocity at 1 bar and (b) total pressure at 1 m/s on the outlet concentration of C_2H_6 . Conditions: CH_4/O_2 vol. ratio = 2.5, inlet temperature = 600 K

Chapter 8

CONCLUSIONS

This thesis deals with the development and evaluation of a detailed kinetic mechanism able to describe oxidation and partial oxidation of light alkanes (C_1 - C_4) in the intermediate and high temperature regime. The kinetic scheme was evaluated by comparing experimental data of ignition delay times measured in shock-tubes and by comparing species concentrations obtained in stirred reactors at several temperatures and pressures.

To develop the mechanism, a set of automatically generated reactions was added to the previously developed high-temperature C_4 kinetic mechanism. These reactions were implemented to include missing reactions paths, which occur in the low and intermediate temperature regimes. The existing C_4 mechanism was optimized to describe high temperature oxidation at typical combustion conditions, where fuel/oxygen ratio is close to the stoichiometric ratio as is typical in flames.

The newly added steps describe the low-temperature chemistry through a scheme which includes oxygen addition reactions to the parent radical, isomerization of the newly formed radical and the formation of cyclical oxygenate species and their decomposition.

In order to improve the accuracy of the automatically generated mechanism, experimental data completed by several authors were considered, and different reactions steps identified by their experiments were coupled to our mechanism increasing the accuracy of the predictions as was discussed in Chapters 4 and 6.

Some of the significant steps added to the existing automatic scheme (see Section 4.3, Fig. 4.1) take into account reactions expected to occur during alkene oxidation at low temperature:

- The initial hydroxyl radical addition to the parent fuel (Alkene + OH = $*C_2H_{2n}OH$)
- Further decomposition of the $*C_2H_{2n}OH$ radical into ketone, aldehydes and small radicals,
- The direct O-heterocycle formation from the fuel and hydroperoxy radical reaction (Alkene + HO_2 = O-heterocycle + OH).

These steps are already described in Section 4.3.7 (Figure 4.2), and they account for most of the cyclical compounds formed at low and intermediate temperatures, as shown in the simulations. The computed data showed an agreement with the reported experimental results, demonstrating the accuracy of the scheme adopted.

Additionally, the inclusion of several radical-radical reactions and initial radical-fuel reactions proved to be useful in describing the oxidation of hydrocarbons under rich mixtures conditions occurring during the partial oxidation of fuels.

For the original high-temperature mechanism a number of kinetic coefficients have been updated for several reactions according to new experimental information available: Additional reactions were included, of which most of the new information was taken from the NIST database. A wide explanation related to the new reactions was included, and the kinetic parameters were given in Section 4.4.

The evaluation of the mechanism was performed by comparing experimental results with computed data of ignition delay times for hydrogen, methane, ethane, propane and butane. In each case the reaction between oxygen and hydrogen was the most sensitive for hydroxyl production. Additionally, when methane was doped with either hydrogen, ethane or propane, the initial decomposition of the added fuel started the ignition process. The reaction of the formed alkyl radical with oxygen was most sensitive for the ignition delay time. Moreover, when the experimental ignition delay times were evaluated at stoichiometric and rich conditions, the proposed mechanism accurately described these ignition delay times.

A further evaluation was carried out by simulating partial oxidation of methane and oxidation of propane and butane at intermediate temperature in rich mixture conditions.

During the noncatalytic partial oxidation of methane, the main inconvenience is connected with the high stability of the methane molecule, especially at the very rich methane concentrations used to run the process. Experimentally, it has been found that carbon monoxide and other couple species are the main products formed. The numerical results predicted this characteristic well, where carbon monoxide, ethane and ethylene were the main products.

Experimentally, when the partial oxidation of propane occurs (at temperatures around 1000 K, at low pressure, and with a rich propane-air ratio $\phi = 2.8$), it has been shown that olefins (ethylene and propylene) are the main species produced. Other minor species, e.g., methane, ethane and carbon monoxide are also present in the final products. In the numerical simulations, olefin production was explained by two main channels. One is the scission of the n-propyl radical and the second the decomposition of the cyclical species formed by the addition of oxygen to the parent radicals. The latter, is characteristic of the low-temperature oxidation of hydrocarbons. Similarly, when experiments describing the oxidation of butane were simulated, the main products formed (ethylene and propylene) were also accurately described.

It was observed in the experimental data for ethylene and propylene oxidation that their respective oxides were the main species formed. By performing a sensitivity and flow analysis the key reactions describing the product's formation were identified, and the kinetic scheme proposed in Sections 4.3.6 and 4.3.7 was proven to be accurate. However, there are some kinetic data in particular the decomposition steps leading to radicals formation, which need to be reconsidered.

All these intermediate channels, added, are especially important in order to describe properly the partial oxidation process. After including the automatically generated reaction set and adding the experimental kinetics information, the final mechanism consists of 1428 reactions made up of 146 species.

The catalytic partial oxidation of a single gauze reactor was studied using a three-dimensional numerical simulation of the flow field coupled with heat transport, multi-step gas-phase and surface reaction mechanism.

Simulations have been performed using two different approaches: In the first one the gauze was assumed to be a channel. This channel has an active surface similar to the one of the gauze, and the initial velocity for the mixture was calculated such that the contact time between the reactive mixture and the catalyst was guaranteed to be similar to the one in the experiments. The second model used includes in detail all the geometrical characteristics of the gauze, and no simplification was done for its representation. With this latter approach a better understanding for the flow patterns was obtained, and it was observed how some physical constrains like catalyst distribution can effect chemical variables like selectivity and reactant conversions.

By using the two-dimensional simulation of the gauze it was possible to describe the main species formation and give important information about the proposed chemical kinetic mechanism for methane partial oxidation on the surface. Selectivities and reactants consumption were correctly predicted, and these data were later used during the 3D modeling of the gauze. The advantage of the two-dimensional model is, that is easier to implement, and that it requires a shorter computation time, which makes it preferable to investigate chemical kinetics.

The three-dimensional model used had the advantage of closely representing the real conditions of the real gauze, by avoiding simplifications, which reduce uncertainties at the moment of result evaluation.

In addition, it was possible to study in more detail the effects on the chemical system of different variables. These included the distribution of the catalyst, its shape, flow pattern, temperature and species concentration, all of which helped to gain a better understanding of the overall process. After including detailed reaction mechanisms, it was observed how the geometrical characteristics of the gauze affected the conversion and species selectivities.

Both models can now be used to explore the reactor behavior at varying operating conditions. For instance, it was shown that the decrease of the initial velocity produces an increase in the conversion of CH_4 and O_2 and has the potential for significant gas-phase chemistry leading to the formation of coupling products (C_2H_6). The significance of the gas-phase reactions is expected to become larger after setting the required physical conditions, which means time, pressure and temperature.

The effect of the gas-phase reactions was more pronounced after increasing reaction time by setting the initial velocity at a lower value. The radical species observed in the gas phase were HO_2 which appeared first, then H_2O_2 and later OH . This scheme follows the one proposed for the intermediate temperature regime (Section 4.3). For the simulations the reduced reaction path shown in Figure 7.4 was included, and couple products (C_2H_6 , C_2H_4) were observed in the latest stages of the gas-phase.

Current work on propane dehydrogenation is ongoing using the methodology applied here: A kinetic surface mechanism is being developed and its initial evaluation has been done using a 2D model before its further application in a 3D model. Butane and other high alkanes are also feasible to be modeled. The gas-phase mechanism for each case should be reduced and adapted to the experimental conditions before its implementation in the CFD program; the advantage is that a wider range of conditions can be considered using the extended mechanism developed.

LIST OF FIGURES

- 2.1 Schematic explosion diagram for hydrocarbons: The blue zone at the right represents the different conditions (of temperature and pressure) where the mixture can explode 7
- 2.2 Shock tube diagram: In the shock tube, reactions are initiated by a temperature jump behind a shock wave. The shock wave is generated by the pressure jump after a foil which separates the high and the low pressure section is bursting or collapses due to the high pressure induced 10
- 2.3 Rapid compression machine: A rapid compression machine is designed to simulate a single engine cycle of an internal combustion engine. The conditions inside the combustion chamber are easily controlled and cleaner than in the traditional internal combustion engines. Above: Rapid compression machine. Down: Details of the combustion chamber 12
- 2.4 Stirred reactors and concentration changes with the time and space: a) Batch reactor; b) Plug-flow tubular reactor (PFTR); c) Continuously stirring tank reactor (CSTR) 13
- 3.1 Characteristic dependence on the pressure for the rate coefficient (k). At low pressure $k \sim k_0 \cdot [M]$, in the fall-off region $k = f(T, [M])$. At high pressure $k = k_\infty \neq f([M])$ 24
- 3.2 Activation energy for the catalytic and non-catalytic pathway for a chemical reaction 27
- 4.1 Schematic mechanism for the combustion of hydrocarbons at 500K - 800K. $R = C_nH_{2n+1}$; $Q = C_nH_{2n}$; $Q' = C_nH_{2n-1}$. First step involves a hydrogen abstraction from the fuel to yield the alkyl radical. At low temperature, the alkyl formed is oxidized and peroxy radicals appears: Further they are decomposed into aldehydes (main species found during experiments in cold flames [88]) ketones and others small radicals 42

-
- | | | |
|------|---|----|
| 4.2 | Schematic mechanism for the combustion of hydrocarbons at 500 K – 800 K, including additional steps proposed in [66]. Blue zone represents the new paths considered: Hydroxyl addition to the olefin, decomposition of the hydroperoxy radical into olefin, and ether formation via HO ₂ addition to the olefin $R = C_nH_{2n+1}$; $Q = C_nH_{2n}$; $Q' = C_nH_{2n-1}$ | 51 |
| 4.3 | Schematic mechanism for the combustion of hydrocarbons at high temperature | 52 |
| 5.1 | Ignition delay times (τ) for H ₂ /O ₂ /Ar mixtures as function of the initial temperature and inlet mixture composition. | 66 |
| 5.2 | Sensitivity analysis for a H ₂ /O ₂ /Ar mixture calculated at $p = 1$ bar and $\phi = 1.4.0\%$. H ₂ : 2.0%, O ₂ : 90% Ar | 67 |
| 5.3 | Ignition delay times (τ) for methane-oxygen-argon mixture as function of the initial temperature: | 68 |
| 5.4 | Ignition delay times CH ₄ :H ₂ mixtures as function of the initial temperature and mixture composition. | 69 |
| 5.5 | Sensitivity analysis for a CH ₄ /O ₂ /H ₂ /Ar mixture. | 70 |
| 5.6 | Ignition delay times (τ) for CH ₄ /O ₂ /C ₂ H ₆ /Ar mixture as function of the initial temperature and inlet composition. CH ₄ /O ₂ /C ₂ H ₆ /Ar (vol.%) | 70 |
| 5.7 | Sensitivity analysis for a CH ₄ /O ₂ /C ₂ H ₆ /Ar mixture | 71 |
| 5.8 | Ignition delay times (τ) for CH ₄ /O ₂ /C ₃ H ₈ /Ar mixtures | 72 |
| 5.9 | Sensitivity analysis for a CH ₄ /O ₂ /C ₃ H ₈ /Ar mixture | 73 |
| 5.10 | C ₂ H ₆ ignition delay times for C ₂ H ₆ /O ₂ /Ar mixtures as function of the initial temperature and composition. | 74 |
| 5.11 | Sensitivity analysis for C ₂ H ₆ /O ₂ /Ar mixtures | 75 |
| 5.12 | C ₃ H ₈ ignition delay times as a function of the initial temperature. C ₃ H ₈ /O ₂ /Ar | 76 |

| | | |
|------|--|----|
| 5.13 | Sensitivity analysis for high pressure propane combustion ($C_3H_8/O_2/Ar$): Stoichiometric and rich conditions | 77 |
| 5.14 | Calculated species mole fraction prior to ignition: In early stages propylene is formed, later ethylene appears in the system preceding the ignition | 77 |
| 5.15 | Ignition delay times for a $C_4H_{10}/O_2/Ar$ mixture as a function of the initial temperature | 78 |
| 5.16 | Sensitivity analysis for a $C_4H_{10}/O_2/Ar$ mixture. | 79 |
| 5.17 | Mole fraction profiles for the main species formed prior to ignition during the C_4H_{10} ignition | 80 |
| 6.1 | Comparison between the simulated results using the gas-phase mechanism and the results reported by Zhu et al. [159] for partial oxidation of a complex methane mixture. (a) Methane and oxygen consumption and carbon dioxide production. (b) Main species reported: Carbon monoxide, hydrogen and coupling products ethylene and ethane. | 83 |
| 6.2 | Reaction path analysis for the partial oxidation of the complex mixture presented in Table 6.1. Methane main consuming paths are due to radicals attack: OH, H and HO_2 (85% of the decomposed fuel is through this channel). Methoxy radicals (CH_3O) consume the 15% left. Coupling product (C_2H_6) is produced due to recombination of the methyl radicals formed in the first stage of the fuel decomposition, ethylene is secondary specie produced from the ethane decomposition | 84 |
| 6.3 | Comparison between calculated results and experimental data for the high temperature partial oxidation of propane. Initial conditions: $\phi = 2.8$, $[C_3H_8]_0 = 0.0175\%$ mole, $p = 4$ bar, $T_0 = 1033$ K. (a) Propane consumption and olefins production (C_2H_4 and C_3H_6), (b) Methane, carbon monoxide and ethane vol. fraction. At high temperature the decomposition of propyl radicals into CH_3 and C_2H_4 (main product) leads to high yields of methane (methyl further reacts with the fuel) which is similar to those for propylene | 85 |
| 6.4 | Reaction flow analysis for the partial oxidation of propane. Initially propane is attacked by radical species leading to n(i)-propyl formation. Ethylene (largest species formed) is produced mainly from n-propyl decomposition in early stages of the reaction. Propylene, another of the largest species experimentally found, is formed during the reaction between i-propyl and radicals species ($iC_3H_7+R\leftrightarrow C_3H_6+RH$). Other reaction paths involving oxygen addition, isomerization of the peroxide radical formed and its decomposition are responsible for nearly 14% of the C_3H_6 obtained | 86 |

-
- 6.5 Comparison between calculated results and experimental data for the high temperature partial oxidation of butane. (a) Butane consumption and olefins production, yields of ethylene and propylene are similar at < 0.09 s, after propylene is consumed and higher concentration of ethylene was found. (b) Methane production increases continuously: Initially methane is formed via reactions between methyl radicals and butane; in later stages reactions involving decomposition of ethane, ethylene and aldehydes drive methane formation 89
- 6.6 Reaction flow analysis for the high temperature partial oxidation of butane. Propylene is mainly formed (95%) from scission of 2-butyl radical ($2C_4H_9 \leftrightarrow C_3H_6 + CH_3$), this step consumes almost all the butyl radicals being formed (88%). Ethylene formation includes two main channels: 1. Direct decomposition of 1-butyl radicals ($1C_4H_9 \leftrightarrow C_2H_4 + C_2H_5$) (45% of the C_2H_4 formed). 2: Decomposition of the ethyl radicals formed ($C_2H_5 \leftrightarrow C_2H_4 + H$) (41% of the C_2H_4 produced). In later stages, propylene to ethylene conversion accounts for the 10% left of the ethylene yield. Formation of C_2H_6 occurs by methyl recombination. Methane formation is explained by the reaction of methyl radical with butane 90
- 6.7 Comparison between the calculated species profiles and the experimental data reported in [66] for the C_2H_4 oxidation at low temperature. 94
- 7.1 Schematic illustration of the reactor used by Smet et al. [179,181] for the study of methane partial oxidation. (a) The illustration of the Pt gauze builds up using a single Pt wire. (b) Pt gauze geometry. (c) Reactor set-up. Original figure from [181] 98
- 7.2 Comparison between measured temperature at the catalyst surface and the gas-phase bulk temperature. Conditions: $p_{tot} = 130$ kPa, $F_{tot} = 1 \cdot 10^{-2}$ mol s^{-1} , $W/F_{CH_4,O} = 39.9$; $CH_4/O_2/He$: 14.3/5.7/80.0. Experiments of Smet et al. [179] 99
- 7.3 Conversion and selectivity as a function of the catalyst temperature. $p_{tot} = 130$ kPa, $F_{tot} = 1 \cdot 10^{-2}$ mol s^{-1} . $CH_4/O_2/He = 14.3/5.7/80.0$. Experimental data [179] 100
- 7.4 Reaction path analysis for methane oxidation in the gas phase. Percentages in the flow analysis quantify the consumption of the species due to that elementary step. Conditions: CH_4/O_2 ratio = 2.5 (vol.), $T = 1050$ K, $p = 1$ bar. The residence time was fixed in order to achieve a methane conversion of 5% 102

-
- 7.5 Mole fraction calculated inside the channel for the different species. X = distance from the channel inlet (m), Y = radial distance from the channel center (m), Z = corresponding variable 106
- 7.6 Selected domain used for the 3D simulations of the catalytic gauze, the reactive mixture flows from the right side to the left and crosses the first catalytic wire at $X=0$. Due to geometrical symmetry only half of both (horizontally and vertically placed) wires have been included 108
- 7.7 Calculated temperature and velocity profiles: $p_{\text{tot}} = 130\text{kPa}$, $V_0 = 10\text{ m/s}$, $T_0 = 600\text{K}$ CH₄/O₂/He: 14.3/5.7/80.0 110
- 7.8 Main species concentration: CH₄, CO and CO₂. $p_{\text{tot}} = 130\text{kPa}$, $V_0 = 10\text{ m/s}$, $T_0 = 600\text{K}$. CH₄/O₂/He= 14.3/5.7/80.0 112
- 7.9 Gas-phase effects: Radicals and coupling products. HO₂, OH, CH₃ and C₂H₆ formed after increasing the contact time between the mixture and the catalyst. $V_0 = 1\text{m/s}$, $p = 1\text{bar}$, $T_0 = 1175\text{ K}$ 114
- 7.10 Impact of (a) inlet gas velocity at 1 bar and (b) total pressure at 1 m/s on the outlet concentration of C₂H₆. Conditions: CH₄/O₂ vol. ratio = 2.5, inlet temperature = 600 K 115

LIST OF TABLES

| | | |
|------|---|----|
| 4.1 | Arrhenius parameters for the reaction: $R^* + O_2 \leftrightarrow RO_2^*$ | 43 |
| 4.2 | Arrhenius parameters for the internal H abstraction $RO_2^* \rightarrow QOOH^*$. Kojima[78] | 44 |
| 4.3 | Arrhenius parameters for the reverse internal H abstraction $QOOH^* \rightarrow RO_2^*$. Kojima[78-80] | 45 |
| 4.4 | Arrhenius parameters for the external H abstraction: $RO_2^* + RH \rightarrow ROOH + R^*$. Wilk [84] | 45 |
| 4.5 | Arrhenius parameters for the disproportionation reaction: $RO_2^* + RO_2^* \rightarrow 2RO^* + O_2$ Adachi [98] | 46 |
| 4.6 | Arrhenius parameters for the decomposition of hydroperoxides: $RO_2H \rightarrow RO^* + O$. Sahetchian [105] | 46 |
| 4.7 | Arrhenius parameters for the decomposition of hydroperoxyalkyl QO_2H^* radical: $QO_2H^* \rightarrow QO + OH$. Kojima [78] | 47 |
| 4.8 | Arrhenius parameters for the reaction: $C_nH_{2n} + HO_2 \leftrightarrow QO + OH$ | 48 |
| 4.9 | Arrhenius parameters for the reaction: $2 C_4H_9 + O_2 \leftrightarrow OH + QO$. Baker [119] | 50 |
| 4.10 | O-Heterocyclic in the C_4 mechanism | 50 |
| 4.11 | Arrhenius parameters for the decomposition $RH \rightarrow R^* + R'^*$; and $RH \rightarrow R^* + H$. | 53 |

| | | |
|------|--|-----|
| 4.12 | Arrhenius parameters for the decomposition of alkyl radical $R^* \rightarrow R^* + \text{Alkene}$, and $R^* \rightarrow H + \text{Alkene}$. Annex I includes references used for those reactions | 54 |
| 4.13 | Arrhenius parameters for the alkyl radical and oxygen reaction $R^* + O_2 \rightarrow HO_2 + \text{Alken}$. Annex I includes the references | 55 |
| 4.14 | Arrhenius parameters for the aldehydes reactions | 55 |
| 6.1 | Selected operation conditions for oxidative coupling of methane | 82 |
| 7.1 | Conditions used for the simulations with the channel reactor model | 104 |
| 7.2 | Boundary conditions used during the 3D simulation | 108 |
| 7.3 | Results 3D numerical simulation | 109 |

ANNEX I

GAS PHASE MECHANISM

Elementary reactions in the H₂-CO-C₁-C₂-C₃-C₄-O₂ system for intermediate and high-temperature combustion and partial oxidation.

Rate coefficients are presented in the modified Arrhenius form $k = A^*T^b \exp(-Ea/RT)$; only the forward reaction is considered; the reverse reaction may be calculated using thermodynamic data. The estimated uncertainty of the reaction rate is given. The collision efficiencies used are:

$$M_{(1)} = [\text{H}_2] + 6.5[\text{H}_2\text{O}] + 0.4[\text{O}_2] + 0.4[\text{N}_2] + 0.75[\text{CO}] + 1.5[\text{CO}_2] + 3.0[\text{CH}_4] + 0.35[\text{Ar}]$$

$$M_{(2)} = [\text{H}_2] + 2.5[\text{H}_2\text{O}] + 0.4[\text{O}_2] + 0.4[\text{N}_2] + 0.75[\text{CO}] + 1.5[\text{CO}_2] + 3.0[\text{CH}_4] + 0.15[\text{Ar}]$$

$$M_{(3)} = [\text{H}_2] + 6.5[\text{H}_2\text{O}] + 0.4[\text{O}_2] + 0.4[\text{N}_2] + 0.75[\text{CO}] + 1.5[\text{CO}_2] + 3.0[\text{CH}_4] + 0.29[\text{Ar}]$$

$$M_{(4)} = [\text{H}_2] + 6.5[\text{H}_2\text{O}] + 0.4[\text{O}_2] + 0.4[\text{N}_2] + 0.75[\text{CO}] + 1.5[\text{CO}_2] + 0.7[\text{CH}_4] + 0.35[\text{Ar}]$$

The mechanism is presented in the CD annexed.

The pre-exponential factor A is given in units of $(\text{cm}^3 \text{mol}^{-1})^{n-1} \text{s}^{-1}$ and the activation energy Ea in kJ mol^{-1} .

The double arrow, shows that the reverse reaction may be calculated using the thermodynamic data.

ANNEX II

SURFACE MECHANISM

Elementary reactions in the H₂-CO-C₁-O₂ system on platinum surfaces. Rate coefficients are presented in the modified Arrhenius form $k = A * T^\beta \exp(-Ea/RT)$. The pre-exponential factor A is given in units of (cm, mol, s); activation energy Ea in kJ mol⁻¹.

$$k_{jk} = A_k T^{\beta k} \exp\left[-\frac{E_{ak}}{RT}\right] \prod_{i=1}^{N_s} \Theta_i^{\mu_{ik}} \exp\left[\frac{\varepsilon_{ik} \Theta_i}{RT}\right] \quad (1)$$

This expression takes into account coverage dependences using the parameter μ_{ik} and ε_{ik} , which should be specified for several surface reactions. Under steady-state, the time variation of the surface coverage (Θ) is zero, then:

$$\frac{\partial \Theta_i}{\partial t} = \frac{\dot{s}_i}{\Gamma} = 0 \quad (i=N_g+1, \dots, N_g+N_s) \quad (2)$$

The concentration $[X_i]$ of an adsorbed species is given in mol/m² and equals to surface coverage (Θ_i) multiplied by the surface site density (Γ).

The surface site density: $2.72 * 10^{-09}$ mol/cm²

The mechanism is presented in the CD annexed.

| Adsorption | A | β | Ea | μ_{ik} | ε_{ik} | (a) | Ref. |
|--|------------------------|---------------------------|-----------|------------------------------|--------------------------------------|-----------------|-------------|
| $H_2 + Pt_{(s)} + Pt_{(s)} \rightarrow H_{(s)} + H_{(s)}$ | 0.046 | 0.0 | 0.0 | -1.0 | 0.0 | $\Theta_{(Pt)}$ | [1] |
| $O_2 + Pt_{(s)} + Pt_{(s)} \rightarrow O_{(s)} + O_{(s)}$ | $1.89 \times 10^{+21}$ | -0.5 | 0.0 | | | | [1] |
| $CH_4 + Pt_{(s)} + Pt_{(s)} \rightarrow CH_{3(s)} + H_{(s)}$ | 9.00×10^{-04} | 0.0 | 72.0 | | | | [2] |
| $CH_4 + O_{(s)} + Pt_{(s)} \rightarrow CH_{3(s)} + OH_{(s)}$ | $5.00 \times 10^{+18}$ | 0.7 | 42.0 | 0.0 | -8.0 | $\Theta_{(O)}$ | [2] |
| $CH_4 + OH_{(s)} + Pt_{(s)} \rightarrow CH_{3(s)} + H_2O_{(s)}$ | 1.00×10^{-00} | 0.0 | 10.0 | | | | [2] |
| $H_2O + Pt_{(s)} \rightarrow H_2O_{(s)}$ | 7.50×10^{-01} | 0.0 | 0.0 | | | | [1] |
| $CO_2 + Pt_{(s)} \rightarrow CO_{2(s)}$ | 5.00×10^{-03} | 0.0 | 0.0 | | | | [2] |
| $CO + Pt_{(s)} \rightarrow CO_{(s)}$ | 8.40×10^{-01} | 0.0 | 0.0 | | | | [1] |
| Desorption | A | β | Ea | μ_{ik} | ε_{ik} | (a) | |
| $H_{(s)} + H_{(s)} \rightarrow Pt_{(s)} + Pt_{(s)} + H_2$ | $3.70 \times 10^{+21}$ | 0.0 | 67.4 | 0.0 | 10.0 | $\Theta_{(H)}$ | [1] |
| $O_{(s)} + O_{(s)} \rightarrow Pt_{(s)} + Pt_{(s)} + O_2$ | $3.70 \times 10^{+21}$ | 0.0 | 235.5 | 0.0 | 188.28 | $\Theta_{(O)}$ | [1] |
| $H_2O_{(s)} \rightarrow H_2O + Pt_{(s)}$ | $4.50 \times 10^{+12}$ | 0.0 | 41.8 | | | | [2] |
| $CO_{(s)} \rightarrow CO + Pt_{(s)}$ | $1.00 \times 10^{+15}$ | 0.0 | 146.0 | 0.0 | 33.0 | $\Theta_{(CO)}$ | [2] |
| $CO_{2(s)} \rightarrow CO_2 + Pt_{(s)}$ | $1.00 \times 10^{+13}$ | 0.0 | 27.07 | | | | [1] |
| Surface reaction | A | β | Ea | μ_{ik} | ε_{ik} | (a) | |
| $C_{(s)} + O_{(s)} \rightarrow CO_{(s)} + Pt_{(s)}$ | $3.70 \times 10^{+19}$ | 0.0 | 0.0 | | | | [2] |
| $CO_{(s)} + Pt_{(s)} \rightarrow C_{(s)} + O_{(s)}$ | $3.70 \times 10^{+19}$ | 0.0 | 236.5 | 0.0 | 33.0 | $\Theta_{(CO)}$ | [2] |
| $CO_{(s)} + O_{(s)} \rightarrow CO_{2(s)} + Pt_{(s)}$ | $3.70 \times 10^{+19}$ | 0.0 | 117.6 | 0.0 | 33.0 | $\Theta_{(CO)}$ | [2] |
| $CO_{2(s)} + Pt_{(s)} \rightarrow CO_{(s)} + O_{(s)}$ | $3.70 \times 10^{+19}$ | 0.0 | 173.3 | 0.0 | -94.14 | $\Theta_{(O)}$ | [2] |
| $CO_{(s)} + OH_{(s)} \rightarrow CO_{2(s)} + H_{(s)}$ | $1.00 \times 10^{+19}$ | 0.0 | 38.7 | 0.0 | 30.0 | $\Theta_{(CO)}$ | [2] |
| $CO_{2(s)} + H_{(s)} \rightarrow CO_{(s)} + OH_{(s)}$ | $1.00 \times 10^{+19}$ | 0.0 | 8.4 | | | | [2] |
| $CH_3_{(s)} + Pt_{(s)} \rightarrow CH_2_{(s)} + H_{(s)}$ | $1.26 \times 10^{+22}$ | 0.0 | 70.3 | | | | [2] |
| $CH_2_{(s)} + H_{(s)} \rightarrow CH_3_{(s)} + Pt_{(s)}$ | $3.09 \times 10^{+22}$ | 0.0 | 0.0 | 0.0 | 2.8 | $\Theta_{(H)}$ | [2] |
| $CH_2_{(s)} + Pt_{(s)} \rightarrow CH_{(s)} + H_{(s)}$ | $7.31 \times 10^{+22}$ | 0.0 | 58.9 | 0.0 | -50.0 | $\Theta_{(C)}$ | [2] |
| $CH_{(s)} + H_{(s)} \rightarrow CH_2_{(s)} + Pt_{(s)}$ | $3.09 \times 10^{+22}$ | 0.0 | 0.0 | 0.0 | 2.8 | $\Theta_{(H)}$ | [2] |
| $CH_{(s)} + Pt_{(s)} \rightarrow C_{(s)} + H_{(s)}$ | $3.09 \times 10^{+22}$ | 0.0 | 0.0 | 0.0 | 2.8 | $\Theta_{(H)}$ | [2] |
| $C_{(s)} + H_{(s)} \rightarrow CH_{(s)} + Pt_{(s)}$ | $1.25 \times 10^{+22}$ | 0.0 | 138.0 | | | | [2] |
| $H_{(s)} + O_{(s)} \rightarrow OH_{(s)} + Pt_{(s)}$ | $1.28 \times 10^{+21}$ | 0.0 | 11.2 | | | | [2] |
| $OH_{(s)} + Pt_{(s)} \rightarrow H_{(s)} + O_{(s)}$ | $7.39 \times 10^{+19}$ | 0.0 | 77.30 | 0.0 | 73.22 | $\Theta_{(O)}$ | [2] |
| $H_2O_{(s)} + Pt_{(s)} \rightarrow H_{(s)} + OH_{(s)}$ | $1.15 \times 10^{+19}$ | 0.0 | 101.4 | 0.0 | -167.4 | $\Theta_{(O)}$ | [2] |
| $OH_{(s)} + OH_{(s)} \rightarrow H_2O_{(s)} + O_{(s)}$ | $7.40 \times 10^{+20}$ | 0.0 | 74.0 | | | | [2] |
| $H_2O_{(s)} + O_{(s)} \rightarrow OH_{(s)} + OH_{(s)}$ | $1.00 \times 10^{+20}$ | 0.0 | 43.1 | 0.0 | -240.6 | $\Theta_{(O)}$ | [2] |
| Additional steps | A | β | Ea | μ_{ik} | ε_{ik} | (a) | |
| $H_2 + C_{(s)} \rightarrow CH_2_{(s)}$ | 4.00×10^{-02} | 0.0 | 29.7 | 0.0 | -4.6 | $\Theta_{(C)}$ | [2] |
| $CH_2_{(s)} \rightarrow C_{(s)} + H_2$ | $7.69 \times 10^{+13}$ | 0.0 | 25.1 | 0.0 | -50.0 | $\Theta_{(C)}$ | [2] |
| $H_{(s)} + OH_{(s)} \rightarrow H_2O_{(s)} + Pt_{(s)}$ | $2.04 \times 10^{+21}$ | 0.0 | 66.22 | | | | [2] |
| $CH_3_{(s)} + H_{(s)} \rightarrow CH_4 + Pt_{(s)} + Pt_{(s)}$ | $3.30 \times 10^{+21}$ | 0.0 | 50.0 | 0.0 | 2.8 | $\Theta_{(H)}$ | [2] |
| $CH_3_{(s)} + H_2O_{(s)} \rightarrow CH_4 + OH_{(s)} + Pt_{(s)}$ | $3.70 \times 10^{+21}$ | 0.0 | 110.6 | | | | [2] |
| $CH_3_{(s)} + OH_{(s)} \rightarrow CH_4 + O_{(s)} + Pt_{(s)}$ | $3.70 \times 10^{+21}$ | 0.0 | 87.9 | | | | [2] |

(a) Denotes the species i, to which the parameter μ_{ik} and ε_{ik} refer to, Eq. (1)

[1] O. Deutschmann, R. Schmidt, F. Behrendt, J. Warnatz, Proc. Combust. Inst. 26 (1996) 1747, see also <http://www.detchem.com/mechanisms>.

[2] D.K. Zerkle, M.D. Allendorf, M. Wolf, O. Deutschmann, J. Catal. 196 (2000) 18.

REFERENCES

- [1] D.B. Spalding, *Combustion and Mass Transfer*. New York, Pergamon Press, 1979.
- [2] M. Ourania-Nektaria, *Entwicklung und Validierung verbesserter Teil-Modelle für transiente Sprays mit Verbrennung*. Laboratorium für Aerothermochemie und Verbrennungssysteme, Zürich, 2005.
- [3] S.M. Eisen, *Visualisierung der dieselmotorischen Verbrennung in einer schnellen Kompressionsmaschine*. Dissertation, Fakultät für Maschinenwesen, Technische Universität München, 2003.
- [4] R.B. Bird, W.E. Stewart, and E.N. Lightfoot, *Transport Phenomena*. New York, John Wiley & Sons, Inc., 1960.
- [5] S.V. Patankar, *Numerical Heat Transfer and Fluid Flow*. New York, McGraw-Hill, 1980.
- [6] J. Warnatz, R.W. Dibble, and U. Maas, *Combustion, Physical and Chemical Fundamentals, Modeling and Simulation, Experiments, Pollutant Formation*. New York, Springer-Verlag, 1996.
- [7] A.M. Kanury, *Introduction to Combustion Phenomena*. New York, Gordon and Breach, 1975
- [8] J. Warnatz, *Influence of Transport Models and Boundary Conditions on Flame Structure*. Numerical Methods in Flame Propagation, N. Peters and J. Warnatz. Wiesbaden, Eds. Friedr. Vieweg and Sohn, 1982.
- [9] G. Dixon-Lewis, "Flame Structure and Flame Reaction Kinetics". *Proc. Roy. Soc. A*, Vol. 307, 1968, 111–135.
- [10] R.J. Kee, G. Dixon-Lewis, J. Warnatz, M.E. Coltrin, and J.A. Miller, "A Fortran Computer Code Package for the Evaluation of Gas-Phase Multicomponent Transport Properties". Sandia National Laboratories Report. SAND86-8246, 1986.
- [11] T.G. Cowling and S. Chapman, *Mathematical Theory of Non-Uniform Gases*. Cambridge University Press, Second Edition, 1951.

-
- [12] M.W. Chase, C.A. Davis, J.R. Downey, D.J. Frurip, R.A. McDonald, and A.N. Syverud, JANAF Thermochemical Tables. Third Edition, *J. Phys. Chem. Ref. Data*, Vol. 14, 1985.
- [13] R.J. Kee, F.M. Rupley, and J.A. Miller, The Chemkin Thermodynamic Database. Sandia National Laboratories Report, SAND87-8215, 1987.
- [14] A. Burcat, Thermochemical Data for Combustion. In *Combustion Chemistry*, W.C. Gardiner. New York, Eds. Springer, 1984.
- [15] S.W. Benson, Thermochemical Kinetics. New York, John Wiley & Sons, 1976.
- [16] S. Gordon and B.J. McBride, Computer Programm for Calculation of Complex Chemical Equilibrium Compositions, Rocket Performance, Incident and Reflected Shocks and Chapman-Jouguet Detonations. NASA SP-273, 1971.
- [17] K.H. Homann, Reaktionskinetik. Darmstadt, Steinkopff, 1975.
- [18] S. Arrhenius, Über die Reaktionsgeschwindigkeit bei der Inversion von Rohrzucker durch Säuren. *Z. Phys. Chem.*, 4, 1889, 226.
- [19] J. Warnatz, Rate Coefficients in the C/H/O/System in Combustion Chemistry, Kapitel 5, W.C. Jr. Gardiner (Hrsg.). New York, Springer-Verlag, 1984, 197-360.
- [20] W. Forst, Theory of Unimolecular Reactions. New York, Academic Press, 1973.
- [21] R.G. Gilbert, K. Luther, and J. Troe, Theory of Thermal Unimolecular Reactions in the Fall-off Range. II. Weak Collision Rate Constants. *Ber. Bunsenges. Phys. Chem.* 87, 1983, 169-177.
- [22] J. Troe, Theory of Thermal Unimolecular Reactions in the Fall-off Range. I. Strong Collision Rate Constants. *Ber. Bunsenges. Phys. Chem.* 87, 1983, 116-169.
- [23] F.A. Lindemann, Discussion on The Radiation Theory of Chemical Action. *Trans. Farad. Soc.*. Vol. 17, 1922, 599.
- [24] K.A. Holbrook, M.J. Pilling, and S.H. Robertson, Unimolecular Reactions. Chichester, Wiley, 2nd Edition, 1996.
- [25] D.L. Baulch, C.J. Lobos, R.A. Cox, C. Esser, P. Frank, Th. Just, J.A. Kerr, M.J. Pilling, J. Troe, R. Walker, and J. Warnatz, Evaluated Kinetic Data for Combustion Modelling. *J. Phys.Chem Ref. Data*. Vol. 13, 1984, 1259.
- [26] D.L. Baulch, C.J. Lobos, R.A. Cox, C. Esser, P. Frank, Th. Just, J.A. Kerr, M.J. Pilling, J. Troe, R. Walker, and J. Warnatz, Evaluated Kinetic Data for Combustion Modelling. *J. Phys.Chem Ref. Data*. Vol. 21, 1994, 411.
- [27] M.E. Coltrin, R.J. Kee, and F.M. Rupley, Surface CHEMKIN (Version 4.0): A Fortran Package for Analyzing Heterogeneous Chemical Kinetics at a Solid-Surface - Gas-Phase Interface. Sandia National Laboratories Report, SAND90-8003B, 1990.

-
- [28] O. Deutschmann, Interactions Between Transport and Chemistry in Catalytic Reactors. Habilitationsschrift, Universität Heidelberg, 2001.
- [29] O. Deutschmann, R. Schmidt, F. Behrendt, and J. Warnatz, Numerical Modeling of Catalytic Combustion. Proc. Combust. Inst., 26, 1996, 1747-1754.
- [30] W.C. Gardiner, Gas Phase Combustion Chemistry. Ed.: W.C. Jr. Gardiner, 1999.
- [31] U. Maas and J. Warnatz, Ignition Processes in Hydrogen-Oxygen Mixtures. Combustion and Flame, 74, Issue 1, 1988, 53-69.
- [32] C. Chevalier, Entwicklung eines detaillierten Reaktionsmechanismus zur Modellierung der Verbrennungsprozesse von Kohlenwasserstoffen bei Hoch- und Niedertemperaturbedingungen. Dissertation, Universität Stuttgart, 1993.
- [33] V. Karbach, Aktualisierung und Validierung eines detaillierten Reaktionsmechanismus zur Oxidation von Kohlenwasserstoffen bei hohen Temperaturen. Diplomarbeit, Universität Heidelberg, 1997.
- [34] V. Warth, N. Stef, P.A. Glaude, F. Battin-Leclerc, G. Scacchi and G.M. Côme, Computer Aide Design of Gas-Phase Mechanisms - Application to the Modeling of Normal Butane Oxidation. Combustion and Flame, Vol. 114, Issues 1-2, 1998, 81-102.
- [35] C. Chevalier, J. Warnatz, and H. Melenk, Automatic Generation of Reaction Mechanism for the Description of the Oxidation of Higher Hydrocarbons. Ber. Bunsenges. Phys. Chem., Vol. 94, 1990, 1362-1367.
- [36] E. Ranzi, T. Faravelli, P. Guffuri, and A. Goldaniga, A Primary Pyrolysis and Oxidation Reactions of Linear and Branched Alkanes. Ind. Eng. Chem. Res., Vol. 36 (8), 1997, 3336-3344.
- [37] T. Asaba, K. Yoneda, N. Kakihara, and T. Hikita, A Shock Tube Study of Ignition of Methane Oxygen Mixtures. 9th Symposium (International) on Combustion, 1963.
- [38] D. J. Seery and C. T. Bowman, An Experimental and Analytical Study of Methane Oxidation Behind Shock Waves. Combustion and Flame, Vol. 14, 1970, 37-47.
- [39] A. Lifshitz, K. Scheller, A. Burcat, and G.B. Skinner, Shock-Tube Investigation of Ignition in Methane-Oxygen-Argon Mixtures. Combustion and Flame, Vol. 16, Issue 3, 1971, 311-321.
- [40] C.J. Jachimowski, Kinetics of Oxygen Atom Formation During the Oxidation of Methane Behind Shock Waves. Combustion and Flame, Vol. 23, Issue 2, 1974, 233-248.
- [41] T. Tsuboi and H. Wagner, Homogeneous Thermal Oxidation of Methane in Reflected Shock Waves. 15th Symposium (International) on Combustion, 1974, 883.
- [42] P. Roth and Th. Just, Kinetics of the High Temperature, Low Concentration CH₄ Oxidation Verified by H and O Atom Measurements. 20th Symposium (International) on Combustion, 1984, 807-818.

-
- [43] L.J. Spadaccini and M.B. Colket, Ignition Delay Characteristics of Methane Fuels. *Prog. Energy Combust. Sci.*, Vol. 20, 1994, 431-460.
- [44] H. Zanthoff and M. Baers, Oxidative Coupling of Methane in the Gas Phase: Kinetic Simulation and Experimental Verification. *Industrial Engineering Chemical Res.*, Vol. 29, 1990, 2-10.
- [45] N. Cohen and K.R. Westberg, Evaluation and Compilation of Chemical Kinetic Data. *J. Phys. Chem. Ref. Data*, Vol. 83 (1), 1979, 46-50.
- [46] C.T. Goralski and L.D. Schmidt, Modeling Heterogeneous and Heterogeneous Reactions in the High Temperature Combustion of Methane. *Chemical Engineering Science*, Vol. 54, 1999, 5791-5807.
- [47] G.P. Smith, D.M. Golden, M. Frenklach, N.W. Moriarty, B. Eiteneer, M. Goldenberg, C.T. Bowman, R. Hanson, S. Song, W.C. Gardiner, V. Lissianski, and Z. Qin, GRI-Mech 3.0 [HTTP://WWW.ME.BERKELEY.EDU/GRI_MECH/](http://www.me.berkeley.edu/GRI_MECH/).
- [48] J. Mantzaras, Numerical Modelling of Turbulent Catalytically Stabilized Channel Flow Combustion. *Cat. Today*, Vol. 59 (1), 2000, 3-17.
- [49] Q. Chen, P.M. Couwenberg, and G.B. Marin, The Oxidative Coupling of Methane with Cofeeding of Ethane. *Cat. Today*, Vol. 21, Issues 2-3, 1994, 309-319.
- [50] Q. Chen, P.M. Couwenberg, and G.B. Marin, Effect of Pressure on the Oxidative Coupling of Methane in the Absence of Catalyst. *AIChE J.*, Vol. 40, Issue 3, 1994, 531.
- [51] M. Baerns, Oxidative Coupling of Methane for the Utilization of Natural Gas. In *Chemical Reactor Technology for Environmental Safe Reactors and Products*, H. I. de Lasa and H. De Laso, Ed.: G. Dogu, 1993, 283-316.
- [52] K. Wiele, J.W. Geerts, and J.M. Kasteren, Elementary Reactions and Kinetic Modeling of the Oxidative Coupling of Methane. Eindhoven University of Technology, Laboratory of Chemical Process Technology, Netherlands, 1990.
- [53] W. Tsang and R.F. Hampson, Chemical Kinetic Database for Combustion Chemistry, Part I: Methane and Related Compounds. *J Phys. Chem. Ref. Data*, Vol. 16, 1986, 471.
- [54] F. Westley and J.T. Herron, Compilation of Kinetics Data for Combustion Chemistry. Part I: Nonaromatic C, H, O, N and S Containing Compounds. US Government Printing Office.
- [55] I.A. Vardanyan and A.B. Nalbandyan, On the Mechanism of Thermal Oxidation of Methane. *Inter. J. Chem Kinetic*, Vol. 17, 1985, 901-924.
- [56] P. Dagout, M. Cathonnet, and J.C. Boettner, Experimental Study and Kinetic Modeling of Propane Oxidation in a Jet Stirred Flow Reactor. *J. Phys. Chem.*, 1988, 661-671.

-
- [57] L.F. Allbright, B.L. Crynes, and W.H. Corcoran, *Pyrolysis, Theory and Industrial Practice*. New York, Academic Press, 1983.
- [58] D.F. Cooke and A. Williams. A Shock Tube Studies of the Ignition and Combustion of Ethane and Slightly Rich Methane Mixtures with Oxygen. 13th Symposium (International) on Combustion, 1971, 757-766.
- [59] N.M. Marinov, W.J. Pitz, C.K. Westbrook, M.J. Castaldi, and S.M. Senkan, Modeling of Aromatic and Polycyclic Aromatic Hydrocarbon Formation in Premixed Methane and Ethane Flames. *Comb. Sci. and Tech*, Vol. 116-117, 1996, 211-287.
- [60] W. Tsang, Chemical Kinetic Data Base for Combustion Chemistry. Part V. Propene. *J. Phys. Chem. Ref. Data.*, Vol. 20, 1991, 221-273.
- [61] W. Tsang, Chemical Kinetic Data Base for Combustion Chemistry. Part III. Propane. *J. Phys. Chem. Ref. Data*, Vol. 17, 1988, 1887.
- [62] W.J. Pitz, C.K. Westbrook, and W.K. Lepard, Auto Ignition Chemistry of C₄ Olefins Under Motore Engine Conditions: A Comparison of Experimental and Modeling Results. *SAE Transactions*, 1991, SAE Paper 912315.
- [63] J.A. Miller and C.F. Melious, Kinetic and Thermodynamic Issues in the Formation of Aromatic Compounds in Flames of Aliphatics Fuel. *Combustion and Flame*, Vol. 91 (1), 1992, 21-39.
- [64] R. Rota, R. Fiandaca, M. Morbidelli and S. Carrá. Experimental Analysis of the Combustion of Mixtures of C₁-C₂ Hydrocarbons. *Ind. Eng. Chem. Res.*, Vol. 38, 1999, 897-905.
- [65] C. Westbrook, M. Thornton, W. Pitz and P. Maltes. A Kinetic Study of Ethylene Oxidation in a Well Stirred Reactor. 22th Symposium (International) On Combustion, 1988, 863-871.
- [66] R. Wilk, W. Pitz, C. Westbrook and N. P. Cernansky. Chemical Kinetic Modeling of Ethene Oxidation at Low and Intermedia Temperatures. 23th Symposium (International) on Combustion, 1990, 203-210.
- [67] D.J. Ray and D. Waddington, Gas Phase Oxidation of Alkenes—Part II. The Oxidation of 2-methylbutene-2 and 2,3-dimethylbutene-2. *Combustion and Flame*, Vol. 20, 1973, 327-334
- [68] D. Zerkle, M. Allendorf, M. Wolf and O. Deutschman. Understanding Homogeneous Contributions to the Platinum Catalyzed Partial Oxydation of Ethane in a Short Contact Time Reactor. *Journal Catalysis*, Vol. 196, 2000, 18-39.
- [69] F.N. Egolfopoulos, D.L. Zhu, and C.K. Law, Laminar Flame Speeds of Methane-Air Mixtures Under Reduced and Elevated Pressures. *Combustion and Flame*, Volume 76, Issues 3-4, 1989, Pages 375-391.

-
- [70] P. Dagaut, M. Cathonnet, and J.C. Boettner, Kinetics of Ethane Oxidation. *International Journal of Chemical Kinetics*, Vol. 23, Issue 5, 1991, 437-455.
- [71] A. Burcat and A. Lifshitz, Investigation of Ignition of Propane-Oxygen-Argon Mixtures. 13th Symposium (International) on Combustion, 1971, 745-755.
- [72] A. Burcat and K. Radhakrishnan, High Temperature Oxidation of Propane. *Combustion and Flame*, Vol. 60, 1985, 157-169.
- [73] M. Cathonnet, J.C. Boettner, and H. James, Experimental Study and Numerical Modelling of High Temperature Oxidation of Propane and n-Butane. 18th Symposium (International) on Combustion. 1981, 903-913.
- [74] M. Baerns and O. Buyevskay, Simple Chemical Processes Based on Low Molecular-Mass Alkanes as Chemical Feed-Stocks. *Catal. Today*, Vol. 45, Issue 1, 1998, 13-22.
- [75] M. Huff and L. D. Schmidt, Olefin Formation by Direct Catalytic Oxidation of Propane and Butane at Short Contact Times. *Journal Catalysis*, Vol. 149, 1994, 127-141.
- [76] A. Beretta, L. Piovesant, and P. Forzatti, An Investigation on the Role of a Pt/Al₂O₃ Catalyst in the Oxidative Dehydrogenation of Propane in Annular Reactor. *Chem. Eng. Sci.*, Vol. 54 (6), 1999, 765-773.
- [77] A. Beretta, P. Forzatti, and E. Ranzi, Production of Olefins via Oxidative Dehydrogenation of Propane in Autothermal Conditions. *Journal Catalysis*, Vol. 184, 1999, 469-478.
- [78] S. Kojima, Detailed Modeling of n-Butane Autoignition Chemistry. *Combustion and Flame*, Vol. 99, 1994, 87-136.
- [79] S. Kojima and T. Suzuoki, Autoignition Delay Measurement over Lean to Rich Mixtures of n-Butane Under Swirl Conditions. *Combustion and Flame*, Vol. 92, 1993, 254-265.
- [80] S. Kojima, R&D Review of Toyota. CRDL, 28-4, 1993.
- [81] A. Burcat, K. Scheller, and A. Lifshitz, Shock-Tube Investigation of Comparative Ignition Delay Times for C₁-C₅ Alkanes. *Combustion and Flame*, Vol. 16, 1971, 29-33.
- [82] M. Nehse, Automatische Erstellung von detaillierten Reaktionsmechanismen zur Modellierung der Selbstzündung und laminarer Vormisflammen von gasförmigen Kohlenwasserstoff - Mischungen. Dissertation. Ruprecht Karls Universität Heidelberg, 2001.
- [83] National Institute of Standard and Technology NIST. Chemical Kinetics Database on the Web, Standard Reference Database 17, Version 7.0 (Web Version), Release 1.2, [HTTP://WWW.NIST.GOV](http://www.nist.gov).

-
- [84] R.D. Wilk, N.P. Cernansky, W.J. Pitz and C.K. Westbrook, Propene Oxidation at Low and Intermediate Temperatures: A Detailed Chemical Kinetic Study. *Combustion and Flame*, Vol. 77, 1989, 145-170.
- [85] C.F. Cullis and Sir C.N. Hinshelwood, The Mechanism of the Hydrogen-Oxygen Reaction V. The Reaction in Vessels Coated with Alkali Iodides, *Proceedings of the Royal Society of London. Series A, Mathematical and Physical Sciences*, Vol. 186, No. 1007 (Sep. 24, 1946), pp. 469-472
- [86] N.N. Semenov, *Some Problems of Chemical Kinetics and Reactivity*. London, Pergamon, 1962.
- [87] A. Fish, *The Cool Flames of Hydrocarbons*. *Angew Chemie (International Ed)*, Vol. 7, 1968, 45.
- [88] R.T. Pollard, *Gas Phase Combustion in Comprehensive Chemical Kinetics*. Vol. 17, C. H. Bamford and C. F. H. Tipper, New York, Elsevier, 1977, 249-367.
- [89] J.H. Knox, A New Mechanism for the Low Temperature Oxidation of Hydrocarbons in the Gas Phase. *Combustion and Flame*, Vol. 9, Issue 3, 1965, 297-310.
- [90] R. Atkinson, D. Baulch, R. Cox, J. Crowley, R. Hampson, J. Kerr, M. Rossi, and J. Troe, *Summary of Evaluated Kinetic and Photochemical Data for Atmospheric Chemistry*. IUPAC, 2001.
- [91] I.R. Slage, Y. J. Park, and D. Gutman, Experimental Investigation of the Kinetics and Mechanism of the Reaction of n-Propyl Radicals with Molecular Oxygen from 297 K to 635 K. 20th Symp (International) on Combustion, 1985, 733-743.
- [92] R.P. Ruiz and K.D. Bayes, Rates of Reaction of Propyl Radicals with Molecular Oxygen. *J. Phys. Chem.*, Vol. 88, 1984, 2592.
- [93] T.M. Lenhardt, C.E. McDade, and K.D. Bayes, Rates of Reaction of Butyl Radicals with Molecular Oxygen. *J. Chem. Phys.*, Vol. 72, 1980.
- [94] R.R. Baker, R.R. Baldwin, A. R. Fuller and R. W. Walker, Addition of nC₄H₁₀ to Slowly Reacting Mixtures of Hydrogen and Oxygen at 480°C. Part 1. Formation of Hydrocarbons Products. *J. Chem. Soc. Faraday Trans. 1*, Vol. 1, 1975.
- [95] A. Fish, I. A. Read, W. S. Affleck and W. W. Haskell. The Controlling Role of Cool Flames in Two-Stage Ignition. *Combustion and Flame*, Vol. 13, Issue 1, February 1969, 39-49.
- [96] R.R. Baldwin and R.W. Walker, Rate Constants for Reactions of HO₂ Radicals with Alkanes, Aldehydes and Related Compounds. 17th Symposium (International) on Combustion, 1979.
- [97] R. Simonaitis and J. Heicklen, Reactions of CH₃, CH₃O and CH₃O₂ Radicals with O₃. *J. Phys. Chem.*, 79, 1975, 298.

-
- [98] H. Adachi and N. Basco, Spectra of Propylperoxy Radicals and Rate Constants for Mutual Interaction. *Int. J. Chem. Kin.*, Vol. 14, 1982.
- [99] T.J. Wallington, P. Dagaut, and M.J. Kurylo, Ultraviolet Absorption Cross Sections and Reaction Kinetics and Mechanism for Peroxy Radicals in the Gas Phase. *Chem. Rev.*, Vol. 92, 1992, 667-710.
- [100] P.D. Lightfoot, R.A. Cox, J. Crowley, M. Destriau, G. Hayman, M. Jenkin, G. K. Moortgat, F. Zabel, Organic Peroxy Radicals: Kinetics Spectroscopy and Tropospheric Chemistry. *Atmos. Environ. Part A*, Vol. 26, 1992.
- [101] L.R. Sochet and M. Lucquin, Analogy Between Gas Phase and Liquid Phase Oxidation of Hydrocarbons in the Final Stages of the Reaction: 'Pic d'arrêt and Oxygen cut-off. *Combustion and Flame*, Vol. 13, Issue 3, 1969, 319-322.
- [102] M. Lucquin and S. Antonik, Multistage Ignition in Hydrocarbon Combustion. *Combustion and Flame*, Vol. 19, Issue 2, 1972, 311-313.
- [103] J.A. Barnard and A. Cohen. Reaction of Methyl Radicals With Oxygen. *Trans. Faraday Soc.* 64, 1968, 396
- [104] A.D. Kirk and J.H. Knox, The Pyrolysis of Alkyl Hydroperoxides in the Gas Phase. *Trans. Faraday Soc.*, Vol. 56, 1960, 1296-1303.
- [105] K.A. Sahetchian, R. Rigny, and J. Maleissye, The Pyrolysis of Organic Hydroperoxides (ROOH). 24th Symposium (International) on Combustion, 1992, 637-643.
- [106] S.W. Benson, Effects of Resonance and Structure on the Thermochemistry of Organic Peroxy Radicals and the Kinetics of Combustion Reactions. *J. Am. Chem. Soc.* Vol. 87, 1965, 972.
- [107] A.C. Hindmarsh, Report UCID-30001. Lawrence Livermore Laboratory, 1974.
- [108] C.F. Cullis, M. Saeed, and D. Trimm, Quantitative Aspects of Alkylperoxy Radical Isomerization During Hydrocarbon Combustion. *Proceedings of the Royal Society of London. Series A, Mathematical and Physical Sciences*, Vol. 300, No. 1463, 1967, 455-467.
- [109] P. Barat, F. Cullis, and R. Pollard, Studies of the Combustion of Branched Chain Hydrocarbons. *Proceedings Royal Soc. London. Ser: A.* 1971, 325.
- [110] S.S. Devush, Z.P. Prisyazhnyuk, and A.M. Koval'skaya, Kinetics of the Thermal Gas Phase Decomposition of C₁-C₄ Organic Peracids. *Kinet. Catal.*, Vol. 24, 1983.
- [111] D.L. Baulch, C.J. Lobos, R.A. Cox, C. Esser, P. Frank, Th. Just, J.A. Kerr, M.J. Pilling, J. Troe, R. Walker, and J. Warnatz, Evaluated Kinetic Data for Combustion Modeling: Supplement II. *J. Phys. Chem. Ref. Data*, Vol. 34, 2005, 757.

-
- [112] R. Baldwin, M. Hisham, and R. Walker, Elementary Reactions Involved in the Oxidation of Propene: Arrhenius Parameters for the Reaction $\text{HO}_2 + \text{C}_3\text{H}_6 \leftrightarrow \text{C}_3\text{H}_6\text{O} + \text{OH}$. Symp. (International) Combustion, Vol. 20, 1985.
- [113] N. Stothard and R. Walker, Arrhenius Parameters for the Addition of HO_2 Radicals to (E) But-2-ene Over the Range 400-520°C. J. Chem. Soc. Faraday Trans., Vol. 86, 1990.
- [114] D.J. Bogan and C.W. Hand, Absolute Rate Constant, Kinetic Isotope Effect and Mechanism of the Reaction of Ethylene Oxide with Oxygen(3P) Atoms. J. Phys. Chem., Vol. 82, 1978, 2067.
- [115] R.R. Baldwin, A. Keen, and R.W. Walker, Studies of the Decomposition of Oxirane and of its Addition to Slowly Reacting Mixtures of Hydrogen and Oxygen. J. Chem. Soc. Faraday Trans.1, Vol. 80, 1984, 435.
- [116] A. Lifshitz and H. Ben-Hamou, Thermal Reactions of Cyclic Ethers at High Temperatures: 1. Pyrolysis of Ethylene Oxide Behind Reflected Shocks. J. Phys. Chem., Vol. 87, 1983, 1782.
- [117] J. Chen, V. Young, P.A. Hooshiyar, H. Niki and M.D. Hurley, FTIR Spectroscopic Study of the Cl-Atom-Initiated Reactions of Ethylene Oxide in O_2/N_2 Diluent. J. Phys. Chem., Vol. 99, 1995, 4071-4077.
- [118] M.G. Duke and K.A. Holbrook, Reactions of Methyl Radicals with Oxetan, 2-Methyloxetan and 2,4-Dimethyloxetan. J. Chem. Soc. Faraday Trans. 1, Vol. 76, 1980, 1232.
- [119] R.R. Baker and R.W. Walker, Addition of n-Butane to Slowly Reacting Mixtures of Hydrogen and Oxygen at 480°C. Part 2. Formation of Oxygenated Products. J. Chem. Soc. Faraday Trans. 1, 1971, 71.
- [120] L. Zalatoi, T. Berces, and F. Marta, Collisional Energy Transfer in the Decomposition of 2-Methyloxetan: I. Gas/Gas Collisions. React. Kinetic Catalyst Lett., Vol. 42, 1990.
- [121] A. Lifshitz, M. Bidani, and S. Bidani, Thermal Reactions of Cyclic Ethers at High Temperatures. 2 Pyrolysis of Tetrahydrofuran Behind Reflected Shocks. J. Phys. Chem., Vol. 90, 1986.
- [122] M. Nehse, J. Warnatz, and C. Chevalier, Kinetic Modeling of the Oxidation of Large Aliphatic Hydrocarbons. Twenty-Sixth Symposium (International) on Combustion, The Combustion Institute, Pittsburgh (1996)
- [123] W.J. Pitz and C.K. Westbrook, Chemical Kinetics of the High Pressure Oxidation of n-Butane and its Relation to Engine Knock. Combustion and Flame, Vol. 63, Issues 1-2, 1986, 113-133.
- [124] A.M. Dean, Predictions of Pressure and Temperature Effects upon Radical Addition and Recombination Reactions. J. Phys. Chem, Vol. 89, 1985, 4600.

-
- [125] Y. Hidaka, T. Nakamura, H. Tanaka, A. Jinno and H. Kawano, Shock Tube and Modeling of Propene Pyrolysis. *Int. J. Chem. Kin.* Vol. 24, 1992, 761-780.
- [126] P. Barbe, R. Martin, D. Perrin, and G. Scacchi, Kinetics and Modeling of the Thermal Reaction of Propene at 800 K. Part I. Pure Propene. *Int. J. Chem. Kinet.*, Vol. 28, 1996, 829-847.
- [127] T. Berces and F. Marta, Reactions of Methyl Radicals with Acetaldehyde and Acetaldehyde-d1 II BEBO Calculations of the Temperature Dependence of the Rate Constants. *Int. J. Chem. Kinet.*, Vol. 8, 1976, 295-306.
- [128] D.L. Singleton, R.S. Irwin, and R.J. Cvetanovic, Arrhenius Parameters for the Reactions of O(3P) Atoms with Several Aldehydes and the Trend in Aldehydic C-H Bond Dissociation Energies. *Can. J. Chem.*, Vol. 55, 1977, 3321.
- [129] R.R. Baldwin, D. H. Langford, M.J. Matchan, R.W. Walker and D.A. Yorke, The High Temperature Oxidation of Aldehydes. 13th Symp. (International) on Combustion, Vol. 13, 1971.
- [130] R. Birrell and A.F. Trotman, The Reactions of Alkyl Radicals, Part VI: The Reactions of Methyl Radicals with Aliphatic Aldehydes. *J. Chem. Soc.* 1960, 2059-2063.
- [131] R. Baldwin, C. Cleugh, J. Plaistowe, and R. Walker, Oxidation of Isobutylaldehyde in Aged Boric Acid Coated Vessels. *J. Chem. Soc. Faraday Trans. 1*, Vol. 75, 1979, 1433-1446.
- [132] T.M. Sloane, Ignition and Flame Propagation Modeling With an Improved Methane Oxidation Mechanism. *Combustion Science Tech.* Vol. 63, 1989, 287-313.
- [133] R. Deters, M. Otting, H. Gg. Wagner, F.B. Temps, B. László, S. Dób, T.A. Bérces, A Direct Investigation of the Reaction CH_3+OH : Overall Rate Constant and CH_2 Formation at $T=298$ K. *Bunsenges. Phys. Chem.* 102 (1), 1998, 58-72.
- [134] Y. Hidaka, High Temperature Pyrolysis of Methane in Shock Waves: Rates for Dissociative Recombination Reactions of Methyl Radicals and for Propyne Formation Reaction. *Int. J. Chem. Kinet.*, Vol. 22, 1990, 701.
- [135] C.L. Yu, C. Wang, and M. Frenklach, Chemical Kinetics of Methyl Oxidation by Molecular Oxygen. *J. Phys. Chem.*, Vol. 99, 1995, 14377-14387.
- [136] E. Hassinen and J. Koskikallio, Flash Photolysis of Methyl Acetate in Gas Phase. Products and Rate Constants of Reactions between Methyl, Methoxy and Acetyl Radicals. *Acta Chem. Scand. A.*, Vol. 33, 1979, 625.
- [137] W. Tsang, Chemical Kinetic Data Base for Combustion Chemistry. Part II. Methanol. *J. Phys. Chem. Ref. Data.*, Vol. 16, 1987.
- [138] H. Thiesemann and C.A. Taatjes, Temperature Dependence of the Reaction $\text{C}_2\text{H}(\text{C}_2\text{D}) + \text{O}_2$ Between 295 K and 700 K. *Chem. Phys. Lett.*, Vol. 270, 1997, 580-586.

-
- [139] K. Devriendt and J. Peeters, Direct Identification of the C₂H. *J. Phys. Chem. A.*, Vol. 101, 1997, 2546-2551.
- [140] J. Peeters, H. Van Look, and B. Ceursters, Absolute Rate Coefficients of the Reactions of C₂H with NO and H₂ Between 295 K and 440 K. *J. Phys. Chem.*, Vol. 100, 1996, 15124-15129.
- [141] V.D. Knyazed and I.R. Slage, Kinetics of the Reaction of Vinyl Radical With Molecular Oxygen. *J. Phys. Chem.*, Vol. 99, 1995, 2247-2249.
- [142] J.W. Bozzelli and A.M. Dean, Hydrocarbon Radical Reactions with O₂: Comparison of Allyl, Formyl, and Vinyl to Ethyl. *J. Phys. Chem.*, Vol. 97, 1993, 4427.
- [143] A.M. Mebel, E.W.G. Diau, M.C. Lin, and K.J. Morokuma, Ab Initio and RRKM Calculations for Multichannel Rate Constants of the C₂H₃ + O₂ Reaction. *J. Am. Chem. Soc.*, Vol. 118, 1996, 9759.
- [144] M. Bartels, M.J. Edelbuttel-Einhaus, and K. Hoyer mann, The Detection of CH₃CO, C₂CHO by Rempi/Mass Spectrometry and the Application to the Study of the Reactions H + CH₃CO and O + CH₃CO. 23th Symposium (International) on Combustion, 1991, 131-138.
- [145] L. Costa, M.P. Luda, G.G. Cameron, M.Y. Qureshi, The Thermal Oxidation of Poly(propyleneoxide) and its Complexes with LiBr and LiI. *Polymer Degradation and Stability*, Vol. 53, 1996, 301-310.
- [146] H-X. Zhang and M.H. Back, Rate Constants for Abstraction of Hydrogen from Ethylene by Methyl and Ethyl Radicals over the Temperature Range 650 K-770 K. *Int. J. Chem. Kinet.*, Vol. 22, 1990, 21.
- [147] S.I. Ahonkhai and H.M. Back, Relative Rate Constants for Abstraction of Hydrogen by Methyl Radicals from Ethane and from Ethylene. *Canadian J. Chem.*, Vol. 66, 1988, 578.
- [148] S.I. Ahonkhai, X.H. Lin, and M.K. Back, Rate Constants for Abstraction of Hydrogen from Ethylene by Methyl and Ethyl Radicals Relative to Abstraction from Propane and Isobutane. *Int. J. Chem. Kinet.*, Vol. 21, 1989, 1.
- [149] R.M. Marshall, The Rate Constant for the Intramolecular Isomerization of Pentyl Radicals. *Int. J. Chem. Kinet.*, Vol. 22, 1990, 935.
- [150] J.C. Thynne, Reactions of Alkyl Radicals. *Trans. Faraday Soc.*, Vol. 58, 1962, 1533.
- [151] P.Y. Yampol'skii, Reactivity of Primary and Secondary Carbon-Hydrogen Bonds in Radical Processes. *React. Kinet. Catal. Lett.*, Vol. 2, 1975, 449.
- [152] A. Burcat, Third Millennium Ideal Gas and Condensed Phase Thermochemical Database for Combustion. Technion Aerospace Engineering (TAE) Report #867, January 2001.

-
- [153] A. Konnov, Detailed Reaction Mechanism for Small Hydrocarbons Combustion. 2000, Release 0.5, <http://homepages.vub.ac.be/~akonnov>.
- [154] C. Muller, V. Michel, G. Scacchi and G.M. Come, THERGAS: A Computer Program for the Evaluation of Thermochemical Data of Molecules and Free Radicals in the Gas-Phase. *J. Chem Phys.*, Vol. 92, 1995, 1154-1178.
- [155] M. Frenklach and D.E. Bornside, Shock-Initiated Ignition in Methane-Propane Mixtures. *Combustion and Flame*, Vol. 56, 1984, 1-27.
- [156] R.W. Crossley, The Effect of Higher Alkanes on the Ignition of Methane-Oxygen-Argon Mixtures in Shock Waves. *Combustion and Flame*, Vol. 19, Issue 3, 1972, 373-378.
- [157] I.R. Slagle, Kinetics of Polyatomic Free Radicals Produced by Laser Photolysis. 3: Reaction of Vinyl Radicals With Molecular Oxygen. *J. Am. Chem. Soc.*, Vol. 106, 1984, 4356.
- [158] J. Bozzelli and A. Dean, Hydrocarbon Radical Reactions With O₂: Comparison of Allyl, Formyl, and Vinyl to Ethyl. *J Phys. Chem.*, Vol. 97, 1993, 4427-4441.
- [159] J.Y. Zhu, R. Dittmeyer, and H. Hofmann, Application of Sensitivity Analysis to the Reduction of a Complex Kinetic Model for the Homogeneous Oxidative Coupling of Methane. *Chemical Engineering and Processing*, Vol. 32, 1993, 167-176.
- [160] M.J. Pilling, T. Turanyi, K.J. Hughes and A.R. Clague, Leeds Methane Oxidation Mechanism Version: 1.4. <http://www.chem.leeds.ac.uk/combustion/>.
- [161] S.C. Li and F.A. Williams, Experimental and Numerical Studies of Two-Stage Methanol Flames. 26th Symposium (International) on Combustion, 1996, 1017-1024.
- [162] K. Spindler and H. Wagner, Zum thermischen unimolekularen Zerfall von Methanol. *Ber Bunsenges. Phys. Chem.*, Vol. 86, 1982, 2.
- [163] K.J. Mintz and D.J. Le Roy, Kinetics of Radical Reactions in Sodium Diffusion Flames. *Can. J. Chem.*, Vol. 56, 1978, 941.
- [164] D.J. Hautman, R.J. Santoro, F.L. Dryer, I. Glassman, An Overall and Detailed Kinetic Study of the Pyrolysis of Propane. *Int. J. Chem. Kinet.* 13, 1981, 149.
- [165] W. Moller, E. Mozzhukhin, and H.G. Wagner, High Temperature Reactions of CH₃. 2. H-Abstraction from Alkanes. *Ber. Bunsenges. Phys. Chem.*, Vol. 91, 1987, 660.
- [166] Y.P. Yampol'skii, Reactivity of Primary and Secondary Carbon Hydrogen Bonds in Radical Processes. *React. Kinet. Catal. Lett.*, Vol. 2, 1975.
- [167] M. Sway, Kinetics of Abstraction Reactions of Methyl Radicals in Gas Phase. *Indian J. Chem.*, Vol. 29, 1990, 748.
- [168] M.M. Thornton, P.C. Malte, and A.L. Crittenden, WSSCI Paper, Fall Meeting of the Western States Section. The Combustion Institute, 1985, 85-35.

-
- [169] R.D. Wilk, D.L. Miller, and N.P. Cernansky, WSSCI Paper, Joint Spring Meeting of the Canadian and Western States Section. The Combustion Institute, 1986, 86-6.
- [170] R.R. Baldwin, C.E. Dean, and R.W. Walker, Relative Rate Study of the Addition of HO₂ Radicals of C₂H₄ and C₃H₆. *J. Chem. Soc. Faraday Trans. 2*, Vol. 82, 1986, 1445.
- [171] R.R. Baldwin and R.W. Walker, Elementary Reactions in the Oxidation of Alkenes. 18th Symposium (International) on Combustion, 1981, 819.
- [172] R.R. Baldwin, J.P. Bennet, and R.W. Walker, Addition of Pentenes to Slowly Reacting Mixtures of Hydrogen and Oxygen at 480°C. *J. Chem. Soc., Faraday Trans. 1*, Vol. 76, 1984, 2396.
- [173] D.J. Ray, D.R. Ruiz, and D.J. Waddington, Gas-Phase Oxidation of Butene-2: The Role of Acetaldehyde in the Reaction. 14th Symposium (International) on Combustion, The Combustion Institute, 1973, 259.
- [174] C.T. Goralski and L.D. Schmidt, Modeling Heterogeneous and Homogeneous Reactions in the High Temperature Catalytic Combustion of Methane – A Numerical Algorithm for Varying Solid Phase Peclet Numbers. *Chem. Eng. Sci.*, Vol. 54, Issue 24, 1999, 5791-5807.
- [175] D.A. Hickman and L.D. Schmidt, Steps in CH₄ Oxidation on Pt and Rh Surfaces: High Temperature Reactor Simulations. *AIChE*, Vol. 39, 1993, 1164.
- [176] O. Deutschmann and R. Schmidt, Two-Dimensional Modeling of Partial Oxidation of Methane on Rhodium in a Short Contact Time Reactor. 27th Symposium (International) on Combustion, The Combustion Institute, Pittsburg, 1998, 2283-2291.
- [177] A.S. Bodke, S.S. Bharadwaj, and L.D. Schmidt, The Effect of Ceramic Supports on Partial Oxidation of Hydrocarbons over Nobel Metal Coated Monoliths. *J. Catalysis*, Vol. 179, 1998, 138-149.
- [178] R. Schwiedernoch, Partial and Total Oxidation of Methane in Monoliths and Short Contact Times Reactors. PhD Dissertation, Universität Heidelberg, 2005.
- [179] C.R.H. de Smet, M.H.J.M. de Croon, R.J. Berger, G.B. Marin, and J.C. Schouten, An Experimental Reactor to Study the Intrinsic Kinetics of Catalytic Partial Oxidation of Methane in the Presence of Heat-Transport Limitations. *Applied Catalysis A, General*, Vol. 187, 1999, 33-48.
- [180] Fluent 6.0 (2000), copyright Fluent Incorporated, Lebanon, NH, see also www.fluent.com.
- [181] M.F. Reayniers, C.R. de Smet, P. Govin, and G. Marin, Catalytic Partial Oxidation: Part I, Catalytic Processes to Convert Methane: Partial or Total Oxidation. *CATTECH*, Vol. 6, 2002, 140-149.

-
- [182] H.K. Hofstad, T. Sperle, O.A. Rokstad, and A. Holmen, Partial Oxidation of Methane to Synthesis Gas Over a Pt/10% Rh Gauze. *Catal. Lett.*, Vol. 45, 1997, 97-105.
- [183] D.A. Hickman and L.D. Schmidt, Synthesis Gas Formation by Direct Oxidation of Methane Over Pt Monoliths. *J. Catal.*, Vol. 138, 1992, 267-282.
- [184] J.C. Mackie, Partial Oxidation of Methane: The Role of the Gas-Phase Reactions. *Catal. Rev. Sci. Eng.*, Vol. 33, 1991, 169-240.
- [185] G.E. Keller and M.M. Bhasin, Synthesis of Ethylene Via Oxidative Coupling of Methane. I Determination of Active Catalyst. *J. Catalysis*, Vol. 73, 1983, 9-19.
- [186] T. Ito, J. Wang, C.H. Lin, and J.H. Lunsford, Oxidative Dimerization of Methane Over a Lithium-Promoted Magnesium Oxide Catalyst. *J. American Chem. Soc.*, Vol. 107, 1985, 5062-5068.
- [187] K.D. Campbell, E. Morales, and J.H. Lunsford, Gas-Phase Coupling of Methyl Radicals During the Catalytic Partial Oxidation of Methane. *J. Am. Chem Soc.*, Vol. 109, 1987, 7900-7901.
- [188] D. Wolf, M. Höhenberger, and M. Baerns, External Mass and Heat Transfer Limitations of the Partial Oxidation of Methane over Pt/MgO, Consequences for Adiabatic Reactor Operation. *Ind. Eng. Chem. Res.*, Vol. 36, 1997, 3345-3353.
- [189] G. Vesper and J. Frauhammer, Modeling Steady State and Ignition During Catalytic Methane Oxidation in a Monolith Reactor. *Chem. Eng. Sci.*, Vol. 55, 2000, 2271-2286.
- [190] O. Deutschmann, S. Tischer, C. Correa, D. Chatterjee, S. Kleditzsch, V.M. Janardhanan, DETCHEM software package, 2.0 ed., Karlsruhe, 2004, see also www.detchem.com.

ERKLÄRUNG

Eidesstattliche Erklärung

Ich erkläre hiermit, dass ich die vorgelegte Dissertation selbst verfasst und mich keiner anderen als der von mir ausdrücklich bezeichneten Quellen und Hilfen bedient habe.

Heidelberg, 16.11.2007

Raul Quiceno Gonzalez

